CRANFIELD UNIVERSITY

Nelia Jurado Pontes

# Experimental and modelling studies of coal/biomass oxy-fuel combustion in a pilot-scale PF combustor

School of Applied Sciences

PhD

Academic Year: 2013 - 2014

Supervisors: Prof J.E. Oakey and Dr H.G. Darabkhani
August 2014

CRANFIELD UNIVERSITY

School of Applied Sciences

Doctor of Philosophy

Academic Year 2013 - 2014

**Nelia Jurado Pontes**

# Experimental and modelling studies of coal/biomass oxy-fuel combustion in a pilot-scale PF combustor

Supervisors: Prof J.E. Oakey and Dr H.G. Darabkhani
August 2014

This thesis is submitted in partial fulfilment of the requirements for the degree of Doctor of Philosophy

# ABSTRACT

This thesis focuses on enhancing knowledge on co-firing oxy-combustion cycles to boost development of this valuable technology towards the aim of it becoming an integral part of the energy mix. For this goal, the present work has addressed the engineering issues with regards to operating a retrofitted multi-fuel combustor pilot plant, as well as the development of a rate-based simulation model designed using Aspen Plus®. This model can estimate the gas composition and adiabatic flame temperatures achieved in the oxy-combustion process using coal, biomass, and coal-biomass blends. The fuels used for this study have been Daw Mill coal, El Cerrejon coal and cereal co-product. A parametric study has been performed using the pilot-scale 100$kW_{th}$ oxy-combustor at Cranfield University and varying the percentage of recycle flue gas, the type of recycle flue gas (wet or dry), and the excess oxygen supplied to the burner under oxy-firing conditions. Experimental trials using co-firing with air were carried out as well in order to establish the reference cases. From these tests, experimental data on gas composition (including $SO_3$ measurement), temperatures along the rig, heat flux in the radiative zone, ash deposits characterisation (using ESEM/EDX and XRD techniques), carbon in fly ash, and acid dew point in the recycle path (using an electrochemical noise probe), were obtained. It was clearly shown during the three experimental campaigns carried out, that a critical parameter was that of minimising the air ingress into the process as it was shown to change markedly the chemistry inside the oxy-combustor.

Finally, part of the experimental data collected (related to gas composition and temperatures) has been used to validate the kinetic simulation model developed in Aspen Plus®. For this validation, a parametric study varying the factors that most affect the oxy-combustion process (the above mentioned done for the experiments, plus the amount of air ingress) was done. The model was found to be in a very good agreement with the empirical results regarding the gas composition.

Keywords: Co-firing, $SO_3$, heat flux, ash deposits, Aspen Plus® simulation

*For my mother, Cornelia Pontes Pedrajas, and my brothers, Manuel Antonio and Miguel Angel Jurado Pontes*

Thank you for your moral support over the years and for believing in me even more than myself

# ACKNOWLEDGEMENTS

Firstly I would like to thank my supervisors John Oakey and Hamid Darabkhani for their valuable guidance during the course of this PhD. Also, I would like to show my gratitude to Nigel Simms for his advice in experimental tests and to Giacomo Pellegrini for guiding me with the modelling work.

I would like to thank Ben Anthony for his exceptional support during the second part of this PhD and for taking the time to review my work.

Great acknowledgement to the team of technicians of Building 43A; especially to Martin Roskilly and Howard Smith without whose help this PhD would not have been possible.

A big thanks to all PhD students, past and present, and staff of Building 40, particularly to Philippa, Ali and Andy for their friendship and their patience peer-reviewing my work during these years.

Finally, thanks to my family for all your support despite the distance.

# TABLE OF CONTENTS

# LIST OF FIGURES

# LIST OF TABLES

# LIST OF EQUATIONS

# LIST OF ABBREVIATIONS

| | |
|---|---|
| ADP | Acid dew point |
| A-F | Air-firing |
| ASU | Air separation unit |
| CCM | Controlled condensation method |
| CCP | Cereal co-product |
| CCS | Carbon, capture and storage |
| DA | High-volatile bituminous coal |
| DA-RE | High-volatile bituminous coal and biomass-eucalyptus |
| db | Dry basis |
| DM | Daw Mill coal |
| DTG | Digital thermal gauge |
| EC | El Cerrejon coal |
| EDX | Energy dispersive X-ray spectroscopy |
| EIS | Electrochemical impedance spectroscopy |
| EN | Electrochemical noise |
| EPA | Environmental Protection Agency |
| ESEM | Environmental scanning electron microscope |
| FB | Fluidised bed |
| FGD | Flue gas desulfurisation |
| FGU | Flue gas treatment unit |
| FTIR | Fourier transform infrared spectroscopy |
| HPC | High pressure column |
| ID | Induced draft |
| LPC | Low pressure column |
| O-F | Oxy-firing |
| PC | Pulverised coal-fired power plant |
| PF | Pulverised fuel |
| RC | Recirculation |
| RFG | Recycled flue gas |
| SCR | Selective catalytic reduction |
| TGA | Thermogravimetric analysis |
| TL | Total loss |

| | |
|---|---|
| UC | Unburnt carbon |
| VOCs | Volatile organic compounds |
| wb | Wet basis |
| XRD | X-Ray diffraction |

# NOMENCLATURE LIST

| | | |
|---|---|---|
| A | Pre-exponential factor published data | $\frac{{}^{kg}/_{s \cdot m^2_{fuel\ part}}}{\left(\frac{N}{m^2}\right)^{\sum \alpha_i}}$ |
| A' | Pre-exponential factor in the dimensions required by Aspen Plus® | $\frac{{}^{kgmol}/_{s \cdot m^3_{Reactor}}}{\left(\frac{N}{m^2}\right)^{\sum \alpha_i}}$ |
| ADP | Acid dew point | K |
| $A_g$ | Specific pore-surface area | $m^2/kg$ |
| $A_p$ | Particle surface | $m^2$ |
| $A_{probe}$ | Area of the probe participating in the heat transfer | $m^2$ |
| $A_{r,j}$ | Pre-exponential factor coefficient | $kmol/s \cdot m^3$ |
| $C_{fuel,initial}$ | Percentage of carbon in the fuel initially, prior to oxy-firing | % |
| $C_g$ | Oxygen concentration in bulk gas | $kg/m^3$ |
| $C_j$ | Diffusion constant for the oxidant species | |
| $C_{O2}$ | Oxygen concentration in combustion gas | $kmol/m^3$ |
| $c_{p,\ air}$ | Heat capacity of the air | kJ/kg·K |
| $D_e$ | Effective diffusion coefficient in porous solid | $m^2/s$ |
| $d_p$ | Particle diameter | m |
| $DW_{105}$ | Dry weight of the sample heated at 105ºC for 12-24 hours | g |
| $DW_{550}$ | Weight of the sample after heating at 550ºC for 4 hours | g |
| E | Activation energy in Aspen Plus® | ${}^{kgmol}/_{m^3_{Reactor} \cdot \left(\frac{N}{m^2}\right)}$ |

| | | |
|---|---|---|
| $E_{r,j}$ | Activation energy | J/kmol |
| $F_{char,\ i}$: | Flux of the char particles entering the $i^{th}$ interval | kg/s |
| $F_{solid,\ i}$ | Flux of solids entering the $i^{th}$ interval | $m^3/s$ |
| H | Fraction of hydrogen in the fuel | % wt. |
| h | Heat transfer coefficient | $kW/m^2 \cdot K$ |
| I | Current | A |
| k | Pre-exponential factor coefficient in Aspen Plus® | $\mathrm{kgmol} \cdot \mathrm{K}^{-n_{Aspen}} \Big/ \mathrm{s} \cdot \mathrm{m}^3_{\mathrm{Reactor}} \cdot \left(\frac{\mathrm{N}}{\mathrm{m}^2}\right)^{\sum \alpha_i}$ |
| $k_{cr}$ | Chemical reaction rate constant | m/s |
| $k_{d,j}$ | Diffusion rate constant | $kg/s \cdot m^2 \cdot Pa$ |
| $k_{r,j}$ | Kinetic rate constant | $kg/s \cdot m^2 \cdot Pa$ |
| m | True order of reaction | |
| $m_{cooling\ air}$ | Cooling air mass flowrate | kg/s |
| $\dot{m}_i$ | Flowrate of fuel *i* | kg/h |
| $MW_C$ | Molecular weight of carbon | kg/kmol |
| n | Apparent order of reaction | |
| $n_{Aspen}$ | Temperature exponent in Aspen Plus® | |
| NR | Noise resistance | Ω |
| $P_i$ | Partial pressure species *i* | bar |
| $p_j$ | Partial pressure of the oxidant species in the bulk phase | Pa |
| $Q_{method1}$ | Convective heat flux calculated using method 1 | kW |
| $Q_{method2}$ | Convective heat flux calculated using method 2 | $kW/m^2$ |
| *R* | Ideal gas constant | $J/kmol \cdot K$ |
| R | Resistance | Ω |
| r | Reaction rate in Aspen Plus® | $\mathrm{kgmol} \Big/ \mathrm{s} \cdot \mathrm{m}^3_{\mathrm{Reactor}}$ |
| $r_C$ | Mean coal particle radius | m |

| | | |
|---|---|---|
| $R_i$ | Intrinsic rate coefficient | $kg/m^2 \cdot s \cdot (atm)^n$ |
| $R_{r,j}$ | Heterogeneous reaction rate | kg/s |
| S | Fuel sulfur fraction | % wt. |
| t | Time | s |
| $T_{dewpoint,i}$ | Temperature estimated for acid dew point considering species *i* | K |
| $T_g$ | Gas temperature | K |
| $T_p$ | Particle temperature | K |
| $T_{probe}$ | Local probe temperature | K |
| $T_s$ | Coal particle temperature | K |
| V | Voltage | V |
| VM | Volatile matter in the fuel | % wt. |
| WS | Weight of the air-dried sample | g |
| $X_c$ | Fraction of carbon oxidized | % |
| $X_{c(i)}$ | Fraction of carbon oxidized of fuel *i* | % |
| $X_i$ | Fractional conversion of species *i* | |
| $\alpha_i$ | Concentration exponent of the $i^{th}$ specie in Aspen Plus® | |
| $\gamma$ | Characteristic size of the particle | m |
| $\varepsilon_c$ | Pulverised fuel porosity | $\frac{m^3_{void)\ fuel\ particle}}{m^3_{total(gas+solid)\ fuel}}$ |
| $\varepsilon_{F,R}$ | Voidage in the combustor | $\frac{m^3_{void)stream\ \ gas+fuel}}{m^3_{total\ combustor}}$ |
| $\epsilon_c$ | Char porosity | |
| $\epsilon_i$ | Mean axial voidage in the $i^{th}$ interval of the riser | |
| $\eta$ | Effectiveness factor (Smith, 1982) | |

| | | |
|---|---|---|
| $\eta_{O2}$ | Effectiveness factor (Sotudeh-Gharebaagh et al., 1998) | |
| $\eta_r$ | Effectiveness factor (Vascellari and Cau, 2009) | |
| $\rho$ | Density | $kg/m^3$ |
| $\rho_B$ | Bulk density | $kg/m^3$ |
| $\rho_{c,comb}$ | Actual (observed) rate of combustion of carbon per unit external surface of the particle | $kg/m^2 \cdot s$ |
| $\rho_{c,comb}^{m}$ | Maximum reaction rate | $kg/m^2 \cdot s$ |
| $\rho_{char}$ | Char particles density | $kg/m^3$ |
| $\sigma$ | Particle density | $kg/m^3$ |
| $\chi$ | Ratio $\rho_{c,comb} / \rho_{c,comb}^{m}$ | |

# 1 INTRODUCTION

## 1.1 Background

The rapid increase in emissions of greenhouse gasses has led to new policies being developed to mitigate this problem. Amongst the most important initiatives, are the Kyoto Protocol (1998) and the Intergovernmental Panel on Climate Change (IPCC, 2007).

As a first consequence of new regulations, the use of renewable sources of energy such as hydro power, solar, wind or biomass are being promoted by the governments of developed countries. However, the use of fossil fuel power plants is still necessary to address rising energy demands. Therefore, the second consequence of the new policies is changes to fossil fuel-fired power generation technologies to satisfy the current regulations regarding reduction of greenhouse gas emissions. As a result, several carbon capture and storage (CCS) technologies are being developed.

Oxy-combustion is one option being considered for the capture of $CO_2$ from fossil fuel-fired power generation. The generation of a gas stream with a high percentage of $CO_2$ in the combustor, permitting the use of much more compact flue gas conditioning equipment downstream of the furnace are examples of the advantages that this technology presents over other carbon capture technologies (pre-combustion and post-combustion). However, the main disadvantage of the use of the oxy-fuel combustion technology remains the elevated cost associated with producing high purity $O_2$ by cryogenic distillation. Oxy-combustion can be combined with the use of biomass as a fuel to allow a near-zero emission process to produce electricity.

## 1.2 Scope

This thesis will focus on the engineering issues with respect to running a retrofitted multi-fuel oxy-combustor pilot plant, as well as the development of a rate-based simulation model designed using Aspen Plus® to predict the gas composition and temperatures achieved in the oxy-combustion process using coal, biomass, and blends of these fuels. The research presented here

concentrates on determining operating key parameters and the simulation of the oxy-combustion process co-firing coal and biomass. As relatively little information is available in the literature on this subject, the knowledge base in this area must be expanded if oxy-fuel combustion is to be developed to its full potential.

This work has been carried out at Cranfield University, as part of the OxyCAP project, funded and lead by UK Engineering and Physical Sciences Research Council (EPSRC).

## 1.3 PhD aim

Oxy-combustion with coal and biomass co-firing is a technology that could revolutionise fossil fuel power generation. It can significantly reduce harmful greenhouse gas emissions and permit the continued use of plentiful coal supplies and thereby secure our future energy needs without the severe environmental impacts expected if fossil fuels are used without CCS. The aim of this work is to improve and extend the information available on co-firing oxy-combustion cycles allowing this valuable technology to become an integral part of the future energy mix.

## 1.4 PhD objectives

This work was conducted by means of experimental tests co-firing coal and biomass under oxy-combustion conditions, followed by the development of a kinetic simulation model for an oxy-combustion plant.

A number of key objectives have been defined to address the aim of this research:

1. Asses the differences in operation when performing oxy-combustion of the pulverised solid fuels (coal and biomass) in comparison to the air-firing case. In particular, perform a parametric study with respect to the effect of recycled ratio and fuel variability on gas composition, temperatures, heat flux, burn-out and ash deposition.

2. Study the oxy-combustion process, co-firing blends of coal and biomass, through a rate-based simulation model. The validated model can then be used as a tool to select future test parameters.
3. Evaluate the input parameters for a retrofitted oxy-combustor at pilot scale and establish the intermediate step between bench and demonstration scale plant. Additionally, this objective would allow for the collection of experimental data that can be used to develop further the rate-based simulation model.
4. Evaluate the possible compensation in heat transfer resulting from the higher heat capacity and emissivity of the gases in the oxy-combustion process as compared to the air-firing case. This was done by the use of blends of coal and biomass in the retrofitted pilot plant at Cranfield University.

The list below describes the main tasks necessary for the fulfilment of the aforementioned objectives.

A. Identify the necessary changes in the combustor to convert it into an oxy-combustor and carry out the modifications on: the recycled flue gas (RFG) system, the new layout of the pipelines, the burner's swirler, and the pulverised fuel (coal and biomass) feeding system.
B. Perform tests in the retrofitted oxy-combustor. Analyse the experimental data on: the gaseous emissions, paying special attention to the presence of $CO_2$, $H_2O$ vapour, CO, $SO_x$, $NO_x$, and HCl; the characterisation of ash deposition and its corrosive potential; and the percentage of carbon in the ash.
C. Design a kinetic simulation model to study the oxy-combustion process through the co-firing of coal and biomass blends.
D. Validate the simulation model through comparison with the experimental data produced here.
E. Design and install a system to remove the water vapour and acid species from the flue gas, to produce a dry recycled flue gas. The layout of the system was developed to allow for operation with wet or dry recycled flue gas, depending on the test, to provide for flexibility of the rig.

F. Develop the rate-based simulation model further by including the system for water vapour and acid species removal.
G. Measure $SO_3$ concentrations.
H. Measure radiative and convective heat flux inside the oxy-combustor. Additionally, develop a thermocouple system in the pilot plant able to measure higher temperatures in locations close to the flame.
I. Integrate the oxy-combustor kinetic model with a module dedicated to air separation, and a module for power generation using a steam turbine.

## 1.5 Summary of thesis structure

The outline of this thesis, including a brief description for each chapter, is provided below.

*Chapter 2.* This chapter presents a critical literature review undertaken on the technical aspects related to oxy-combustion, co-firing of coal-biomass blends, formation and characterisation of ash deposits, formation and measurement of $SO_3$, measurement of acid dew point in the recycled flue gas and other aspects required to allow modelling of pulverised fuels combustion under oxy-firing conditions.

*Chapter 3.* This chapter describes the 100$kW_{th}$ pilot-scale down-fired combustor at Cranfield University and the retrofitting process carried out to convert it into an oxy-combustor. Additionally, provides a detailed explanation of the stages completed for the development of the kinetic simulation model, as well as the continuous feedback between experimental and modelling results to select parametric studies done during this PhD work.

*Chapter 4.* This chapter provides experimental data from the operation of the pilot-scale oxy-combustor with regards to gas composition, temperatures reached, heat fluxes generated, analysis of ash deposits and fly ash, $SO_3$ measured and acid dew point evaluation for the three campaigns of experiments completed.

*Chapter 5.* This chapter describes the parametric studies carried out for each stage of the model development, equilibrium and kinetic based, as well as the

results generated, from which the operating parameters that optimize the oxy-combustion process are suggested.

*Chapter 6*. This chapter provides an overall discussion on the experimental and modelling results including a bench mark against the main existing oxy-combustion pilot scale facilities and the diagnosis with regards to the model validation.

*Chapter 7.* This final chapter presents the main conclusions for the experimental and modelling outcomes of this PhD work, as well as the technological implications of this work, and recommendations for future research.

## 1.6 Dissemination from PhD thesis

The list below describes the main contributions regarding work published related to this PhD by attendance as presenter in international conferences.

- Jurado, N., Gohari Darabkhani H., Anthony, E.J., Oakey, J. E., "Experimental and simulation studies of oxy-fuel combustion for carbon capture and sequestration (CCS) from a coal/biomass power plant", 13th International Conference on Clean Energy (ICCE 2014), 8-12 June 2014, Istanbul, Turkey. Oral presentation and proceedings.
- Jurado, N., Gohari Darabkhani H., Anthony, E.J., Oakey, J. E., Oral presentation: "Co-firing Performance of a Retrofitted Oxy-Combustor burning Coal/Biomass Blends: Experimental and Simulation Study", 3rd Oxyfuel Combustion Conference, 9- 13 September 2013, Ponferrada, Spain. Poster also presented: "OxyCAP UK: Oxyfuel Combustion - Academic Programme for the UK", University of Cambridge: S. Balusamy, J. Dennis, S. Hochgreb, S. Scott; Cranfield University: H. Darabkhani, N. Jurado, J. Oakey; University of Edinburgh: H. Chalmers, J. Gibbins, I. Trabadela; Imperial College London: M. Al-Jeboori, F. Cavallo Marincola, P. Fennell, B. Franchetti, A. Kempf, N. McGlashan, S. Navarro-Martinez, F. Wigley; University of Kent: L. Gao, M. Hossain, S. Li, G. Lu, D. Sun, Y. Yan; University of Leeds: S. Black, A. Clements, L.

Ma, W. Nimmo, M. Pourkashanian , A. Pranzitelli, J. Szuhánszki; University of Nottingham: T. Farrow, H. Liu, C. Snape, C-G. Sun.

- Jurado, N., Gohari Darabkhani, H., Anthony, E. J., Oakey, J. E., “Kinetic Simulation of a 100kW$_{th}$ Oxy-Combustor using Aspen Plus”, 12$^{th}$ Carbon Capture, Utilization & Sequestration Conference, May 13-16, 2013, Pittsburgh, Pennsylvania, USA. Oral presentation.
- Jurado, N., Gohari Darabkhani H., Oakey, J. E., “Simulation of Oxy-combustion co-firing Coal and Biomass with ASU and Steam Turbine using Aspen Plus” Sixth International Conference on Clean Coal Technologies (CCT2013), 12-16 May 2013, Thessaloniki, Greece. Oral presentation.
- Gohari Darabkhani, H., Jurado, N., Simms, N., Oakey, J., “Co-firing of Coal/Biomass in a Pilot-scale Oxy-combustor: Experiences and the Experimental Results,” in the proceedings book "Fuelling the future: advances in science and technologies for energy generation, transmission and storage", pp. 34-38, 2012, Brow Walker Press, Boca Raton, Florida, USA.
- Gohari Darabkhani, H., Jurado, N., Simms, N., Oakey, J., “Retrofitting Practice of a 100kW$_{th}$ Coal/Biomass Air-firing Combustor to the Oxy-firing Mode: Experiences and the Experimental Results”, the Energy and Materials Research Conference (EMR2012), 20-22 June 2012, Malaga, Spain.
- Jurado N., Gohari Darabkhani H., and Oakey, J., “Oxy-combustion of Coal/Biomass Mixtures in a 100kW$_{th}$ Combustor”, the 11$^{th}$ Annual Carbon Capture, Utilization and Sequestration Conference, Paper No. 240, April 30 - May 3, 2012. , Pittsburgh, Pennsylvania, USA. Oral presentation.

The paper below has been accepted for poster presentation and will be included in Proceedings of International Conference on Greenhouse Gas Technologies (GHGT) to be held 5-9 October 2014, University of Texas at Austin, Texas, USA:

- Jurado, N., Gohari Darabkhani H., Anthony, E.J., Oakey, J. E., “Oxy-combustion studies into the co –firing of coal and biomass blends: effects on heat transfer, gas and ash compositions”, Poster and proceedings in Energy Procedia.

# 2 LITERATURE REVIEW

## 2.1 Introduction

This chapter critically assesses the existing knowledge available on the technical aspects of oxy-firing of pulverised fuels, and the effect of using a non-fossil fuel, specifically biomass (co-combustion), in the process. It also examines issues related to corrosion problems, such as characterisation of ash deposits, the measurement of $SO_3$ and the determination of the acid dew point, since they have been found to be of high importance under these experimental conditions. Finally, a summary of the main elements of model development carried out to allow the process to be effectively simulated.

## 2.2 Technical aspects on oxy-combustion

### 2.2.1 Percentage of recycled flue gas

In the oxy-combustion process, it is necessary to recycle part of the flue gas to act as an inert and control the temperature inside the combustor, otherwise, the temperatures experienced by boiler internals would be too high for the materials normally used in a pulverised fuel boiler. Consequently, it is necessary to determine the optimal degree of recycle. There are two criteria with regards to this specification: some authors (Wall et al., 2009) suggest that the percentage of recycle must be set so as to reach similar temperatures inside the combustor to the air-firing case, whereas other authors [(Smart et al., 2010b); (Haykiri-Acma et al. 2010); (Payne et al., 1989)] recommend adjusting this parameter to achieve a similar heat flux to the air–firing case. Conventional combustion is usually considered as reference, so the outcomes of this work can be applied to both: existing (i.e. retrofit) and new-built plants.

The fact of recycling the flue gas has several consequences for the combustion process (Smart et al., 2010a):

- Decrease of NO in the flue gas as consequence of NO being reduced or re-burnt

- The $SO_x$ emissions per unit energy of fuel combusted are reduced as the sulfur is retained at higher levels in the ashes and/or deposits. Therefore, the composition of the ashes is different from those generated under the air-firing conditions. The deposits generated may have a more acidic nature (Wall et al., 2009), which is an important factor to be considered with regards to its implication for material's corrosion
- Different heat transfer properties as consequence of the different gas composition inside the combustor (higher presence of $CO_2$ and $H_2O$, and lower presence of $N_2$ in comparison with the air-firing case), which would lead to an increase in the radiative heat transfer
- As an additional consequence of the change in the gas composition there will also be changes in mass flows and velocities of flows due to the different average density of the gas, which would affect the residence time of the fuel particle.

The published literature suggests the following guidelines listed below, with respect to the amount and conditions of the recycle flue gas:

- The percentage of recycled flue gas varies between 60 and 80%; and its temperature should be in the range of 200-350$^0$C (Toftegaard et al., 2010)
- Generally, two currents of recycled flue gas are needed [(Santos, 2008); (Toftegaard et al., 2010); (Strömberg et al., 2009)]:
    - The primary recycle, which is used for conveying the pulverised fuel up to the burner, must be cooled and scrubbed as part of its pre-treatment, to ensure that $SO_2$ is removed from the flue gas to avoid later corrosion in the coal mills, if the recycled flue gas is used for coal drying. After this step, the flue gas must be dried and reheated to 250$^0$C in order to be able to dry the coal. This stage is important to prevent humid coal clogging the coal mills
    - The secondary recycle, that is the equivalent stream to the secondary and tertiary ones in the air-firing case. Usually, it is only treated to filter the particles so to avoid the accumulation of solids in the furnace. However, acid gases ($NO_x$, $SO_x$, HCl, HF)

are not removed from this stream in order to minimise the energy penalty associated with reheating the recycle.

### 2.2.2 Type of recycle flue gas: wet/dry

The reasons for the existence of two different recycles, wet and dry, have been explained above. There are several configurations depending on the type of recycle flue gas, according to Nakayama et al. (1992) and these are illustrated in Figure 1. The main differences between these configurations are:

- The location from where the recycle is taken: before or after the pre-heater (upstream of the cooler for the wet recycle cases, and downstream of the cooler for dry recycle ones)
- Whether the recycle is pre-heated together with the oxygen fed or not

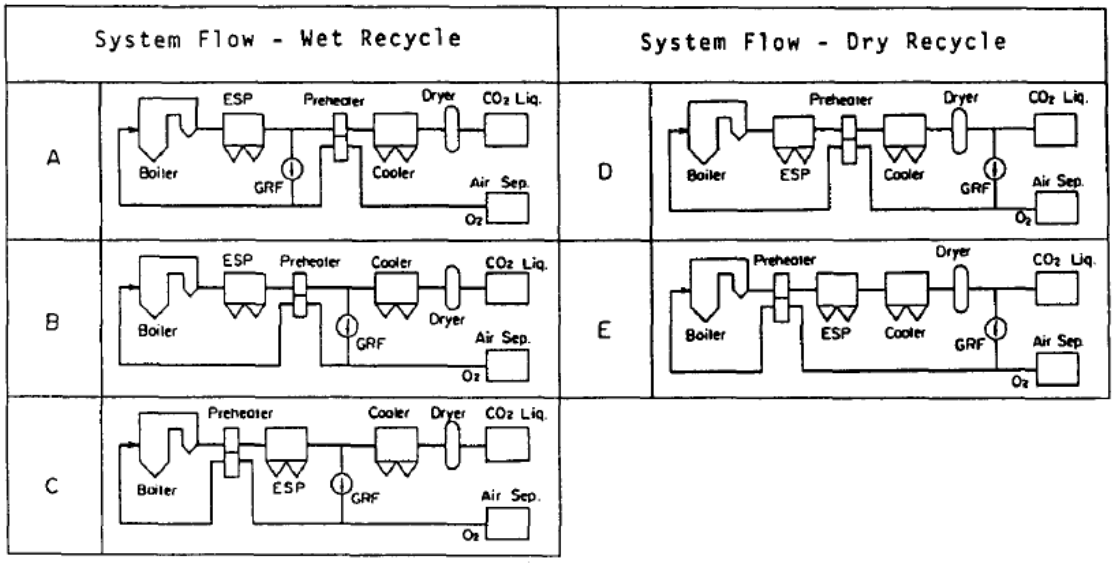


**Figure 1.Possible configurations for oxy-fuel combustion with dry/wet recycle. Image taken from Nakayama et al. (1992)**

However, the cases shown in Figure 1 do not consider configurations combining wet and dry recycle.

In a process using only wet recycle one would expect an increase in the level of acid gases inside the boiler (up to 3-4 times higher than in air-firing case according to Buhre et al. (2005)) and supporting data from this work are presented in Table 1.

**Table 1 Example of the effect of recycle strategy on $SO_2$ concentration in the flue gas, based on 1000 ppmv without recycle. Data taken from Buhre et al. (2005)**

| Fraction of total flue gas recycled | 0.7 | 0.6 | 0.5 | 0.4 | 0.3 | 0.2 | 0.1 | 0 |
|---|---|---|---|---|---|---|---|---|
| Sulfur concentration in flue gas (ppmv) | 3110 | 2370 | 1920 | 1650 | 1390 | 1230 | 1080 | 1000 |

Buhre et al. (2005) also emphasized the fact that corrosion problems are likely to appear in the boiler when coals with medium and high content of S, Cl, and F are used. In addition, much of the $SO_x$ produced will ultimately be retained in the fly ashes, so the use of these ashes for cement or concrete production could be problematic (Toftegaard et al., 2010).

### 2.2.3 Effect of oxygen injection

The injection of the oxygen into an oxy-combustion process can be done at different locations: into the primary recycle (which is the stream that conveys the pulverised fuel to the burner assembly), into the secondary recycle or directly into the burner.

Regarding the position for oxygen injection into the primary recycle, there are different opinions. Several authors [(Dillon et al., 2005), (Zanganeh and Shafeen, 2007)] have objected to this, due to safety reasons, and suggested that the oxygen injection should not occur prior to the primary recycle passing by the mills. This is to avoid the combustion starting before the entrance of this stream to the furnace. However, Dillon et al. (2005) suggest one should consider the larger thermal capacity of $CO_2$ in comparison with $N_2$ (U.S. Environmental Protection Agency, 2000), as a factor that would allow for the concentration of oxygen to be increased above 21% without inducing a risk of explosion. But Dillon et al. (2005) does not support this statement with any experimental data. Flower et al. (2009) have reported experimental data on to this topic suggesting concentrations of $O_2$ in $CO_2$ between 25 and 35% are necessary to achieve similar ignition of coal to that occurred with air.

For oxygen injection into the secondary stream, bearing in mind the safety guidelines, all the oxygen required must be injected either mixed with the secondary recycled stream or directly to the burner [(Toftegaard et al., 2010), (Strömberg et al., 2009)]. The latter option, could be carried out through the burner itself or by using over-fire ports according to Zanganeh and Shafeen, (2007). Table 2 summarizes the main advantages and drawbacks for each type of oxygen injection.

**Table 2 Advantages and disadvantages of each alternative to inject oxygen in oxy-firing combustion. Taken from Toftegaard et al. (2010)**

| Option | Advantage(s) | Disadvantage(s) |
|---|---|---|
| Before coal mills | (1) Sufficient space in recirculation duct to ensure adequate mixing<br>(2) The stream to the mills will be drier than without oxygen<br>(3) With oxygen in primary stream burner design is expected to be closer to that for conventional air burners | (1) Risk of zones with very high-oxygen concentrations if mixing is inadequate, with increased risk of combustion/explosions in mills<br>(2) Primary stream will be cooled due to the low temperature of the oxygen |
| After mills, before burners | (1) No risk of explosion in mills<br>(2) Possible to obtain the same oxygen concentration in the burner as is the case for operation on air | (1) Significant risks are associated with the injection of nearly pure oxygen into a high temperature stream of coal and flue gas |
| Directly in burners (either pure oxygen lance or with the secondary stream) | (1) No risk of explosion in mills or flue gas ducts<br>(2) No expenses for mixing in primary stream<br>(3) Oxygen lance provides increased control of the mixing of oxygen and fuel in the near-burner zone | (1) Burner has to be re-designed<br>(2) Limited capacity for coal drying in mills |

### 2.2.4 Heat flux characterisation

There are several factors, inherent to the oxy-combustion process, which contribute to the heat transfer generated under these conditions being different from that of the air-firing case. The main causes are: the different composition of the environment inside the furnace, and the effect of the recycle on the flame.

In this section, the most suitable techniques found in the relevant literature to measure the heat transfer under oxy-combustion conditions are described, as well as discussing the main outcomes from investigations published on this topic.

With regards to the techniques to measure heat flux, Smart et al., (2010c) suggested two different methods: one for radiative and one for convective heat transfer measurement. The first method consists of the use of a MEDTHERM digital radiation heat flux meter. This sensor is located in ports along the radiant section of the furnace wall in the same axis of the burner centreline. For the convective heat flux measurement, an in-house air-cooled probe was developed by these authors. The air flow was controlled to set a surface temperature of the probe of 570K. Two methods were used to calculate the convective heat flux. This allowed a comparison between the results, and agreement within 5% was obtained. The first method, suggested by Smart et al., (2010c), used the flue gas mass flowrate ($m_{flue\ gas}$), and the measured flue gas temperature local to the probe ($T_{probe}$), to calculate the heat transfer coefficient (h). As one knows the probe area participating in the heat transfer ($A_{probe}$) exposed to the flue gas, the convective heat flux ($Q_{method1}$) per area unit, can be calculated by Equation 1:

$$Q_{method1} = h \cdot A_{probe} \cdot \left(T_{gas} - T_{probe}\right) \qquad \textbf{Equation 1}$$

[Note: for the convective heat flux ($Q_{method1}$) to be in the units that Smart et al., (2010c) suggest kW/m$^2$, the factor $A_{probe}$ should not be included in Equation 1. This equation has been taken from their paper]

The second method is based on the cooling air mass flowrate ($m_{cooling\ air}$), the inlet ($T_{air,in}$) and outlet air temperature ($T_{air,out}$), the heat capacity of the air ($c_{p,air}$),

and the exposed probe area ($A_{probe}$). Equation 2 shows the way by which the convective heat flux ($Q_{method2}$) is calculated.

$$Q_{method2} = {m_{cooling\ air} \cdot C_{P.air} \cdot \left(T_{air,out} - T_{air,in}\right)}\Big/{A_{probe}} \qquad \textbf{Equation 2}$$

Considering the main outcomes from previous studies, it is evident that the different chemical composition (higher presence of $CO_2$ and $H_2O$, and lower presence of $N_2$) inside the oxy-combustor, ensures that this gas has different characteristics: thus there is an increase in the emissivity which will have a direct effect on the heat transfer [(Andersson et al., 2008); (Park et al., 2013)]. On the other hand, Andersson et al. (2008) highlighted in their work the importance of the large contribution to the radiation from the particles present in the flame because they emit over a continuous spectrum. Furthermore, these authors note, as one of the main conclusions of their studies, that when using pulverised fuels, the larger effect of the particles on the radiation ensures that the difference in specific emissivity that occurs, for the change in the environment from air to oxy-firing conditions, does not provide the decisive effect on the process. Andersson et al. (2008) provided an in-depth analysis of the heat fluxes, and specified that the increase in the total emissivity changing from air to oxy-firing when using dry recycle is only around 5%, whereas when using wet recycle it is more than 20%. In consequence, the moisture content in the flue gas is much more important than the $CO_2$ content with respect to gas radiation.

In the case of the recycle rate, Andersson et al. (2008) proposed adjusting this parameter as a way of controlling the temperature inside the oxy-combustor and therefore as a means to regulate the distribution of heat. Studies on this subject have also been conducted by Smart et al., (2010b), who concluded that the radiation flux peak decreases and slightly moves downstream in the furnace when the percentage of recycled flue gas increases. The decrease in this peak is mainly due to the higher mass flow that exists when the percentage of recycled flue gas is increased, which causes a reduction in the flame temperature. The shift of the peak is also related to the higher mass flow, which

has a direct effect on the level of oxygen enrichment, which is lower. As a consequence, the flame generated is longer and “lazier”, having the maximum for the radiative heat flux delayed, in comparison to the cases with lower recycle. According to these authors, similar radiative heat flux to air-firing case can be achieved, when the recycle ratio is set to 72% with 3% oxygen at the furnace exit. Conversely to the situation with the radiative heat transfer, there is an increase in the peak of convection flux when the percentage of recycle flue gas increases. This is a consequence of the higher mass flow and temperature of the flue gas in the convective zone.

## 2.3 Technical aspects on co-combustion of coal and biomass

The use of biomass to generate power, by itself or by when blended with coal, strongly influences the combustion process, due to its different elemental and mineral composition. A crucial aspect related to the use of biomass, as fuel, is its variability, especially with respect to its volatile fraction, particle size and nitrogen content (Holtmeyer et al., 2012). The volatile fraction of a fuel is an aspect of this process that has direct effects on its ignition temperature. Generally, biomass has higher volatile content than coal, which makes it easier to use for start-up, as it has a lower ignition temperature. The nitrogen content of the biomass is an important characteristic to look at because it can affect the NO emissions.

The co-combustion of biomass and coal has been suggested as an alternative method to varying of the recycle flue gas to control heat transfer under oxy-firing conditions (Haykiri-Acma et al., 2010). These authors concluded this as consequence of having observed that similar conversion values of the fuel are reached at lower temperatures when co-firing coal-biomass blends, using between 5 and 20% share of biomass, compared to the oxy-coal case.

### 2.3.1 Heat flux and ignition temperatures during co-combustion under oxy-firing conditions

#### Heat flux

Results from experiments where co-firing coal and biomass under conventional and oxy-combustion conditions have been reported by Smart et al., (2010c). These workers have shown that there is an inverse relation between the peak radiative heat flux and the recycle ratio. By contrast, there is an increase in the peak of convection flux when the percentage of recycle flue gas increases. These authors pointed out that similar peak radiative and convective heat fluxes to the air-firing case can be obtained under oxy-firing conditions using coal or coal-biomass blends. However, they do not occur at the same percentage of recycled flue gas, as they are fuel dependent.

#### Ignition temperature

Delay in ignition of the fuel under oxy-combustion conditions is a topic of great interest, as demonstrated by the fact that many authors have extensively researched it. However, there is no general agreement on this issue. On one hand, the works of Toftegaard et al. (2010), and Arias et al. (2008), suggest that the delay of the ignition occurs only when firing coal, but not when the process involves co-firing coal and biomass. This fact is explained as a consequence of the greater ease of achieving ignition of coal-biomass blends, as demonstrated by the studies of these authors, where lower ignition temperatures are observed. On the other hand, Yuzbasi and Selçuk (2011) claim that the delay in ignition always occurs during co-combustion of coal-biomass comparing air to oxy-firing at the same level of oxygen (these workers carried out tests by replacing $N_2$ with $CO_2$). However, as the content of oxygen increases, these authors effectively agree with Toftegaard et al. (2010), and Arias et al. (2008), by concluding that lower ignition temperatures occur. The reasons for these different conclusions may be due to several factors. One of them could be the type of coal burned, which is very different in the case of Arias et al. (2008), where high rank coals are used, compared to the work of Yuzbasi and Selçuk (2011), where low rank coal is burnt. Another possible cause could be due to

the different oxygen levels used for each of these studies. An additional issue to consider is that while Arias et al. (2008) provide a very precise definition of the ignition temperature (Faúndez et al. 2005), Yuzbasi and Selçuk (2011) give a very simple definition “the ignition temperature is defined as the temperature at which coal starts burning”. In consequence, it is probably more reasonable to follow conclusions of Arias et al. (2008).

The oxygen content in the oxy-combustion cycle has a greater effect on ignition temperature than changing the composition of the fuel (coal or coal-biomass blends) [(Arias et al., 2008), (Toftegaard et al., 2010)]. This statement is supported by the data included in Figure 2, provided by Arias et al. (2008), shown below.

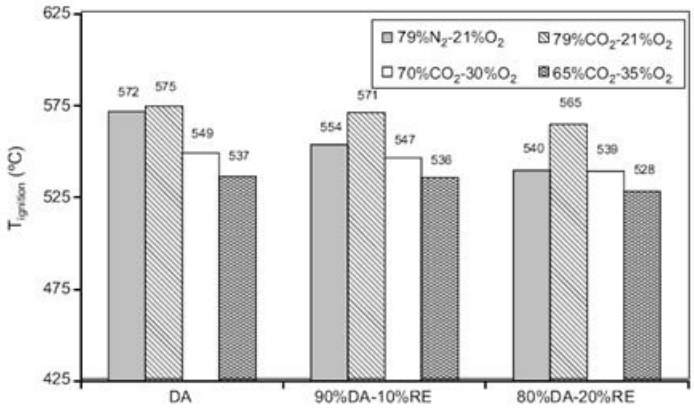


**Figure 2 Ignition temperatures of high-volatile bituminous coal (DA) and blends with biomass (DA-RE). Taken from Arias et al. (2008)**

The trend observed for the ignition temperature is to decrease as the concentration of oxygen in the oxidizer increases (Toftegaard et al., 2010). The reason for this, is explained by Arias et al. (2008) is due to increase in the reaction rate, associated with the higher presence of oxygen, that increase the rate of heat release, making the temperature required to ignite the fuel lower. Interestingly, the relative effect of changing the concentration of oxygen in the oxidizer was found to be almost independent of the type of fuel, according to these authors. On the other hand, using air as oxidizer, there are noticeable differences regarding the type of fuel used. Ignition temperature tends to decrease when the amount of biomass is higher in the fuel. This fact is a direct

consequence of the high reactivity and volatiles content of the biomass, which makes easier to start the combustion with this fuel rather than with coal [(Arias et al., 2008), (Toftegaard et al., 2010)].

However, it is important to note that the decrease in ignition temperature is smaller when coal-biomass blends are burnt than in the case of coal. This point can be explained as a consequence of two effects: firstly, the coal has a higher heating value than the biomass; secondly, the rich $CO_2$ atmosphere needs a higher amount of heat to increase its temperature, (Arias et al., 2008). An additional conclusion is that more heat, and consequently, a higher ignition temperature, are needed in the case of oxy-combustion than in conventional combustion, the other factors remaining the same according to Toftegaard et al. (2010). The increase in the ignition temperature when nitrogen is replaced by $CO_2$ is a consequence of the higher specific heat of $CO_2$ in comparison to $N_2$. Thus, more heat is needed to increase the temperature in $CO_2$ rich atmospheres, and therefore, a delay in ignition occurs in these cases (Arias et al., 2008).

According to the experiments carried out by Yuzbasi and Selçuk (2011), in which low rank coal (lignite) and biomass (olive residue) are co-fired, together with, for some of the tests, replacement of $N_2$ by $CO_2$, there is a slight delay in the ignition; this fact has been observed to be more important in the case of olive residue. For the pyrolysis experiments performed, there is no interaction between coal and biomass both in $N_2$ rich and in $CO_2$ rich atmospheres, and therefore, no deviation from theoretical curves occurs. In combustion experiments carried out by these authors, as long as oxygen concentration increases the trends found are:

- DTG (Digital Thermal Gauge) profiles move to lower temperatures, although a delay in ignition is observed for all the oxy-firing combustion tests
- A complete combustion of the fuel is achieved at lower temperatures
- There is an increase in the rate of weight loss.

In the experiments done for the study accomplished by Yuzbasi and Selçuk (2011), there are deviations from the theoretical predictions for co-combustion of coal and biomass. These deviations are suggested to be consequence of synergistic interactions between the parent fuels.

### 2.3.2 Burnout

Earlier research (Murphy and Shaddix, 2006) has indicated that char combustion rate, using coal as fuel, increases in oxygen rich environments in comparison with air-firing conditions. However, this work was carried out using $N_2$ as inert gas instead of $CO_2$. In consequence, it is necessary to consider others authors' studies to obtain conclusions more directly related to the oxy-combustion of coal and biomass blends, as is the case in the investigations carried out by Arias et al. (2008).

According to the burnout tests performed by Arias et al. (2008), the percentage of burnout rises with increasing oxygen concentration in the oxidant stream (higher burnout levels than in air-firing case when using oxygen concentrations between 30 and 35%(v/v)). However, the degree of burnout is higher in conventional combustion than in oxy-combustion when the percentage of oxygen is set to 21% (v/v) under oxy-firing conditions. On the other hand, although an improvement in the degree of burnout could be expected for coal-biomass blends due to the higher volatile content of the biomass, the increase of burnout is almost negligible in the work of Arias et al. (2008), as it can be seen in Figure 3. The explanation provided for this fact is related to the changes occurred in the reactor regarding oxygen and temperatures profiles due to the feeding of a more reactive fuel, such as the biomass.

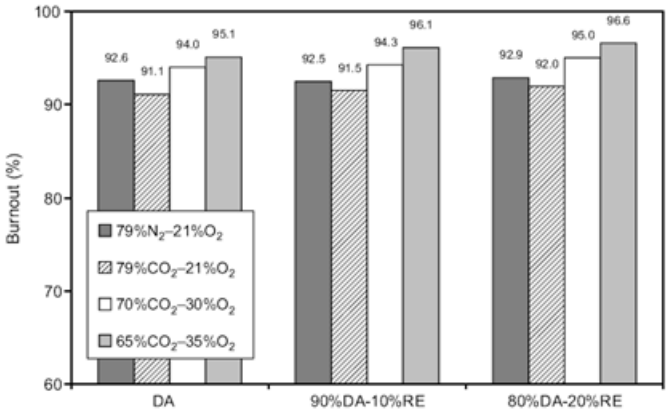


**Figure 3 Burnouts of DA–RE blends at a fuel ratio of 0.8. Taken from Arias et al. (2008)**

Similar conclusions can be obtained from the experiments to study the carbon in ash performed by Smart et al., (2010c). The improvement in the percentage of burnout is a consequence of two effects. Firstly, the fact of burning coal-biomass blends, where the higher volatile content and reactivity of the biomass influence the percentage of carbon in ash, causing burnout to decrease. Secondly, the improvement in the burnout due to firing the fuel under oxy-combustion conditions, where there is a high level of oxygen, causes an increase of the char oxidation rate. These authors pointed out that the calculations to set up a certain content of oxygen (3%v/v) at the exit of the combustor were made by considering the oxygen present in the fuel. In consequence, at the beginning of the combustion process the coal "sees" less oxygen than the biomass. This makes the analysis and modelling of burnout data in this case (oxy-firing of coal and biomass) extremely complex according to Smart et al., (2010c).

Borrego et al. (2009) carried out a study using only biomass as fuel, under air and oxy-firing conditions. Their experiments showed that the atmosphere has a strong influence on the development of porosity in the chars produced. However, the type of biomass used was identified as a factor contributing to this porosity development, in some cases this resulted in enlarging, or in others cases making the pore volume smaller in the chars generated. Nevertheless,

overall results showed that similar characteristics were found in terms of morphology, specific surface area, optical texture and reactivity of the chars.

**Characterisation of carbon in ash**

Traditionally, the loss on ignition (LOI) method has been used to measure the remaining unburnt carbon in fly ash [(Santisteban et al., 2004), (Vassilev and Vassileva, 2005)]. For this method, a relation between the LOI at 550°C and organic carbon, as well as, between LOI at 950°C and inorganic carbon are taken as basis of the characterisation. Considering that organic carbon in the ash is approximately half of the LOI at 550°C (empirically calculated (Santisteban et al., 2004)), Equation 3 and Equation 4 would allow for the calculation of unburnt carbon in ash:

$$Burnout(\%) = 100 \cdot \left( C_{fuel,initial}(\%) - \left( {}^{LOI_{550}(\%)}/_{2} \right) \Big/ C_{fuel,initial}\,(\%) \right) \qquad \textbf{Equation 3}$$

$$LOI_{550}(\%) = 100 \cdot {}^{(DW_{105} - DW_{550})}/_{WS} \qquad \textbf{Equation 4}$$

Where $C_{fuel,initial}$ is percentage of carbon in the fuel initially (prior to oxy-firing), $DW_{105}$ is dry weight of the sample heated at 105ºC for 12-24 hours, $DW_{550}$ is weight of the sample after heating at 550ºC for 4 hours, WS is weight of the air-dried sample.

However, Fan and Brown (2001) and Zhao et al. (2013) have demonstrated that the LOI method overestimates the unburnt carbon for those cases from their work studying coal and biomass ash, respectively, for cases where there are significant contents of volatile organic compounds (VOCs). In the study carried out by Fan and Brown (2001), where coal was used, the authors claimed that the degree of overestimation was around 20%. Zhao et al. (2013) studied the characteristics of ash generated from burning biomass, stating that the positive bias given by $LOI_{550}$ is due to the effect of both: release of VOCs in the ash, and also, because at the ashing temperature, a small amount of carbonates may decompose, contributing to the weight loss. The presence of carbonates in the

fly ash generated under oxy-firing conditions has been identified by Wigley (2010) to be a consequence of the reduced decomposition of the carbonates, present as minerals in the original fuel, at high partial pressures of $CO_2$.The method to measure the carbon in ash that Zhao et al. (2013) suggested is by thermogravimetric analysis (TGA), where in the first stage, the sample is heated in an inert atmosphere ($N_2$), liberating the volatile matter. Then, the ash is exposed to an oxidizing atmosphere, to cause the unburnt char carbon to react. The weight of the sample is recorded during the entire TGA experiment, producing a curve similar to the one shown in Figure 4, where UC denotes unburnt carbon, and TL denotes total loss.

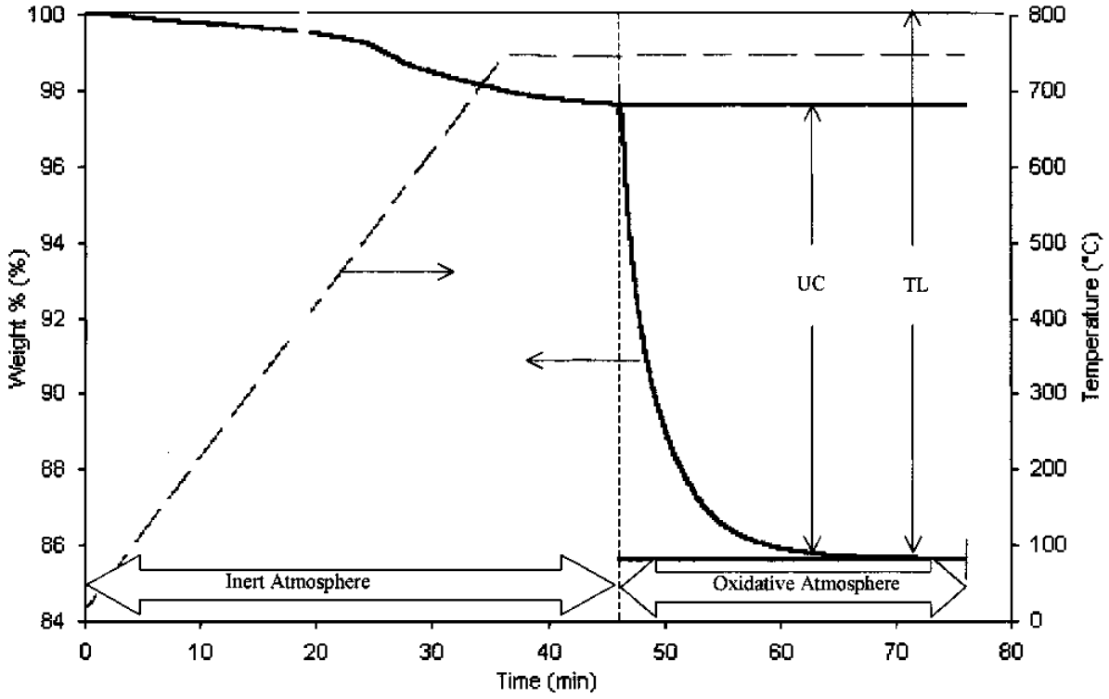


**Figure 4 TGA weight loss curve of a typical fly ash sample. Image taken from Fan and Brown (2001)**

## 2.4 Ash deposits: formation and characteristics under oxy-firing conditions

One important characteristic of the ash generated under oxy-combustion conditions as has been previously mentioned (see p. 12): is that it is likely that corrosion problems will appear in the boiler when coals with medium and high content of S, Cl, and F are used, because of the flue gas recycle. This leads to

the accumulation of certain undesirable species inside the combustor. This combined with a greater sulfur oxides retention in fly ash when burning blends of coal and biomass due to higher alkali content in biomass [(Toftegaard et al., 2010), (Khodier and Simms, 2010), (Bartolomé et al., 2010), (Chamberlain et al., 2013)] can be expected to produce the same type of result as reported by Syed et al. (2012). In their paper, it was concluded that more corrosion damage occurs under oxy-firing conditions of coal and biomass blends in comparison to air-firing combustion.

The propensity to form ash deposits, as well as slagging and fouling issues related to the use of biomass in thermal applications have been addressed by several authors such as (Khodier and Simms, 2010), or Bartolomé et al. (2010). The latter pointed out the influence of $Na_2SO_4$ in the formation of an adhesive layer on the deposits. However, Chen et al. (2012) noted in their paper that there is a lack of literature on the behaviour of ash, mechanisms of slag layer formation and its interaction with char particles, under oxy-combustion conditions. In consequence, it is clear that more research is needed in this field.

## 2.5 $SO_3$ formation and measurement

The higher presence of acid species in the flue gas generated in oxy-combustion has been already mentioned above. Special attention must be paid to the generation of $SO_3$ inside the combustor and the evolution of this species downstream of the furnace, as it has been noted by many authors [(Maddalone et al., 1979), (Ahn et al., 2011), (Eddings et al., 2011), (Spörl et al., 2013)], given the scarcity of experimental data regarding $SO_3$ measurements under oxy-combustion conditions.

The difficulty associated with the measurement of $SO_3$ during operation of a combustor has been identified by some authors as a major issue [(Nielsen, 2003), (Fleig et al., 2012)]. The reasons for this are as follows:

- High reactive nature of the $SO_3$ (leading to high probability of negative bias as consequence of the loss of $SO_3$ due to reaction with $H_2O$ to

generate $H_2SO_4$, by surface reactions in the sampling line, or reactions with the filter cake with the particles)

- The normal low $SO_3$ concentrations in the flue gas, comparatively to $SO_2$, as $SO_3$ is usually around 2% of the sulfur present in the system
- High $SO_2$ concentrations causing interferences, because it can lead to positive bias during the analysis of the sample.

The most commonly used technique for $SO_3$ measurement is the controlled condensation method. This is based on cooling the sampled flue gas down to the dew point of sulfuric acid but above the water dew point, so that the $SO_3$ is collected as an aerosol which condenses on the coil walls or on the back-up glass frit in the collection cell (Maddalone et al., 1979). Later on, the $SO_3$ condensed in the coil, as mist, is measured (using titration or ion chromatography), and together with the measured total volume of flue gas sampled, the concentration of $SO_3$ in the flue gas can be calculated. The main disadvantage of this method is its inability to achieve real-time measurements during the process. Despite this drawback, this technique is the one suggested as standard (EPA Method 8A (NCASI Southern Regional Center, 1996) and ASTM 3226-73T) due to its accuracy. The configuration suggested by EPA Method 8A is illustrated in Figure 5.

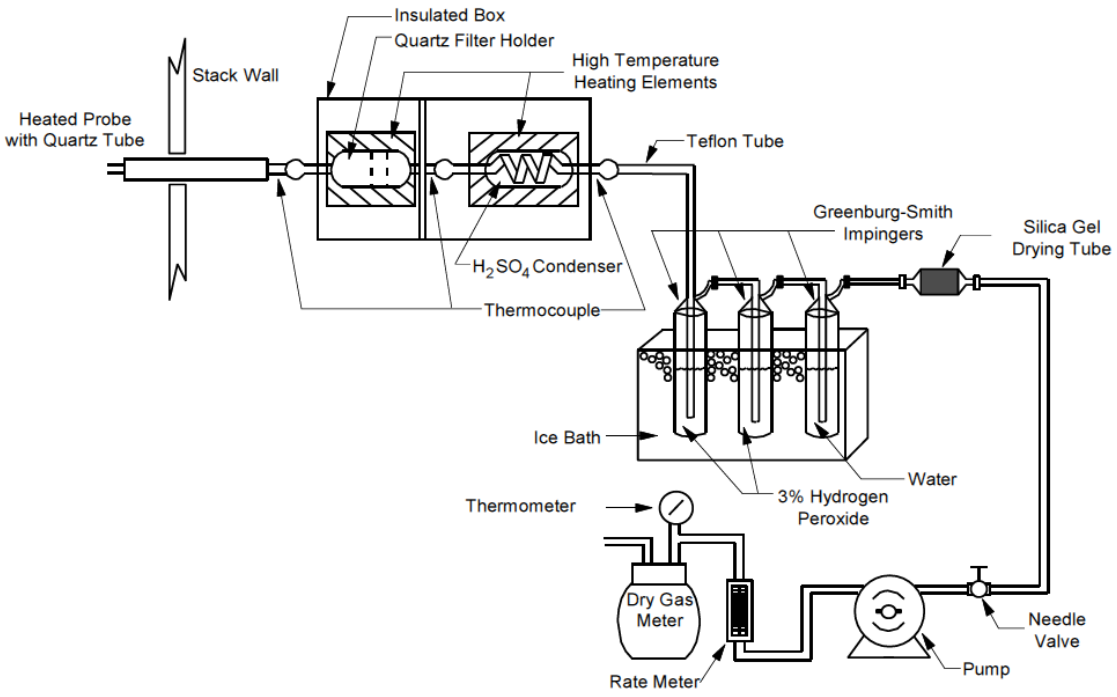


**Figure 5 $SO_x$ sampling train (EPA Method 8A). Image taken from NCASI Southern Regional Center (1996)**

The Method 8A was developed to avoid two important interferences occuring during the $SO_3$ evaluation as consequence of using the Method 8 in kraft recovery furnaces. These interferences are caused by the sulfates present in the fly ash, as these would be collected in the quartz filter, which is not considered in the $SO_3$ estimation; and by the $SO_2$ (for which the controlled condensation technique is applied, based on different condensation temperatures of $SO_2$ in comparison to $SO_3$). It is noteworthy to highlight the increasing importance of the sulfate generation and hence, its potential to cause a bias in the $SO_3$ measurement, when the fuel considered is biomass. This is due to the higher levels of alkalis, K in paticular,which is highly likely to react with $SO_3$ to form sulfates by nucleation when flue gases are cooled down to around 1150K, as Jiménez and Ballester (2005) suggested in their work. These authors found that when burning pure biomass or co-fring it with coke, $K_2SO_4$ appeared to be the only major compound in the submicron particles. In the experiments of Jiménez and Ballester (2005) the biomass was doped with S for the K to react with it instead of with the Cl also present in the biomass; because

KCl presents more corrosive problems than $K_2SO_4$. As a consequence, no K would be available to react with Cl, and this would be emitted as HCl in the flue gas or as $Cl_2$ at temperatures below 300K.

Nielsen (2003) suggested that this method typically had a reproducibility of 10% or less, as a consequence of its complexity. In his work two issues were highlighted as important so not to underestimate the $SO_3$ levels in the gas sampled: the ash filtration step (because $SO_3$ can be captured due to reactions with the filter cake), and $SO_3$ condensation (before the coil). Nielsen used a modification of the ASTM D-3226-73T for his experiment.

The main alternatives to the controlled condensation method are:

- Fourier transform infrared (FTIR) spectroscopy, used by Chamberlain et al. (2013). This method allows for the continuous measurement of $SO_3$ and has the ability of analysing in situ and providing real-time data. The main drawback of this approach according to Fleig et al. (2012) is the likelihood of losing part of the $SO_3$ present during the sampling process. These authors established that the results using this technique compared to the controlled condensation method are around 20% lower. Also, there is a complication implicit with the use of FTIR in relation to the issue of generating the reference spectra for the gases that are going to be measured ($SO_3$ and $H_2O$), due to their relatively weak absorption ranges, making difficult to avoid interferences with other species present (e.g. $H_2S$)
- Salt method, used by Vainio et al. (2013). For this option, a salt is used to capture the $SO_3$ and or $H_2SO_4$ present in the flue gas sampled. Then, the salt is dissolved in water and the content of sulfate ions analysed. The $SO_3$ content can be also measured indirectly by using a FTIR to analyse the HCl, which is generated from the reaction involving the $SO_3/H_2SO_4$ and the salt packed in the tube. This modification allows for a continuous and in-situ analysis. However, when using this technique with solid fuels that contain chlorine, there is problem since the HCl is produced both from the reaction with sulfur compounds and the

combustion product, which leads to a positive bias in the measurement of $SO_3$.

After having enumerated the main advantages and drawbacks for each method, it appears that the best technique to measure the content of $SO_3$ in the flue gas is the spiral tube condensation method [(Stanger and Wall, 2011), (Ahn et al., 2011), (Nielsen, 2003)].

### 2.5.1 Effect of temperature

The effect of the combustion temperature on $SO_x$ has been researched by Ahn et al. (2011): who studied how the equilibrium favours $SO_2$ formation at high temperatures (>1273K) and $SO_3$ formation at lower temperatures; bearing in mind that in all the cases, the amount of $SO_3$ is much less than the amount expected if it were in equilibrium with actual $SO_2$ levels. The conclusions of this study are very useful in selecting the optimum window temperature in which to sample the flue gas and this appears to be ~755K. The equilibrium $SO_3$ concentration reaches a maximum around 600K. However, according to Fleig et al. (2013) and Chamberlain et al. (2013), $SO_3$ is typically kinetically controlled and, as a consequence, the concentrations will depend on the location and residence time. If the gas is sampled at too high temperature, it is very likely that the maximum $SO_3$ formation will not have taken place. On the other hand, if the temperature is too low, part of the $SO_3$ may have condensed out prior to sampling. An additional finding of Ahn et al. (2011) was that, at the optimum sampling temperature, the $SO_3$ concentration was almost four times higher in oxy-combustion than in conventional combustion.

### 2.5.2 Effect of fuel

Most of the studies carried out to analyse the content of $SO_3$ in the flue gas, using air or oxy-firing conditions, have used coal as the fuel [(Maddalone et al., 1979), (Nielsen, 2003), (Ahn et al., 2010), (Eddings et al., 2011), (Spörl et al., 2013)], or propane plus $SO_2$ injected in the oxidizer [(Fleig et al., 2012), (Vainio et al., 2013)]. However, there is only one study published where $SO_3$ has been

measured during co-firing of coal and biomass in an oxy-combustion environment (Tan et al., 2013).

The main findings reported, in relation to $SO_3$ measurements, for the studies using coal under oxy-firing conditions are:

- Measurements taken at around 800K showed that $SO_3$ levels during oxy-firing experiments are four to six times higher than in the air-firing case using a high sulfur bituminous coal. However, in tests when using a low sulfur-content coal, the results in terms of $SO_3$ formation were similar for both: air and oxy-combustion (Ahn et al., 2011)
- Measurements taken at high temperatures, around 1200K, did not indicate any difference between air and oxy-firing cases (Ahn et al., 2011)
- Considering normalized emissions, mass of $SO_3$ per unit energy input, in the case of PC-fired tests, levels measured during air–firing tests were higher than for oxy-firing; whilst for experiments carried out in circulating fluidized bed reactor, both (air and oxy-fired) normalized emissions were comparable (Ahn et al., 2011)
- The $SO_3$ content is less than 2% of the total sulfur compounds in all cases (under air and oxy-firing conditions) (Chamberlain et al., 2013)
- Investigations on sulfur oxide emissions ($SO_2$ and $SO_3$) carried out by Spörl et al. (2013), have shown that the oxygen excess in oxy-firing tests has an important effect on the generation of $SO_x$; as opposed to conventional combustion, where this effect is negligible. In consequence, these authors suggested this operational condition as a key parameter to control the $SO_x$ emissions under oxy-firing conditions.

On the other hand, the main conclusion from Tan et al. (2013) with regards to co-combustion under oxy-firing conditions was that no significant relation could be found between the $SO_3$ levels and the share of biomass in the fuel, suggesting as probable cause for this, the very low measurements obtained for $SO_3$ levels. The low concentrations reported (0.15 - 2.76 ppm) were for all cases: using coal and coal-biomass blends. Allowing for the sampling

conditions described in their paper, it could be expected that these low concentrations are a consequence of the location where the flue gas was sampled, which was downstream of the bag filter, where the temperature was around 370K; so, it is likely, following Ahn et al. (2011) suggestions (see p. 28), that part of the $SO_3$ had condensed prior to the sampling point.

## 2.6 Acid dew point: prediction and measurement

The acid dew point of the flue gas generated under oxy-combustion conditions is expected to be higher from the air-firing case as consequence of the higher content of $SO_x$ and other acid species (HCl and $NO_2$). Interestingly, Stanger and Wall (2011) suggested a quantitative difference, between 14 and 21.6K, for the oxy-fuel acid dew points in comparison with those for conventional combustion. These authors used the ZareNezhad correlation (ZareNezhad, 2009) to predict the acid dew point of the flue gas generated from oxy-firing pulverised coal. This correlation, see Eq 5 below, is a combination of two methods: the Okkes (Okkes, 1987), and Verhoff/Banchero (Verhoff and Banchero, 1974) correlations.

$$T_{dewpoint} = 150 + 11.664 \cdot ln(750 \cdot P_{SO3}) + 8.1328 \cdot ln(750 \cdot P_{H2O}) - 3.83226 \cdot 10^{-1} \cdot ln(750 \cdot P_{SO3}) \cdot ln(750 \cdot P_{H2O}) \quad \textbf{Eq 5}$$

Figure 6 presents the predicted acid dew points resulted from using several methods [(ZareNezhad, 2009), (Okkes, 1987), (Verhoff and Banchero, 1974)] as a function of the sulfur content in the fuel. This figure clearly shows the difference in value for acid dew points under air and oxy- firing conditions.

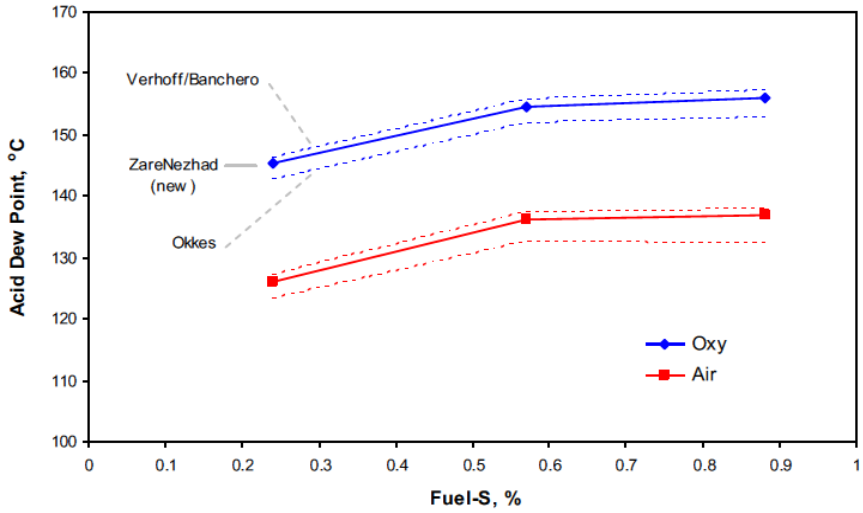


**Figure 6 Comparison of acid dew point correlations (based on the thermodynamic $SO_3$ conversion at 1270K). Image taken from Stanger and Wall (2011)**

The acid dew point estimation can be calculated considering all the acid species, as Huijbregts and Leferink (2004) noted in their paper, using a different correlation for each species ($SO_3$, $SO_2$, HCl, and $NO_2$). The equations adopted by these authors are listed in Table 3.

**Table 3 Correlations for acid dew point estimation**

| | | |
|---|---|---|
| Verhoff and Banchero, (1974) | $T_{dewpoint,SO3} = \frac{1}{(2.276\cdot10^{-3}-2.943\cdot10^{-5}\cdot ln(750\cdot P_{H2O})-8.58\cdot10^{-5}\cdot ln(750\cdot P_{SO3})+6.2\cdot10^{-6}\cdot ln(750\cdot P_{SO3})\cdot ln(750\cdot P_{H2O}))}$ | **Eq 6** |
| Kiang (1981) | $T_{dewpoint,SO2} = \frac{10^3}{(3.9526-1.863\cdot10^{-1}\cdot ln(750\cdot P_{H2O})+8.67\cdot10^{-4}\cdot ln(750\cdot P_{SO2})+9.1\cdot10^{-4}\cdot ln(750\cdot P_{H2O})\cdot ln(750\cdot P_{SO2}))}$ | **Eq 7** |
| Kiang (1981) | $T_{dewpoint,HCl} = \frac{10^3}{(3.7368-1.591\cdot10^{-1}\cdot ln(750\cdot P_{H2O})-3.26\cdot10^{-2}\cdot ln(750\cdot P_{HCl})+2.69\cdot10^{-3}\cdot ln(750\cdot P_{H2O})\cdot ln(750\cdot P_{HCl}))}$ | **Eq 8** |
| Perry and Chilton, (1973) | $T_{dewpoint,NO2} = \frac{10^3}{(3.664-1.446\cdot10^{-1}\cdot ln(750\cdot P_{H2O})-8.27\cdot10^{-2}\cdot ln(750\cdot P_{NO2})+7.56\cdot10^{-3}\cdot ln(750\cdot P_{H2O})\cdot ln(750\cdot P_{NO2}))}$ | **Eq 9** |

For [Eq 5-Eq 9], partial pressures are given in bar and temperatures in K.

### Measurement of acid dew point

For the measurement of acid dew point, the techniques suggested in the literature are the same as that used to measure corrosion rates, as these two

phenomena are intrinsically related. The alternatives for in situ measurements are: electrochemical impedance spectroscopy (EIS) and electrochemical noise (EN) [(Yang et al., 2013), (Mills and Mabbutt, 2000)]. Both methods are based on the use of two (or more) electrodes plus one additional for reference. When the environmental conditions change, due to the acid dew temperature has been reached, the acid will start to condense on the electrodes surface, causing reduction-oxidation reactions which will have an effect on the impedance/conductivity of the electrode. These changes are electronically logged and the measuring system is also provided with a thermocouple to record the temperature at which the changes in impedance or conductivity occur.

## 2.7 Modelling oxy-combustion of pulverised fuels

### 2.7.1 Introduction to simulation and computational software

The importance of using computational and simulation models to predict the behaviour of a process is due to the fact that this approach is considerably cheaper and faster. Some of the commercial packages used to process modelling are: Fluent, CHEMKIN, Aspen Plus, gPROMS, Thermoflex or Hysis. However, before modelling a process involving combustion, it is necessary to obtain data specific to each modality: conventional combustion, fluidised circulating bed combustion, oxy-firing...etc. Previous studies [(Field, 1969). (Baum and Street, 1971), (Smith, 1982), (Musarra et al., 1986), (Makino, 1992), (Murphy and Shaddix, 2006)] have noted the relevance of adequately characterising the char combustion and they have published essential data on this topic. Studies on computational modelling of the combustion of solid fuels have been carried out by Musarra et al. (1986), Vascellari and Cau (2009), Wang et al. (2009), and Li and You (2010). Work on oxy-coal combustion for large-scale boilers using CFD modelling has been carried out by authors like Al-Abbas et al. (2012). Researchers who have investigated the oxy-firing process using Aspen Plus® include: Sotudeh-Gharebaagh et al. (1998) (circulating fluidised bed using coal as fuel in air-firing conditions), Xiong et al. (2011), and Hu and Yan (2012) (both oxy-firing coal, assuming equilibrium conditions).

However, to date few authors have performed simulations on oxy-combustion for co-firing coal –biomass blends using Aspen Plus®.

There are two approaches that can be adopted when simulating an oxy-combustion process:

- Using a method based on the equilibrium reactions. In this method is assumed that all reactions involved in the process reach chemical equilibrium. This is a simplifying hypothesis as real processes do not have sufficient residence time for this to occur
- A kinetics based approach: by using this approach, which is more complex than the previous one, the effect of temperature as well as the presence of critical chemical species and the residence time are considered for the calculation of the combustion products.

Studies published using both approaches are discussed in next subsections.

### 2.7.2 Modelling based on chemical equilibrium

The studies published where the equilibrium approach is taken, usually consider the process of generating the oxygen, necessary to feed to the oxy-combustor, as part of the simulation model. This is the case for the work carried out by Xiong et al. (2011) where the global process of oxy-combustion, from the air separation unit (ASU), the boiler, turbines and feed-water heaters associated, and the flue gas treatment unit (FGU) are simulated to study the interactions between the different modules. The configuration of this model is shown in Figure 38 (see Appendix A.1.2). The main input parameters changed from case to case, by these authors, are the percentage of oxygen in the product stream generated in the ASU, and the percentage of recycled flue gas. Note that these two parameters are combined to supply a specific oxygen concentration (30% mol-based) in the gas mix fed to the furnace. Xiong et al. (2011) included a stream to simulate the air ingress into the process, given that this is the usual situation for retrofitted oxy-combustors. Xiong et al. (2011) specified a flowrate for this stream of 2% of the total gas supplied to the boiler. To establish the

percentage of recycle, these authors used the criterion that their system achieved the same temperature as in the air-firing case.

There are also studies where the ASU is not included in the model, such as the work of Hu and Yan (2012). The authors provide a better definition of the reactions occurred in the selective catalytic reduction reactor (SCR) to reduce the $NO_x$ and in the flue gas desulfurization unit (FGD). The assumptions made are shown in Figure 37, and the configuration of the model in Figure 36 (see Appendix A.1.1). They concluded that it is possible to achieve a percentage of $CO_2$ around 96% mol-based in dry basis after the flue gas cleaning units.

The studies presented thus far provide, mainly, with specifications for the reactors, process configurations, or operating parameters related to the oxy-fuel combustion assuming equilibrium conditions. However, to obtain a global view of the process, it is necessary to consider more complex models incorporating modules for the ASU and the power generation unit. These investigations are discussed below.

**Air separation unit (ASU)**

The simulation of the air separation unit (ASU) process should consist of a multi-stage compressor, a multi-stream heat exchanger, and two distillation columns (one at low and one at high pressure), according to the main references found for this process.

Hu et al. (2010) suggested as goal to obtain a purity of 95% mol-based of oxygen in the product stream; the configuration of the model is presented in Figure 39 (see Appendix A.1.2). For this, the air is compressed up to 6.2 bar and then purified using a condenser and a filter. The compressed air stream is then split in two fractions: the largest stream is conveyed to the high pressure column (HPC), pressure set at 5.5 bar, and the smaller one to the low pressure column (LPC), pressure set at 1.35 bar. The bottom product of the HPC is oxygen rich liquid with a purity of 35-38%, which is fed to the LPC to be further, purified. The selected parameter that controls the purity of oxygen generated is suggested to be the flowrate of oxygen vapour in LPC flow, which is dependant

of the vapour flowrate from the bottom stage and the reflux ratio of the LPC. These authors pointed out that the condensation temperature of the gaseous nitrogen needs to be increased when the purity of the liquid oxygen increases. This is a consequence of the fact that the boiling temperature of the oxygen stream rises with its purity. The need to maintain a fixed pinch point in heat exchanger 2 (see Figure 39 in Appendix A.1.2), where the nitrogen stream transfers heat to the oxygen stream, also means that the condensation temperature of the nitrogen must be increased. Hence, more power has to be consumed to compress the air stream to improve the purity of the oxygen product. They carried out a study to determine the optimum purity of the oxygen, in relation to the specific energy consumption of the ASU. Figure 7 shows that, for a purity of oxygen above 97%, the associated increase in energy consumed is sharp; while from 97 to 80% purity this relation is approximately linear.

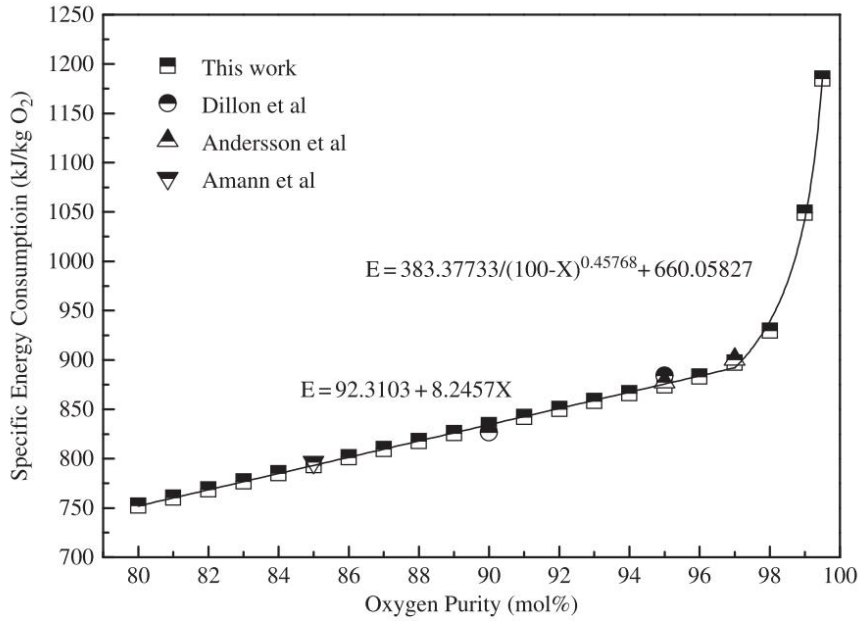


**Figure 7 Specific energy consumption of ASU at different oxygen purity. Image taken from Hu et al. (2010)**

The configuration for the ASU proposed by Raibhole and Sapali (2012) is similar to the one suggested by Hu et al. (2010), but they use different operation

parameters. The pressure and number of stages for each column are: 4 bar and 40 stages for HPC, and 1.2 bar and 56 stages for the LPC.

A more detailed description of the parameters used for the cryogenic air distillation is given by Amarkhail (2010). This process differs from the previous ones in the fact that there is an additional product stream of argon for which there is a required purity as well. In consequence, it is necessary to use two or more distillation columns, see Figure 40 in Appendix A.1.2. Data related to outlet temperatures of the different heat exchangers used to optimise the energetic efficiency of the process are also given in this work.

**Power generation unit**

The power generation unit is defined by the oxy-combustor and the set of steam turbines. Depending on the degree of complexity of the simulation, there can be different options for the system. Xiong et al. (2011) suggested a system formed by nine steam turbines: two high-pressure, two intermediate-pressure, and five low-pressure units, shown in Figure 41 (see Appendix A.1.2). By implementing a power generation unit with several steam turbines, working at different pressures, a more detailed study regarding the heat recovery can be made and consequently, a more accurate analysis of the energetic efficiency of the plant. This could be an opportunity to study and optimise the combined heat and power efficiency of the oxy-combustion process. However, the accuracy of the simulation increases with its degree of complexity. These authors carried out a study of an 800$MW_e$ oxy-combustion power plant with the basic operational parameters to be set for the simulation (see Figure 42 in Appendix A.1.2). Some of these data can be extrapolated to be used in the simulation of a different scale oxy-combustion system.

### 2.7.3 Modelling based on kinetics

As the kinetic approach is more complex, it is usual to make some simplifying hypothesis. The most typical ones are proposed by Edge et al. (2011) and explained below:

- Steady state conditions are assumed to be maintained during the oxy-firing process, so particle characteristics remain constant
- The velocity in the pores of the particle can be neglected, as it is assumed that no diffusion occurs inside the particle
- The temperature of the coal particles is assumed to be homogeneous
- The reactions occurred in the surface of the particle are considered separately from the reactions occurred in the gaseous phase
- The pulverised fuel particles are assumed to be spherical and to have uniform physical and chemical properties
- The combustion of the char is assumed to take place once the existing volatiles in the fuel have been oxidised, even though during the real process the char and volatile combustion are parallel steps
- The char particles are composed exclusively of carbon when the temperature achieved is above 1270K.

**Char combustion**

Different approaches can be considered when kinetically modelling a combustion process, in such cases the main difference is the limiting step selected. The char combustion process can be controlled by:

- Diffusion of the oxygen through the gaseous phase to reach the particle surface where the reaction takes place
- Diffusion rate through the pore of the char particle
- Kinetics of the appropriate chemical reactions

Smith (1982) proposed specific equations depending on the controlling step assumed. For the case in which no limitations are considered regarding mass transfer or pore diffusion, the char reaction rate obeys to Equation 10.

$$\rho_{c,comb}\left({}^{kg}/_{m^2 \cdot s}\right) = \eta \cdot \gamma \cdot A_g \cdot R_i\left[C_g \cdot (1-\chi)\right]^m \qquad \textbf{Equation 10}$$

For the case where the reactions are slow enough (see Equation 11), the pore diffusion does not have any rate-limiting effect, so the concentration of oxygen throughout the pore is the same as on the particle's outer surface.

$$\rho_{c,comb}\left({}^{kg}/_{m^2 \cdot s}\right) = \eta \cdot \sigma \cdot A_g \cdot R_i\left[C_g \cdot (1-\chi)\right]^m \qquad \textbf{Equation 11}$$

The third case presented by Smith (1982), is when both, pore diffusion and chemical reaction provide a strong rate-limiting effect.

$$\rho_{c,comb}\left({}^{kg}/_{m^2 \cdot s}\right) = 2 \cdot \left\{2 \cdot A_g \cdot \sigma \cdot D_e \cdot R_i \cdot {}^{\left[C_g \cdot (1-\chi)\right]^{m+1}}/_{(m+1)}\right\}^{0.5} \qquad \textbf{Equation 12}$$

There are other authors who have suggested less complex equations for the heterogeneous reaction rate, when considering diffusion and kinetic limitations. For instance, Vascellari and Cau (2009) suggested the system (Equation 13-Equation 15) based on Smith (1982), for the case in which the reactions rates are governed by mass transfer through the gaseous phase of the oxidant species as well as by intrinsic kinetics.

$$R_{r,j} = A_p \cdot \eta_r \cdot p_j \cdot \left[{}^{\left(k_{r,j} \cdot k_{d,j}\right)}/_{\left(k_{r,j} + k_{d,j}\right)}\right] \qquad \textbf{Equation 13}$$

$$k_{d,j} = \frac{C_j}{d_p} \cdot \left[\frac{\left(T_p + T_g\right)}{2}\right]^{0.75} \qquad \textbf{Equation 14}$$

$$k_{r,j} = A_{r,j} \cdot \exp\left({}^{-E_{r,j}}/_{R \cdot T_s}\right) \qquad \textbf{Equation 15}$$

The above mentioned equations were suggested by Vascellari and Cau (2009) for the heterogeneous reactions of the char. The reactions governed by these expressions are presented with the numbers assigned by the authors, so not to lead to misunderstandings when displaying additional information related to these reactions. The chemical reactions and the species involved considered by Vascellari and Cau (2009) are listed below:

$C(s) + 0.5O_2 \rightarrow CO$ (6)

$C(s) + CO_2 \rightarrow 2CO$ (7)

$C(s) + H_2O \rightarrow CO + H_2$ (8)

There are also homogenous reactions. These reactions occur when light gases are released from the pulverised fuel, during primary pyrolysis. Vascellari and Cau (2009) proposed the following reactions based on the work of Kim et al. (2008):

$CH_4 + 0.5O_2 \rightarrow CO + 2H_2$ (2)

$CH_4 + H_2O \rightarrow CO + 3H_2$ (3)

$CO + 0.5O_2 \rightarrow CO_2$ (4)

$H_2 + 0.5O_2 \rightarrow H_2O$ (5)

Vascellari and Cau (2009) study provide the expressions for the chemical reactions, information about pre-exponential factors and activation energy. This is illustrated in Figure 43 and Figure 44 (see Appendix A.2)

Sotudeh-Gharebaagh et al. (1998) are the only researchers that have used the rate-based model of the char combustion to date using the software Aspen Plus®. However, the topic of their study is not oxy-firing but circulating fluidized bed combustion and they were considering air-firing. Nonetheless, some key information was produced in their work.

These authors considered for their simulations a staged combustion: in first stage the combustion of the volatiles present in the coal occur, and subsequently the char combustion. This assumption is similar to the one made by Vascellari and Cau (2009).

For the combustion of the volatiles, the reactions considered are listed below:

$C + O_2 \rightarrow CO$ (a)

$S + O_2 \rightarrow SO_2$ (b)

$H_2 + 0.5O_2 \rightarrow H_2O$ (c)

The fraction of the carbon that is oxidized depends on the analysis of the coal and it is given by the Equation 16.

$$X_c = VM - H - S$$ **Equation 16**

Where VM is the volatile matter in the coal (obtained from the proximate analysis), H is the fraction of hydrogen in the coal, and S is the fraction of sulfur in the coal.

For the char combustion, a kinetic model is employed. The fraction of carbon suggested to react is that remaining at the end of the combustion of the volatiles: (1-$X_c$). The reactions considered for this stage are both heterogeneous and homogeneous:

$C + 0.5O_2 \rightarrow CO$ (d)

$CO + 0.5\ O_2 \rightarrow CO_2$ (e)

$C + CO_2 \rightarrow 2CO$ (f)

The third reaction is neglected in this model (Sotudeh-Gharebaagh et al., 1998) as in the case of a circulating fluidised bed combustor the temperature of the particles is not considered to be high enough for this reaction to occur. This is a difference between their work, and the work presented here as higher temperatures are normally achieved in down-fired combustors.

The equation suggested by Sotudeh-Gharebaagh et al. (1998) for the first reaction (d), between the char particle and the oxygen present in the gaseous phase is presented in Equation 17.

$$r_{1,i} = \frac{[3 \cdot \eta_{O2} \cdot k_{cr} \cdot F_{char,i} \cdot (1-\epsilon_i) \cdot C_{O2}]}{[\rho_{char} \cdot r_c \cdot (1-\epsilon_c) \cdot F_{solid,i}]}$$ **Equation 17**

Where $k_{cr}$ is the chemical reaction rate constant and is defined by Equation 18.

$$k_{cr} = k_{01} \cdot \exp\left(-E_1 / R_g \cdot T_p\right)$$ **Equation 18**

$\eta_{02:}$ Effectiveness factor

$k_{cr} = k_{01} \exp(-E_1/R_g\ T_p)$, Chemical reaction rate constant ($m \cdot s^{-1}$)

$F_{char,i}$: Flux of the char particles entering the $i^{th}$ interval ($kg \cdot s^{-1}$)

$\epsilon_i$: Mean axial voidage in the $i^{th}$ interval of the riser

$C_{O2}$: Combustion gas concentration ($kmol \cdot m^{-3}$)

$\rho_{char}$: Density of char particles ($kg \cdot m^{-3}$)

$r_C$: Mean coal particle radius (m)

$\epsilon_C$: Char porosity

$F_{solid,i}$: Flux of solids entering the $i^{th}$ interval ($m^3 \cdot s^{-1}$)

For the second reaction (e), the combustion rate is given by an expression where the order of the reaction for the each species, the concentration of $O_2$, CO and $H_2O$, and the bed temperature are considered.

For the $NO_x$ formation, Sotudeh-Gharebaagh et al. (1998) both, thermal $NO_x$ and $NO_x$ generated as a consequence of the oxidation of the fuel nitrogen, are considered. The reactions considered for the $NO_{x,thermal}$ generation are:

$0.5\ N_2 + 0.5\ O_2 \rightarrow NO$ (g)

$0.5 N_2 + O_2 \rightarrow NO_2$ (h)

$N_2 + 0.5\ O_2 \rightarrow N_2O$ (i)

For the $NO_{x,fuel}$ generation these authors applied a conversion factor ($\alpha_1$), which could vary between 0 and 1. The expression suggested for this step is described in Equation 19.

$\alpha_1\ N_{fuel} \rightarrow \alpha_1 NO_x$ **Equation 19**

The $SO_2$ capture matter is also discussed by these authors. This capture was achieved by $SO_2$ capture via limestone, where the fractional conversion of the $SO_2$ was calculated using a FORTRAN subroutine, with the following reactions:

$CaCO_3 \rightarrow CaO + CO_2$ (j)

$CaO + SO_2 + 0.5\ O_2 \rightarrow CaSO_4$ (k)

In Figure 45 (see Appendix A.2), the information related to the type of reactor used for the different stages is described, as well as the input variables that, according to Sotudeh-Gharebaagh et al. (1998), must be entered in the software Aspen Plus® to run the simulations.

## 2.8 Summary

Having reviewed the experimental data related to oxy-firing of coal-biomass blends and simulation models available in the literature, there are a few aspects that need further study as very little or none work has been published on them.

Firstly, a number of pilot-scale oxy-combustors have been operated using coal or coal-biomass blends (with low shares of biomass) to study the gas composition of the flue gas, the optimum amount of recycled flue gas to use (selected as a function of different criteria, see p. 9), or the effect of the oxygen injection (its excess and location) on the flame characteristics, ignition temperature and burnout content. However, no published data are available for oxy-firing coal-biomass blends or pure biomass with real recycle of the flue gas, as most facilities simulate this stream by mixing $CO_2$ and $H_2O$ in specific proportions. Consequently, a study under these conditions to evaluate the chemistry inside the oxy-combustor and heat fluxes generated seems necessary. Special attention should be drawn, also, to the generation of $SO_3$ (gaseous), $K_2SO_3$ and KCl (aerosols) as if these are retained in the ash deposits, they can increase their corrosive potential in a noticeable way. Studies of the presence of these species inside the furnace have been carried out, but none of them used combined conditions: how oxy-firing coal–biomass blends with high share of biomass affects the generation of these corrosive compounds, and to which extent they are captured in the ash deposits. This together with the ash behaviour, mechanisms of slag layer formation and its interaction with char particles under oxy-combustion conditions have been pointed out as topics of high interest. Another issue related to corrosion is the characterisation of the acid dew point in oxy-firing, where it is particularly important, due to the higher concentrations of acid species ($NO_x$, $SO_x$, HCl) present in the flue gas. Although correlations to estimate theoretical acid dew

points are available in the published literature, there is a lack of experimental data considering co-firing and oxy-combustion simultaneously to assess the accuracy of these theoretical estimations.

Finally, a few models have been presented using different commercial software for the simulation of the oxy-combustion process using pulverized coal. However, none of them includes the simulation of the global process (power generation module -combustor and steam turbine- and air separation module) combined with a rate-based approach for the char combustion, considering the widely used commercial software, Aspen Plus®. Furthermore, no kinetic data are available in the dimensions required by this software, so it seems necessary to develop an equation that permits the use of the kinetic data existing in the literature.

# 3 METHODOLOGY

## 3.1 Introduction

This chapter describes the main operating aspects considered for the realization of the experimental tests (previous retrofitting of the pilot combustor), as well as the steps fulfilled to design the simulation model. The parametric studies carried out for both, the pilot-scale oxy-combustor and the simulation model, have been made on the basis of the suggestions found in the specific literature for these subjects. The two approaches, experimental and modelling, adopted for the study of the oxy-combustion process led to a continuous feedback between them, as they were ran in parallel: e.g. the experimental results were used as inputs for the simulation model, and the results of parametric analyses with the model were used to select forthcoming experiments. Figure 8 illustrates schematically the methodology, described above, implemented for the accomplishment of this PhD work.

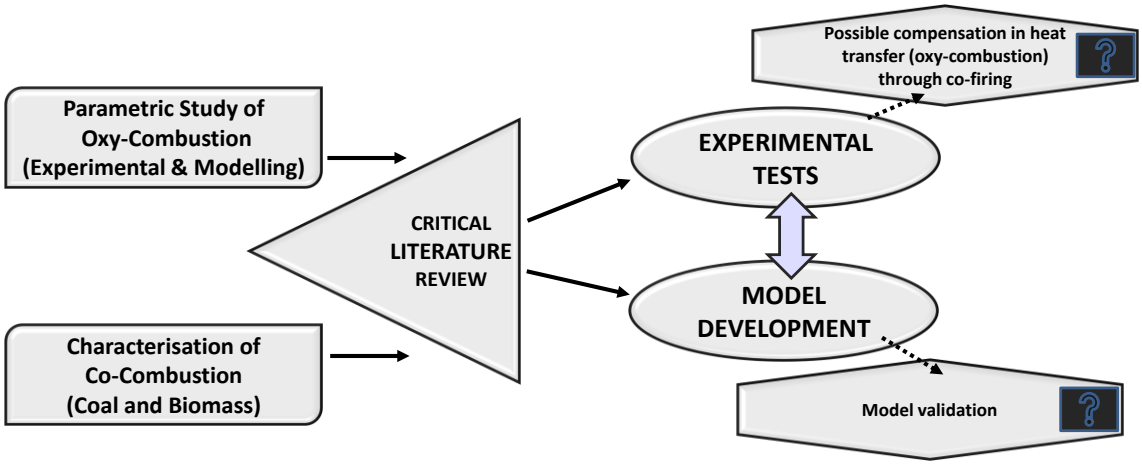


**Figure 8 Overview of the methodology adopted**

For the experimental setup, the pilot scale combustor together with the modifications implemented to convert it into an oxy-combustor, the monitoring equipment, as well as specific techniques applied are described.

The description of the simulation model includes the explanation of the stages, where different parametric studies have taken place, as well as the identification of elements constituting the model and their main characteristics.

## 3.2 Pilot scale oxy-combustor: experimental setup, development and optimisation

The experimental tests under air and oxy-firing conditions were performed in the pulverised fuel (PF) down-fired combustor with a 100kW$_{th}$ capacity located at Cranfield University. This combustor is attached to a 50kW$_{th}$ fluidized bed (FB), which is located prior to the PF as it can be seen in Figure 46. This schematic shows the configuration of the pilot scale previously to all the modifications that have been carried out for the retrofitting process.

For the air-firing experiments, the FB module was used as a preheater for the air, with the pulverised fuel fed directly to the burner associated to the PF combustor. However, for the tests performed under oxy-firing conditions the PF combustor was isolated from the FB combustor by a gate valve located in between. In any case, the fuel fed to the burner corresponds to a heat release of 100kW$_{th}$.

### 3.2.1 Retrofitting process: from air to oxy-fired combustor

#### Rig description

The retrofitting process was carried out through several stages, which are described later on in this section. The resulting configuration is shown in Figure 9.

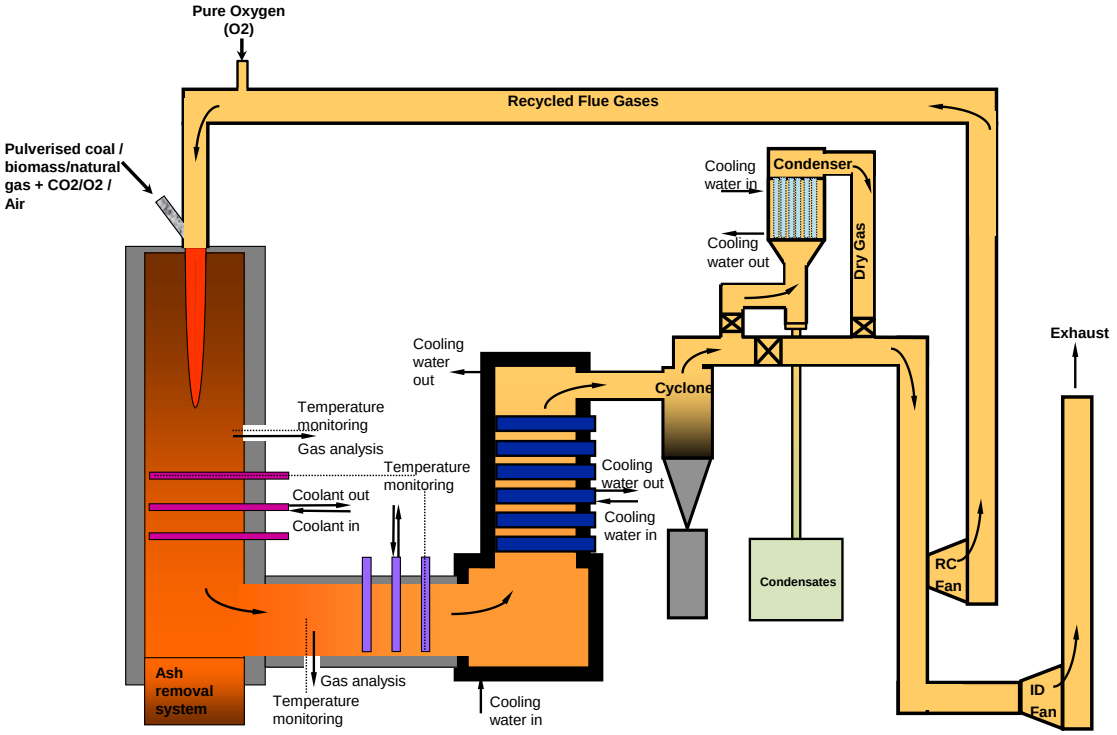


**Figure 9 Schematic diagram of final configuration of 100kW$_{th}$ PF oxy-combustor**

Note that this final configuration was only employed for the third campaign of experiments, as in the case of the first and second campaigns an intermediate rig arrangement was used.

The pulverised fuel is fed to the oxy-combustor at a constant rate using a fuel feeder provided by a metering screw, a vibratory tray and a Venturi eductor (see Figure 47 in Appendix B). Additionally, the feeder has three purge points located: at the main storage hopper, at the feeding hopper, and at the end of the vibratory tray feeder. $CO_2$ is injected through these purge points to keep a positive pressure inside the pulverised fuel feeding system so as to avoid air ingress. Once the pulverised fuel reaches the Venturi eductor, it is fluidised and conveyed to the burner by a stream of pure $CO_2$ gas coming from $CO_2$ cylinders. Prior to this stream being fed to the burner, the primary $O_2$, coming from $O_2$ cylinders, was injected into the stream, when using this option for a particular test.

The combustor is equipped with a down-fired burner, provided with a pilot flame port and a flame detector. The pulverised fuel is combusted in the vertical zone

of the combustor (3.7 m height). The combustor has a square cross-section with sides of 650 mm and thermal isolation with thickness 175 mm (see Figure 48 in Appendix B). The vertical zone has four view ports and ports where sensors are used to measure wall temperatures (six type K thermocouples). The data acquisition system is a Pico Logger Unit-TC-08. More thermocouples are installed along the rig monitoring: inlet and outlet temperature of the water used in the refrigeration system, at the heat exchanger section, temperature after the cyclone, and six more thermocouples to measure the temperature along the recirculation line. These sensors are sampled using the data logger, with 24 sampling ports distributed along the vertical and horizontal sections of the chamber. Three of these ports, located at the bottom part of the vertical section, are used by the deposition probes. To collect the deposits, it was necessary to allow the chamber to cool down for 18 to 24 h, then the ash deposited on the probes was sampled and analysed using ESEM/EDX and XRD. An on-line high-resolution multi-component Fourier Transform Infra-red (FTIR) was used to analyse $CO_2$, $O_2$, $H_2O$, CO, NO, $NO_2$, $N_2O$, $NH_3$, $SO_2$, HCl, HF and $CH_4$. The rig was provided with two sampling points to allow for the FTIR analysis: one located at the vertical section of the chamber (one of the aforementioned ports), and another at the exit of the condenser.

The exhaust gas goes through two water-cooled heat exchangers, one in the horizontal and one in the vertical section, before exiting the oxy-combustor. After leaving the chamber, the gas enters a cyclone where the suspended particles are removed. From here, depending on the type of recycle flue gas used for the experiment, this stream passes by the condenser (dry RFG) or by-passes it (wet RFG). Then, part of the gas is recirculated to the combustion chamber, through RC fan, and the remainder is sent to the stack, through ID fan. The pipelines that convey the recycled flue gas are thermally isolated with a trace heating system to avoid a temperature drop below the acid dew point of the flue gas. The secondary $O_2$ is injected into this stream prior to feeding it to the oxy-combustor. A secondary analyser, an ADC MGA 3000 Multi Gas Analyser which measures $CO_2$, CO, $O_2$ and $SO_2$, samples the gas just before

the entrance to the burner to monitor that the percentage of oxygen is in the range specified (27-35% v/v).

**Primary modifications**

The retrofitting process has been carried out in three stages. The first stage involved the installation of the recirculation line including setting up the recirculation fan (RC fan), gas-tight type, the $O_2$ injection to the recycle flue gas (secondary $O_2$) and trace heating wiring to prevent condensation in the flue gas recirculation lines. Additionally, a line to supply the $CO_2$ was installed to convey the pulverised fuel from the hopper to the burner itself. The second phase covered the design and fitting of a swirl in the air inlet port of the burner; implementation of layout to inject the primary $O_2$, added to the stream conveying the fuel to the combustor; installation of the gas-tight fuel-feed hopper; and the design of a new $CO_2$ supply line, capable to supply higher flow rates, to respond to the design requirements of the new fuel feeder. Figure 49 shows the configuration of the gas panel where the flow rates of $CO_2$ and $O_2$ into the process can be controlled. The modifications accomplished in the third stage were set: to provide the rig with a dry recycled flue gas (implementation of a condenser, see Figure 50 in Appendix B); to enhance the mixture of the secondary $O_2$ injected with the recycle flue gas (see Figure 51 in Appendix B); to improve existing measurements by upgrading the range of measurement of the analysers (FTIR and ADC MGA 3000) used to sample the gas (see Figure 52 and Table 28 in Appendix B); and to apply additional measurements: $SO_3$ content, acid dew point, heat flux inside the combustor and percentage of burnout in ash.

The procedures incorporated to the methodology to measure new aspects of the oxy-combustion process are described below:

- Sulfur trioxide measurement. The method chosen to measure $SO_3$ content in the flue gas is the Controlled Condensation Method developed by the Environmental Protection Agency (EPA Method 8A) (NCASI Southern Regional Center, 1996), which scheme has been already presented in Figure 5. The standard procedure for sampling, sample

recovery and sample analysis is fully described in the reference given for this method. Note that for the sample collection a mistake was made for all the analyses, which was to consider the procedure described in Method 8 (see Appendix C of Method 8A in NCASI Southern Regional Center (1996)): the rinsing water used for the quartz probe and the quartz filter were collected in the same container as well as the washing water from the $SO_3$ condenser. Consequently, the analyses carried out account not only for the $SO_3$ but also for the $SO_4^{2-}$ sampled as aerosols collected on the filter. The location selected to install the $SO_3$ sampling train is the last part of the horizontal section of the oxy-combustor, as it is where the optimum window temperature to sample the flue gas is (see Figure 55 in Appendix B).

- Acid dew point measurement. The acid dew point measurement has been carried out with an electrochemical noise (EN) probe, CAPCIS branded, as previously explained in section 2.6. The location selected is in the pipeline that conveys the recycle flue gas (three metres from the exit of the recirculation fan (RC fan)) in its way to the entrance of the oxy-combustor. See Figure 53 in Appendix B for further explanation.
- Heat flux measurement. Measurements of the radiative and convective flux were scheduled to be performed in the radiative section of the oxy-combustor (vertical section where the flame is located). For the radiative heat flux measurement a HUKSEFLUX water cooled sensor for high temperatures was acquired (see Figure 54 [a), b)] in Appendix B). For the convective heat flux measurement, an in-house air-cooled probe was designed taking into account the guidelines given by Smart et al., (2010c). This probe is shown in Figure 54 -c) in Appendix B. The method intended to be used for the calculations of the convective heat flux was also the one suggested by these authors. The main problem found during the initial tests of the third campaign, when this in-house probe was used, was the practical impossibility in keeping the temperature of the surface probe at the set temperature (300°C) or close enough, even using the maximum amount of cooling air allowed for the rig. The

decision made after having recognized this problem, compounded by the fact that this probe was contaminating by the ash deposits sampled from probes located below it, was not to use this convective heat flux probe for subsequent tests.

- Temperature measurement. New R type thermocouples were acquired to measure the temperature in locations selected close to the flame. This type of thermocouple allows for the measurement of higher temperatures (up to 2020K). The location chosen for these thermocouples, as well as for the other measurement systems is described in Figure 55 in Appendix B.

### 3.2.2 Main operational aspects

The main operating conditions that were scheduled to vary through the experimental plan are listed below.

#### Type of combustion

To study the oxy-combustion process, it is necessary to set a reference case to compare the results generated performing oxy-firing tests. For the experiments carried out at as part of the work of this PhD, the reference case is the combustion with necessary amount of coal required to generate 100 $kW_{th}$. Additionally, as result of the critical literature review done, which suggests that further researching was needed on co-firing coal and biomass blends under air and oxy-firing conditions, it was considered worthwhile also to carry out tests on air-firing cases using coal-biomass blends for comparison purposes.

#### Type of fuel

The fuels used for the experimental tests have varied depending on the campaign planned. The parent fuels selected to carry out the tests were: Daw Mill coal, El Cerrejon coal, and cereal co-product (CCP) biomass. Then, different blends of these fuels were used, as required by the test programme for the specific cases studied. The characteristics of the three parent fuels are given in Table 4, data taken from Khodier (2011) and Asgaryan (2013). (Note that the sum of the ultimate analysis, moisture and ash for Daw Mill and El

Cerrejon coals, are slightly different from 100; however, it was the only data available for the composition of these fuels).

**Table 4 Proximate, ultimate, mineral and ash analyses of the fuels**

| | Daw Mill coal | El Cerrejon coal | CCP |
|---|---|---|---|
| Proximate analysis (% (wt) as received) | | | |
| Moisture | 4.60 | 5.80 | 8.10 |
| Volatile matter | 31.30 | 34.80 | 70.80 |
| Ash | 4.20 | 8.60 | 4.20 |
| Calorific value, (MJ/kg) | | | |
| Gross calorific value | 25.26 | 27.85 | 17.61 |
| Net calorific value | 24.11 | 27.12 | 16.34 |
| Ultimate analysis (% (wt) as received) | | | |
| Carbon | 74.15 | 69.2 | 43.30 |
| Hydrogen | 4.38 | 4.80 | 5.80 |
| Nitrogen | 1.17 | 1.42 | 2.70 |
| Chlorine | 0.20 | 0.02 | 0.17 |
| Sulfur | 1.28 | 0.58 | 0.16 |
| Oxygen | 10.49 | 9.98 | 35.57 |
| Mineral analysis (% (wt)) | | | |
| Kaolinite $Al_4Si_4O_{10}(OH)_8$ | 54 | 16.90 | - |
| Illite $KAl_2(OH)_2(AlSi_3O_{10})$ | - | 9.40 | - |
| Calcite $CaCO_3$ | 14 | - | - |
| Dolomite $CaMg(CO_3)_2$ | 12 | - | - |
| Pyrite $FeS_2$ | 20 | 12.90 | - |
| Quartz $SiO_2$ | - | 54.20 | - |
| Coquimbite $Fe^{-3}{}_2(SO_4)_3 \cdot 9H_2O$ | - | 3.50 | - |
| Bassanite $CaSO_4 \cdot 0.5H_2O$ | - | 3.20 | - |
| Ash analysis (% (wt)) | | | |
| $SiO_2$ | 36.80 | 60.69 | 44.36 |
| $Al2O_3$ | 23.90 | 22.01 | 2.79 |
| $Fe_2O_3$ | 11.20 | 7.43 | 2.47 |
| $TiO_2$ | 1.10 | 0.92 | 0.12 |
| CaO | 12.00 | 2.27 | 7.78 |
| MgO | 2.50 | 2.90 | 3.96 |
| $Na_2O$ | 1.50 | 1.06 | 0.36 |
| $K_2O$ | 0.50 | 2.32 | 24.72 |
| $Mn_3O_4$ | 0.40 | 0.06 | 0.10 |

| | Daw Mill coal | El Cerrejon coal | CCP |
|---|---|---|---|
| $P_2O_5$ | - | 0.21 | 12.04 |
| $SO_3$ | - | - | - |
| BaO | - | 0.11 | 0.05 |

**Recycled flue gas: percentage and type**

The percentage of recycled flue gas set was different for each campaign of experiments, because of the difficulty associated with the controllability of this parameter, given the interaction of two fans (ID and RC fan). In the first two campaigns the recycle was around 50% of the flue gas, while in the third campaign, it was set in the range of 58-65%.

Regardless of the type of flue gas used, it was not until the third stage of modifications when the condenser was installed. So, the third campaign is the only one with both dry and wet recycles flue gas, whereas the first and second campaigns just operated with wet recycle.

**Flowrate of oxygen**

Following the guidelines in the published literature, to ensure safe conditions for the oxygen injection, the oxygen percentage in the primary stream was not permitted to exceed 21% (v/v). This parameter was the same for all the experimental campaigns.

During the first and second campaign, the secondary oxygen was kept under 28% (v/v), because: no literature was found suggesting values above 28% (v/v), and the range of the ADC MGA 3000 Multi Gas Analyser was between 0 and 30% (v/v). However, for the third campaign a new upper limit of 35% (v/v) was set in consequence of new recommendations established in the literature, plus the fact of the upgrade of the analyser. With the higher specification for the $O_2$, values between 2 and 5% (v/v) of $O_2$ at the exit of the combustor were reached (this did not happen in previous campaigns), meaning that there was an excess of oxygen in the initial gas mixture fed to the burner, allowing for a complete combustion of the fuel.

**Pressure**

The operating pressure selected in the oxy-combustor has a direct effect on the amount of air ingress that occurs into the process. This parameter becomes more important in the cases of retrofitted facilities, as it is the case for our reactor at Cranfield University. Air ingress into the oxy-combustion process in retrofitted plants is a common phenomenon as noted by many researchers [(Steinmetz et al., 2011), (Santos, 2008)] as one of the main problems due to this is that it causes a drop in the purity of $CO_2$ seen in the flue gas, which in practise would cause higher costs for the purification of this stream prior to its compression and storage.

For the first and second campaigns of experiments, the operating pressure inside the combustor was set to be below atmospheric for safety and design considerations. However, to minimise the air ingress into the combustion chamber during the test, the pressure was kept as close as possible to atmospheric.

For the third campaign and after having checked during the initial tests that the CO levels were low enough, the tests were run in slightly positive pressure, switching it to be negative when the ports associated to the combustor had to be opened momentarily (change of the FTIR sampling probe, and at the start /end of using the $SO_3$ sampling train).

**Additional aspects**

Several limitations for the operation of the pilot scale oxy-combustor were identified during the different campaigns of experiments. They are described in Appendix B.1.1.

Prior to each test, as part of the preparation of the rig for operation, a list of tasks was carried out in order to ensure good performance. This list is given in Appendix B.1.2. Similarly, some maintenance was required on the rig after each test; the main tasks for this step are described in B.1.3.

During each test, a datasheet was filled as a back-up measure in case that any of the data loggers failed during operation (See Figure 56 in Appendix B.1).

### 3.2.3 Experimental test programme

The experimental test programme consists of a minimum of three tests (varying the fuel composition) under two different combustion conditions (air and oxy-firing), which makes a total of 6 tests, see Table 5. This approach has been adopted in order to allow for a comparative analysis given the primary established operational parameters.

**Table 5 Minimum number of tests -Primary parameters**

| FUEL / COMBUSTION | 100% Coal | 50%Coal-50% Biomass | 100% Biomass |
|---|---|---|---|
| Air-firing | Test 1 | Test 2 | Test 3 |
| Oxy-firing | Test 4 | Test 5 | Test 6 |

Additionally, a number of secondary parameters have been considered, due to their significant effect on the process but bearing in mind their relatively lower importance with respect to the primary parameters. These parameters have been already mentioned in the previous section but are listed as follows: use of a second type of coal, percentage and altering the type of recycle, changing the percentage of oxygen present in the recycle (at the entrance of the oxy-combustor), pressure inside the combustor. The matrix of the completed experimental plan designed to study the effect of both, primary and secondary, operating parameters is presented in Table 6. The code followed to label these tests (XX.YY.Z.(i)) is described in Table 7.

**Table 6 Experimental test programme**

| | | | 100%COAL | | 100%CCP | 50%COAL/50%CCP | | 75%COAL/25%CCP | |
|---|---|---|---|---|---|---|---|---|---|
| | | | DM | EC | | DM/CCP | EC/CCP | DM/CCP | EC/CCP |
| AIR-FIRING | | | FC.DM.A | TC.EC.A | TC.CC.A | | TC.B1.A | | |
| OXY-FIRING | Wet RFG (w/o cond) | RFG 1 (50-55%) | FC.DM.O.(a)<br>FC.DM.O.(b)<br>FC.DM.O.(c)<br>FC.DM.O.(d)<br>SC.DM.O | | SC.CC.O | SC.B1.O | | | |
| | | RFG 2 (58-65%) | | TC.EC.O.(a) | | | | | |
| | Dry RFG (with cond) | RFG 1 (50-55%) | | | TC.CC.O | | TC.B1.O.(a) | | |
| | | RFG 2 (58-65%) | | TC.EC.O.(b)<br>TC.EC.O.(c) | | | TC.B1.O.(b) | | TC.B2.O |

**Table 7 Code for labelling tests**

| | XX. | YY. | Z. | i |
|---|---|---|---|---|
| Options: Meaning | FC: First campaign<br>SC: Second campaign<br>TC: Third campaign | DM: Daw Mill coal<br>EC: El Cerrejon coal<br>CC: Cereal co-product<br>B1: Blend 50/50<br>B2: Blend 75/25 | A: Air-firing<br>O: Oxy-firing | a: First test under XX.YY.Z conditions<br>b: Second test under XX.YY.Z conditions<br>Etc. |

## 3.3 Model development of an oxy-combustor

For the design of the simulation model of a 100kW$_{th}$ oxy-combustor, several stages have been explored. In each of these stages specific parameters have been varied to study their effect on the outputs of the model, as well as to analyse the physical meaning of these effects on the experimental process of co-firing coal and biomass blends under oxy-firing conditions, setting as reference the air-firing case using coal.

In the following sections, the parametric study carried out in each phase of the simulation model's development is described, along with the different versions of the model produced.

### 3.3.1 Parametric study applied to modelling

To permit the parametric study of co-firing coal and biomass under oxy-firing conditions by the use of a simulation model, a limited number of parameters have been varied in each stage; the values applied for these operational parameters are presented in Table 8. The variation of the inputs, which are: type of fuel supplied, energy demand, percentage of recycle flue gas, excess of $O_2$, air ingress into the oxy-combustor, and reactions considered for each reactor defined; as applied for the simulation model, generate results for temperature achieved, gas composition of the flue gas, energy required by ASU process, composition of $CO_2$ product, emissions to air, solid residue, and net efficiency of the process. However, it is necessary to mention that the software used, Aspen Plus®, has two main limitations regarding the outputs generated: the estimation given for the temperature refers to an adiabatic flame temperature, and the solid residue have the same composition as the ash defined as input for the specific fuel used. In consequence, these aspects were only explored based on experimental results, rather than the outcomes from the simulations.

**Table 8 Parametric study applied to simulation model**

| | STAGE | Air/ oxy-firing | RFG (%) | $O_{2,exc}$ (%) (v/v) | $T_{RFG}$ (K) | Air Ingress (% of total gas fed) | Fuel |
|---|---|---|---|---|---|---|---|
| Equilibrium Model | STAGE E1<br>Air-firing case | Air -firing | -- | 21 | -- | -- | El Cerrejon coal |
| | STAGE E2<br>Oxy-firing case with wet recycle | Oxy -firing | 60, 65, 70 | 0,10,21 | 640 | -- | El Cerrejon coal |
| | STAGE E3<br>Oxy-firing case with wet recycle and heat loss | Oxy -firing | 60, 65, 70 | 0,5,10 | 400 | -- | El Cerrejon coal |
| | STAGE E4<br>Oxy-firing case with wet recycle, heat loss and air ingress | Oxy -firing | 60, 65, 70 | 0,5,10 | 400 | 1.7 | El Cerrejon coal |
| Kinetic Model | STAGE K1<br>Air-firing case | Air -firing | -- | 21 | -- | -- | El Cerrejon coal |
| | STAGE K2<br>Oxy-firing case with wet recycle, heat loss and air ingress | Oxy -firing | 55, 60, 65, 70 | 0,5,10 | 400 | 2,10, 18 | Coal (El Cerrejon, Daw Mill), biomass (cereal co-product, Miscanthus), blends coal - biomass (75/25;50/50;25/75) |
| | STAGE K3<br>Oxy-firing case with partial condensation in RFG, heat loss and air ingress | Oxy -firing | 55, 60, 65, 70 | 0,5 | 350 | 0, 10 | Daw Mill coal, CCP, blend Daw Mill - CCP (50/50) |
| | STAGE K4<br>Oxy-firing case with dry recycle, heat loss, air ingress | Oxy -firing | 55, 60, 65 | 0,5 | 400 | 10 | El Cerrejon coal |

| STAGE | Air/ oxy-firing | RFG (%) | $O_{2,exc}$ (%) (v/v) | $T_{RFG}$ (K) | Air Ingress (% of total gas fed) | Fuel |
|---|---|---|---|---|---|---|
| STAGE K5<br>Air-firing case with power generation unit | Air -firing | -- | 21 | -- | -- | El Cerrejon coal |
| STAGE K6<br>Oxy-firing case with dry recycle (constant $\eta_{condenser}$= 95%), heat loss, air ingress, ASU and power generation unit | Oxy -firing | 55, 60, 65 | 0,5 | 400-470 | 10 | El Cerrejon coal, CCP, blend EC-CCP (50/50) |
| STAGE K7<br>Oxy-firing case with dry recycle (variable $\eta_{condenser}$), heat loss, air ingress, ASU and power generation unit | Oxy -firing | 55, 60, 65 | 0,5 | 400-470 | 5, 7, 10 | El Cerrejon coal, CCP, blends EC-CCP (75/25; 50/50) |

### 3.3.2 Simulation model based on chemical equilibrium

The aim of this first phase of the simulation model's development, based on the equilibrium of the reactions, was to provide an initial approach to the process. From this preliminary analysis, with regards to mass and energy balances, a study on the contribution of the factors defined as inputs to the model was carried out. The box-plot of the model is presented in Figure 10.

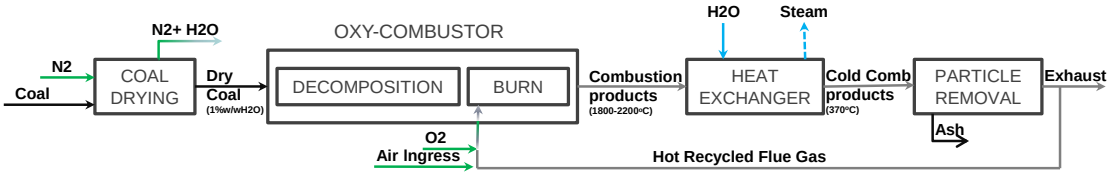


**Figure 10 Box-plot of the equilibrium model**

In a simulation model, not all the reactors defined correspond to an actual reactor in the real process. Thus, the coal first undergoes a drying stage, simulated by a stoichiometric reactor. This step does not take place in a reactor in the experimental setting. The drying process occurs when the pulverised fuel is conveyed from the feeder to the burner. The moisture of the coal after this step is 1 % (wt). The oxy-combustor is simulated using two reactors: the first one to enable the coal to turn into a conventional solid, with the ability to react. This step is necessary because when a new solid component is defined in Aspen Plus®, it belongs to the non-conventional solids group, unable to interact with other species. The second reactor acts as the actual combustor, where all the reactions occur. The hot combustion products pass then through the heat exchanger, where they are cooled down to 640K (370°C in Figure 10). After this, a cyclone removes the suspension solids from the flue gas. From this point, part of the gas is recycled to the oxy-combustor and part goes to the stack. The fraction of gas that is recycled (Hot Recycled Flue Gas in Figure 10), goes through another heat exchanger, in which the heat loss of the RFG in its way back to the combustor is simulated. At the exit of the second heat exchanger, at 400K, the oxygen necessary to burn the fuel is injected. Additionally, a stream of air is fed at this point to re-create the air ingress occurred in real conditions when using retrofitted facilities.

The interface of Aspen Plus® designed for the equilibrium model is presented in Figure 11.

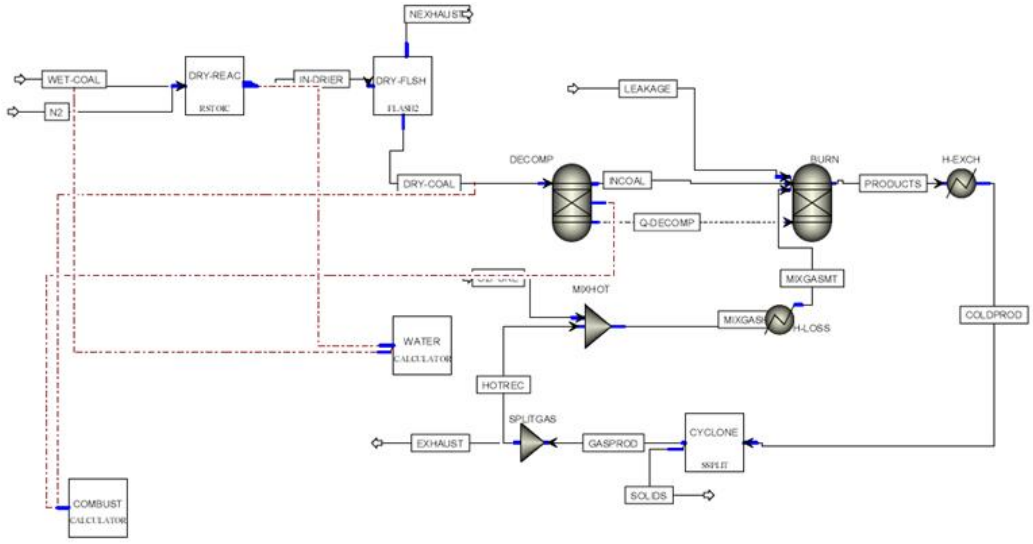


**Figure 11 Interface of the equilibrium model in Aspen Plus®**

The main input parameters necessary to define the reactors simulating the different steps of the process are described in Table 29 (Appendix C). Additionally, a brief description for the types of the reactors available in Aspen® libraries, which have been used in the equilibrium and kinetic models, is given in Table 30 (Appendix C).

### 3.3.3 Kinetic simulation model with wet recycle

The additional output of simulation models based on kinetics is that, this option provides a more realistic approach to the process than the equilibrium one.

The simplifying hypothesis of considering the system as chemically controlled allows the mass transfer of the oxidant species and the pore diffusion in the char particles to be neglected. The kinetic parameters proposed by Vascellari and Cau (2009) have been used in the simulation model. However, some modifications had to be made for the pre-exponential factors of the char combustion reactions. These changes were necessary as a consequence of the differences between the dimensions required by Aspen Plus® and the ones found in the published literature.

The power law expression for the reaction rate used by Aspen Plus® on a partial pressure basis is shown below:

$$r = k \cdot T^n \cdot e^{-E/RT} \cdot \prod (p_i)^{\alpha i} \qquad \textbf{Equation 20}$$

The dimensions for the pre-exponential factor (called “k” in Aspen Plus®, and usually named “A” in Arrhenius equation) required by the commercial package are:

$$kgmol \cdot K^{-n} \Big/ sec \cdot m^3_{Reactor} \left(\frac{N}{m^2}\right)^{\sum \alpha_i}$$

All data found in the references for pre-exponential factors have different dimensions compared to Aspen Plus® requirements, as in the denominator there is a factor corresponding to the char particle surface, instead of the volume of the reactor.

To convert the dimensions of the published data to the dimensions required by Aspen Plus®, the formula shown below has been developed:

$$A' = A \cdot \left[\frac{3 \cdot (1 - \varepsilon_c) \cdot \left(1 - \varepsilon_{F,R}\right)}{r_c \cdot MWc}\right] \qquad \textbf{Equation 21}$$

The main drawback of this method is the necessity of calculating a pre-exponential factor ($A'$) for each case simulated, as every time the total volume of gases involved in the process changes (e.g., when the percentage of recycled flue gas varies), so does the voidage in the reactor ($\varepsilon_{F,R}$) and, hence, the pre-exponential factor ($A'$). On the other hand, this is the only method currently available due to the lack of published data for the dimensions required by Aspen Plus®. Figure 12 presents the box-plot for the kinetic base case.

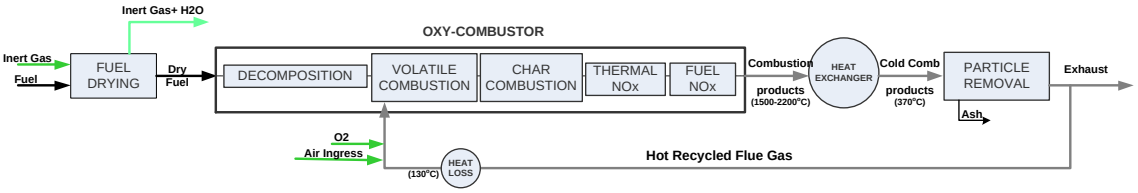


**Figure 12 Box-plot of the basic kinetic model**

A variation of the previous case study has been considered, in which an additional block was implemented to simulate the partial condensation of $H_2O$ vapour during recirculation of the flue gas to the oxy-combustor. This set of simulations was necessary so as to have a kinetic model with operating conditions as close as possible to the second campaign of experimental tests performed in the pilot plant. The box-plot for the rate-based case with partial condensation is presented in Figure 13.

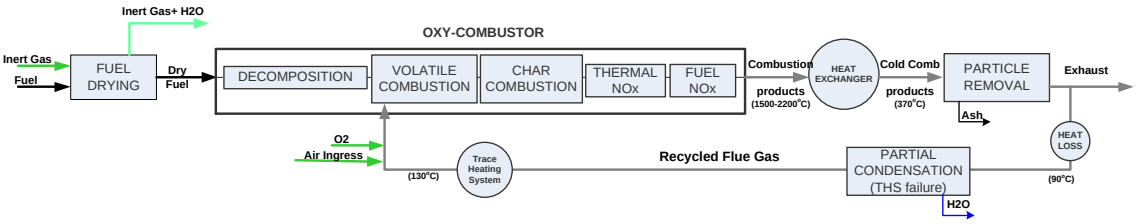


**Figure 13 Box-plot of the kinetic model with partial condensation in RFG**

Here, the drying process has been defined so that 5% (wt.) of the fuel moisture is included in the gas stream. The oxy-combustor is simulated using five reactors: the first one converts the fuel, nonconventional solids, to conventional ones; a reactor to perform the combustion of the volatile species of the fuel (where the fraction of C that reacts is Xc =VM-H-S (Sotudeh-Gharebaagh et al., 1998)); a reactor to simulate the combustion of the char; a reactor where the thermal $NO_x$ is generated; and lastly, a reactor to simulate the generation of $NO_x$ from the fuel N. The hot combustion products then go to the heat exchanger, where they are cooled down to 640K (370°C in Figure 13) Then, a cyclone is in charge of removing the suspended solids from the flue gas. From this point, part of the gas is recirculated to the oxy-combustor and the rest sent to the exhaust. The fraction of gas that is recirculated goes through a heat exchanger, where the heat loss of the RFG on its way back to the combustor is simulated, as this fact occurred during the experimental tests of the second campaign. Then, there is a split reactor where the condensed $H_2O$ vapour (due to heat loss) is removed from the flue gas stream. To define the amount of $H_2O$ vapour that condenses in this reactor, the saturation vapour pressure of the $H_2O$ at the minimum temperature reached in the flue gas was considered. This value established the maximum concentration in the gaseous phase that is

possible for the $H_2O$ vapour. Thus, if the $H_2O$ vapour concentration is higher, it condenses.

After the partial condenser, a heat exchanger simulates the trace heating system of the actual pilot plant. Then, the oxygen is injected together with an air stream to recreate the air ingress that takes place during the experimental tests. An additional heat exchanger is implemented prior to the feeding of RFG to the chamber, to ensure that the temperature is set according to the specifications.

The interface of Aspen Plus® when using the kinetic model with partial condensation in the RFG is shown in Figure 14, and the types of reactors used for the different steps, the main input parameters and the reactions defined in them are presented in Table 31 (Appendix C).

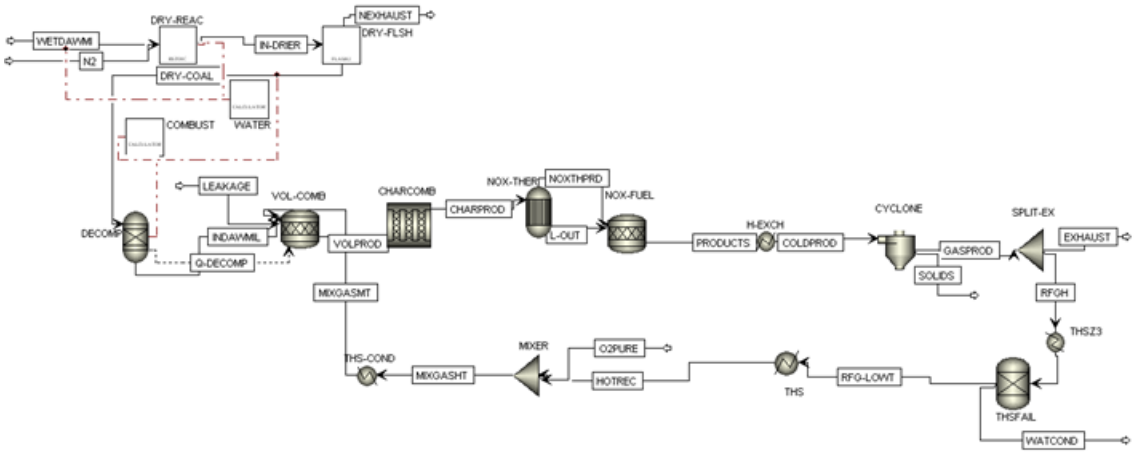


**Figure 14 Interface of the kinetic model with partial condensation in RFG**

Additional fixed input parameters in the simulations related to the geometry of the combustor, flow rates and fuel properties are shown in Table 32 (Appendix C), and the analysis of the fuels has been already presented in Table 4.

The methodology adopted to compare results from simulations and experimental data from the second campaign was, first, to set up operating conditions as similar as possible to the experiments; and second, to perform the simulations comparing the results generated by the model in Aspen Plus® regarding gas composition and temperatures reached. For the first step (establish similar operating conditions), it was necessary to determine the

amount of air ingress into the process which occurred during the experiments. This was accomplished using mass balances based on the experimental data. Additionally, air ingress was varied in the model, until analogous values generated by the simulations to the empirical gas composition were obtained. Although the air ingress is an unknown variable that needed to be characterised, other operating parameters were changed in the simulations to find out the combination that best represented the experimental conditions during the tests. These parameters were: percentage of RFG, excess of $O_2$ supplied, and amount of water vapour condensed.

### 3.3.4 Kinetic simulation model with dry recycle

The design of the process for the simulations using dry recycle differs from the presented in previous subsection (kinetic model with partial condensation in RFG) in: the generation of HCl as combustion product in the oxy-combustor block, the condensation of $H_2SO_4$, $HNO_3$ and HCl in the condenser (additionally to $H_2O$ vapour), and in the location where the exhaust gas is split from the recirculated stream. The last aspect was changed in order to prepare the model in case of the implementation of a $CO_2$ conditioning unit for future simulations. The box-plot and interface in Aspen Plus®, used for stages K6 and K7, are presented in Figure 15 and Figure 16, respectively.

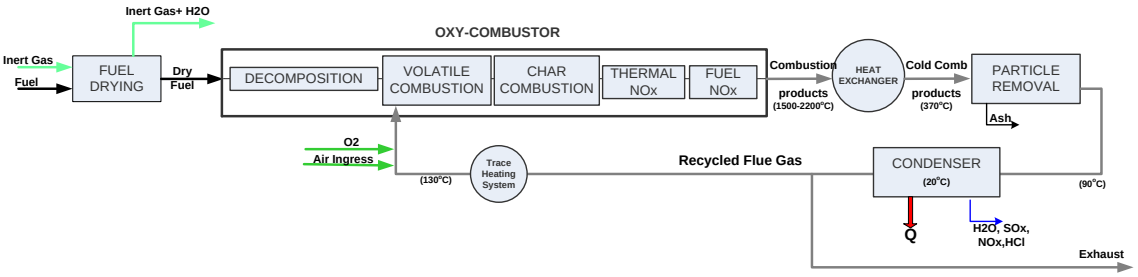


**Figure 15 Box-plot for kinetic model with dry recycle**

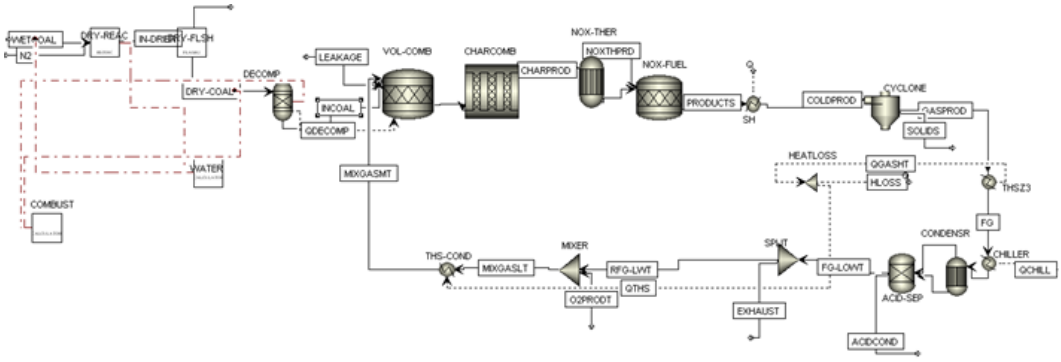


**Figure 16 Interface of the kinetic model with dry recycle in Aspen Plus®**

The main parameters defined in those blocks of the simulation model in which chemical reactions occur are presented in Table 33 (see Appendix C).

A variation of this model was provided in order to meet the operational conditions of the experimental plant during the third campaign of tests. The main difference in operation for this model is the variable efficiency applied to the condenser depending on the fuel used. This step was included after noticing that the condenser performed differently when using biomass or blends with high share of biomass. Additionally, the parametric study applied in this stage was adjusted with regards to: the blends of coal biomass used, and the amount of air ingress supplied to the oxy-combustor. The last change, related to the air ingress, which was required as consequence of the better sealing of the rig achieved prior to the third campaign of tests. Thus, a study to find out the quantitative effect of this action had to be carried out.

The main parameters defined for the reactors remain the same as the presented in Table 33, with the only difference being the specification type for the ACID SEP block (part of the condenser); the values considered for this stage of modelling, K7, are described in Table 34 (see Appendix C). Other fixed input parameters to the model are included in the aforementioned Table 32 (Appendix C).

### 3.3.5 Kinetic simulation model integrated with air separation and power generation units

For the final configuration of the kinetic model, two additional modules were implemented. The ASU is the section of the process where the oxygen to be fed to the oxy-combustor is generated with a specified purity. In the oxy-combustor section, the fuel and the oxygen are supplied so the combustion process occurs. The high temperature flue gas generated enters into a heat exchanger to produce the steam that will be fed to the last section, the steam turbine. Here, the pressurised steam provides the thermal energy to the turbine which will extract it as mechanical work (see Figure 17).

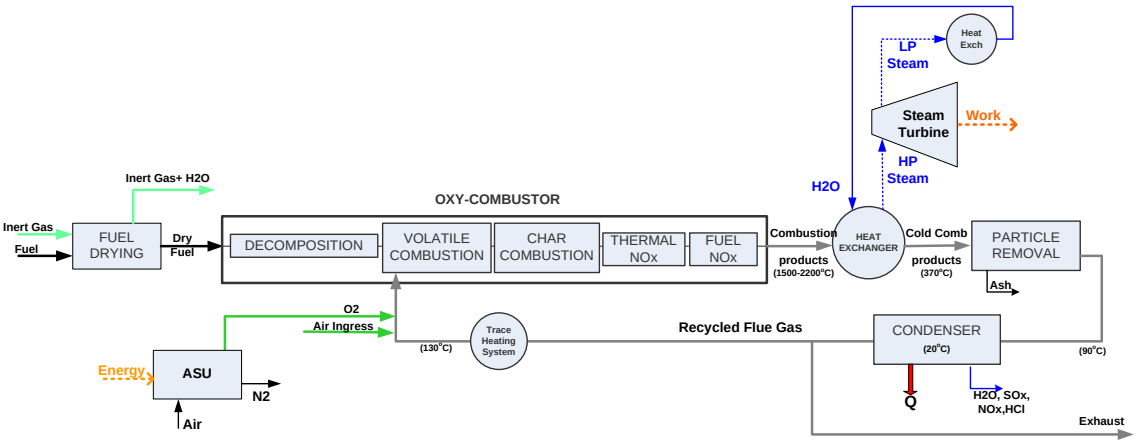


**Figure 17 Box-plot of the ASU, oxy-combustor and steam turbine**

#### Air separation unit

The ASU process simulated consists of a multi-stage compressor, a multi-stream heat exchanger, and two distillation columns (one at low and one at high pressure).

The four-stage intercooling compressor produces air at 6.3 bar, pressure necessary to generate a stream of oxygen with 95% mol purity. The pressurised air is split into two streams, and fed to the multi-stream heat exchanger (HE1) where it works as the hot fluid, and its exit temperature is 143K (-130ºC). The stream of air with higher flowrate is supplied to the high pressure column (HPC), which is defined by 40 stages, a total condenser and a reflux ratio of 1.2. Note that the condenser of the HPC provides with the heat needed by the reboiler of

the low pressure column (LPC). The stream that exits the HPC in the distillates section has more content of nitrogen, as this specie has higher vapour pressure than the oxygen. The stream of the bottom of the HPC is, consequently, enriched in oxygen, of around 47% mol purity. Both streams are cooled in a multi-stream heat exchanger (HE2), and expanded using valves prior to feed them to the LPC. The LPC has a total of 56 stages, and the streams are fed as follows: the air on the 10$^{th}$ stage, the oxygen rich stream (bottom of HPC) on the 23$^{rd}$ stage, and the nitrogen rich stream (top of HPC) on the 1$^{st}$ stage. The reflux fraction value for this column is 0.5712. The diagram used for the ASU simulations can be seen on Figure 18.

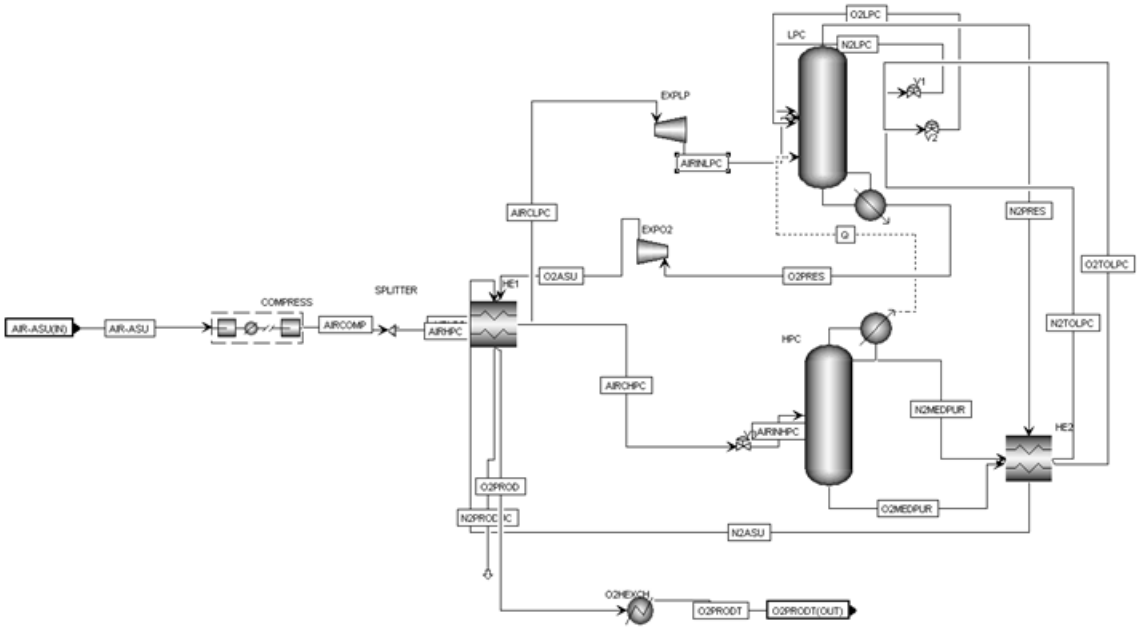


**Figure 18 ASU process interface in Aspen Plus®**

### Power generation unit

The power generation unit consists of the oxy-combustor and the steam turbine. The heat released by the combustion products is used (inside the super-heater (SH)) to increase the temperature and the pressure of the steam that will be fed to the turbine. The thermal energy of the steam is converted into mechanical work in the steam turbine, as the steam is expanded down to 0.06 bar, as it is proposed by Xiong et al. (2011). The low pressure vapour is fed to another heat

exchanger to return to the pressure and temperature conditions at which is set to be fed to the first heat exchanger (S-SH).

The interface in Aspen Plus® for the comprehensive system simulated is presented in Figure 19.

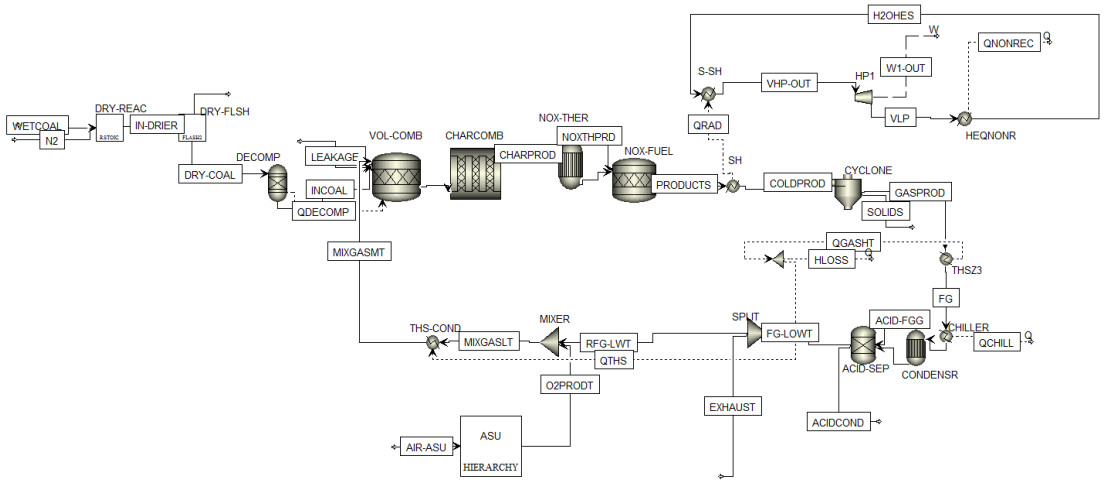


**Figure 19 Interface of oxy-combustor integrated with ASU and steam turbine in Aspen Plus®**

# 4 EXPERIMENTAL RESULTS AND ANALYSIS

This section describes the main aspects studied here (gas composition, temperatures and heat flux, ash deposits and fly ash characterisation, $SO_3$ analysis and acid dew point of the flue gas) by operating the retrofitted oxy-combustor using coal, biomass and coal-biomass blends. For each topic, the work has been structured according to the three experimental campaigns that have been carried out for this PhD.

## 4.1 Gas composition

### 4.1.1 First campaign: results from preliminary tests

The results obtained for the gas composition, during the first experimental campaign, are reported in Table 9 and Table 10. In Table 9, the average compositions (*) reached inside the combustor are presented for the air-firing test (FC.DM.A), and for the four oxy-firing tests performed [FC.DM.O (a-d)]; all of them using Daw Mill coal. Note that the conditions for the main operating parameters for these tests have been previously defined in Table 6, and the system to name each test is given in Table 7.

**Table 9 Average gas composition (*) under air and oxy-firing conditions and RFG during first campaign**

| | $CO_2$ %(v/v) | $H_2O$ %(v/v) | $O_2$ %(v/v) | $NO_x$ ppmv | CO ppmv | $SO_2$ ppmv | $CH_4$ ppmv | HCl ppmv | RFG % |
|---|---|---|---|---|---|---|---|---|---|
| FC.DM.A | 11.30 | 11.40 | 2.80 | 95 | 5271 | 324 | 193 | 37 | - |
| FC.DM.O(a) | 28.92 | 16.42 | 7.01 | 114 | 11337 | 714 | 272 | 57 | 55 |
| FC.DM.O(b) | 34.25 | 19.95 | 6.85 | 99 | 13817 | 851 | 480 | 28 | 58 |
| FC.DM.O(c) | 36.22 | 14.34 | 7.85 | 99 | 9297 | 786 | 238 | 46 | 58 |
| FC.DM.O(d) | 39.51 | 23.08 | 0.25 | 177 | 17464 | 1527 | 1077 | 97 | 57 |

(*) *Selected data for periods under steady operation*

As already mentioned in the methodology section, the goal of these tests was to tune the pilot plant after the initial modifications made in the early stage of the retrofitting process. Actually, as can be seen from the table above, the level of $CO_2$ improves in each succeeding test.

However, the CO levels do not follow a clear trend, and are very high for the last test. This fact, high concentrations of CO due to partial combustion, is a direct consequence of the lack of excess $O_2$ during this test FC.DM.O (d), as the $O_2$ average value was 0.25% (v/v). With regards to the $NO_x$ levels, there is almost no difference between the air-firing case and the three first oxy-firing tests [FC.DM.O (a-c)]; this trend is supported by the literature (Toftegaard et al., 2010), as in oxy-firing conditions, due to the reduction of the $N_2$ into the process, air, a reduction in the thermal and prompt $NO_x$ are expected, resulting in a reduction in the $NO_x$ emitted between one third and half of the levels of $NO_x$ seen in air-firing. For the $SO_2$ concentrations, the levels seen for the oxy-firing tests are between two and three times higher than in the air-firing case, as consequence of the flue gas recycle.

In Table 10 the existing gas composition for the moment in which the maximum $CO_2$ concentration was reached for each test, is presented.

**Table 10 Gas composition during oxy-combustion tests when $CO_{2,max}$ was reached, first campaign**

| | $CO_2$ %(v/v) | $H_2O$ %(v/v) | $O_2$ %(v/v) | $NO_x$ ppmv | CO ppmv | $SO_2$ ppmv | $CH_4$ ppmv | HCl ppmv |
|---|---|---|---|---|---|---|---|---|
| FC.DM.O(a) | 36.65 | 19.43 | 4.20 | 114 | 7469 | 1205 | 118 | 84 |
| FC.DM.O(b) | 36.17 | 19.38 | 2.20 | 124 | 25108 | 854 | 888 | 26 |
| FC.DM.O(c) | 42.49 | 13.96 | 6.99 | 80 | 6726 | 1027 | 254 | 62 |
| FC.DM.O(d) | 48.06 | 26.03 | 0 | 176 | 2587 | 2311 | 1765 | 343 |

From the table above, a noticeable difference for the levels reached in the minor species between the first three oxy-firing tests [FC.DM.O (a-c)] and the last test [FC.DM.O (d)] of this campaign can be identified, except for the case of CO which is the lowest when the maximum $CO_2$ occurs. The results regarding gas composition of the test FC.DM.O (d) are more similar to the ones obtained during the tests of the second campaign. This can be explained by the fact that in this last test of the first campaign, the flowrate of coal was increased, by feeding the burner with a flowrate closer to the design specifications of the combustor. The values for the flow rates used in each experimental test are presented in Table 35 (see Appendix D).

The evolution of the gas species inside the oxy-combustor for one of the tests of this campaign [FC.DM.O (d)] is illustrated in Figure 57 to Figure 59 (see Appendix

D.1.1.). These graphs clearly show the moments when the old fuel feeder had to be refilled, as air ingress then occurred together with momentary disruption of the fuel fed. The direct consequence of the air ingress was the decrease in $CO_2$ levels. The disruption of the fuel feed also had effects on the minor species: causing disturbances in the flame with resulting changes in the gas products composition, which are reflected mainly in terms of increase in the CO and $CH_4$ concentrations.

### 4.1.2 Second campaign: results with wet recycle

The main modification in the configuration of the rig for this second campaign was the installation of the new fuel feeder, which has been already presented in Figure 47 (see Appendix B), providing with a constant flowrate of fuel to the process, avoiding the fluctuations in the gas composition noticed in the earlier tests.

The results of the tests carried out during the second experimental campaign are reported in Table 11.The average composition (*) for the main and minor species is presented here, as well as the maximum $CO_2$ level reached in each test.

**Table 11 Gas composition (*) and RFG for oxy-combustion tests of second campaign**

| | $CO_{2\ max}$ %(v/v) [db] | $CO_{2\ max}$ %(v/v) [wb] | $CO_2$ %(v/v) [wb] | $H_2O$ %(v/v) [wb] | $O_2$ %(v/v) [wb] | $NO_x$ ppmv [wb] | CO ppmv [wb] | $SO_2$ ppmv [wb] | HCl ppmv [wb] | $CH_4$ ppmv [wb] | RFG % |
|---|---|---|---|---|---|---|---|---|---|---|---|
| SC.DM.O | 73.59 | 56.67 | 49.86 | 24.55 | 1.24 | 245 | 3577 | 2008 | 237 | 90 | 51 |
| SC.B1.O | 71.13 | 53.02 | 50.42 | 26.39 | 1.50 | 249 | 925 | 1092 | 296 | 1 | 52 |
| SC.CC.O | 64.93 | 45.71 | 44.05 | 30.35 | 2.40 | 88 | 2648 | 51 | 31 | 118 | 52 |

(*) *Selected data for periods under steady operation*

No significant differences are observed for the tests SC.DM.O and SC.B1.O, except for the levels of CO and $CH_4$, which are much lower in the case using the coal-biomass blend, denoting a complete oxy-combustion; and for the $SO_2$ concentration that is half the value in test SC.B1.O compared to the concentration generated using 100% Daw Mill coal (SC.DM.O). The latter observation is in line with expectations considering that given the sulfur content in Daw Mill coal is almost ten times the sulfur content in CCP (see Table 4). The water vapour content should also be higher in the case of the test SC.CC.O, but some condensation was observed during this test, as consequence of a failure in the trace heating system. The low values obtained for $NO_x$, $SO_2$ and HCl in SC.CC.O do not follow the trend set by the tests

SC.DM.O - SC.B1.O. This is assumed to be a consequence of the condensation occurred in this test (SC.CC.O), as the species showing too low levels are the acid ones that would have condensed in case of a fall in the temperature below the acid dew point of the flue gas. Finally, the excess oxygen is relatively low in the tests in the second campaign, a fact that explains the relatively high CO levels reached.

One of the main characteristics attending to the gas composition profiles obtained for this second campaign is their stability, enabled by the gas-tight fuel feeder. This can be seen in Figure 60 (see Appendix D.1.2), in comparison with the fluctuations observed from the graphs generated during the first campaign of experiments.

### 4.1.3 Third campaign: final results with wet and dry recycle

For the last stage of experiments, the rest of the modifications planned for the rig were put in place, the main one being the installation of the condenser, in the recirculation line, providing us with the possibility of studying the effects of using dry recycled flue gas. Another important difference in the operation conditions, during this last campaign, was the fact that the slightly positive pressure over the atmospheric ($\Delta P$=0.002 bar) in the oxy-combustor reduced air ingress into the process.

The results for the tests performed under air and oxy-firing conditions varying the composition of the fuel, as regards to the average gas composition (*), as well as the maximum $CO_2$ levels reached, identifying the percentage of RFG used for each test, are reported in Table 12.

**Table 12 Gas composition (*) and RFG for oxy-combustion tests of third campaign**

| | $CO_{2max}$ %(v/v) [db] | $CO_{2max}$ %(v/v) [wb] | $CO_2$ %(v/v) [wb] | $H_2O$ %(v/v) [wb] | $O_2$ %(v/v) [wb] | $NO_x$ ppmv [wb] | CO ppmv [wb] | $SO_2$ ppmv [wb] | HCl ppmv [wb] | $CH_4$ ppmv [wb] | RFG %, type |
|---|---|---|---|---|---|---|---|---|---|---|---|
| TC.EC.A | | 11.79 | 11.12 | 7.40 | 4.98 | 634 | 37 | 305 | 8 | 0 | - |
| TC.B1.A | | 12.74 | 12.33 | 9.39 | 2.27 | 404 | 99 | 274 | 37 | 2 | - |
| TC.CC.A | | 12.65 | 12.44 | 12.19 | 2.71 | 391 | 668 | 88 | 39 | 57 | - |
| TC.EC.O.(a) | 70.73 | 52.38 | 47.51 | 26.38 | 2.23 | 560 | 1393 | 771 | 6 | 89 | 60, wet |
| TC.EC.O.(b) | 67.45 | 52.89 | 49.31 | 24.13 | 5.46 | 753 | 29 | 689 | 6 | 1 | 58, dry |
| TC.EC.O.(c) | 81.22 | 66.08 | 62.13 | 19.80 | 3.56 | 1077 | 356 | 820 | 20 | 8 | 70, dry |

| | $CO_{2max}$ %(v/v) [db] | $CO_{2max}$ %(v/v) [wb] | $CO_2$ %(v/v) [wb] | $H_2O$ %(v/v) [wb] | $O_2$ %(v/v) [wb] | $NO_x$ ppmv [wb] | CO ppmv [wb] | $SO_2$ ppmv [wb] | HCl ppmv [wb] | $CH_4$ ppmv [wb] | RFG %, type |
|---|---|---|---|---|---|---|---|---|---|---|---|
| TC.B2.O | 77.19 | 61.22 | 60.56 | 21.59 | 4.70 | 594 | 226 | 654 | 31 | 13 | 67, dry |
| TC.B1.O.(a) | 74.60 | 55.29 | 48.89 | 29.15 | 4.16 | 508 | 1352 | 516 | 56 | 78 | 48, dry |
| TC.B1.O.(b) | 78.46 | 65.10 | 58.61 | 20.59 | 6.26 | 998 | 29 | 438 | 29 | 0 | 60, dry |
| TC.CC.O | 80.36 | 65.21 | 57.05 | 25.35 | 6.55 | 612 | 21 | 108 | 100 | 1 | 54, dry |

(*) *Selected data for periods under steady operation*

The results, as shown in Table 12, indicate that the maximum $CO_2$ level reached, on a wet basis, occurs in the case of 100% coal [TC.EC.O.(c)], as expected given the elemental analysis of the fuels. Interestingly, similar values for the $CO_2$ levels in dry basis were achieved when using both parent fuels, in tests TC.EC.O.(c) and TC.CC.O. For the $H_2O$ content, the results obtained are higher than expected after the installation of the condenser, even though its effect can be seen in the last repeat of the tests with each fuel [TC.EC.O.(c)- TC.B2.O- TC.B1.O.(b)- TC.CC.O], where the average value is around 20-25%(v/v), being the maximum for the case when using 100% CCP. The $O_2$ in excess was improved during this third campaign, and was between 3.5 and 6.5 %(v/v), in most cases. The CO levels reached are much lower in comparison with previous campaigns, as a consequence of a better combustion of the fuels. With regards to the $NO_x$ concentrations, the data shows that TC.EC.O.(c) and TC.B1.O.(b) reached around 1000ppms, and did not follow the trend set by the rest of oxy-firing tests (550-750ppmv); the possible reasons for this will be explored in the discussion section. The data reported regarding the $SO_2$ levels agrees with the expectation considering the fuels analysis, higher range (680-820ppmv) in the tests using 100% coal, medium range (440-650ppmv) for those tests using coal-biomass blends, and the lowest concentration (around 100ppmv) for the case using only biomass. Likewise, the levels measured inside the combustor for HCl, also follow the trend set by the ultimate analysis of the fuels: increasing with the share of biomass. The concentrations reported for the $CH_4$ are very low, which supports the belief that we have achieved effectively complete combustion for the tests of this third campaign, and as consequence, concentration levels are very low for intermediate combustion products such as CO and $CH_4$.

From the data presented in Table 12, the average gas composition obtained under air and oxy-firing conditions can be compared. For the main species ($CO_2$, $H_2O$) and some minor species ($SO_2$, HCl) the effect of recycling flue gas is noticeable, causing the levels to increase twice to three times their value in comparison to the air-firing case using the same fuel, however, the $NO_x$ levels remain similar for most cases. This means an actual decrease of $NO_x$ emissions per unit of energy produced, according to Buhre et al. (2005). It is worth highlighting that the higher concentration in $SO_2$ levels inside the oxy-combustor, noted previously, do not consider the normalisation per unit of energy released from the fuel, and this also follows trends reported by Buhre et al. (2005).

Some of the tests performed during this third campaign are plotted in Appendix D.1.3, to illustrate: the transition from operating with wet RFG to dry RFG during test TC.EC.O (b) in Figure 61 and Figure 62; the change of the FTIR sampling port from the primary (inside the combustor) to the secondary (after the condenser) during operation using biomass under oxy-firing (test TC.EC.O (b)) in Figure 63 and Figure 64, and air-firing conditions (test TC.CC.A) in Figure 65 and Figure 66.

### 4.1.4 Summary of findings

This section summarizes the main findings with regards to gas composition that have resulted as outcomes after the accomplishment of the three experimental campaigns.

The results for one test using coal under oxy-firing conditions for each of the experimental campaigns are shown in Table 13. These data allows visualizing the improvement in the performance of the rig achieved through the retrofitting process, showing an increase in the $CO_2$ levels higher than 20% in wet basis. Additionally, it can be seen that the results presented here suggest steady progress towards “better combustion” performance considering the low levels for CO and $CH_4$ seen for the test TC.EC.O.(c), in comparison to the high concentrations of CO in the two first campaigns, denoting partial combustion of the fuel.

**Table 13 Comparison of gas composition using coal in oxy-combustion over the three campaigns**

| | $CO_{2max}$ %(v/v) [db] | $CO_{2max}$ %(v/v) [wb] | $CO_2$ %(v/v) [wb] | $H_2O$ %(v/v) [wb] | $O_2$ %(v/v) [wb] | $NO_x$ ppmv [wb] | CO ppmv [wb] | $SO_2$ ppmv [wb] | HCl ppmv [wb] | $CH_4$ ppmv [wb] | RFG %, type |
|---|---|---|---|---|---|---|---|---|---|---|---|
| FC.DM.O(d) | 63.18 | 48.06 | 39.51 | 23.08 | 0.25 | 177 | 17464 | 1527 | 97 | 1077 | 57, wet |
| SC.DM.O | 73.59 | 56.67 | 49.86 | 24.55 | 1.24 | 245 | 3577 | 2008 | 237 | 90 | 51, wet |
| TC.EC.O.(c) | 81.22 | 66.08 | 62.13 | 19.80 | 3.56 | 1077 | 356 | 820 | 20 | 8 | 70, dry |

The gas compositions obtained for all the tests carried out during the second and third campaigns are presented in Figure 20 (main species) and Figure 21 (minor species). The results of the first campaign haven't been included here because, as it was mentioned at the beginning of this chapter, they were preliminary tests.

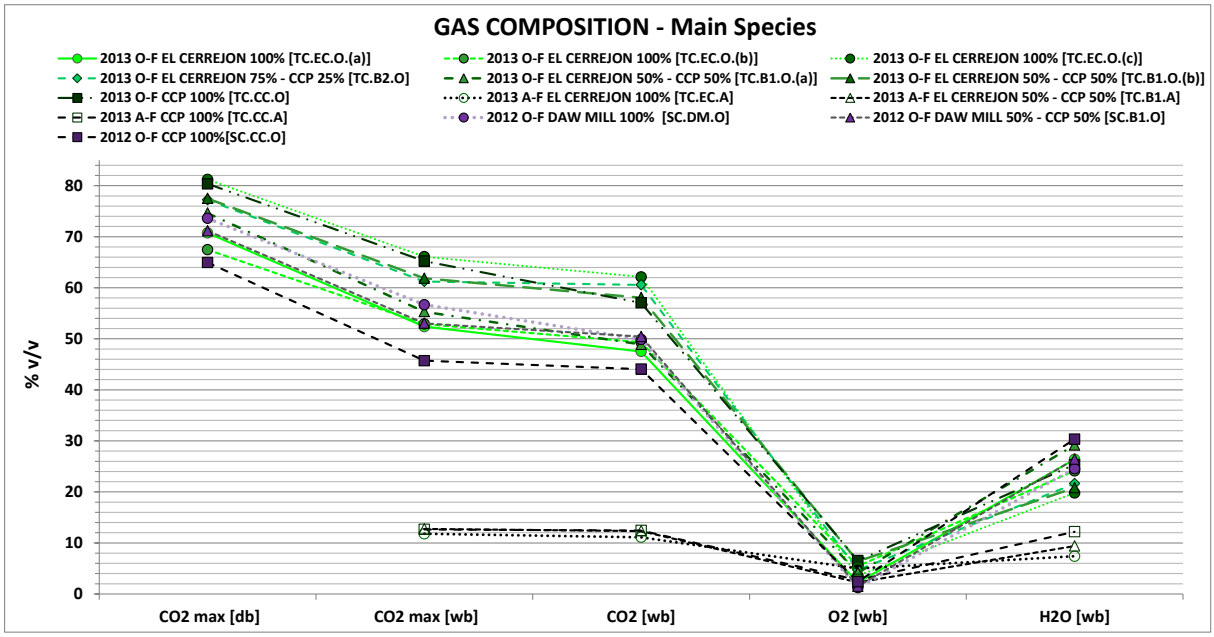


**Figure 20 Summary gas composition_ Main species**

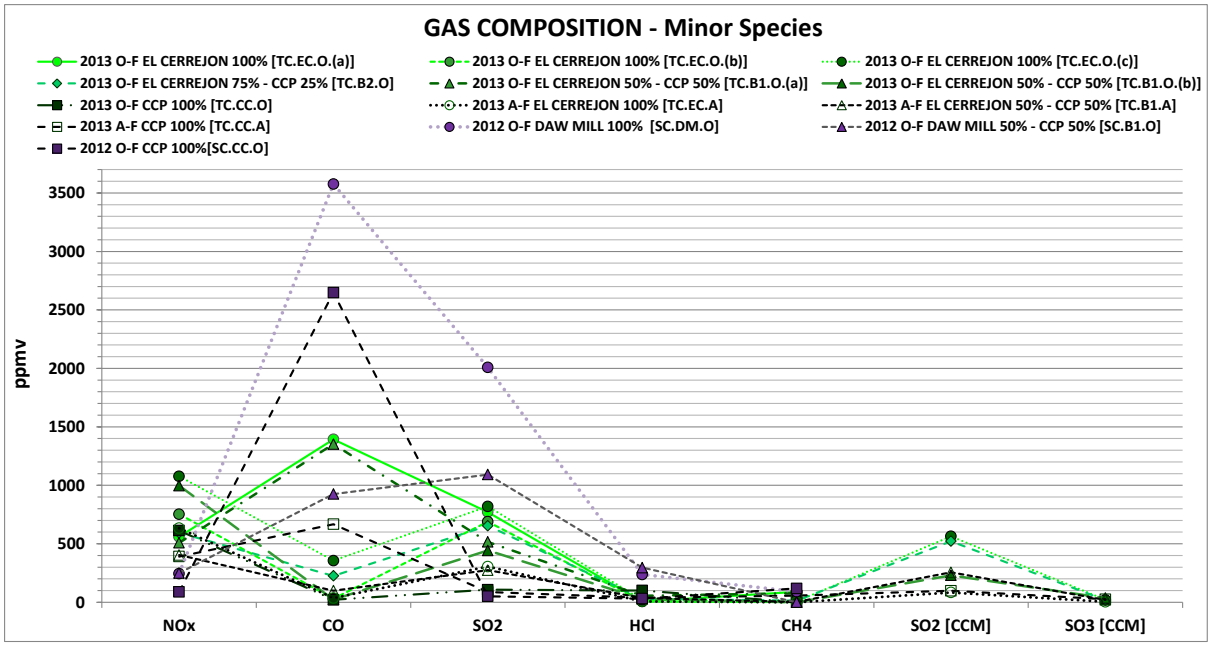


**Figure 21Summary gas composition_ Minor species**

## Effect of recycled flue gas: percentage and type

The main operational difference between air and oxy-firing combustion is the use of recycled flue gas. A direct consequence of this parameter is the accumulation of the chemical species in the recycled gases, a fact that is positive from the perspective of generating a stream with high $CO_2$ concentration. However, it also leads to the accumulation of undesirable corrosive species in the boiler.

From Figure 20 it can be observed that the levels of $CO_2$ obtained under oxy-combustion are five times the concentrations reached in the air-firing cases. The same is true for the $H_2O$ content, although these are at lower level, with the concentrations up to three times higher than in conventional combustion. Analysing Figure 21, the main difference between air and oxy-combustion results with regards to the minor species are increases in the $SO_2$ concentrations, which are up to 2.6 times higher when using coal in oxy-combustion compared to the same case under air-firing conditions.

The optimum range for percentage of RFG, for which higher $CO_2$ levels were achieved, was found to be between 65 and 70%. The type of recycle that contributed to these higher concentrations was using dry RFG.

**Effect of fuel**

- *Coal vs. biomass*. The results presented in Figure 20 show that although the maximum $CO_2$ levels in wet basis are achieved for those cases oxy-firing coal, considering dry basis the maximum $CO_2$ values using 100% coal or 100% biomass are similar and over 80%(v/v). This is a significant finding, as one might have expected that due to the lower carbon content in the elemental analysis of biomass, this would affect the $CO_2$ concentration of the flue gas generated. However, this 80% is still far from the purity in $CO_2$ required by the sequestration process, which is around 98% (Buhre et al., 2005), so a $CO_2$ purification unit would be still needed when using retrofitted facilities. Regarding the $H_2O$ levels, it is clear that the flue gas generated using biomass before any flue gas treatment will have higher $H_2O$ content, as a consequence of the higher $H_2$ and $O_2$ concentrations of the biomass; so precautions should be taken to avoid reaching the acid dew point temperature. With regards to the minor species, it can be observed in Table 12 and Figure 21 the main differences when increasing the share of biomass in the fuel is that the $SO_2$ levels decrease and the HCl levels increase, as expected given the ultimate analysis of the parent fuels.
- *Daw Mill vs. El Cerrejon*. The most relevant difference observed when varying the type of coal is in relation to the minor species in Table 13 (neglecting the high CO levels, which have been already commented), the high $SO_2$ and HCl concentrations obtained for those cases using Daw Mill coal. This is an effect of the higher contents of S and Cl in the ultimate analysis of Daw Mill coal in comparison with El Cerrejon coal. Additionally, the $NO_x$ level presented in Table 13 for TC.EC.O.(c) is not representative of the rest of the cases using El Cerrejon coal. However, this is not believed to be a factor dependent of the type of coal, as it will be explained in the discussion section.

**Effect of oxygen injection**

From the data in Table 13 and Figure 20, it is obvious that the third campaign was the only one with an acceptable excess $O_2$ concentration. In these tests the $O_2$ concentration in the feeding stream to the burner, after the $O_2$ injection to the RFG,

was around 35% (v/v), not taking 28% (v/v) as maximum as in the previous campaigns.

**Effect of pressure inside oxy-combustor**

One of the operational parameters changed in the last experiments from previous campaigns was the pressure inside the combustor, making it slightly positive with respect to the atmospheric case (0.002 bar higher). This was done to reduce air leakage, since given the low CO concentrations observed in the first tests of the third campaign this posed no danger to staff working on this experimental campaign.

As a consequence of this variation in the operation mode, a decrease in the air ingress was observed. This fact will be quantitatively explained in the section dedicated to results of model validation vs. third campaign's experimental data.

## 4.2 Temperatures and heat fluxes

### 4.2.1 First campaign: temperatures for Daw mill coal under air and oxy-firing conditions

The maximum temperatures reached inside the combustor during the first experimental campaign are presented in Table 14. These results are displayed, together with the average value for the percentage of RFG as well as the thermal power that should have been generated considering the fuel supplied to the burner (see Table 35 in Appendix D for further information). The specific location, where these temperatures were measured, is presented in Figure 55 (Appendix B).

**Table 14 Maximum temperatures reached inside the combustor during first campaign**

| | [0] Top vert (K) | [1] Flame 1 (K) | [2] Flame 2 (K) | [3] Flame 3 (K) | [4] Bottom vert (K) | RFG (%) | Power (kW) |
|---|---|---|---|---|---|---|---|
| FC.DM.A | 785 | 826 | 918 | - | 853 | - | 56 |
| FC.DM.O(a) | 850 | 959 | 1064 | - | 1025 | 55 | 56 |
| FC.DM.O(b) | 954 | 971 | 1061 | 1069 | 1007 | 58 | 56 |
| FC.DM.O(c) | 972 | 969 | 1047 | 1048 | 990 | 58 | 56 |
| FC.DM.O(d) | 895 | 1019 | 1093 | - | 1056 | 57 | 88 |

From these data it is clear that the maximum temperatures are reached in the location labelled 'Flame 3'. The highest temperature, over all the tests carried out

during this first campaign, was 1093 K, which was achieved during the last oxy-firing test [FC.DM.O(d)]. This is reasonable considering that this was the test where a higher flowrate of coal was fed to the reactor, although it was not possible to supply enough fuel to fulfil the nominal specifications of the combustor (100$kW_{th}$).

A comparison between the temperatures reached under air and oxy-firing conditions can be made, for those cases with similar power, observing the data presented in Table 14. The main outcome from this comparison is that during the oxy-combustion tests, the maximum temperature seen was in the range of 130 to 145K higher than the maximum temperature for air-firing, which is a substantial increment.

### 4.2.2 Second campaign: temperatures for oxy-firing Daw Mill coal/cereal co-product

The maximum temperatures reached for the tests carried out in the second experimental campaign, varying the fuel composition under oxy-firing conditions, are presented in Table 15. The RFG percentage and thermal power expected, as consequence of the fuel flowrate supplied to the burner, are also included for a better analysis of the results.

It is necessary to take into account that these tests were the first ones after the installation of the air-tight fuel feeder. As a consequence, even though calibrations were carried out with the different fuels, the flowrate set initially for the fuel to be supplied in each test, was rarely obtained. Another fact is that after the completion of the first campaign, the thermocouples located at [0], [1] and [2] were found to be installed in such a way that they were measuring the refractory temperatures. So, their position was modified to measure the temperatures in the centre of the transversal section of the combustor, at the beginning of the second campaign. The effect of this modification can be observed comparing the temperatures reached for the aforementioned locations between Table 14 and Table 15.

**Table 15 Maximum temperatures reached inside the combustor during second campaign**

| | [0] Top vert (K) | [1] Flame 1 (K) | [2] Flame 2 (K) | [3] Flame 3 (K) | [4] Bottom vert (K) | RFG (%) | Power (kW) |
|---|---|---|---|---|---|---|---|
| SC.DM.O | 917 | 1243 | 1373 | 1332 | 1259 | 51 | 120 |
| SC.B1.O | 730 | 1267 | 1267 | 1250 | 1192 | 52 | 80 |
| SC.CC.O | 813 | 1120 | 1122 | 1087 | 1027 | 52 | 99 |

The maximum temperatures achieved in this second campaign were for the test using 100% Daw Mill coal [SC.DM.O], reaching 1373K in the location labelled 'Flame2'. This is assumed to be a consequence, at least partially, of the fact that this was the experiment where higher flowrate of fuel was supplied, as it can be seen comparing the values for thermal power expected in each test.

A comparison of the effect of varying the fuel oxy-fired can be made considering the data presented in Table 15. It is noticeable that even though in the test using biomass [SC.CC.O] the thermal power expected was 20kW$_{th}$ higher than in the case using the coal-biomass blend [SC.B1.O], the temperatures reached in the latter was 145K higher than in the test using 100% biomass; and 106K lower than in the test using 100% coal. Another effect caused by the variation of the fuel used, that can be seen from the temperatures reached in the top of the vertical combustor [0] comparing the tests [SC.DM.O] and [SC.B1.O], is the change in the location of the flame downwards when increasing the share of biomass. However, it is necessary to double check this conclusion by looking at the results from the third campaign, where more tests were carried out, so a better analysis can be done.

### 4.2.3 Third campaign: temperatures and heat fluxes co-firing coal-biomass blends under air and oxy-firing conditions

Table 16 summarises the maximum temperatures as well as maximum and average heat fluxes reached during the third experimental campaign. Additionally the RFG percentage and the thermal power expected are included to allow for a better analysis of the results.

**Table 16 Maximum temperatures and heat fluxes reached inside the combustor during third campaign**

| | [0] Top vert (K) | [1] Flame1 (K) | [2] Flame2 (K) | [3] Flame3 (K) | [4] Bottom vert (K) | Heat $flux_{Max}$ ($kW/m^2$) | Heat $flux_{Av}$ ($kW/m^2$) | RFG (%) | Power (kW) |
|---|---|---|---|---|---|---|---|---|---|
| TC.EC.A | 803 | 1345 | 1346 | 1230 | 1135 | 42.9 | 35.8 | - | 108 |
| TC.B1.A | 797 | 1384 | 1381 | 1226 | 1126 | 33.7 | 29.2 | - | 108 |
| TC.CC.A | 819 | 1377 | 1374 | 1224 | 1110 | 85.5 | 31.4 | - | 101 |
| TC.EC.O.(a) | 847 | 1437 | 1430 | 1339 | 1158 | 191.7 | 153.8 | 60 | 119 |
| TC.EC.O.(b) | 819 | 1401 | 1393 | 1307 | 1204 | - | - | 58 | 101 |
| TC.EC.O.(c) | - | 1508 | 1501 | 1373 | 1238 | 188.5 | 149.9 | 70 | 125 |
| TC.B2.O | 799 | 1379 | 1377 | 1251 | 1139 | 38.8 | 33.6 | 67 | 105 |
| TC.B1.O.(a) | 860 | 1418 | 1422 | 1305 | 1195 | - | - | 48 | 114 |
| TC.B1.O.(b) | | 1384 | 1380 | 1255 | 1161 | 82.7 | 63.8 | 60 | 105 |
| TC.CC.O | 873 | 1378 | 1382 | 1247 | 1174 | 150.6 | 109.9 | 54 | 118 |

**Temperature**

From the table above, the maximum temperatures are achieved at the locations labelled ‘Flame1’ and ‘Flame 2’, so the flame was situated closer to the burner. In contrast the second campaign, no evidence of movement of the flame to be more detached from the burner when increasing the share of biomass supplied is found seeing the data reported in Table 16.

The maximum temperature reached was 1508K when oxy-firing El Cerrejon coal in the test labelled TC.EC.O.(c). The noticeable difference between the temperatures obtained in this test compared to the rest, 70K in the best case, is assumed to be a consequence of the higher flowrate of coal supplied during this test.

Analysing the effects of changing the type of combustion, it can be observed that the temperature reached for the case where oxy-firing 100% El Cerrejon coal [TC.EC.O.(b)] was 55K higher than in the corresponding case [TC.EC.A] under air-firing conditions, considering tests with similar thermal power expected. However, for

those tests using coal-biomass blends and pure biomass, the thermal levels reached under air and oxy-firing conditions were equivalent.

Comparing the temperatures reported when using different coal-biomass shares under oxy-firing conditions, the cases with 100% El Cerrejon coal were the ones with maximum thermal profiles, and these were 20K higher than the cases using blends and 100% biomass. Interestingly, using air-fired combustion, the temperatures reached are higher for those cases using coal- biomass blends and pure biomass. Note that no final conclusions should be inferred from the differences observed from case to case. This is because the temperatures measured near the flame were taken in three specific locations; but the transversal gradients of temperature can be very pronounced inside the chamber and different between cases.

**Heat flux**

Previously to the analysis of the data reported with regards to heat fluxes, it is necessary to bear in mind that some problems were observed in the performance of the heat flux sensor. The readings obtained were exceptionally low for some of the tests ([TC.EC.A], [TC.B1.A], [TC.B2.O], [TC.B1.O.(b)]). It is believed that for a few of these tests ([TC.EC.A], [TC.B2.O], [TC.B1.O.(b)]) the cause of the low measurements was ash deposition on the sensor lens. However, test [TC.B1.A] shows no evidence of this possible cause for the malfunctioning, as the sensor was cleaned before the test and re-calibrated after finishing the third experimental campaign to double check that no drift had occurred.

The comparison of the results for heat fluxes were based on the average value measured, and extrapolated to achieve the same thermal power expected for those cases where it was necessary. The effect of changing the type of combustion can be analysed considering the tests using 100% biomass [TC.CC.A] and [TC.CC.O], to avoid using results from the tests where the measurements of the sensor seems not to be reliable. The averaged values reported for heat fluxes in Table 16, show that the heat flux for oxy-firing conditions is three times higher compared to air-firing. The reported data also shows that changing the type of fuel, from 100% biomass [TC.CC.O] to 100% El Cerrejon coal [TC.EC.O.(a)], increases the heat flux by 1.4 times. It is further observed that the maximum heat flux value for oxy-firing is double the air-firing case. When changing the type of fuel from biomass to coal under oxy-

firing conditions, the maximum heat flux increases by 1.25 times. However, to be able to draw more definitive conclusions, it would be necessary to consider the wall effect on the heat fluxes reached. Unfortunately, the temperatures of the wall were not measured nearby where the heat flux sensor was located, so this evaluation of the contribution of radiation from the wall cannot be accomplished.

The evolution of the temperatures and heat flux inside the combustor is illustrated for tests using 100% biomass under air [TC.CC.A] and oxy-firing [TC.CC.O] conditions, as well as for 100% El Cerrejon coal in oxy-combustion [TC.EC.O.(a)] in Figure 67.

### 4.2.4 Summary of findings

This section summarizes the main findings with regards to temperatures reached and heat fluxes obtained inside the combustor. The temperatures reached in the different locations along the combustor are illustrated in Figure 22.

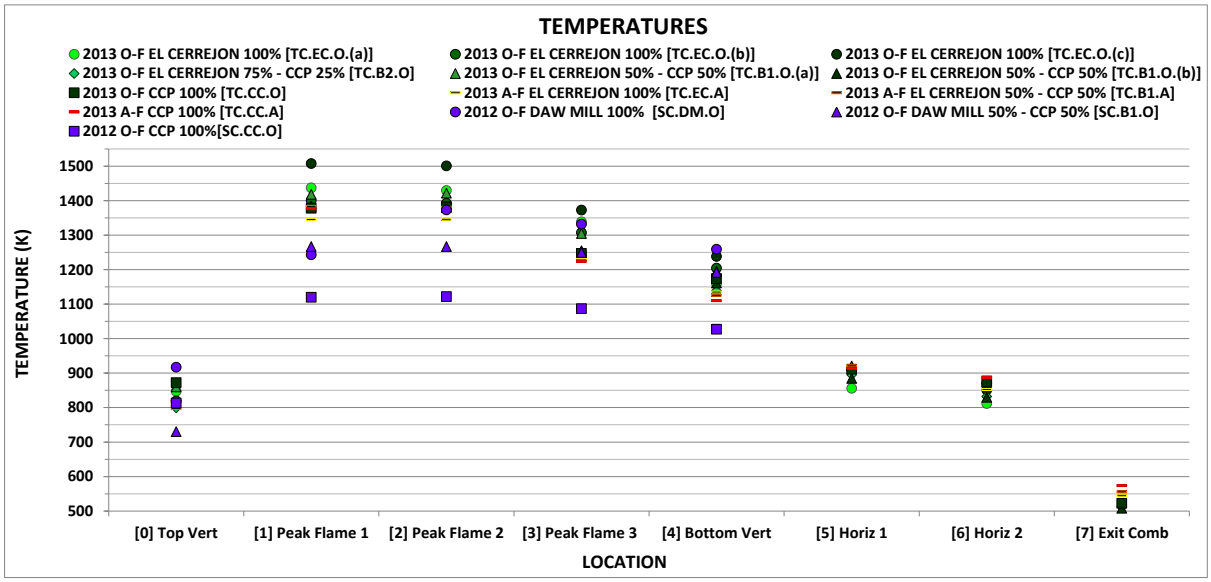


**Figure 22 Summary_ Temperatures**

#### Effect of mode of combustion: air against oxy-firing

Comparing the temperatures obtained under air and oxy-firing conditions for the last experimental campaign, the main outcome is that higher thermal profiles are achieved in the oxy-combustion process reaching temperatures around 50K higher, on average, than in conventional combustion with air, allowing for similar thermal power expected as consequence of the flowrate of fuel supplied.

The results obtained for heat fluxes achieved show that the values obtained under oxy-firing conditions are up to three times the heat fluxes generated in air-firing, looking at the averaged values, and doubles the air-firing case for the maximum heat flux reached.

**Effect of fuel**

- *Coal vs. biomass*. The data presented in Table 16 and Figure 22 suggest that while similar temperatures are reached in air-firing when varying from coal to biomass (with similar thermal power expected), there is a noticeable difference when changing the type of fuel under oxy-firing conditions. In the case of oxy-firing El Cerrejon coal temperatures 20K higher than for 100% biomass or coal-biomass blends were seen. Regarding the results obtained for heat fluxes, the increase obtained as consequence of using El Cerrejon coal was 1.4 times higher than the heat flux using 100% biomass under oxy-firing conditions (averaged values), and 1.25 times higher comparing maximum heat fluxes reached using pure coal. No significant difference was observed when varying the type fuel in combustion with air.
- *Daw Mill vs. El Cerrejon.* The main difference observed in Figure 22 is the higher temperatures reached in the cases where using El Cerrejon coal compared to when using Daw Mill coal. This is believed to be a consequence of two facts: the higher calorific value of El Cerrejon coal and the better performance of the rig during the last experimental campaign.

## 4.3 Ash deposits and fly ash

The analysis and characterisation techniques used for the ashes sampled are listed below:

- ESEM/EDX: Environmental Scanning Electron Microscope and Energy Dispersive X-ray Spectroscopy. This analysis provides with information of the elements present on the surface of the sample.
- XRD: X-ray diffraction. This analysis is particularly recommended for crystalline samples providing information about existing chemical compounds. It is less effective for amorphous materials.
- Modified technique based on thermogravimetric analysis using consecutively inert and oxidizing atmospheres [(Fan and Brown, 2001), (Zhao et al., 2013)].

This method is used to characterise the remaining carbon in the ash sampled. However, the sample's weight is not measured during all the process, but: at the beginning, after passing one hour in an inert-atmosphere ($N_2$) furnace at 1023K, and after passing one hour in an oxidizing- atmosphere (air) furnace at 1023K.

### 4.3.1 Analysis of ash deposits from oxy-firing Daw Mill coal/cereal co-product

The results from the ESEM/EDX analyses of the ashes sampled are reported in Table 17. For their evaluation, a comparison with the previous analysis of the deposits generated from parent fuels produced under air-firing conditions provided in Table 4 will be done.

**Table 17 ESEM/EDX Analyses (% wt.) for Daw Mill coal/CCP under oxy-firing conditions**

| | FC.DM.O(d) | SC.DM.O | SC.B1.O | SC.CC.O |
|---|---|---|---|---|
| O | 47.81 | 40.94 | 50.15 | 45.42 |
| Na | 1.34 | 0.97 | 0.00 | 0.00 |
| Mg | 0.51 | 0.00 | 0.90 | 1.35 |
| Al | 13.77 | 8.98 | 4.50 | 4.15 |
| Si | 18.55 | 13.88 | 22.60 | 19.25 |
| P | 0.00 | 0.00 | 2.51 | 3.58 |
| S | 0.64 | 1.01 | 0.94 | 2.35 |
| K | 2.03 | 2.04 | 8.48 | 16.94 |
| Ca | 1.04 | 2.00 | 5.37 | 5.65 |
| Ti | 0.83 | 0.59 | 0.00 | 0.00 |
| Fe | 12.78 | 29.59 | 4.55 | 0.68 |
| Cu | 0.71 | 0.00 | 0.00 | 0.47 |
| Cl | 0.00 | 0.00 | 0.00 | 0.16 |

It can be seen from the data reported in Table 4 compared to Table 17, that for elements such as K, Mg, Fe, and Ti, the trend followed agrees with the previous analysis: in the cases of K and Mg increasing with the percentage of biomass, and for Fe and Ti rising with the percentage of coal. Other elements (O, Si) do not show a clear pattern. The molar ratio of oxygen to silicon was studied to see if $SiO_2$ was the main Si-compound formed. A ratio of around 2 would confirm this, but the results

showed ratios in the range of 3.8 to 5.2. The ratio Al/Si corresponds to the previous analysis of the parent fuels for the cases using 100% Daw Mill coal and the coal-biomass blend. However, for the case of 100% CCP, the Al/Si resulted is three times higher than expected. Ca content increases with the share of biomass, showing an opposite behaviour to that expected.

The S content in ash increases with the share of biomass in the fuel fired; contrary to expectations, given the elemental analysis of the parent fuels shown in Table 4 (the S content in Daw Mill coal is eight times higher than in biomass). It is possible that this is due to the higher content of K in deposits generated from 100% CCP, as higher K in the fuel means more $K_2SO_4$ is likely to form. The fact of the higher content in S of the ash sampled from the tests using biomass, as a blend or pure, will be further analysed in the discussion section.

Cl content was only detected in the deposits generated when oxy-firing 100% cereal co-product. This result is explained considering the fuel composition (see Table 4), where the ultimate analysis shows similar Cl contents for Daw Mill coal and the biomass; and the ash analysis presents higher K presence for CCP. This leads to formation of KCl in the case of the biomass, while in the case of Daw Mill coal, the K available is only enough to react with the sulfur present, as this reaction is in competition and more favoured than the KCl generation reaction. This is an important observation due to the high corrosive characteristics of KCl. Further justifications for this will be presented in the discussion section.

The images generated as result of the ESEM/EDX analyses are presented in Figure 68 to Figure 71 (see Appendix D.2). From these pictures, it can be clearly seen that the particle size increases with the share of biomass.

### 4.3.2 Analyses of ash deposits and fly ash from co-firing coal-biomass blends under air and oxy-firing conditions

Figure 23 illustrates the deposit probes during the ash sampling for six of the tests accomplished in the third campaign. Images from a) to c) correspond to air–firing tests and d) to f) correspond to oxy-firing cases, varying the type of fuel: 100% El Cerrejon coal, 50% El Cerrejon coal-50% CCP and 100% CCP.

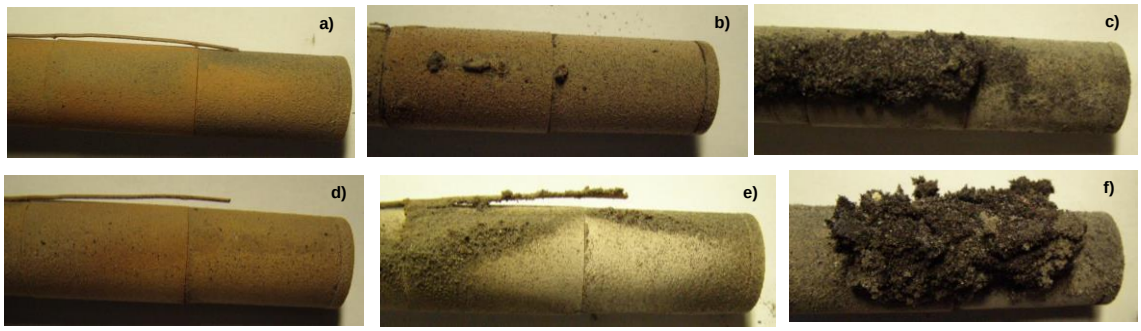


**Figure 23 Ash deposit probes for tests: a) [TC.EC.A] b) [TC.B1.A] c) [TC.CC.A] d) [TC.EC.O.(c)] e) [TC.B1.O.(b)] f) [TC.CC.O]**

From these images, it is noteworthy the fact that when using 100% CCP the structure of the deposit is more fibrous and porous than when oxy-firing 100% El Cerrejon coal or the coal-biomass blend. No significant difference in the aspect of the deposits can be observed comparing the cases under oxy and air-firing conditions.

#### 4.3.2.1 ESEM/EDX Results

The results from the ESEM/EDX analyses of the ashes sampled at high temperature in the third experimental campaign are reported in Table 18. To evaluate these results, a comparison with the previous analysis of the deposits generated from parent fuels produced under air-firing conditions provided in Table 4 was made.

**Table 18 ESEM/EDX Analyses (% wt.) for El Cerrejon coal/CCP under air and oxy-firing conditions_ High temperature probe (1023K)**

| | TC.EC.A | TC.B1.A | TC.CC.A | TC.EC.O. (b) | TC.EC.O. (c) | TC.B1.O. (a) | TC.B1.O. (b) | TC.B2.O | TC.CC.O |
|---|---|---|---|---|---|---|---|---|---|
| O | 45.45 | 45.05 | 41.74 | 41.05 | 43.91 | 46.04 | 45.06 | 43.62 | 42.72 |
| Na | 1.45 | 0.93 | 0.34 | 2.08 | 1.15 | 0.58 | 0.50 | 0.96 | 0.80 |
| Mg | 0.91 | 1.10 | 1.17 | 1.04 | 0.82 | 1.11 | 0.96 | 0.83 | 1.15 |
| Al | 14.85 | 7.29 | 0.84 | 14.24 | 8.80 | 4.39 | 5.12 | 9.55 | 0.69 |
| Si | 19.73 | 20.47 | 17.38 | 17.69 | 15.04 | 20.60 | 22.57 | 19.96 | 21.73 |
| P | 0.36 | 1.53 | 2.64 | 0.16 | 0.94 | 2.31 | 1.63 | 0.75 | 2.62 |
| S | 3.18 | 3.77 | 5.26 | 1.19 | 4.54 | 3.35 | 3.37 | 2.05 | 4.19 |
| K | 1.72 | 11.56 | 21.3 | 1.28 | 11.08 | 13.00 | 11.85 | 5.21 | 19.46 |
| Ca | 3.83 | 4.15 | 5.28 | 4.20 | 2.75 | 4.84 | 4.15 | 3.52 | 4.77 |
| Ti | 1.23 | 0.43 | 0.00 | 1.09 | 0.66 | 0.30 | 0.34 | 0.81 | 0.00 |
| Fe | 6.59 | 3.73 | 0.79 | 15.27 | 9.21 | 3.47 | 4.44 | 5.32 | 0.77 |
| Cl | 0.00 | 0.00 | 0.00 | 0.00 | 0.00 | 0.00 | 0.00 | 0.00 | 1.09 |

| | TC.EC.A | TC.B1.A | TC.CC.A | TC.EC.O. (b) | TC.EC.O. (c) | TC.B1.O. (a) | TC.B1.O. (b) | TC.B2.O | TC.CC.O |
|---|---|---|---|---|---|---|---|---|---|
| Ba | 0.71 | 0.00 | 0.00 | 0.70 | 0.00 | 0.00 | 0.00 | 0.00 | 0.00 |
| Cr | 0.00 | 0.00 | 0.00 | 0.00 | 1.10 | 0.00 | 0.00 | 0.00 | 0.00 |

From the data presented in the table above, the majority of the elements detected follow the trend set by the previous analysis of parent fuels, shown in Table 4. The trend observed for Na, Al, Ti and Fe is to increase with the share of El Cerrejon coal. On the other hand, the contents of Mg, P, K, Ca and Cl increase with the percentage of biomass used in the fuel. For the particular case of P, this trend is less marked than it should be considering the previous analysis of the parent fuels. It is interesting also that the low K contents obtained for the tests using 100% El Cerrejon, are consistent with the fact that, generally, in coals, this element tends to be mixed with the clay present, preventing its release; contrarily to what happens in the case of biomass where there is no clay present.

The two elements that do not show clear patterns are Si and S, similarly to the results for previous campaigns. The Si contents are similar for all the cases reported, even though it should be higher for those cases with more percentage of El Cerrejon coal. The tests with maximum Si levels are those using the coal-biomass blend B1 and 100% CCP. An evaluation of the molar ratio of oxygen to silicon was carried out to see if it was around 2. However, the results showed that these ratios presented values between 3.4 and 5.1, so there was a low possibility of $SiO_2$ forming as the main species. Another interesting ratio to examine is the relation between aluminium and silicon. The Al/Si ratio detected for cases using coal-biomass blends and pure biomass corresponds to the ratios in the parent fuels in Table 4. However, the Al/Si ratio resulted for the cases using 100% El Cerrejon coal, under air and oxy-firing, is twice the value of the ratio expected. For the S content, similar values are observed when using pure biomass or coal, even though the ultimate analysis, presented in Table 4, shows that El Cerrejon coal has 3.5 times more sulfur that the CCP. This observation could have the same explanation mentioned in the previous subsection, where results from using Daw Mill coal/CCP were analysed: the higher content of K in deposits generated when using biomass, makes more likely $K_2SO_4$ to form.

Ba content has been only detected for the cases when using 100% El Cerrejon coal, under air-and oxy-firing conditions. This observation is in agreement with the low level of Ba presented in the previous analysis of CCP (see Table 4).

The results obtained from the ESEM/EDX analyses carried out to ash deposited on the medium temperature probe (923K) are presented in Table 19.

**Table 19 ESEM/EDX Analyses (% wt.) for El Cerrejon coal/CCP under air and oxy-firing conditions_ Medium temperature probe (923K)**

| | TC.EC.A | TC.B1.A | TC.CC.A | TC.EC.O.(c) | TC.B1.O.(b) | TC.B2.O | TC.CC.O |
|---|---|---|---|---|---|---|---|
| O | 45.45 | 46.67 | 46.60 | 43.91 | 45.06 | 43.58 | 47.61 |
| Na | 1.45 | 0.72 | 0.43 | 1.15 | 0.50 | 1.71 | 0.41 |
| Mg | 0.91 | 1.27 | 1.19 | 0.82 | 0.96 | 1.14 | 1.41 |
| Al | 14.85 | 4.24 | 0.69 | 8.80 | 5.12 | 7.41 | 0.00 |
| Si | 19.73 | 21.88 | 26.04 | 15.04 | 22.57 | 14.31 | 20.36 |
| P | 0.36 | 2.04 | 2.09 | 0.94 | 1.63 | 1.78 | 3.23 |
| S | 3.18 | 3.77 | 1.45 | 4.54 | 3.37 | 5.60 | 2.71 |
| K | 1.72 | 10.34 | 15.76 | 11.08 | 11.85 | 12.96 | 16.14 |
| Ca | 3.83 | 5.14 | 4.77 | 2.75 | 4.15 | 2.78 | 5.23 |
| Ti | 1.23 | 0.35 | 0.00 | 0.66 | 0.34 | 0.55 | 0.00 |
| Fe | 6.59 | 3.60 | 0.96 | 9.21 | 4.44 | 8.18 | 0.91 |
| Ba | 0.71 | 0.00 | 0.00 | 0.00 | 0.00 | 0.00 | 0.00 |
| Cr | 0.00 | 0.00 | 0.00 | 1.10 | 0.00 | 0.00 | 0.00 |

The observations made for the ashes sampled at high temperature (1023K) are valid, in general, for the results from the ESEM/EDX analyses to the ash deposits at medium temperature (923K) presented in the table above, except for two elements: Si and S.

The presence of silicon has been analysed together with the contents obtained for oxygen in case it showed evidence of being forming $SiO_2$, but the ratios observed were too high for this, between 3.4 and 5.3. This fact can be further evaluated when the results of the XRD analyses are presented (see next subsection). For the Al/Si ratios, similar results to the ones at high temperature are observed: keeping the ratio of the previous analyses shown in Table 4 those cases using coal-biomass blends and pure biomass.

The S levels reported show a maximum for the tests using coal-biomass blends, and the minimum when using 100% CCP. However, the levels reached for the tests with 100% CCP are still higher than expected considering the ultimate analysis of the parent fuels, being the most probable explanation to this fact the $K_2SO_4$ formation already described. These observations have been made considering air and oxy-firing cases.

The images resulted from the ESEM/EDX analyses are presented in Figure 72 to Figure 78 (see Appendix D.2). From these pictures, it can be seen that the larger size of the ash particles occur when increasing the percentage of biomass, as in previous campaigns.

#### 4.3.2.2 XRD Results

In this section, the results from the XRD analyses are presented comparing the air case versus oxy-firing for a given type of fuel; or making the comparison between results generated varying from 100% coal to 100% biomass maintaining the combustion mode.

For the case using 100% El Cerrejon coal, the spectra generated for ashes sampled under air-firing (black) and under oxy-firing conditions (red) are illustrated in Figure 24. The peaks corresponding to compounds observed to be different between the two cases are highlighted in the graph.

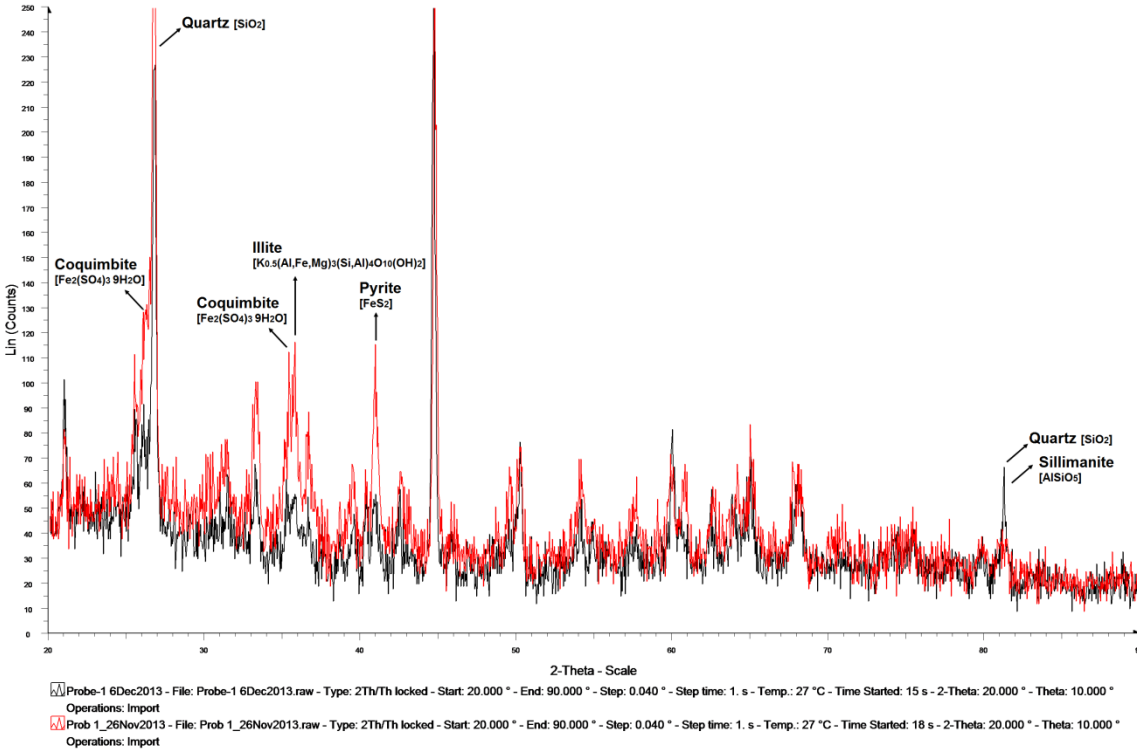


**Figure 24 XRD charts for El Cerrejon coal ashes collected at 970K; test [TC.EC.A] (black spectrum) against [TC.EC.O (c)] (red spectrum)**

From the graph above, it can be seen that under oxy-firing conditions using 100% coal, compounds such as quartz, coquimbite, illite, or pyrite are present at higher levels than in the air-firing case. The only compound found to have higher contents in air combustion is sillimanite. Additionally, Figure 79, Figure 80 and Figure 81 (see Appendix D.3) illustrate the specific XRD results where the main compounds are labelled, allowing for a more precise analysis to identify in which form Si is presented. From these charts, it can be seen that Si apart from forming quartz: also forms nickel-silicate-nickel-olivine, olivine, aluminium-iron-silicon, illite, kaolinite, mullite and sillimanite. However, the last compound was only found in ashes generated under air-firing conditions.

For the case using 50% El Cerrejon coal-50% CCP, the spectra generated for ashes sampled under air-firing (red) and under oxy-firing conditions (black) are illustrated in Figure 25.

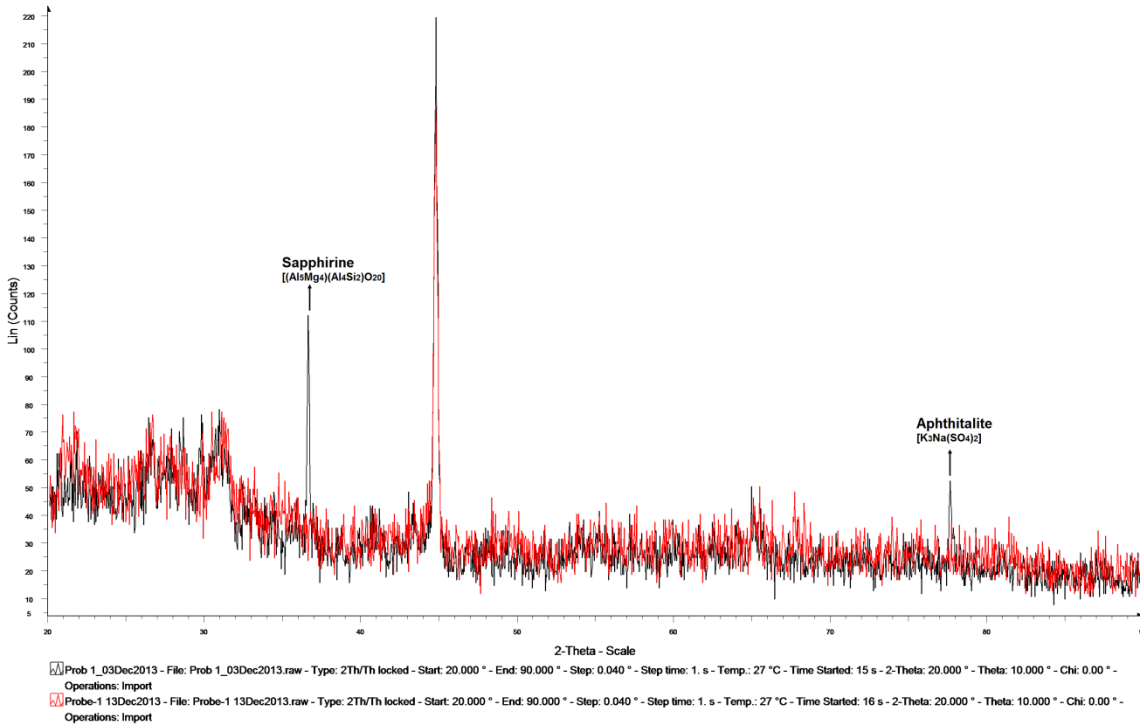


**Figure 25 XRD charts for 50% El Cerrejon coal-50% CCP ashes collected at 920K; test [TC.B1.A] (red spectrum) against [TC.B1.O (b)] (black spectrum)**

From the graph above it can be seen that the main compounds that are observed to be different in the oxy-combustion case for the coal-biomass blend are sapphirine and aphthitalite.

For the case using 100% CCP, the spectra generated for ashes sampled under air-firing (red) and under oxy-firing conditions (black) are illustrated in Figure 26.

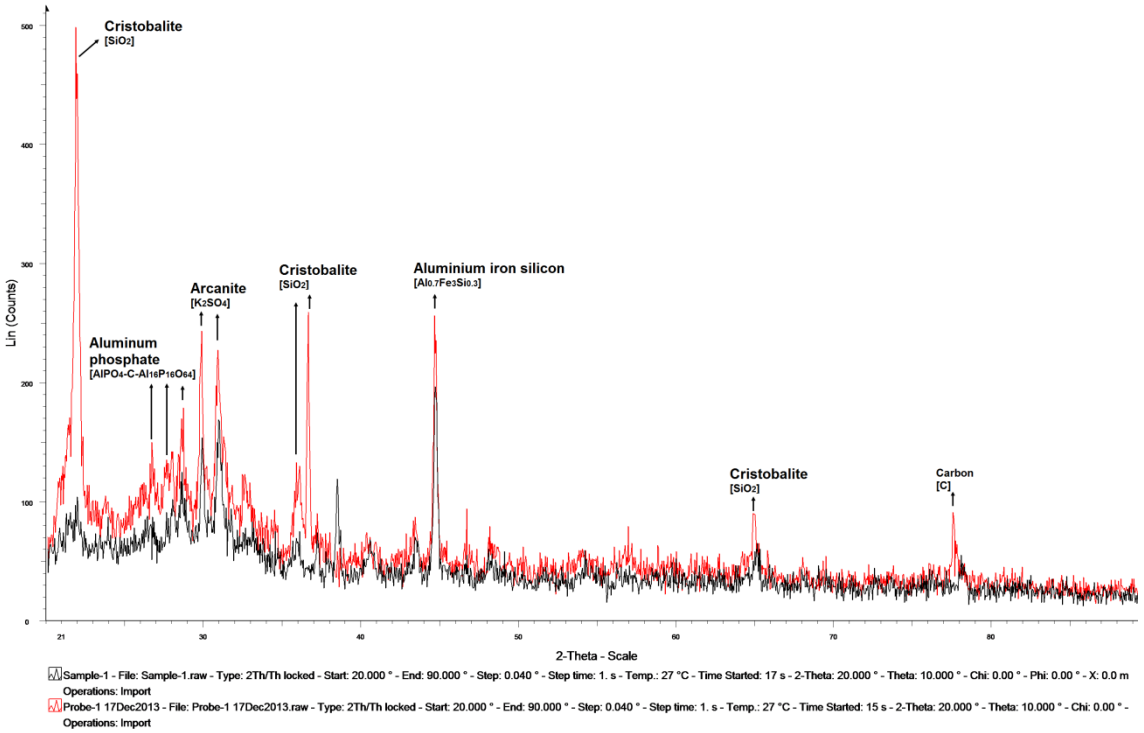


**Figure 26 XRD charts for 100% CCP ashes collected at 940K; test [TC.CC.A] (red spectrum) against [TC.CC.O] (black spectrum)**

Contrary to the situation for 100% coal and coal-biomass blend, using 100% CCP leads to higher levels of a range of different compounds for the air-firing case. Silicon appears to form mainly cristobalite ($SiO_2$), but also some aluminium iron silicon compounds. Other compounds such as aluminium phosphate and arcanite ($K_2SO_4$) appear to have a higher concentration under air-firing conditions.

For the comparison of the results obtained for 100% El Cerrejon coal and 100% CCP under oxy-firing conditions, the corresponding spectra are presented in Figure 27.

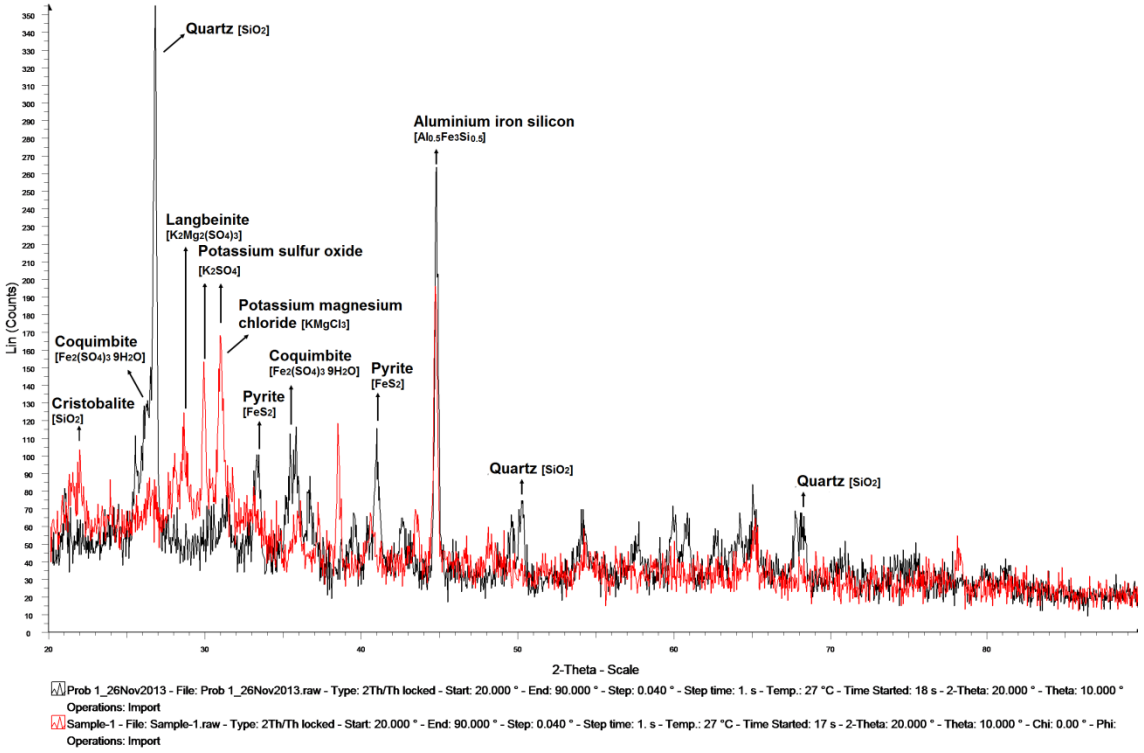


**Figure 27 XRD charts for 100% El Cerrejon coal and 100% CCP ashes collected at 970K; test [TC.EC.O (c)] (black spectrum) against [TC.CC.O] (red spectrum)**

From the figure above, it can be seen that compounds such as quartz ($SiO_2$), aluminium iron silicon, coquimbite and pyrite are dominant for ashes generated oxy-firing El Cerrejon coal. On the other hand, when using 100% CCP the levels of cristobalite ($SiO_2$), potassium sulfur oxide and potassium magnesium chloride are higher than for the pure coal case.

### 4.3.2.3 Characterisation of particles: size distribution and shape

An attempt to determine the size distribution of the ash deposit particles as well as their shape has also been carried out. The average results are displayed in Table 20.

**Table 20 Average grain size and shape of ash deposit and parent fuels particles**

| | EC | CCP | TC.EC.A | TC.B1.A | TC.CC.A | TC.EC.O. (c) | TC.B1.O. (b) | TC.CC.O |
|---|---|---|---|---|---|---|---|---|
| Spherical (μm) | - | 23.84 | 24.86 | 36.34 | 36.57 | 39.36 | 51.32 | 36.21 |
| Non Spherical (μm) | 80.70 | 42.48 | 59.20 | 55.42 | 55.37 | 61.89 | 70.17 | 82.9 |
| Total (μm) | - | 40.29 | 46.81 | 49.15 | 46.71 | 52.88 | 63.40 | 67.34 |

The data presented in the table above shows what it had been already anticipated at the beginning of this subsection 4.3.2: that we observe smaller size of the particles as the share of coal increases. This occurs for all the cases considering spherical particles, and for half of the cases analysed regarding the fraction of non-spherical particles. It is also noticeable that the non-spherical particles are larger, typically in the range of 1.4 to 2.6 times bigger, compared to the spherical ones. Another interesting observation is the relationship between particle's sizes of parent fuels and ashes generated: while El Cerrejon coal's particles decrease their size down to 75% of their original size after the oxy-combustion, the biomass particles show an increase in the range of 1.2 to 1.6 times their initial size.

The results of the size distribution analyses carried out for the parent fuels are displayed in Figure 82 and Figure 83, Appendix D.4. Additionally, charts showing the size distribution for ashes generated from oxy-firing 100% El Cerrejon coal and 100% CCP are presented in Figure 84 and Figure 85 (see Appendix D.4). From these data, the uneven size distribution for both cases presented is clear, and in general this applies for all the analyses performed.

#### 4.3.2.4 Carbon in ash results

The results obtained after performing the carbon in ash evaluation using the technique explained at the beginning of this section (see p. 86) are presented in Table 21.

**Table 21 Carbon in ash results (%). Location A: Probe 1; B: Probe 2; B*: Horizontal chamber; C: Cyclone**

| LOC | TC.EC.A | TC.B1.A | TC.CC.A | TC.EC.O. (b) | TC.EC.O. (c) | TC.B1.O. (a) | TC.B1.O. (b) | TC.B2.O | TC.CC.O |
|---|---|---|---|---|---|---|---|---|---|
| A | 0.0 | 0.0 | 0.0 | 0.0 | 0.0 | 0.0 | 0.0 | 0.0 | 0.0 |
| B | 31.4* | 0.0 | 0.0 | 0.0 | 43.5* | :0.0 | 0.0 | 30.5* | 0.0 |
| C | 38.3 | 33.2 | 30 | 9.4 | 7.38 | 11.4 | 16.15 | 8.9 | 8.3 |

From these data, it is clear that the ashes sampled nearby the flame (locations A and B) do not contain any unburnt carbon. For the ashes sampled further from the flame location, in the horizontal section of the combustor (denoted with B*) the unburnt carbon is quite high, similarly to what is observed for the case of the fly ashes sampled from the cyclone (location C). However, there is a significant decrease for

the unburnt carbon in the oxy-firing cases compared to the percentages obtained under air-firing conditions. This may be consequence of the higher temperatures and $O_2$ concentration for the oxy-firing tests. A possible reason for the overall high levels in unburnt carbon observed for fly ashes could be the size distribution, with excessive fraction of large particles, in which El Cerrejon coal was supplied.

Images of the crucibles containing the ashes evaluated, before and after the carbon in ash test, are presented in Figure 86 for different fuels under oxy-firing conditions (see Appendix D.5). It can be seen in these pictures that there is always a dummy crucible. This empty crucible was used to allow for changes in measurements resulting from variations in environmental conditions, which would cause changes in weight readings which were not due to the mass loss of the sample during the combustion process.

### 4.3.3 Summary of findings

This section summarizes the main findings with regards to ash deposits composition and size distribution, as well as carbon in ash remaining after the combustion of the fuel under air and oxy-firing conditions.

Regarding the appearance of the ash deposits collected, these results show they are more fibrous and porous for ashes sampled when increasing the share of CCP in the fuel. This fact is supported by the results obtained for size distribution where cases using biomass showed higher average particle sizes.

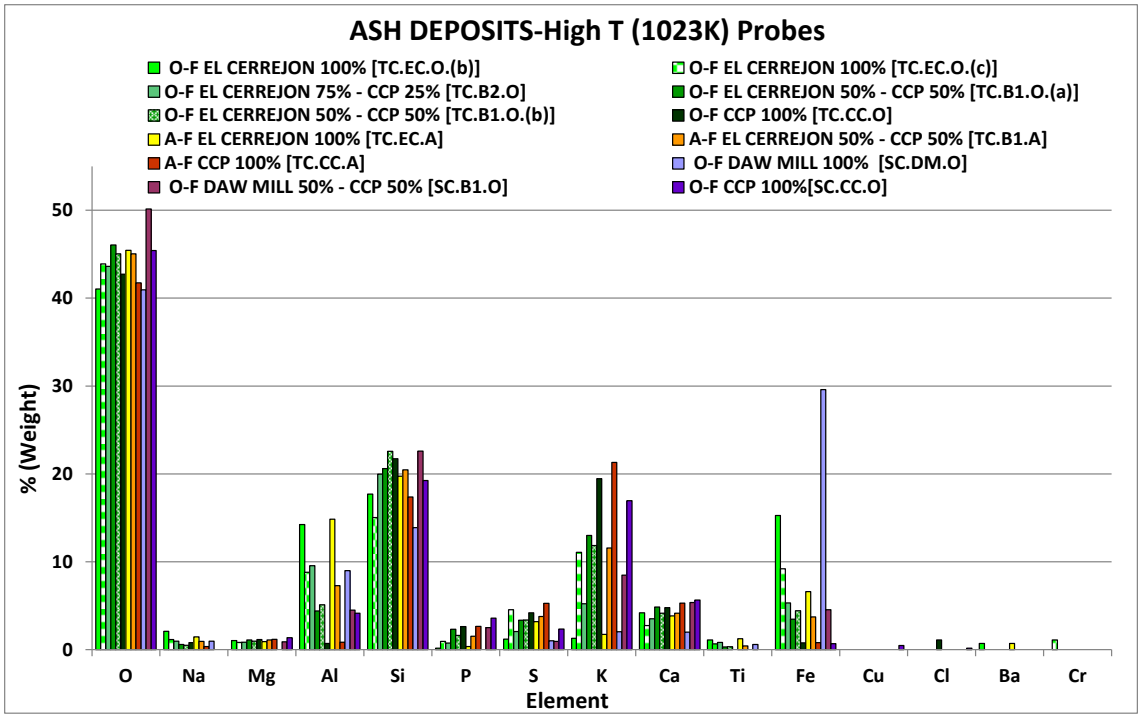


**Figure 28 Summary_ ESEM/EDX Results**

From the results obtained for the ESEM/EDX analyses, similar trends have been found at high (1023K) and medium (923K) sampling temperatures, where most of the elements followed the trend demonstrated by the previous analyses of the ashes under air-firing conditions. The ESEM/EDX results for the second and the third campaign at high temperature are illustrated in Figure 28. The main exceptions found to these trends have been S and Si. The similar S levels reached in all cases, even though Daw Mill coal and El Cerrejon coal have 8 and 3.5 times more S than CCP, respectively, and this has been explained by the fact that the higher K levels contained in the biomass would lead to much larger formation of $K_2SO_4$. The Si contents reported were analogous as well for all the tests, although the trend expected was to increase with the percentage of coal used. The XRD results have shown that the case of oxy-firing CCP presented much higher $SiO_2$ levels than the air–firing case using this fuel. Additionally, the Al/Si ratios reported when using coal-biomass blends and pure biomass correspond to the ratios set by the parent fuels, contrary to what happens with the case using 100% El Cerrejon coal where the Al/Si ratio resulted is twice the value expected. The low K contents obtained for cases using Daw Mill and El Cerrejon are consistent with the fact that this element tends to be mixed with the clay present in coals, preventing their release. Chlorine has been only detected in the ash deposits for the cases using pure biomass under oxy-firing

conditions; a result that is supported by the XRD analyses comparing pure coal and pure biomass where higher presence of potassium magnesium chloride is observed for the case using 100% CCP.

The main outcomes from the XRD analyses are:

- When using 100% coal under oxy-firing conditions, compounds as quartz, coquimbite, illite, or pyrite are present higher levels than in the air-firing case
- When using 100% biomass under oxy-firing conditions, Si forms mainly cristobalite ($SiO_2$)
- When using 100% biomass under air-firing conditions, higher levels of aluminium phosphate and arcanite ($K_2SO_4$) are observed

It is worth noting that the XRD results are complementary to the ESEM/EDX analyses as the X-Ray Diffraction technique evaluates only crystalline forms and most content of the ash deposits in this project are amorphous.

The results for the carbon in ash have shown that for the ashes sampled in the locations nearby the flame, the unburnt C was zero for all the cases. However, high percentages of carbon in ash have been reported for ashes sampled from the horizontal section and the cyclone. Elevated levels for unburnt C were observed for air-firing cases compared to oxy-firing, where the combustion process is assumed to be enhanced by the higher $O_2$ concentrations and higher temperatures reached. However, no clear trend was found by varying the type of fuel.

## 4.4 $SO_3$ Results from third campaign: air and oxy-firing cases

The results for $SO_2$ and ($SO_3$+$SO_4^{2-}$) analyses applying the controlled condensation method (NCASI Southern Regional Center, 1996) with the modification in the procedure, mentioned in section 3.2.1, to evaluate the levels of these species under air and oxy-firing conditions for different fuels are presented in Table 22. The results obtained are displayed against the average $SO_2$ values recorded using the FTIR for the same period of time when the $SO_x$ sampling train was operating. Additionally, the concentrations resulted from the CCM technique are presented in ppmv and in $mg/m^3$ to simplify the comparison of these values with data published in the literature referenced.

**Table 22 SOx Results**

| | $SO_2$ [FTIR] | $SO_2$ [CCM] | | $(SO_3+SO_4^{2-})$ [CCM] | | $(SO_3+SO_4^{2-})$ /$SO_2$ | $(SO_3+SO_4^{2-})$ /$SO_2$ |
|---|---|---|---|---|---|---|---|
| | (ppmv) | (ppmv) | ($mg/m^3$) | (ppmv) | ($mg/m^3$) | (%) ppmv | (%) $mg/m^3$ |
| TC.EC.A | 305.2 | 83.5 | 218.7 | 3.0 | 11.9 | 3.6 | 5.5 |
| TC.B1.A | 274.3 | 245.8 | 643.5 | 16.6 | 66.3 | 6.7 | 10.3 |
| TC.CC.A | 87.6 | 98.9 | 258.9 | 20.8 | 83.4 | 21.0 | 32.2 |
| TC.EC.O.(c) | 819.6 | 566.8 | 1483.7 | 16.9 | 67.8 | 3.0 | 4.6 |
| TC.B2.O | 654.3 | 525.2 | 1374.7 | 13.8 | 55.1 | 2.6 | 4.0 |
| TC.B1.O.(b) | 442.2 | 231.4 | 605.7 | 29.5 | 118.1 | 12.7 | 19.5 |

From the table above, it can be seen that similar $(SO_3+SO_4^{2-})$ levels were obtained for tests carried out under air and oxy-firing conditions: rising as the percentage of biomass increases. Also, the results obtained for oxy-firing exceed the levels analysed in the air-firing cases. The $SO_2$ levels increase with the share of coal; the higher concentrations reached for the oxy-firing cases compared to the ones resulted under air-firing conditions and its explanation have been already discussed in section 4.1.3.

The ratio $(SO_3+SO_4^{2-})/SO_2$ seems to be highly dependent on the fuel used, increasing with the share of biomass. A possible cause for this fact could be the high levels of alkalis contained in the fly ashes resulting from coal-biomass blends or pure biomass, act as catalyst for the conversion of $SO_2$ to $SO_3$ as it is suggested by several authors [(Mars and Maessen, 1968);(Hill et al., 2011)]. A second effect of the high content in alkalis of the biomass is its reaction with the $SO_3$ generated to produce sulfates aerosols by nucleation [(Jiménez and Ballester, 2005), (Kuuluvainen et al., 2015)]. Note that the products of this second phase of reactions (aerosols formation) caused one of the interferences that the Method 8A (NCASI Southern Regional Center, 1996) tries to eliminate; however, the procedure followed during the analyses, leads to the evaluation of $(SO_3+SO_4^{2-})$ present in the gas sampled, not only the $SO_3$ content, as it was the original goal. This will be further commented in the discussion section.

The case of air-firing pure coal where the ($SO_3$+$SO_4^{2-}$) and $SO_2$ contents detected, using CCM, are much lower than for the rest of the cases evaluated, this is assumed to be due to an error during the sampling process. It seems that part of the sample was missed, most likely during the rinsing of the sampling train. The complexity of this method and its low reproducibility has already been noted earlier (see section 2.5).

To evaluate the levels of $SO_2$ measured using the CCM, a confidence interval of 95% (Diez et al., 2012) was used. The results of this evaluation show that the only cases where the $SO_2$ concentrations were not within the 95% confidence interval [182.6, 678.4] were TC.EC.A and TC.CC.A. This confidence interval was calculated using the measurements taken with FTIR analyser. This means that 14% of the samples measured with CCM were out of the confidence range established (without considering the case TC.EC.A to calculate this percentage as for this test some sample loss occurred during the analysis).

## 4.5 Acid dew point

In this section the acid dew point of the flue gas generated under oxy-firing conditions will be analysed attending to two criteria:

- Theoretical predictions using experimental gas composition data and the correlations already presented (see section 2.6)
- Experimental data acquired by using electrochemical noise (EN) techniques (see Figure 53 in Appendix B)

### 4.5.1 Theoretical acid dew points

The values calculated for the acid dew points applying the correlations presented in Eq 7 to Eq 9, are presented in Table 23. To carry out these calculations, experimental data from the tests performed during the second and third campaigns were used to provide average concentrations of $H_2O$, $SO_2$, HCl and $NO_2$.

**Table 23 Theoretical acid dew points based on correlations for $SO_2$, HCl and $NO_2$ concentrations**

| | $T_{ADP}$ $SO_2$ (K) | $T_{ADP}$ HCl (K) | $T_{ADP}$ $NO_2$ (K) |
|---|---|---|---|
| SC.DM.O | 335.93 | 340.52 | 322.20 |
| SC.B1.O | 337.18 | 342.38 | 323.54 |
| SC.CC.O | 338.73 | 340.31 | 318.48 |
| TC.EC.A | 311.93 | 311.72 | 296.70 |
| TC.B1.A | 316.23 | 319.17 | 298.32 |
| TC.CC.A | 320.75 | 323.82 | 303.68 |
| TC.EC.O.(a) | 337.02 | 334.22 | 325.30 |
| TC.EC.O.(b) | 335.10 | 332.41 | 324.24 |
| TC.EC.O.(c) | 331.10 | 331.22 | 321.39 |
| TC.B2.O | 332.77 | 333.74 | 321.72 |
| TC.B1.O.(a) | 338.95 | 340.75 | 327.86 |
| TC.B1.O.(b) | 331.86 | 332.92 | 322.65 |
| TC.CC.O | 335.31 | 339.30 | 325.21 |

As can be observed from the above data, comparing acid dew points calculated for tests of the second campaign show higher values, in general, than those calculated for the third campaign conditions. This is explained by the fact that during the second campaign, the condenser had not been installed, so there was more accumulation of acid species causing the acid dew point (ADP) to rise. In the second campaign, the compound causing the highest ADP, between 340 and 342 K, is the HCl regardless the fuel used.

For the ADP estimated considering the conditions of the third campaign, the lowest values for ADP are shown for the air-firing cases, in the range of 311 to 324 K, as it might be expected given the lower concentrations of acid species (see Table 12). The physical meaning of this is that the temperatures of the flue gas can be allowed to fall to lower values without acid condensation occurring. The worst-damage cases considering the oxy-combustion tests during the third campaign are TC.B1.O.(a) and TC.CC.O, between 339 and 341 K, due to HCl condensation. For the rest of the cases, the species causing the highest ADP, and so being the limiting factor, varies between $SO_2$ and HCl.

### 4.5.2 Experimental acid dew points

Data for potential and current were collected using the electrochemical noise probe, through the electrodes connected to its surface, during the oxy-combustion tests. The resistance can be then calculated, from Ohm's Law, working out the potential/current ratio (see Equation 22). These data allow one to estimate the noise resistance (see Equation 23), which is defined by standard deviation for the potential divided by the standard deviation of the current over a period of time, which is a parameter that is inversely proportional to the reaction rate. This relationship is due to the fact that higher rate of reaction give rise to higher current gradients, due to the red-ox reactions occurring on the surface of the probe between the condensed acid species and the metal of the probe. This situation can be represented by Equation 25 and Equation 26.

Ohm's Law:

$$R(\Omega) = \frac{V(V)}{I(A)} \qquad \textbf{Equation 22}$$

Definition of noise resistance:

$$NR(\Omega) = \frac{std(V)}{std(I)} \qquad \textbf{Equation 23}$$

Considering the electrochemical aspect:

$$Reaction\ rate_{Corrosion} \propto \frac{\partial I}{\partial t} \qquad \textbf{Equation 24}$$

Consequently, the relationship between noise resistance and reaction rate is:

$$\uparrow I \ \rightarrow \uparrow \left(\frac{\partial I}{\partial t}\right) \ \rightarrow \uparrow Reaction\ rate_{Corrosion}\ \&\ \downarrow NR \qquad \textbf{Equation 25}$$

$$\downarrow I \ \rightarrow \downarrow \left(\frac{\partial I}{\partial t}\right) \ \rightarrow \downarrow Reaction\ rate_{Corrosion}\ \&\ \uparrow NR \qquad \textbf{Equation 26}$$

This method allows for the identification of periods with high and low noise resistance as a function of any electrochemical activity: the higher the noise resistance the lower the rate of reaction occurring, so little or no acid species condensation is occurring for that time period. This is the basis allowing one to

evaluate the graphs presented below, where the noise resistance is plotted against the temperature of the probe, showing also the theoretical range for acid dew point calculated. Note that the fluctuations in the temperature of the probe represented, labelled as $T_{CAPCIS\ PROBE}$, are a consequence of the different flow rates of cooling air applied to the probe, to see its effect on the electrochemical noise generated.

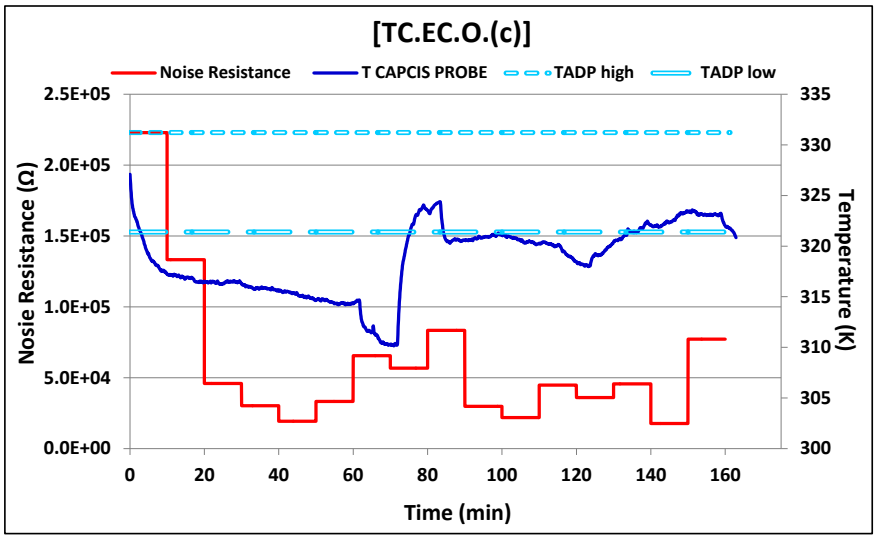


**Figure 29 Electrochemical noise for test TC.EC.O.(c)**

The figure above illustrates the results for the test oxy-firing 100% el Cerrejon coal, and shows how during the periods where the temperature of the probe surface is below the low $T_{ADP}$, the noise resistance decreases sharply, which means that more corrosion is occurring. When the temperature of the probe is between the high and low values for $T_{ADP,}$ there is still corrosion although less, as the noise resistance increases by one order of magnitude.

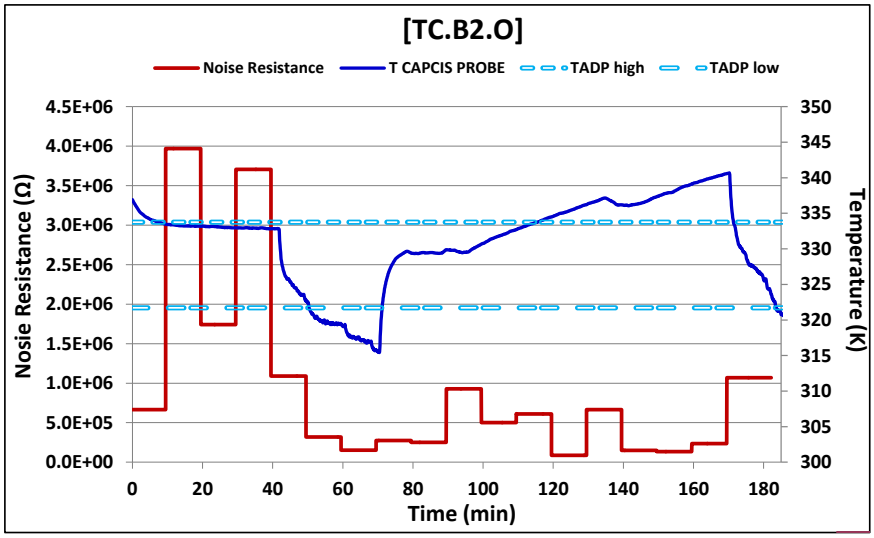


**Figure 30 Electrochemical noise for test TC.B2.O**

The development of noise resistance as a function of time obtained for the test using 75% coal-25% biomass is presented in Figure 30. It can be seen that at the beginning of the test, at temperatures close to the theoretical high $T_{ADP}$, the noise resistance is very high so the corrosion rate is negligible, around 334K. However, there is an intermediate drop of the resistance in that period for which no apparent cause can be found, as the temperatures remain stable. From minute 40, as the temperature of the probe's surface starts to drop, the noise resistance decreases sharply, this suggests that the corrosion rate is speeding up. The value for the noise resistance remains around $5 \cdot 10^5$ Ω, with a few fluctuations until ten minutes before ending the test. The low levels reached for the noise resistance through the end of the test, around $10^5$ Ω, does not correspond with the expected results as the temperature goes over the high $T_{ADP}$ from minute 120. A possible explanation for this could be that, even when the acid species had stopped condensing (the existing temperature is higher than the $T_{ADP}$), the surface of the probe is still soaked with the condensates, so until they evaporate the corrosion continues, and the noise resistance does not start to increase.

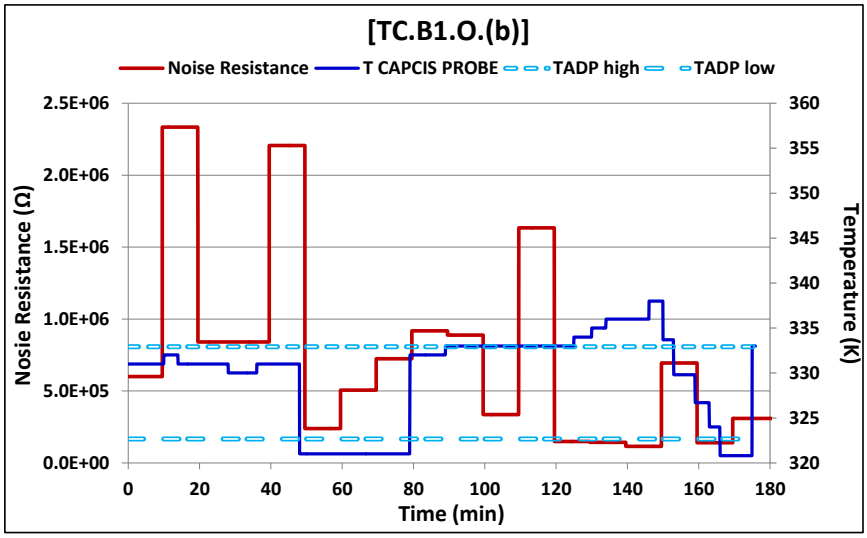


**Figure 31 Electrochemical noise for test TC.B1.O.(b)**

Figure 31 shows the profile obtained for the electrochemical noise in the case of oxy-firing 50% coal- 50%biomass. The noise resistance observed, between $10^6$ and $2 \cdot 10^6$ Ω, when the temperature is slightly below the high $T_{ADP}$ indicates the negligible reaction rate of corrosion during that period of the test. From minute 50, there is an abrupt decrease in the surface temperature of the probe below the low $T_{ADP,}$ which causes the noise resistance to drop down $2.3 \cdot 10^5$Ω, increasing the corrosion rate. From minute 80, the temperature rises until it is close to the high $T_{ADP}$, causing the noise resistance to increase sharply. Towards 120 minutes, there is an inexplicable drop of the resistance, while the temperature of the probe remains over the estimated high $T_{ADP}$. This could mean that the real $T_{ADP}$ is higher than the theoretical estimation, so that the corrosion starts at higher temperatures.

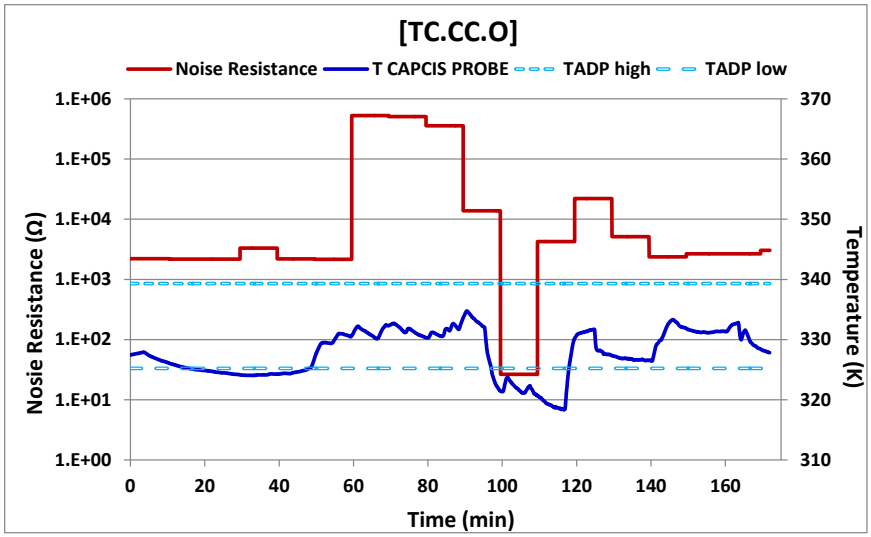


**Figure 32 Electrochemical noise for test TC.CC.O**

The figure above illustrates the electrochemical noise occurring for the case of oxy-firing 100% CCP. The noise resistance remains at low values, around $2 \cdot 10^3 \Omega$, when the temperature of the probe's surface is close to the low $T_{ADP,}$ indicating the high reaction rate of corrosion for that period. From minute 60 there is an increase in the noise resistance up to $5 \cdot 10^5 \Omega$, associated with the rise in the temperature to 330K, middle point between high and low estimated $T_{ADP}$. Later on, there is another drop as a result of the temperature going below the low $T_{ADP}$, and a final increase in the noise resistance as the temperature rises again. In summary for this test, the effect of the surface temperature on the noise resistance seems to be in agreement with the values estimated for the high and low $T_{ADP.}$

### 4.5.3 Summary of findings

As result of the global evaluation carried out, it seems that the relationship between noise resistance and temperature of the probe's surface shows that the corrosion rates are maximum when the temperature goes below the low $T_{ADP}$ estimated; but is not noticeable for the periods where the temperature is between the range set by the high and low $T_{ADP}$. This could mean that the actual acid dew point is lower than the estimated values for the high $T_{ADP}$. So the correlations used result in conservative estimations for the acid dew points.

# 5 MODEL DEVELOPMENT AND RESULTS

This section describes the results produced using the simulation model designed with Aspen Plus® for the main stages for a 100$kW_{th}$ oxy-combustor. These results are compared to the experimental data obtained from running the pilot scale oxy-combustor using different types of fuel and recycle. Subsequently, the agreement between experimental data and results from simulations will be assessed to proceed to the validation of the model.

If validated, the model could be used as a predictive tool to allow for the analysis of effects on the process of key operating conditions and establish the best parameters to optimise the oxy-combustion process using solid pulverised fuels.

## 5.1 Results from equilibrium modelling

The parametric study carried out during the development of the equilibrium model, evaluated the effect on the process caused by the variation of the percentage of recycled flue gas (RFG) and the percentage of oxygen in excess supplied. Table 24 shows the results generated for gas composition and temperatures reached for the last stage of the equilibrium modelling named E4, with the configuration illustrated in Figure 11. For this stage, as it was described in Table 8, the conditions are: 100% El Cerrejon coal, wet recycle (only particle removal), heat loss applied through the recycle so the temperature at which the RFG enters the combustor is 400K, and existence of air ingress into the process that is defined as 1.7%(v/v) of the total gas supplied to the oxy-combustor.

**Table 24 Simulation results_ Gas composition and temperatures-Stage E4**

| RFG (%) | $O_{2,Exc}$ (%) | $O_{2,IN}$ %(v/v) | $O_{2,OUT}$ %(v/v) | $H_2O_{,OUT}$ %(v/v) | $CO_{2,OUT}$ %(v/v) | $CO_{,OUT}$ (ppmv) | $SO_{2,OUT}$ (ppmv) | T (K) | Heat Transfer (kW) |
|---|---|---|---|---|---|---|---|---|---|
| Air-firing | 21 | 21 | 2.76 | 6.3 | 14.71 | 2500 | 465 | 1996 | 80.56 |
| 60 | 0 | 33.83 | 3.92 | 25.33 | 53.57 | 78443 | 1908 | 2458 | 80.76 |

| RFG (%) | $O_{2,Exc}$ (%) | $O_{2,IN}$ %(v/v) | $O_{2,OUT}$ %(v/v) | $H_2O_{,OUT}$ %(v/v) | $CO_{2,OUT}$ %(v/v) | $CO_{,OUT}$ (ppmv) | $SO_{2,OUT}$ (ppmv) | T (K) | Heat Transfer (kW) |
|---|---|---|---|---|---|---|---|---|---|
| | 5 | 35.79 | 6.21 | 24.79 | 53.89 | 58404 | 1856 | 2445 | 82.45 |
| | 10 | 37.70 | 8.61 | 24.17 | 53.60 | 43764 | 1801 | 2423 | 83.64 |
| 65 | 0 | 29.70 | 2.18 | 25.93 | 58.00 | 41818 | 1932 | 2288 | 83.50 |
| | 5 | 30.85 | 4.70 | 25.30 | 57.82 | 25272 | 1875 | 2269 | 84.86 |
| | 10 | 33.02 | 7.42 | 24.54 | 56.77 | 16284 | 1814 | 2240 | 85.46 |
| 70 | 0 | 23.77 | 1.00 | 26.24 | 60.94 | 15008 | 1940 | 2079 | 84.67 |
| | 5 | 26.23 | 3.93 | 25.44 | 59.75 | 5996 | 1874 | 2051 | 85.23 |
| | 10 | 28.70 | 6.98 | 24.56 | 57.86 | 3276 | 1806 | 2016 | 85.16 |

As can be seen from the table above, the $CO_2$ levels achieved increase with the percentage of recycle, as a consequence of the accumulation in the process of the gaseous species. The $O_2$ contents obtained in the combustion products are between 2 and 6%, in most cases for 0 - 5% of oxygen in excess, which is in agreement with the general guidelines for a good combustion. The CO levels are noticeably high for the cases where there is no excess oxygen, showing evidence for partial combustion. It can be observed the effect of dilution of the $SO_2$ concentrations as the oxygen in excess supplied increases. Considering the heat transfer results, the data show how they increase as the percentage of recycle and oxygen in excess rise, being the case-studies comparable to the reference case (air-firing) the ones using 60% RFG. As for the temperatures reached (adiabatic flame temperatures), the values reported show that they are higher as the percentage of recycle decreases.

## 5.2 Results from kinetic modelling-Wet recycle

This section summarizes the results generated by the kinetic model for the stages K1, K2 and K3 presented in Table 8. A parametric study varying the type of fuel, percentage of recycle, excess of oxygen and air ingress into the process was carried out for this phase. Note that results from stage K2 report data using

wet recycle, while for stage K3 partial condensation was applied in the cases using 100% CCP. This change was made to obtain results from the model using similar operating conditions to the experiments performed in the pilot oxy-combustor plant, where some condensation was observed due to failure of the trace heating system associated to the RFG pipeline.

### 5.2.1 Gas composition and temperatures

The results generated using the simulation model with wet recycle are displayed in Table 25. Note that these data are only a sample of all the cases simulated for the stages K1 to K3 of the modelling, here results are presented when using 5% of oxygen in excess and recycling 55% of the flue gas. Additionally, more data generated from simulations where varying the percentage of recycle are reported in Table 36 (see Appendix E).

**Table 25 Simulation results_ Gas composition and temperatures using 5% $O_{2,excess}$ and 55% RFG-Stages K1, K2, K3**

| Fuel | $Air_{Ingress}$ (%) | $O_{2,IN}$ %(v/v) | $O_{2,OUT}$ %(v/v) | $H_2O_{,OUT}$ %(v/v) | $CO_{2,OUT}$ %(v/v) | $CO_{,OUT}$ (ppmv) | $SO_{2,OUT}$ (ppmv) | T (K) | Heat Transfer (kW) |
|---|---|---|---|---|---|---|---|---|---|
| | | | | *K1* | | | | | |
| DM | Air-firing | 21 | 3.28 | 5.24 | 14.83 | 0 | 928 | 1825 | 76.47 |
| | | | | *K2* | | | | | |
| DM | 2 | 40.21 | 4.23 | 22.77 | 64.29 | 0 | 4030 | 2412 | 81.9 |
| B1 | 2 | 34.98 | 3.32 | 30.93 | 57.32 | 5 | 2526 | 2278 | 78.63 |
| CCP | 2 | 31.32 | 0.98 | 42.7 | 48.27 | 0 | 650 | 2105 | 74.99 |
| DM | 10 | 38.24 | 6.70 | 19.32 | 54.41 | 0 | 3409 | 2211 | 80.55 |
| B1 | 10 | 34.51 | 4.82 | 28.09 | 48.46 | 0 | 2135 | 2119 | 79.30 |
| CCP | 10 | 27.45 | 0.57 | 41.83 | 40.31 | 0 | 543 | 2029 | 81.22 |
| DM | 18 | 36.32 | 9.08 | 16.07 | 45.48 | 0 | 2848 | 2005 | 78.70 |
| B1 | 18 | 33.84 | 8.29 | 22.15 | 41.22 | 0 | 1817 | 1911 | 75.19 |
| CCP | 18 | 29.70 | 6.78 | 30.57 | 35.53 | 0 | 479 | 1775 | 70.43 |

| Fuel | $Air_{Ingress}$ (%) | $O_{2,IN}$ %(v/v) | $O_{2,OUT}$ %(v/v) | $H_2O_{,OUT}$ %(v/v) | $CO_{2,OUT}$ %(v/v) | $CO_{,OUT}$ (ppmv) | $SO_{2,OUT}$ (ppmv) | T (K) | Heat Transfer (kW) |
|---|---|---|---|---|---|---|---|---|---|
| | | | | *K3* | | | | | |
| DM | 10 | 38.25 | 6.68 | 19.35 | 54.47 | 0 | 3412 | 2213 | 80.56 |
| B1 | 10 | 33.13 | 4.23 | 29.47 | 48.23 | 0 | 2048 | 2209 | 86.48 |
| CCP | 10 | 32.65 | 4.19 | 33.94 | 43.91 | 0 | 592 | 1994 | 72.61 |

Comparing the data from the table above with the experimental data reported for the second experimental campaign (see Table 11) it can be observed that the $CO_2$ levels are quite similar to the simulations where 10% of air ingress was applied. For the case in which 18% of air ingress was supplied, the flue gas appears to be more diluted than in the experimental data, which means that this percentage of air ingress is probably higher than the actual air entering the process during experiments. Regarding the $H_2O$ vapour content, the case using CCP and 18% air ingress, gives a better estimation compared to the experimental data. However this last aspect, steam $H_2O$ levels, should not be a decisive factor in evaluating the percentage of air ingress into the process due to the condensation observed in the recycle line during the experimental test using 100% CCP. Thus, the actual percentage of $H_2O$ for this case study would be lower. For the $O_2$ levels at the exit of the oxy-combustor, the simulations using 2 and 10% of air ingress, give a better approximation in comparison to the experimental data. The simulation model implementing 10% of air ingress was the one used to analyse the effect of the partial condensation, whose results will be used for the validation of the model using wet recycle.

Regarding the temperatures, it is noticeable the difference between the much higher values generated by the model in comparison to the temperatures reached during the second campaign presented in Table 15. As previously mentioned, these results are not equivalent as the simulation model calculates the adiabatic flame temperature, not the real temperature achieved inside the combustor.

### 5.2.2 Model validation against experimental data (second campaign)

The comparison between the results generated using the kinetic simulation model with 10% of air ingress, 55%RFG and partial condensation, and the experimental results from the second campaign, using 52% RFG, is illustrated in Figure 33.

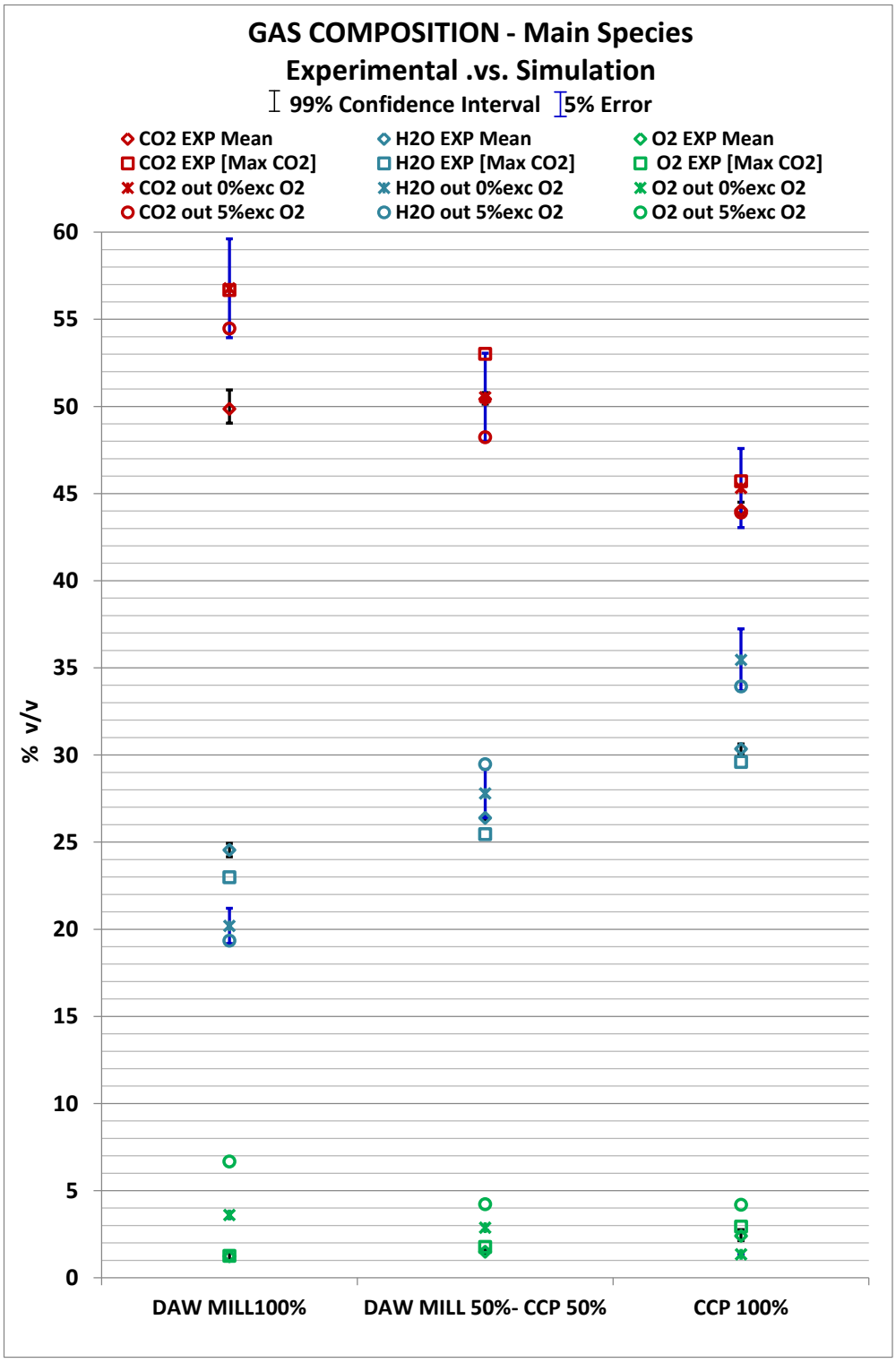


**Figure 33 Model validation_Mean values with error bars for comparing modelled outputs from oxy-combustion using wet recycle and 10% air ingress to sampled data (confidence interval of 99% from the sampled mean values and +/-5% error from the modelled results)**

From the chart above, an optimal agreement for the gas composition between the estimation made by the kinetic model and the experimental results can be observed, as the experimental data are in most cases within the range established by the +/-5% error from the modelled outputs. The confidence intervals from the mean sampled have been included in this chart, to present the range of plausible values that would be measured for these species, with a 99% confidence level, if new tests were done under those operating conditions. It can be seen that there is an accurate prediction regarding the $CO_2$ levels, better for pure fuels than for the blend. For the $H_2O$ contents, the estimation given by the kinetic model is satisfactory and more precise when using the coal-biomass blend. As for the $O_2$ contents, the graph shows a better agreement with the simulation case applying 0% $O_2$; this agrees with the observation made when the experimental results were presented, see subsection 4.1.2, with the explanation that not enough oxygen was supplied during these experiments.

As regards to the temperatures reached, as it has been mentioned above, the results generated by the model are not comparable to the temperatures achieved inside the combustor experimentally. This is because the model estimates the adiabatic flame temperatures, which does not consider heat transfer to the surroundings, incomplete combustion, or dissociation, leading to much higher temperatures than the empirical ones.

## 5.3 Results from kinetic modelling- Oxy-combustor using dry recycle integrated with air separation and power generation units

This section summarizes the data resulted from the parametric study performed varying the percentage of recycle, oxygen in excess and air ingress in the kinetic model applying dry recycle. In this phase of the model development, two additional units were integrated to produce a global picture of the oxy-combustion process, by simulating the air separation unit that generates the oxygen that is supplied to the oxy-combustor and the power generation module. The configuration for this model is illustrated in Figure 17, Figure 18 and Figure 19, corresponding to the stages K6 and K7 described in Table 8.

### 5.3.1 Gas composition, temperatures and net power generated

The results presented in this subsection correspond to stage K6, in which the condenser efficiency was considered 95% for all the cases. The purity of the oxygen generated in the ASU is 95%, and the net power has been calculated by subtracting the energy consumed by the ASU to the power generated in the steam turbine. The reference case is air-firing 100% El Cerrejon coal.

Table 26 shows the results for the combustion products generated for cases applying 60%RFG, 5% of oxygen in excess and 10% of air ingress into the process. More data generated from simulations carried out at this stage can be found in Table 37 (see Appendix E).

**Table 26 Simulation results_ Gas composition, temperatures and net power generated using 60%RFG, 5% $O_{2,Excess}$ and 10% air ingress-Stages K5 and K6**

| Fuel | $O_2$ %(v/v) | $H_2O$ %(v/v) | $CO_2$ %(v/v) | CO (ppmv) | $SO_2$ (ppmv) | HCl (ppmv) | NO (ppmv) | $NO_2$ (ppmv) | T (K) | Net power ($kW_e$) |
|---|---|---|---|---|---|---|---|---|---|---|
| | | | | | *K5* | | | | | |
| EC | 3.48 | 6.05 | 14.42 | 0.00 | 447 | 13 | 459 | 32 | 2070 | 24.1 |
| | | | | | *K6* | | | | | |
| EC | 7.65 | 10.59 | 61.14 | 0.53 | 759 | 23 | 779 | 59 | 2765 | 17.4 |
| B1 | 7.38 | 14.75 | 56.73 | 0.55 | 560 | 128 | 467 | 52 | 2529 | 17 |
| CCP | 2.12 | 20.45 | 50.47 | 4870 | 255 | 107 | 96 | 40 | 2265 | 16.5 |

The results obtained from the kinetic model using dry recycle show that $CO_2$ decrease and $H_2O$ increase by 10% changing from pure coal to pure biomass. For the minor species, it can be seen that there is a marked decrease for $SO_2$ and NO contents when increasing the share of biomass, while the HCl levels show an increasing trend. No significant variation can be observed for $NO_2$ in relation to the type of fuel used. Comparing the results from the table above with the data generated using wet recycle, presented in Table 25, there is a noticeable increase in the $CO_2$ levels, between 7 and 10% higher in the combustion products when using dry recycle. Note that this increase doubles if

the location considered for the comparison is downstream the condenser, as the data presented in these tables is for the flue gas at the exit of the oxy-combustor.

Regarding the values presented for net power generated, in Table 26 and Table 37, there is a decreasing trend as the share of biomass rises. It can be observed also that the power generation is enhanced when lower percentages of recycle are used, as there is a lower volume of gases to heat up, therefore the combustion products reach higher temperatures. The same effect occurs with the use of lower excess of oxygen.

### 5.3.2 Model validation against experimental data (third campaign)

For the ultimate model validation, the results generated in stage K7 are compared to the experimental results obtained during the third campaign. For this, variable condenser efficiencies will be considered as the condenser did not performed equally when varying the fuel used during the experiments in the pilot scale oxy-combustor. Also, a new parametric study has been carried out to evaluate the air ingress into the process, so to assess the effect of an improved sealing of the rig as part of the last stage of modifications in the pilot plant. Table 27 reports data related to gas composition only, as the temperatures generated by the simulation model (adiabatic flame temperatures) are not comparable to the empirical ones obtained in the oxy-combustor. The effect on the net power generated is not considered here, as the general trends observed have been already analysed using the results from stage K6.

**Table 27 Simulation results_ Gas composition using 60%RFG, 5% $O_{2,Excess}$ -Stage K7**

| Fuel | $\eta_{cond}$ (%) | $Air_{Ingress}$ (%) | $O_2$ %(v/v) | $H_2O$ %(v/v) | $CO_2$ %(v/v) | CO (ppmv) | $SO_2$ (ppmv) | HCl (ppmv) | NO (ppmv) | $NO_2$ (ppmv) |
|---|---|---|---|---|---|---|---|---|---|---|
| EC | 50 | 5 | 5.6 | 17.13 | 63.48 | 0 | 784 | 23 | 805 | 60 |
| B2 | 54 | 5 | 5.84 | 18.50 | 62.19 | 0 | 696 | 76 | 521 | 58 |
| B1 | 57 | 5 | 4.56 | 21.09 | 61.12 | 0 | 592 | 137 | 509 | 57 |
| CCP | 86 | 5 | 4.51 | 23.12 | 59.56 | 0 | 321 | 137 | 124 | 52 |

| Fuel | $\eta_{cond}$ (%) | $Air_{Ingress}$ (%) | $O_2$ %(v/v) | $H_2O$ %(v/v) | $CO_2$ %(v/v) | CO (ppmv) | $SO_2$ (ppmv) | HCl (ppmv) | NO (ppmv) | $NO_2$ (ppmv) |
|---|---|---|---|---|---|---|---|---|---|---|
| EC | 50 | 7 | 6.61 | 16.70 | 59.76 | 0 | 742 | 22 | 762 | 57 |
| B2 | 54 | 7 | 6.62 | 17.56 | 59.13 | 0 | 661 | 72 | 495 | 55 |
| B1 | 57 | 7 | 6.04 | 19.80 | 58.52 | 0 | 566 | 131 | 487 | 54 |
| CCP | 86 | 7 | 4.61 | 22.95 | 59.09 | 0 | 319 | 136 | 123 | 52 |
| EC | 50 | 10 | 7.48 | 15.70 | 56.15 | 0 | 698 | 21 | 716 | 53 |
| B2 | 54 | 10 | 6.77 | 17.30 | 55.38 | 0 | 620 | 67 | 464 | 52 |
| B1 | 57 | 10 | 6.79 | 16.90 | 55.72 | 0 | 530 | 123 | 456 | 51 |
| CCP | 86 | 10 | 5.44 | 21.50 | 53.93 | 0 | 291 | 124 | 112 | 47 |

As can be seen from the table above, $CO_2$ contents increase with the percentage of coal used but more moderately than the trend observed for stage K6. In the case of using pure coal, no matter the degree of air ingress applied, $CO_2$ percentages are around 1-4% higher than for pure biomass. For the $H_2O$ contents, the trend is to rise with the share of biomass, being on average 6% higher for the cases using pure CCP compared to the cases using 100% El Cerrejon coal. Regarding the oxygen contents only the cases applying 5% of air ingress, result in values in the range of 4.5-5% which responds to the guidelines to promote a good combustion. However, the rest of the cases, with 7 and 10 % of air ingress, have oxygen levels above 6% which could be considered to be excessive, even more bearing in mind the energy penalty associated with the generation of the $O_2$ pure stream in the ASU. For the minor species, it can be observed that using only coal $SO_2$ levels double the levels reached using biomass. The opposite occurs as regards to the HCl percentage which is 6 times higher in the cases using pure CCP. This is thought to be consequence of the higher Cl percentages found in the biomass as seen from the ultimate analysis. For the NO contents, there is a significant difference for the cases using pure coal which present 6.5 times more NO than using pure biomass; this seems to be consequence of the $NO_x$ thermal generation, considering the $NO_x$ generated from the N-fuel, this should be higher in the case of biomass. On the

other hand, $NO_2$ levels seem to be similar for all the cases although there is a slightly increasing trend in the presence of coal.

For the model validation, the data from simulations presented in Table 27, are compared to the experimental data resulted from the third campaign (see Table 12). From this comparison, it can be deduced that the cases which present most similarities regarding the gas composition are those using 5% air ingress. This means that the air ingress into the process has been reduced by 5%, as it was hoped for after the last modifications made to the pilot scale oxy-combustor.

The comparison for the gas composition between the results from simulations using 5% of air ingress and the experimental data for the third campaign is illustrated in Figure 34 for main species and in Figure 35 for minor species. The confidence intervals from the experimental mean values have been included in these graphs, to present the range of plausible values that would be measured for the main and minor species, with a 99% confidence level, if new tests were done under those operating conditions. Also, to compare the results generated using the simulation model with the experimental data, the range established by +/- 5% error from the modelled results was used.

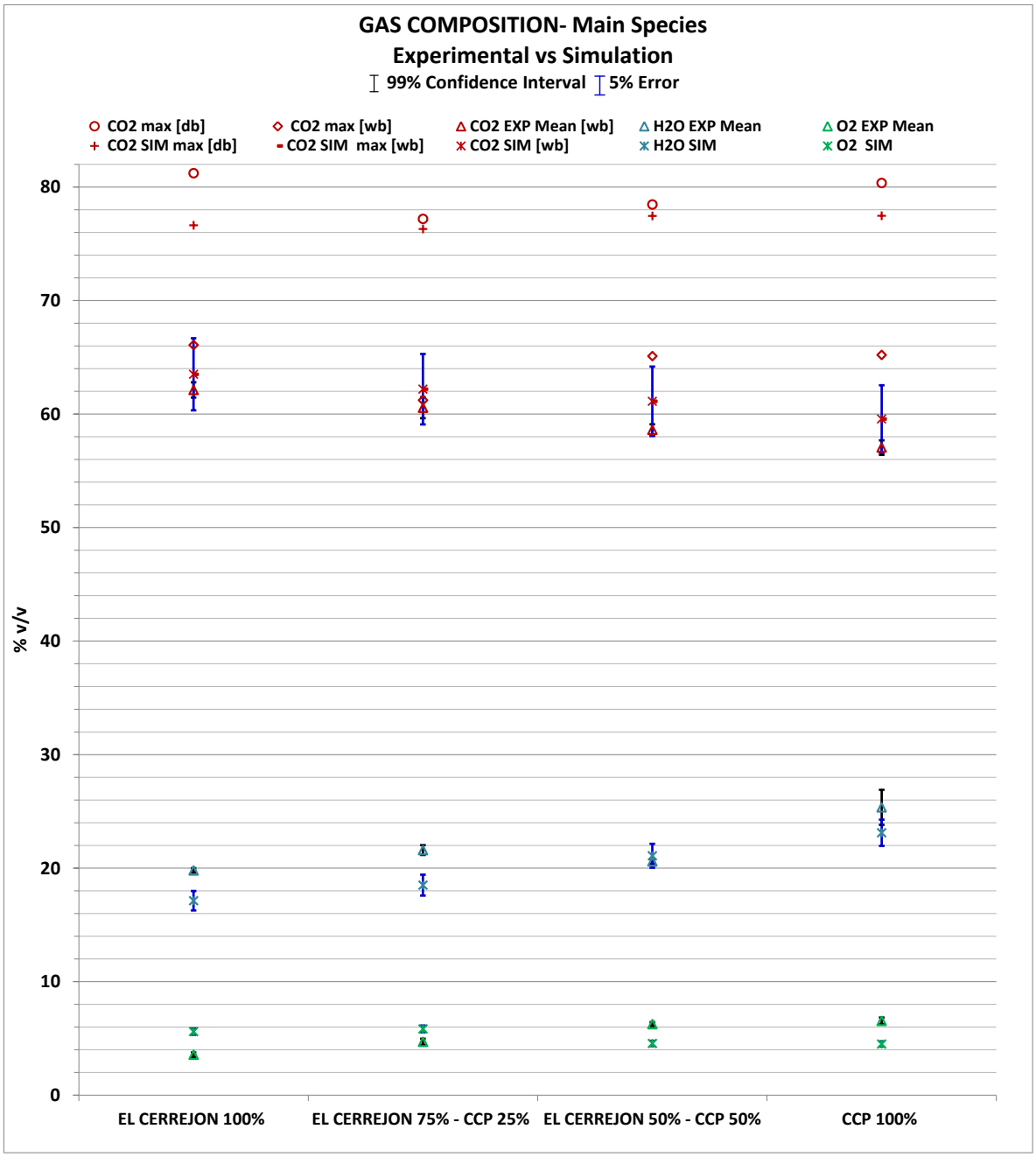


**Figure 34 Model validation_Main species mean values with error bars for comparing modelled outputs from oxy-combustion using dry recycle and 5% air ingress to sampled data (confidence interval of 99% from the sampled mean values and +/-5% error from the modelled results)**

From the comparison for the main species, it can be observed that the experimental data are within the range established using an error of +/-5% from the modelled outputs for all the cases regarding $CO_2$, and are very close to

these ranges in what respects to $H_2O$ data. Consequently, it can be inferred that the estimations made by the model are very reasonable.

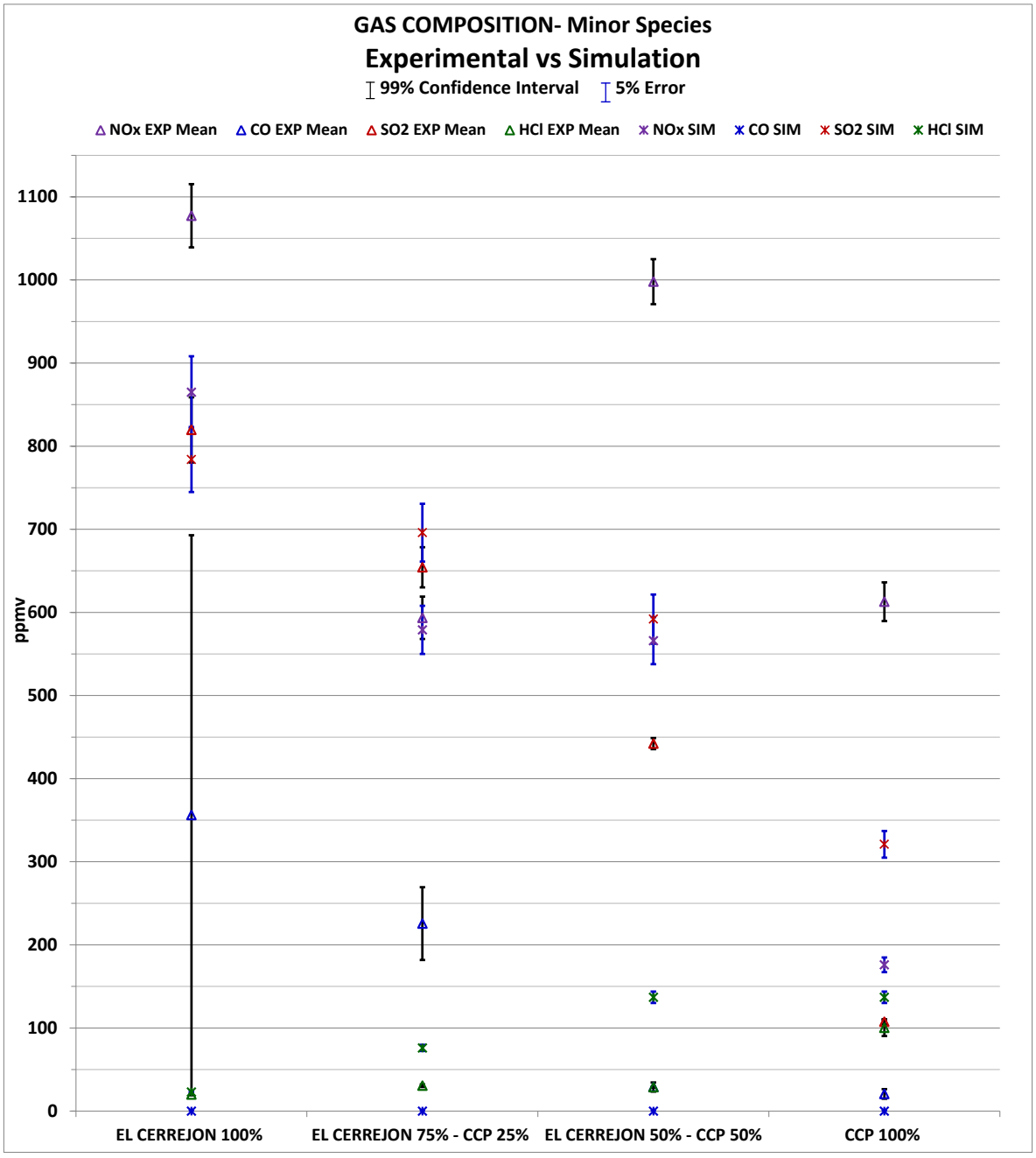


**Figure 35 Model validation_Minor species mean values with error bars for comparing modelled outputs from oxy-combustion using dry recycle and 5% air ingress to sampled data (confidence interval of 99% from the sampled mean values and +/-5% error from the modelled results)**

For the minor species there is a good agreement with the experimental data as regards to $SO_2$ levels considering pure coal and coal-biomass blend B2, and the estimations given for HCl are close enough to the sampled values. However, there is an overestimation for the $SO_2$ content in the range of 1.3 to 3 times higher than the experimental values when increasing the share of biomass, in cases simulated for B1 and pure CCP. The model underestimates by 18% the $NO_x$ levels for the case using pure coal and by 65% for pure biomass. However, the agreement for the coal-biomass blend B2 case is very accurate.

## 5.4 Summary of findings

The ultimate validation of the kinetic model using dry recycle has been found to be highly accurate for $CO_2$ and $H_2O$; and for the most important minor species considering their corrosive effects ($SO_2$ and HCl). It should be noted that the estimation made by the simulations for the minor species is highly dependent on the condenser efficiency defined in the model. This value was selected according to the values observed in the experimental tests, during which the performance of the condenser was found to be inherent to the type of fuel used (coal, blends or biomass).

The thermal profiles have not been subjected to validation with the experimental temperatures reached inside the pilot oxy-combustor as the model generates values for adiabatic flame temperature that does not take into consideration heat losses to the surroundings, incomplete combustion of the fuel or dissociation of intermediate combustion products. However, the general trends were found to be similar to the experimental temperatures: higher when increasing the share of coal.

From the evaluation of the net power generated, it has been concluded that this decreases with a higher percentage of biomass in the fuel. It was found as well, that this is enhanced at lower recycle ratios and for minimum excess as expected, as there is less volume of gases to heat up. Additionally, the energy penalty associated to the oxy-combustion process has been assessed

compared with the air-firing case, which gives higher values for net power generated for all oxy-firing cases, because of the power required by the ASU.

The main outcomes from the parametric studies carried out during the kinetic model development are: the selection of 60% RFG as the optimal recycle ratio that optimises the $CO_2$ reached, and the evaluation of the amount of air ingress occurred into the process for the experimental tests. The air ingress has been estimated to be of 10% of the total volumetric flowrate supplied to the oxy-combustor for the second campaign, and 5% for the third campaign.

# 6 GENERAL DISCUSSION

This chapter discusses the findings presented in the results sections for the experimental campaigns and modelling final stage. It also evaluates how well the aims and objectives set in Chapter 1 have been addressed, as well as presenting the limitations seen in the course of this PhD work.

## 6.1 Review progress vs. Objectives

The aim set for this PhD project defined in the introductory section was to enhance the knowledge of co-firing oxy-combustion cycles. For this, four objectives were outlined and they are reviewed below, to evaluate if they have been fulfilled appropriately, considering the results generated from this work.

1. The assessment of the differences in operation comparing the conventional and oxy-combustion processes has been satisfactorily achieved. The parametric studies to evaluate the effect of the recycle ratio or the fuel variability on the chemistry of the process, thermal profiles reached, heat transfer generated or burn-out and ash deposits characterisation have been successfully performed.
2. A kinetic simulation model has been designed to study the oxy-combustion process by co-firing coal-biomass blends. The model was provided with optimal estimations in its different stages, using wet and dry recycle, so it could be used to select subsequent experimental tests: which would maximise the $CO_2$ concentrations.
3. The evaluation of the operating conditions on the gas composition, temperatures and heat fluxes reached in the context of a retrofitted oxy-combustor was accomplished. The result of this study was the determination of optimal conditions regarding recycle ratio, oxygen supplied, and the fuel or blends of fuels that performed best. It was noted as well, that an important factor to consider in retrofitted facilities, is an assessment of the air ingress occurred into the process as it appears to have high influence on the chemistry inside the oxy-combustor.

4. The heat fluxes were evaluated under air and oxy-firing conditions, demonstrating noticeably difference which makes it improbable that one can compensate for this factor through the use of coal-biomass blends.

From the above review of the progress done against the objectives that were initially set for this PhD work, all of them have been met satisfactorily.

## 6.2 Summary of results

### 6.2.1 Experimental findings

#### Gas composition

The tests run in the pilot-scale oxy-combustor have demonstrated very good performance, as similar $CO_2$ levels to those achieved in other oxy-combustion pilot scale facilities have been seen during the third experimental campaign. For the cases using 100% El Cerrejon coal, a maximum of 81% of $CO_2$ (dry basis) was reached, which is very close to the 85%, with absence of any air ingress, as reported by Steinmetz et al. (2011), or to the 89% with 5% of air ingress suggested by Spörl et al. (2013). Furthermore, the value achieved in the oxy-combustor at Cranfield University is higher than the range between 70 and 80% suggested by Wall et al. (2009). Looking at data to compare the $CO_2$ levels reached using pure biomass, 80% (dry basis) are surprisingly close to the reached with 100% coal, however no publications are available on tests using pure biomass under oxy-firing conditions using real recycled flue gas (non-synthetic). The maximum share of biomass blended with coal, for which published data exists regarding gas composition of main species, is 50%-50% investigated by Tan et al. (2013) who achieved 85% $CO_2$ (dry basis). This value is similar to the percentages suggested by the aforementioned authors for pure coal, so it can be concluded that similar $CO_2$ levels can be expected from co-firing coal-biomass blends or even when pure biomass is used under oxy-combustion conditions. An additional output from this comparison is the confirmation that oxy-firing pure coal, coal-biomass blends or pure biomass, produces $CO_2$ concentrations more than five times higher than $CO_2$ levels reached in conventional combustion. Looking at the $CO_2$ levels obtained using

the oxy-combustor at Cranfield University, it can be inferred that these concentrations are still far from the purity of 98% which is usually set as a requirement at the entrance of the sequestration train (Buhre et al., 2005); so it seems that a $CO_2$ purification unit would be still needed when using retrofitted facilities.

For the $H_2O$ content in the flue gas, the levels reached during the last experimental campaign are between 20% (pure coal) and 29% (blend B1), using dry recycle. This range shows that the concentrations reached for $H_2O$ are three times higher in oxy-firing compared to air-firing. The only published data available in the literature, with analogous operating conditions, are the results reported by Spörl et al. (2013) generated in a 500kW facility using wet recycle and with 5% of air ingress, where they reached 28% of $H_2O$ using pure rich lignite. This value is very similar to the 26.4% of $H_2O$ obtained in the test TC.EC.O (a) using wet recycle in the oxy-combustor at Cranfield University. No published data is available in the literature reviewed using coal-biomass blends or pure biomass with real recycle of the flue gas, as most of the facilities simulate this stream by mixing $CO_2$ and $H_2O$ gases in specific proportions. This shows the uniqueness of the experimental data for coal-biomass blends using oxy-combustion obtained and presented in this work.

Regarding the minor species, special attention was paid to $NO_x$, $SO_x$, and HCl levels and observed values are similar to those seen in the available literature. The levels reported for the oxy-firing tests for $NO_x$ are in the range of 550-750 ppmv, slightly higher than in the air-firing case, where the $NO_x$ reached were between 400 and 630 ppmv. This increment for oxy-combustion is thought to be due to the higher oxygen percentage supplied to the burner, 21% in air-firing against 35% in oxy-firing, assumption that would be supported by the trends for NO and $NO_x$ reported by Riaza et al. (2013) and Spörl et al. (2013) in their investigations. The cases not following the trends set by the rest of the tests, TC.EC.O.(c) and TC.B1.O.(b), were highlighted in the results section because they presented $NO_x$ levels around 1000ppm. The high $NO_x$ concentration reached in the case using pure coal [TC.EC.O.(c)] may be explained by the $NO_x$

thermal generation being promoted due to the high temperatures reached in this test, maximum over all the third campaign. On the other hand, some authors [(Riaza et al., 2013), (Pawlak-Kruczek et al., 2013)] have speculated that increasing the excess of oxygen supplied to the burner, lead to an enhancement of NO production from the N-fuel. This could explain the results obtained for the test using 50%-50% blend [TC.B1.O.(b)], which presented an excess in oxygen, after the oxy-combustion of 6.4%. Regarding the averaged $SO_2$ concentrations reached for oxy-fuel during the third experimental campaign for coal (750ppmv), blends (550ppmv) and biomass (100ppm), are in agreement with the trends suggested by Pawlak-Kruczek et al. (2013). However, their data for the pure coal case showed higher $SO_2$ values, due to higher sulfur contents in the coal used by these authors. On average, the $SO_2$ levels from experiments in the oxy-combustor at Cranfield University were 2.6 times higher than the values reached under air-firing conditions. The $SO_3$ levels reached under air and oxy-firing conditions are similar and comparable to the results presented by Wall et al. (2009). These authors established a relation between the levels reached under oxy-combustion (around 18ppm, for the coal with similar S-content to El Cerrejon coal) and air-firing (around 6ppm). Ahn et al. (2010) also observed similar values to those obtained at Cranfield University, when using low-S content coal, around 10ppm. However, if the comparison is done considering the levels reported by Spörl et al. (2013), as they used a high-S content coal (3.5 times higher than El Cerrejon coal), the results would need to be extrapolated. Making this comparison, the values obtained at Cranfield University are of the same order of magnitude although 20% lower than the value extrapolated. The trend observed for the ($SO_3$+$SO_4^{2-}$) concentrations as the type of fuel is changed, increases with increasing biomass share. It has not been possible to benchmark this tendency as the only study published where $SO_3$ was measured oxy-firing coal-biomass blends, was done by Tan et al. (2013) who reported very low $SO_3$ concentrations, around 1-2 ppm, for coal and coal-biomass blends. These authors also sampled the gas after the bag filter, where the temperatures were very low (370K) and probably the $SO_3$ present in the flue gas had already condensed. An interesting observation was made in

the results section regarding the $(SO_3+SO_4^{2-})/SO_2$ ratio obtained when varying the fuel. While in the cases using pure coal or coal-biomass blends this ratio is around 4-5%, which is in agreement with the ratios suggested by Spörl et al. (2013) of 5%; the cases using pure or high shares of biomass, for air and oxy-firing, presented ratios in the range of 20-32%. This fact could be explained by assuming that the conversion from $SO_2$ to $SO_3$ may be promoted by the alkalis contained in the fly ashes, as these species (K and Na) have been used by several authors [(Mars and Maessen, 1968);(Hill et al., 2011)] as catalysts, together with $V_2O_5$ to enhance the conversion from $SO_2$ to $SO_3$. This, combined with the fact that the K content is noticeably higher for biomass than for coal and its tendency to form sulfates aerosols with the sulfur present as $SO_x$, as pointed out by Jiménez and Ballester (2005), suggests given this assumption that this is the most likely explanation for the high $(SO_3+SO_4^{2-})/SO_2$ ratios obtained. For the levels of HCl seen, all the results show the increase of concentration with the share of biomass. It gives similar values for air and oxy-firing when using pure coal and blends, but doubles in concentration when using pure biomass and switching from air-firing to oxy-firing conditions.

**Temperature and heat flux**

For the thermal profiles obtained in the pilot-scale oxy-combustor at Cranfield University the maximum reached was using 100% El Cerrejon coal: over 1500K. This temperature is similar to the data reported by Toporov et al. (2008) and Andersson et al. (2008) from tests performed with a 100 $kW_{th}$ vertical pilot-scale oxy-combustors using lignite. Looking at larger scale pilot plants, the results are comparable, although lower, than the temperatures achieved by Yamada and Misawa (2007), of around 1670K, in their 400-800 $kW_{th}$ oxy-combustor using a bituminous coal. No published experimental data for temperatures has been found for pilot-scale facilities co-firing coal and biomass, other than for electrically heated reactors [(Pawlak-Kruczek et al., 2013), (Riaza et al., 2013), (Fryda et al., 2008)].

The heat fluxes presented for the oxy-firing cases reached values up to three times higher (averaged values), and two times higher (maximum heat flux) than

the values achieved for air-firing. This trend is consistent with the values reported for emissivities observed by Wall et al. (2009). These authors suggested values for gas emissivity in oxy-firing about 2.2 times higher than in air-firing, when considering a 200$kW_{th}$ pilot facility, as the differences between air and oxy-firing diminish as the scale of the of the furnace increases. Another interesting outcome observed was the effect of varying the fuel under oxy-firing conditions which resulted in heat fluxes 1.4 times higher (in average) and 1.25 times higher for maximum heat flux reached, when using 100% El Cerrejon coal than with 100% cereal co-product. A similar trend is reported by Smart et al., (2010c) for heat fluxes when using 60%coal-40%biomass blends in a 500$kW_{th}$ combustion facility. The effect of changing the combustion mode suggested by these authors agrees with the effect observed in the pilot facility used for this PhD work, and is higher for the oxy-fuel cases. The tendency suggested by Smart et al., (2010c), around 1.1-1.3 times higher in oxy-firing, is similar to the trend observed in the oxy-combustor at Cranfield University during the last experimental campaign.

**Ash deposits and fly ash**

The ESEM/EDX results presented for the ash deposits have shown that the species do not follow the trends established by the previous analysis of the ashes are S and Si. For the S levels, it has been explained that the analogous concentrations were observed for all the cases: varying the fuel (coal and biomass) and the firing mode (air and oxy), while the tendency expected was to decrease with the share of biomass used. This fact is believed to be a consequence of the retention of S as sulfate, due to its reaction with K, which is present in significant quantities in the biomass ash, producing high levels of $K_2SO_4$. This has been supported by the presence of arcanite ($K_2SO_4$) in the ash deposits for the case oxy-firing 100% CCP observed in the XRD analyses. Regarding the Si contents none of the molar ratios showed evidence that $SiO_2$ had formed as the main compound, as the values obtained were too high (between 3.1 and 5.3). However for the cases using biomass, pure or blended with coal, the XRD analyses showed the presence of $SiO_2$, as well as other

compounds containing Si. Looking at Al/Si and Cl/S mass ratios, the Al/Si ratio is similar to the ultimate analysis of the parent fuels for the cases using coal-biomass blends and pure biomass. For the Cl contents, this element was only found for those cases oxy-firing 100% biomass. This has been justified by the higher availability of K present when using CCP as fuel, which leads to KCl generation, as this reaction is in competition with $K_2SO_4$ generation, although less favoured. Due to the lower S presence when using high shares of biomass, after part of the K has reacted with $SO_x$ to generate $K_2SO_4$, there is still K available to produce KCl; fact that does not occur when using high shares of coal, as all the K seems to react to generate sulfates. This observation is also in agreement with the Cl/S ratio for the biomass of 1, while for the cases of El Cerrejon coal and Daw Mill coal such ratios are much lower, at 0.35 and 0.15 respectively. It was therefore not expected to find Cl in the deposits using high shares of coal.

Other important aspects highlighted from the XRD results, are the higher levels of quartz, coquimbite, illite, or pyrite when oxy-firing 100% coal in comparison to the air-firing case. This observation is in agreement with the suggestions made by Wigley (2010). Regarding the observations presented for the cases using 100% biomass, it has been shown that under air-firing conditions, higher levels of aluminium phosphate and arcanite ($K_2SO_4$) were produced; and, under oxy-firing conditions Si forms mainly cristobalite ($SiO_2$).

The results presented for carbon in ash, showed high levels for fly ash sampled from the last section of the oxy-combustor and the cyclone. This can be explained by the fact of the fuel size was too large together with the lower residence time associated with the scale of the oxy-combustor at Cranfield University. Additionally, higher contents of unburnt carbon were observed for air-firing cases in comparison with the oxy-combustion tests, which is a consequence of the enhanced combustion in oxygen enriched atmospheres which promoted higher combustion temperatures.

**Acid dew point**

The acid dew points calculated with the correlations suggested by Verhoff and Banchero (1974), Kiang (1981), and Perry and Chilton (1973) using the experimental gas compositions obtained in the oxy-combustor at Cranfield, have shown that lower acid dew points are expected for air-firing in comparison with oxy-firing cases. This observation is in agreement with the suggestion made by Wall et al. (2009). Furthermore, these estimations have been compared with the results generated from the measurements using the electrochemical noise probe located in the recycle line. The conclusion of this comparison was that corrosion rates are maximum when the temperature goes below the low $T_{ADP}$ estimated; but it is less clear when the temperature is between the high and low $T_{ADP}$. This could mean that the actual acid dew point is lower than the estimated values for the high $T_{ADP}$, leading one to infer that the correlations found in the literature produce conservative estimations for the acid dew points.

### 6.2.2 Model validation

The validation of the kinetic model using dry recycle has been achieved by comparing the modelling results with the experimental gas composition, this provides a very accurate estimation for main species ($CO_2$ and $H_2O$) and minor species of high interest, due to their corrosive properties, ($SO_2$ and HCl). This means that the equation suggested to convert the kinetic data available in the literature to the dimensions required by Aspen Plus® has been shown to work suitably.

Once the model was validated, one of its main outputs is the allowance for the evaluation of the quantity of air ingress into the process.

It should be noted, for the model validation, the temperatures have not been considered, as the model calculates values for the adiabatic flame temperature which are always considerably higher than the temperatures reached in the pilot-scale combustor, as no losses to the surroundings are taken into account in the simulations. However, the temperatures generated by the model have

been validated against other values of adiabatic flame temperatures for similar conditions. The results of this PhD modelling work have been compared with the results calculated using the FACT program, allowing for flame dissociation and gave very similar results to the Aspen Plus® calculation. Additionally, the temperature estimation given by the model is in good agreement with the measurements of adiabatic flame temperatures suggested by Smart et al., (2010c) for a 500 $MW_{th}$ test rig.

Another aspect from the summary of findings from the modelling results is the difference in net power generated when comparing air-firing, higher, to oxy-firing cases, as consequence of the energy penalty associated to the generation of a high purity oxygen stream in the ASU block. However, these values cannot be compared directly as, the $CO_2$ concentration of the exhaust gases generated in air-firing and oxy-firing are very different. In consequence, to perform this comparison, one must carry out techno-economic studies, such as the those by Hadjipaschalis et al. (2009) where the comparison is done evaluating the grams of $CO_2$ emitted per energy unit, the electricity cost, as well the $CO_2$ avoidance cost associated with the combustion of coal under air-firing and oxy-firing conditions. Their final conclusion is that the oxy-fuel combustion plant is the most competitive technology in the field of CCS.

## 6.3 Limitations

Several limiting factors have been met during the course of this PhD. The main ones were associated with the operation of the pilot-scale oxy-combustor and are summarised in Appendix B.1.1. On the other hand, the main limitation determined in regards to the kinetic simulation model, was the inability of such a model to calculate values for temperatures reached, other than the adiabatic flame temperature. However, this drawback has been resolved though benchmarking the results with values generated with other programs.

# 7 FINAL CONCLUSIONS AND FUTURE WORK

This project aimed to enhance the knowledge of co-firing oxy-combustion cycles to boost development of this valuable technology towards becoming an integral part of the energy mix. Four objectives were defined to accomplish this goal in the introductory section, and have been evaluated in the subsection 6.1 as regards to the results presented. The contributions to knowledge are provided below as is the technological implications that these conclusions represent in the context of scale-up to deployment. Finally, some recommendations for future work are suggested.

## 7.1 Conclusions

The main outcomes from this PhD work are explained below, differentiating between those related to the experimental and the modelling aspects of this thesis.

### 7.1.1 Experimental

- Identification of gas composition levels in oxy-fuel combustion using dry recycle:
    - Similar maximum $CO_2$ concentrations can be achieved, on a dry basis, when using pure coal and pure biomass: above 80%;
    - High levels of $H_2O$, between 20 and 29%, are reached even using the condenser (dry recycle);
    - For minor species the ranges observed are 550-750ppmv for $NO_x$, 100-750 for $SO_2$ and 8-100 for HCl;
    - $SO_3$ and $SO_4^{2-}$ contents have been found to be between 16 and 36 ppm, independent from the combustion mode or the fuel fired. Noticeable increase in the $(SO_3+SO_4^{2-})/SO_2$ ratio has been identified when increasing the share of biomass;
- Verification that higher thermal profiles are achieved under oxy-firing conditions in comparison to air-firing, with a maximum temperature of 1508K when using 100% coal;

- Evaluation of the difference in heat fluxes generated under oxy-firing against air-firing conditions. The option selected to compensate the higher heat capacity and emissivity of $CO_2$, was the use of coal-biomass blends. The results have shown that the heat flux for oxy-firing conditions is three times higher compared to air-firing looking at the averaged values, while the use of pure biomass only reduces the heat flux 1.4 times compared to pure coal. It has been further observed that the maximum heat flux value for oxy-firing is double the air-firing case, and when changing the type of fuel from biomass to coal under oxy-firing conditions, the maximum heat flux increases by 1.25 times. In consequence, it is not possible to compensate for the higher heat fluxes produced in oxy-firing by using such fuels of lower heat value;
- Characterisation of ash deposits generated under oxy-fuel combustion has shown:
    - Ash deposits generated from pure biomass and coal-biomass blends with high share of biomass presented higher particle size, and were markedly fibrous and cohesive, leading to ash deposits blocks generation;
    - The ESEM/EDX analyses of the ash deposits showed similar trends at 1023 and 923K. S contents are similar to all oxy-firing cases even when changing from pure coal to pure biomass, possibly as consequence of $K_2SO_4$ generation. Cl has been found only in the deposits generated from oxy-firing 100% biomass, as consequence of KCl generation.
- Verification was provided that lower levels of carbon in ash are present in fly ashes generated under oxy-fuel combustion;
- Evaluation of the accuracy under oxy-firing conditions of the correlations suggested in the literature for acid dew point, allow us to make the conclusion that the experimental acid dew points observed are usually lower than the estimations calculated, so it is a conservative estimation;

- Identification of the necessity of the condenser as an essential additional treatment for the recycle flue gas when using high shares of biomass in blends or pure biomass, due to high $H_2O$ contents reached; and
- Identification of specific efficiencies of the condenser depending of the fuel used.

### 7.1.2 Modelling

- Validation of the kinetic model designed for oxy-firing coal and biomass which allows for the evaluation of the effects caused by the variation of the main operating parameters (type of fuel, %RFG and $O_2$ in excess) and the identification of the amount of air ingress into the process; and
- Validation of the equation suggested for the conversion of the kinetic parameters, published in the relevant literature, to match the format required by Aspen Plus®.

## 7.2 Technological implications

The findings made as part of this PhD will help to establish an intermediate step between bench and demonstration scale plants, aiming as well to set up some basis for operation. An additional outcome of this work is the capability to evaluate the effect of the main operating parameters on the oxy-fuel combustion process, with wet or dry RFG, by using the rate-based simulation model designed. This model is able to provide with realistic predictions as regards to gas composition and adiabatic flame temperatures when using different types of pulverised fuels (co-firing).

As part of the establishment of some basic aspects to scale-up the effects observed during the operation of the oxy-combustor, at Cranfield University, to demonstration scale plants, the main ideas are explained as follows. It has been verified that the retrofitting process of a combustor into an oxy-combustor can lead to satisfactory results, allowing one to reach $CO_2$ concentrations in the exhaust similar to new-built facilities. The main issue associated to the retrofitting of a combustor has been proved to be minimising the air ingress into the process. Regarding the operation when varying the firing mode, it has been

concluded that this together with the type of fuel used (coal, biomass, co-firing) will affect the flexibility with what a higher scale plant should be designed. This is consequence of the variation of the maximum temperatures reached and their location inside the furnace when changing the type of fuel supplied. Another issue suggested by this work to be important, is to provide an adequate trace heating system to the recycle line, to avoid undesirable condensation of steam and acid species along the recycle layout. For co-firing issues, an important implication from using high shares of biomass is the characteristics of the ash deposits. It has been observed that these deposits are highly fibrous and cohesive, which makes necessary a higher maintenance of the water heating tubes located in the radiative section of the furnace, as otherwise whole banks of tubes could see their efficiency drop dangerously.

## 7.3 Recommendations for future research

The work accomplished for this PhD has contributed to the knowledge base in the sense that the effects observed during the operation of the oxy-combustor in Cranfield University co-firing coal and biomass could be used to scale-up the process. However, as a result of the overall analysis carried out, additional issues have been appointed as further gaps in knowledge, and therefore suitable to be addressed in future research. The suggestions below describe the alternatives to continue researching on this topic:

- The use of other coals and biomasses types should be investigated. It is suggested that the use of coals with higher S content and biomasses with higher Na level which would allow for the evaluation of the effects on the $SO_x$ and sulfates aerosols formation, and ash deposits characteristics, respectively;
- Further investigation of the $SO_3/SO_2$ ratio should be performed comparing cases using 100% coal with coal-biomass blends with high shares of biomass, but applying an analysis procedure identical to the one described in Method 8A. This would allow for the verification of the effect presented as one of the conclusions of this PhD work (marked

increase of the ($SO_3$+$SO_4^{2-}$)/$SO_2$ ratio with higher presence of biomass) and evaluation of the presence of $SO_3$ and sulfates separately;

- Further investigation on the heat flux generated when changing the firing mode as well as when varying the type of fuel supplied. Additionally, a way of improving this measurement would be by installing a valve at the port where the heat flux probe is located, so to be able to measure only for a few minutes avoiding the ash deposition on the sensor lens;
- Upgrade the condenser to a larger size as it was observed that after a few hours of operation its efficiency dropped sharply;
- Validation of the kinetic simulation model with experimental data from a larger pilot scale oxy-combustor; and
- The study of the oxy-combustion process using the kinetic simulation model could be complemented with a CFD model to allow for the evaluation of the behaviour of the flame inside the oxy-combustor. This complementary model would provide more realistic values for thermal profiles than the adiabatic flame temperatures generated using Aspen Plus®.

# REFERENCES


Ahn, J., Okerlund, R., Fry, A., Eddings, E.G., 2011. Sulfur trioxide formation during oxy-coal combustion. International Journal of Greenhouse Gas Control 5, S127–S135. doi:10.1016/j.ijggc.2011.05.009

Ahn, J., Overacker, D., Okerlund, R., Fry, A., Eddings, E., 2010. SO3 formation during oxy-coal combustion, in: Proceedings of the 35th International Technical Conference on Clean Coal & Fuel Systems.

Al-Abbas, A.H., Naser, J., Dodds, D., 2012. CFD modelling of air-fired and oxy-fuel combustion in a large-scale furnace at Loy Yang A brown coal power station. Fuel 102, 646–665. doi:10.1016/j.fuel.2012.06.028

Amarkhail, S. shah, 2010. Diploma project. Kabul Polytechnic University, Faculty of chemical technology.

Andersson, K., Johansson, R., Hjärtstam, S., Johnsson, F., Leckner, B., 2008. Radiation intensity of lignite-fired oxy-fuel flames. Experimental Thermal and Fluid Science 33, 67–76. doi:10.1016/j.expthermflusci.2008.07.010

Arias, B., Pevida, C., Rubiera, F., Pis, J.J., 2008. Effect of biomass blending on coal ignition and burnout during oxy-fuel combustion. Fuel 87, 2753–2759. doi:10.1016/j.fuel.2008.01.020

Asgaryan, M., 2013. PhD Thesis. Prediction of the remaining service life of superheater and reheater tubes in coal-biomass fired power plants. Cranfield University.

Bartolomé, C., Gil, A., Ramos, I., 2010. Ash deposition behavior of cynara–coal blends in a PF pilot furnace. Fuel Processing Technology 91, 1576–1584. doi:10.1016/j.fuproc.2010.06.005

Baum, M.M., Street, P.J., 1971. Predicting the combustion behaviour of coal particles. Combustion science and technology 3, 231–243.

Borrego, A.G., Garavaglia, L., Kalkreuth, W.D., 2009. Characteristics of high heating rate biomass chars prepared under N2 and CO2 atmospheres. International Journal of Coal Geology 77, 409–415. doi:10.1016/j.coal.2008.06.004

Buhre, B.J.P., Elliott, L.K., Sheng, C.D., Gupta, R.P., Wall, T.F., 2005. Oxy-fuel combustion technology for coal-fired power generation. Progress in Energy and Combustion Science 31, 283–307. doi:10.1016/j.pecs.2005.07.001

Chamberlain, S., Reeder, T., Stimpson, C.K., Tree, D.R., 2013. A comparison of sulfur and chlorine gas species in pulverized-coal, air- and oxy-combustion. Combustion and Flame 160, 2529–2539. doi:10.1016/j.combustflame.2013.05.008

Chen, L., Yong, S.Z., Ghoniem, A.F., 2012. Oxy-fuel combustion of pulverized coal: Characterization, fundamentals, stabilization and CFD modeling. Progress in Energy and Combustion Science 38, 156–214. doi:10.1016/j.pecs.2011.09.003

Diez, D., Barr, C., Cetinkaya-Rundel, M., 2012. OpenIntro statistics, Second Edition.

Dillon, D., White, V., Allam, R.J., Wall, R., Gibbins, J., 2005. Oxy Combustion Processes for CO2 Capture from Power Plant. Engineering investigation report IEA greenhouse gas R&D research and development programme.

Eddings, E.G., Ahn, J., Okerlund, R., Fry, A., 2011. SO3 emissions in pilot-scale oxy-fired pulverized-coal and circulating-fluid-bed test facilities, in: 2nd IEAGHG International Oxyfuel Combustion Conference (IOCC). Yeppoon, Australia.

Edge, P., Gharebaghi, M., Irons, R., 2011. Combustion modelling opportunities and challenges for oxy-coal carbon capture technology. Chemical Engineering Research and Design 89, 1470–1493. doi:10.1016/j.cherd.2010.11.010

Fan, M., Brown, R.C., 2001. Comparison of the Loss-on-Ignition and Thermogravimetric Analysis Techniques in Measuring Unburned Carbon in Coal Fly Ash. Energy & Fuels 15, 1414–1417. doi:10.1021/ef0100496

Faúndez, J., Arenillas, A., Rubiera, F., García, X., Gordon, A.L., Pis, J.J., 2005. Ignition behaviour of different rank coals in an entrained flow reactor. Fuel 84, 2172–2177. doi:10.1016/j.fuel.2005.03.028

Field, M.A., 1969. Rate of combustion of size-graded fractions of char from a low rank coal between 1200K-2000K. Combustion and Flame 13, 237–252.

Fleig, D., Alzueta, M.U., Normann, F., Abián, M., Andersson, K., Johnsson, F., 2013. Measurement and modeling of sulfur trioxide formation in a flow reactor under post-flame conditions. Combustion and Flame 160, 1142–1151. doi:10.1016/j.combustflame.2013.02.002

Fleig, D., Vainio, E., Andersson, K., Brink, A., Johnsson, F., Hupa, M., 2012. Evaluation of SO3 Measurement Techniques in Air and Oxy-Fuel Combustion. Energy & Fuels.

Flower, M., Man, C., Gibbins, J., Mcglashan, N., 2009. A comparison between i gnition behaviours of 7 different UK and World-Traded coals in air, and in a mixture of oxygen and carbon dioxide gases representative of oxy-combustion conditions, in: 26th Annual International Pittsburgh Coal Conference. pp. 1602–1609.

Fryda, L., Cieplik, M.K., Jacobs, J.M., van de Kamp, W.L., 2008. Study of oxyfuel combustion of coal and biomass in a lab-scale pulverised fuel, in: 16th European Biomass Conference & Exhibition.

Hadjipaschalis, I., Kourtis, G., Poullikkas, A., 2009. Assessment of oxyfuel power generation technologies. Renewable and Sustainable Energy Reviews 13, 2637–2644. doi:10.1016/j.rser.2009.07.001

Haykiri-Acma, H., Turan, A.Z., Yaman, S., Kucukbayrak, S., 2010. Controlling the excess heat from oxy-combustion of coal by blending with biomass. Fuel Processing Technology 91, 1569–1575. doi:10.1016/j.fuproc.2010.06.004

Hill, T., Korner, R., Kramer, M., 2011. Catalyst for the oxidation of SO2 to SO3. US Patent App. 13/084,934. US 2011/0250124 A1.

Holtmeyer, M.L., Kumfer, B.M., Axelbaum, R.L., 2012. Effects of biomass particle size during cofiring under air-fired and oxyfuel conditions. Applied Energy 93, 606–613. doi:10.1016/j.apenergy.2011.11.042

Hu, Y., Li, H., Yan, J., 2010. Integration of Evaporative Gas Turbine with Oxy-Fuel Combustion for Carbon Dioxide Capture. International Journal of Green Energy 7, 615–631. doi:10.1080/15435075.2010.529405

Hu, Y., Yan, J., 2012. Characterization of flue gas in oxy-coal combustion processes for CO2 capture. Applied Energy 90, 113–121. doi:10.1016/j.apenergy.2011.03.005

Huijbregts, W.M.M., Leferink, R.G.I., 2004. Latest advances in the understanding of acid dewpoint corrosion: corrosion and stress corrosion cracking in combustion gas condensates. Anti-Corrosion Methods and Materials 51, 173–188. doi:10.1108/00035590410533129

Jiménez, S., Ballester, J., 2005. Effect of co-firing on the properties of submicron aerosols from biomass combustion. Proceedings of the Combustion Institute 30, 2965–2972. doi:10.1016/j.proci.2004.08.099

Khodier, A., 2011. PhD Thesis. Co-firing fossil fuels and biomass: combustion, deposition and modelling. Cranfield University.

Khodier, A., Simms, N., 2010. Investigation of gaseous emissions and ash deposition in a pilot-scale PF combustor co-firing cereal co-product biomass with coal, in: Conference on Renewable Energies and Power Quality.

Kiang, Y.H., 1981. Predicting Dewpoints of Acid Gases,Chemical Engineering. p. 127.

Kim, J.P., Schnell, U., Scheffknecht, G., 2008. Comparison of Different Global Reaction Mechanisms for MILD Combustion of Natural Gas. Combustion Science and Technology 180, 565–592. doi:10.1080/00102200701838735

Kuuluvainen, H., Karjalainen, P., Bajamundi, C.J.E., Maunula, J., Vainikka, P., Roppo, J., Keskinen, J., Rönkkö, T., 2015. Physical properties of aerosol particles measured from a bubbling fluidized bed boiler. Fuel 139, 144–153. doi:10.1016/j.fuel.2014.08.048

Li, K., You, C., 2010. Particle Combustion Model Simultaneously Considering a Volatile and Carbon Reaction. Energy & Fuels 24, 4178–4184. doi:10.1021/ef100463g

Maddalone, R.F., Newton, S.F., Rhudy, R.G., Statnick, R.M., 1979. Laboratory and Field Evaluation of the Controlled Condensation System for S03 Measurements in Flue Gas Streams Laboratory and Field Evaluation of the Controlled Condensation System for SO3 Measurements in. Journal of the Air Pollution Control Association 29, 626–631. doi:10.1080/00022470.1979.10470834

Makino, A., 1992. An approximate explicit expression for the combustion rate of a small carbon particle. Combustion and flame 90, 143–154.

Mars, P., Maessen, J., 1968. The mechanism and the kinetics of sulfur dioxide oxidation on catalysts containing vanadium and alkali oxides. Journal of Catalysis 12, 1–12.

Mills, D.J., Mabbutt, S., 2000. Investigation of defects in organic anti-corrosive coatings using electrochemical noise measurement. Progress in Organic Coatings 39, 41–48. doi:10.1016/S0300-9440(00)00098-9

Murphy, J.J., Shaddix, C.R., 2006. Combustion kinetics of coal chars in oxygen-enriched environments. Combustion and Flame 144, 710–729. doi:10.1016/j.combustflame.2005.08.039

Musarra, S.P., Fletcher, T.H., Niksa, S., Dwyer, H.A., 1986. Heat and mass transfer in the vicinity of a devolatizing coal particle. Combust. Sci. Technol. 45, 289–307.

Nakayama, S., Noguchi, Y., Kiga, T., Miyamae, S., Maeda, U., Hawai, M., Tanaka, T., Koyata, K., Makino, H., 1992. Pulverized Coal Combustion in 02/CO2 Mixtures on a Power Plant for C02 Recovery. Energy Conversion and Management 33, 379–386.

NCASI Southern Regional Center, 1996. Method 8A - Determination of sulfuric acid vapor or mist and sulfur dioxide emissions from kraft recovery furnaces.

Nielsen, M.T., 2003. On the relative importance of SO2 oxidation to high dust SCR DeNOx units, in: DOE/NETL 2003 Conference on Selective Catalytic Reduction (SRC) and Selective Non-Catalytic Reduction (SNCR) for NOx Control.

Okkes, A.G., 1987. Get acid dew point of flue gas. Hydrocarbon Processing 66, 53–55.

Park, S., Kim, J. a., Ryu, C., Chae, T., Yang, W., Kim, Y.-J., Park, H.-Y., Lim, H.-C., 2013. Combustion and heat transfer characteristics of oxy-coal combustion in a 100MWe front-wall-fired furnace. Fuel 106, 718–729. doi:10.1016/j.fuel.2012.11.001

Pawlak-Kruczek, H., Ostrycharczyk, M., Baranowski, M., Czerep, M., Zgóra, J., 2013. Co-Firing of Biomass with Pulverised Coal in Oxygen Enriched Atmosphere. Chemical and Process Engineering 34, 215–226. doi:10.2478/cpe-2013-0018

Payne, R., CHEN, S., Wolski, A., Richter, W., 1989. CO2 recovery via coal combustion in mixtures of oxygen and recycled flue gas. Combustion Science and Technology 67, 1–16.

Perry, R.H., Chilton, C.H., 1973. Chemical engineers' handbook.

Raibhole, V.N., Sapali, S.N., 2012. Simulation and Parametric Analysis of Cryogenic Oxygen Plant for Biomass Gasification. Mechanical Engineering Research 2, 97–107. doi:10.5539/mer.v2n2p97

Riaza, J., Álvarez, L., Gil, M.V., Pevida, C., Pis, J.J., Rubiera, F., 2013. Ignition and NO Emissions of Coal and Biomass Blends under Different Oxy-fuel Atmospheres. Energy Procedia 37, 1405–1412. doi:10.1016/j.egypro.2013.06.016

Santisteban, J., Mediavilla, R., López-Pamo, E., Dabrio, C.J., Ruiz Zapata, M.B., García, M.J.G., Castaño, S., Martínez-Alfaro, P.E., 2004. Loss on ignition: a qualitative or quantitative method for organic matter and carbonate mineral content in sediments? Journal of Paleolimnology 32, 287–299.

Santos, S., 2008. Oxyfuel Combustion for Coal Fired Power Plant with CO2 Capture.

Smart, J.P., Lu, G., Yan, Y., Riley, G.S., 2010a. Characterisation of an oxy-coal flame through digital imaging. Combustion and Flame 157, 1132–1139. doi:10.1016/j.combustflame.2009.10.017

Smart, J.P., O'Nions, P., Riley, G.S., 2010b. Radiation and convective heat transfer, and burnout in oxy-coal combustion. Fuel 89, 2468–2476. doi:10.1016/j.fuel.2010.03.048

Smart, J.P., Patel, R., Riley, G.S., 2010c. Oxy-fuel combustion of coal and biomass, the effect on radiative and convective heat transfer and burnout. Combustion and Flame 157, 2230–2240. doi:10.1016/j.combustflame.2010.07.013

Smith, I.W., 1982. The combustion rates of coal chars: A review, in: Nineteenth Symposium (International) on Combustion. pp. 1045–1065. doi:10.1016/S0082-0784(82)80281-6

Sotudeh-Gharebaagh, R., Legros, R., Chaouki, J., Paris, J., 1998. Simulation of circulating fluidized bed reactors using ASPEN PLUS. Fuel 77, 327–337. doi:10.1016/S0016-2361(97)00211-1

Spörl, R., Maier, J., Scheffknecht, G., 2013. Sulphur Oxide Emissions from Dust-fired Oxy-fuel Combustion of Coal. Energy Procedia 37, 1435–1447. doi:10.1016/j.egypro.2013.06.019

Stanger, R., Wall, T., 2011. Sulphur impacts during pulverised coal combustion in oxy-fuel technology for carbon capture and storage. Progress in Energy and Combustion Science 37, 69–88. doi:10.1016/j.pecs.2010.04.001

Steinmetz, C., Bergins, C., Weckes, P., Dieter, K., 2011. Oxyfuel Power Plant Design : Retrofit Options for Different Fuels, in: 2nd Oxyfuel Combustion Conference.

Strömberg, L., Lindgren, G., Jacoby, J., Giering, R., Anheden, M., Burchhardt, U., Altmann, H., Kluger, F., Stamatelopoulos, G.-N., 2009. Update on Vattenfall's 30 MWth oxyfuel pilot plant in Schwarze Pumpe. Energy Procedia 1, 581–589. doi:10.1016/j.egypro.2009.01.077

Syed, a. U., Simms, N.J., Oakey, J.E., 2012. Fireside corrosion of superheaters: Effects of air and oxy-firing of coal and biomass. Fuel 101, 62–73. doi:10.1016/j.fuel.2011.03.010

Tan, Y., Jia, L., Wu, Y., 2013. Some Combustion Characteristics of Biomass and Coal Cofiring under Oxy-Fuel Conditions in a Pilot-Scale Circulating Fluidized Combustor. Energy & Fuels 27, 7000–7007.

Toftegaard, M.B., Brix, J., Jensen, P. a., Glarborg, P., Jensen, A.D., 2010. Oxy-fuel combustion of solid fuels. Progress in Energy and Combustion Science 36, 581–625. doi:10.1016/j.pecs.2010.02.001

Toporov, D., Bocian, P., Heil, P., Kellermann, A., Stadler, H., Tschunko, S., Förster, M., Kneer, R., 2008. Detailed investigation of a pulverized fuel swirl flame in CO2/O2 atmosphere. Combustion and Flame 155, 605–618. doi:10.1016/j.combustflame.2008.05.008

U.S. Environmental Protection Agency, 2000. Carbon Dioxide as a Fire Suppressant : Examining the Risks.

Vainio, E., Fleig, D., Brink, A., Andersson, K., Johnsson, F., Hupa, M., 2013. Experimental Evaluation and Field Application of a Salt Method for SO3 Measurement in Flue Gases. Energy & Fuels.

Vascellari, M., Cau, G., 2009. Numerical simulation of pulverized coal oxy-combustion with exhaust gas recirculation. 4th International Conference on Clean Coal Technologies.

Vassilev, S. V., Vassileva, C.G., 2005. Methods for Characterization of Composition of Fly Ashes from Coal-Fired Power Stations: A Critical Overview. Energy & Fuels 19, 1084–1098. doi:10.1021/ef049694d

Verhoff, F.H., Banchero, J.T., 1974. Predicting dew points of flue gases. Chemical Engineering Progress 70, 71–72.

Wall, T., Liu, Y., Spero, C., Elliott, L., Khare, S., Rathnam, R., Zeenathal, F., Moghtaderi, B., Buhre, B., Sheng, C., Gupta, R., Yamada, T., Makino, K., Yu, J., 2009. An overview on oxyfuel coal combustion—State of the art research and technology development. Chemical Engineering Research and Design 87, 1003–1016. doi:10.1016/j.cherd.2009.02.005

Wang, X., Zhao, D., Jiang, L., Yang, W., 2009. The Deposition and Burning Characteristics During Slagging Co-Firing Coal and Wood: Modeling and Numerical Simulation. Combustion Science and Technology 181, 710–728. doi:10.1080/00102200902851776

Wigley, F., 2010. Coal mineral transformations under oxy-fuel combustion conditions Final report for BCURA Project B81 (1 January 2007 – 30 September 2009).

Xiong, J., Zhao, H., Chen, M., Zheng, C., 2011. Simulation study of an 800 MWe oxy-combustion pulverized-coal-fired power plant. Energy & Fuels 2405–2415.

Yamada, T., Misawa, N., 2007. Pilot scale experiments giving direct comparison between air and oxy-firing of coals and implication for large scale plant design, in: 2nd Meeting of the Oxy-Fuel Network. pp. 262–278.

Yang, Y., Zhang, T., Shao, Y., Meng, G., Wang, F., 2013. In situ study of dew point corrosion by electrochemical measurement. Corrosion Science 71, 62–71. doi:10.1016/j.corsci.2013.03.001

Yuzbasi, N.S., Selçuk, N., 2011. Air and oxy-fuel combustion characteristics of biomass/lignite blends in TGA-FTIR. Fuel Processing Technology 92, 1101–1108. doi:10.1016/j.fuproc.2011.01.005

Zanganeh, K.E., Shafeen, A., 2007. A novel process integration, optimization and design approach for large-scale implementation of oxy-fired coal power plants with CO2 capture. International Journal of Greenhouse Gas Control 1, 47–54. doi:10.1016/S1750-5836(07)00035-7

ZareNezhad, B., 2009. New correlation predicts flue gas sulfuric acid dewpoints. Oil & Gas Journal 107, 60–63.

Zhao, M., Han, Z., Sheng, C., Wu, H., 2013. Characterization of Residual Carbon in Fly Ashes from Power Plants Firing Biomass. Energy & Fuels 27, 898–907. doi:10.1021/ef301715p

# APPENDICES

# Appendix A Extended literature review

## A.1 Modelling based on equilibrium

### A.1.1 Examples of oxy-combustor using Aspen Plus

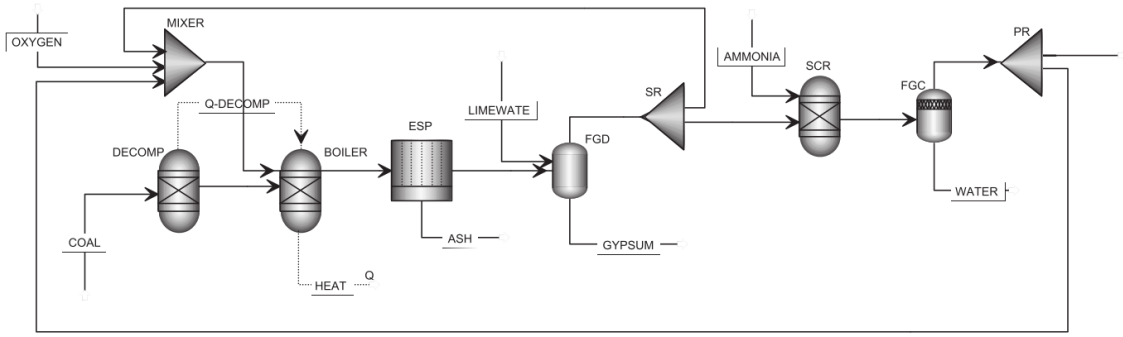


**Figure 36 Flow sheet of oxy-coal combustion process. Image taken from Hu and Yan (2012)**

| | Stoichiometry | Type | Frictional conversion |
|---|---|---|---|
| SCR | $4NO + 4NH_3 + O_2 \leftrightarrow 4N_2 + 6H_2O$ | | 0.95 |
| | $2NO_2 + 4NH_3 + O_2 \leftrightarrow 3N_2 + 6H_2O$* | | 0.95 |
| FGD | $CO_2 + 2H_2O \leftrightarrow H_3O^+ + HCO_3^-$ | Equilibrium | |
| | $CO_3^- + H_2O \leftrightarrow H_3O^+ + CO_3^{-2}$ | Equilibrium | |
| | $SO_2 + 2H_2O \leftrightarrow H_3O^+ + HSO_3^-$ | Equilibrium | |
| | $CO_3^- + H_2O \leftrightarrow H_3O^+ + SO_3^{-2}$ | Equilibrium | |
| | $CaSO_3\ (Solid) \leftrightarrow Ca^{+2} + SO_3^{-2}$ | Salt | |
| | $CaCO_3\ (Solid) \leftrightarrow Ca^{+2} + CO_3^{-2}$ | Salt | |
| | $CaSO_3{\cdot}0.5H_2O\ (Solid) \leftrightarrow Ca^{+2} + SO_3^{-2} + 0.5H_2O$ | Salt | |

* $NO_2$ is small part of $NO_x$ ($NO + NO_2$) with coal combustion, at most 10%, which is not considered in this work.

**Figure 37 Specifications of reaction in SCR and FGD. Image taken from Hu and Yan (2012)**

## A.1.2 Examples of oxy-combustion plant

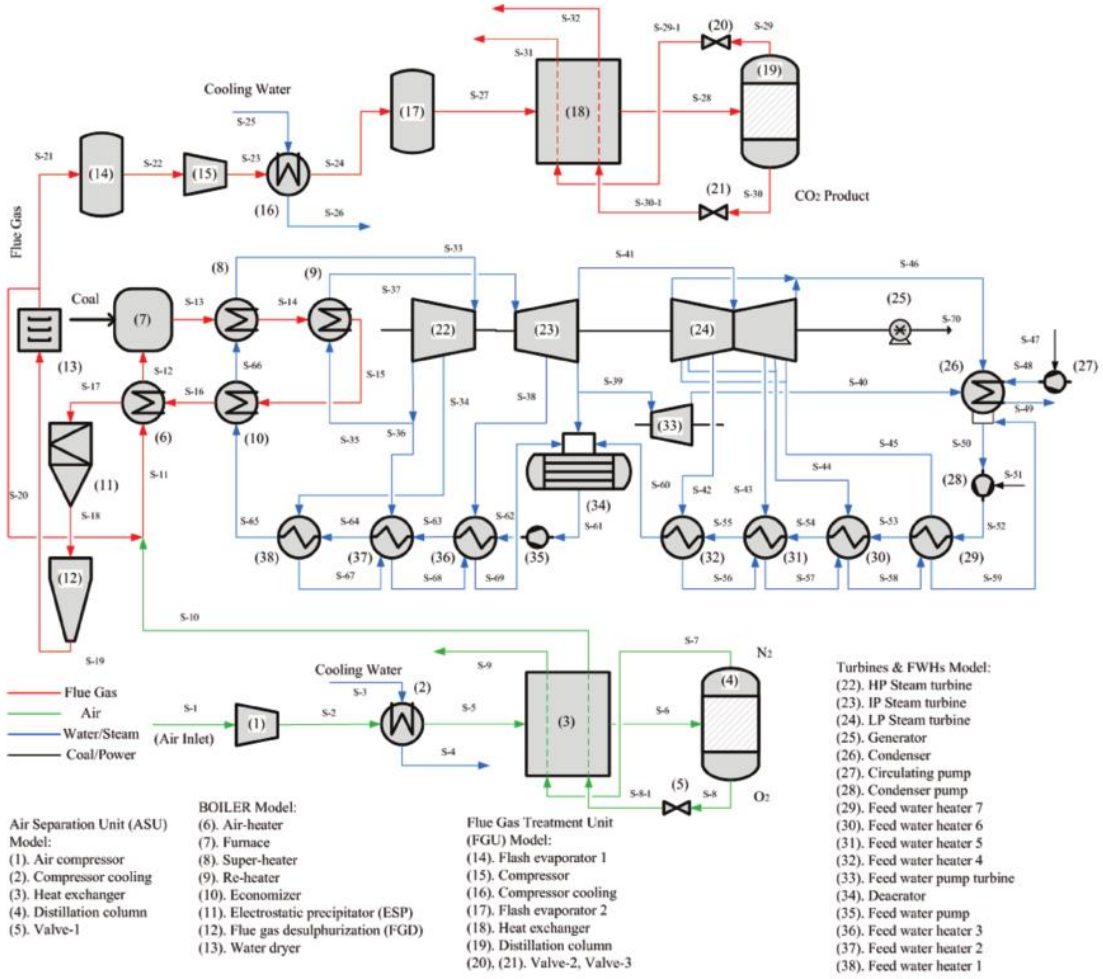


**Figure 38 Schematic diagram of the oxy-combustion PC system including ASU and steam turbines. Image taken from Xiong et al. (2011)**

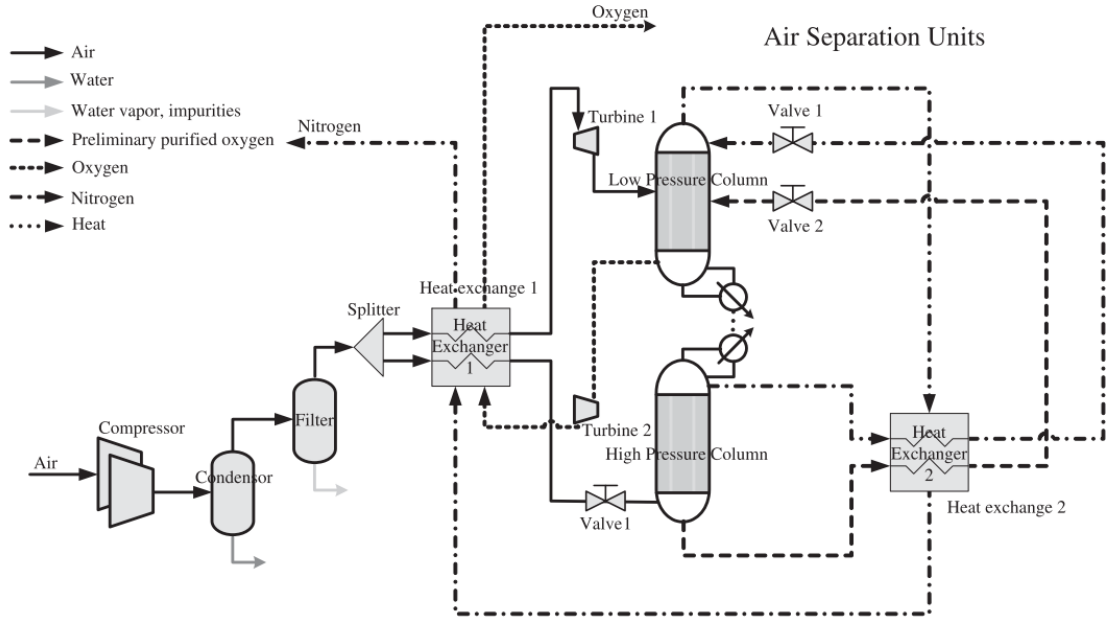


**Figure 39 ASU process flow diagram. Image taken from Hu et al. (2010)**

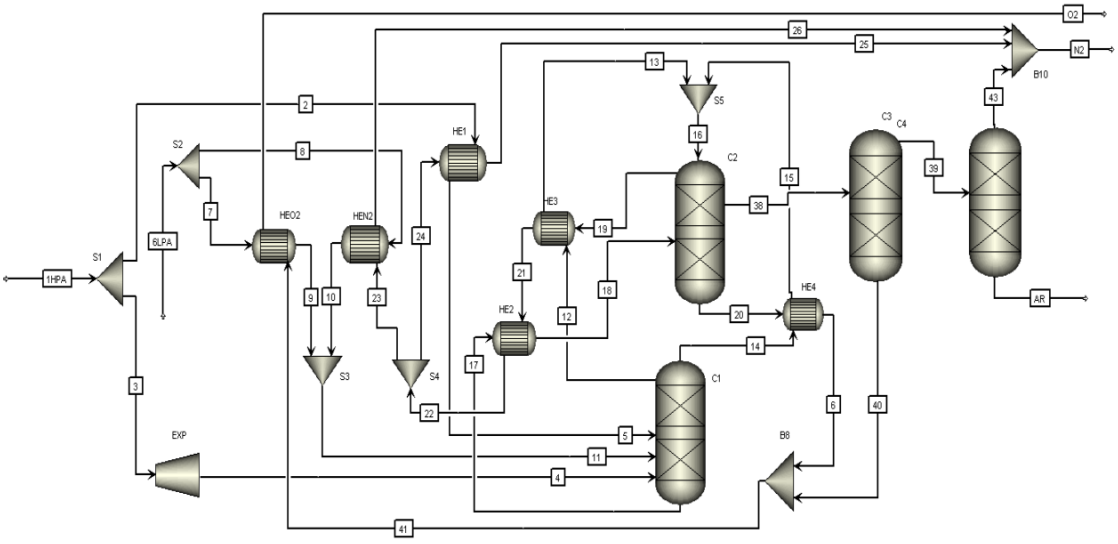


**Figure 40 Scheme of ASU. Image taken from Amarkhail (2010)**

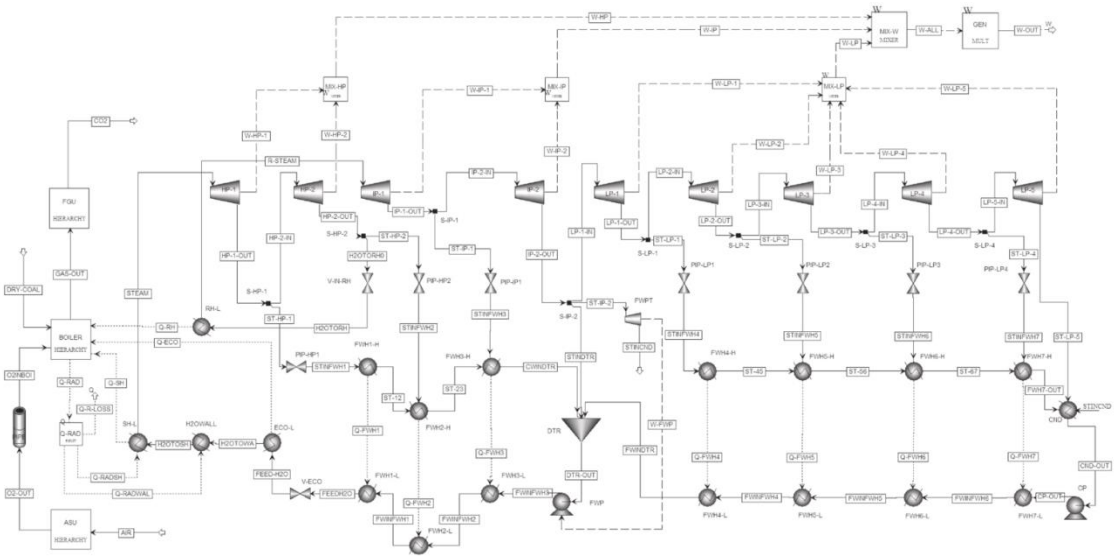

**Figure 41 Oxy-combustion boiler and the steam turbines system. Image taken from Xiong et al. (2011)**

| item | value |
|---|---|
| SH steam | 598.89 °C, 242.35 bar, and 625.994 kg/s |
| RH steam | 621.11 °C and 45.09 bar |
| $O_2$ excess factor | 1.05[36] |
| furnace outlet | 1100 °C and 1 atm |
| recycle ratio | 0.705 |
| air ingress | 15 °C, 1 atm, and 2% of total gas supplied in the boiler |
| condenser outlet | 38.74 °C and 0.368 bar |
| turbine stage discharge pressure (HP1−LP5) (bar) | 77.07, 49.02, 21.36, 9.515, 5.013, 1.323, 0.5771, 0.2473, and 0.0689 |
| TTD (FWH1−FWH7) (°C) | −1.111, 0, −1.111, 2.778, 2.778, 2.778, and 2.778 |
| generator efficiency (%) | 98.58 |

**Figure 42 Basic inputs needed in the simulation. Image taken from Xiong et al. (2011)**

## A.2 Modelling based on kinetics

| | **Reaction,** $\mathrm{kmol/s \cdot m^3}$ | $A_{rj}$ | $E_{rj}/R$, K |
|---|---|---|---|
| 1 | $\frac{d[C_nH_m]}{dt} = A_{r1} \cdot \exp(-E_{r1}/RT_g)\,[C_nH_m][O_2]$ | $3.8 \cdot 10^7$ | 6670 |
| 2 | $\frac{d[CH_4]}{dt} = A_{r2} \cdot \exp(-E_{r2}/RT_g)\,[CH_4]^{0.5}[O_2]^{1.25}$ | $4.4 \cdot 10^{11}$ | 15098 |
| 3 | $\frac{d[CH_4]}{dt} = A_{r3} \cdot \exp(-E_{r3}/RT_g)\,[CH_4][H_2O]$ | $3.1 \cdot 10^8$ | 15098 |
| 4 | $\frac{d[CO]}{dt} = A_{r4} \cdot \exp(-E_{r4}/RT_g)\,[CO][O_2]^{0.3}[H_2O]^{0.5}$ | $2.5 \cdot 10^8$ | 8052 |
| 5 | $\frac{d[H_2O]}{dt} = A_{r5} \cdot \exp(-E_{r5}/RT_g)\,[H_2][O_2]^{0.5}$ | $7.9 \cdot 10^{10}$ | 17614 |

**Figure 43 Kinetic rate of reactions defined by Eq. 1-5. Image taken from Vascellari and Cau (2009)**

| **Reaction** | $A_{rj}, \mathrm{kg/s \cdot m^2 \cdot Pa}$ | $E_{rj}$, J/kmol | Order $n$ | Reference |
|---|---|---|---|---|
| 6 | 0.005 | $74 \cdot 10^6$ | 1 | Field (1969) |
| 7 | $6.3510^{-3}$ | $162 \cdot 10^6$ | 1 | Smoot (1997) |
| 8 | $1.9210^{-3}$ | $147 \cdot 10^6$ | 1 | Smoot (1997) |

**Figure 44 Kinetic rate of surface reaction defined (Eq. 6-8). Image taken from Vascellari and Cau (2009)**

| Phenomena | Reactor block | Input variables |
|---|---|---|
| (1) Devolatilization and volatile combustion | (1) RYIELD | $T_b$, $P$, $F(y)$ |
| | (2) RSTOIC | $T_b$, $P$, $X_C$, $X_H$, $X_S$ chemical reactions |
| (2) Char combustion | (3) RCSTR | $T_b$, $P$, $r_{1,i}$, $r_{CO,i}$ chemical reactions |
| (3) NQ formation | (4) REQUIL | $T_b$, $P$ chemical reactions |
| (4) $SO_2$ capture | (5) RSTOIC | $T_b$, $P$, $X_{CaCO_3}$, $X_{SO_2,i}$ chemical reactions |

**Figure 45 The reactor model parameters utilized in the simulation. Image taken from Sotudeh-Gharebaagh et al. (1998)**

# Appendix B Rig description

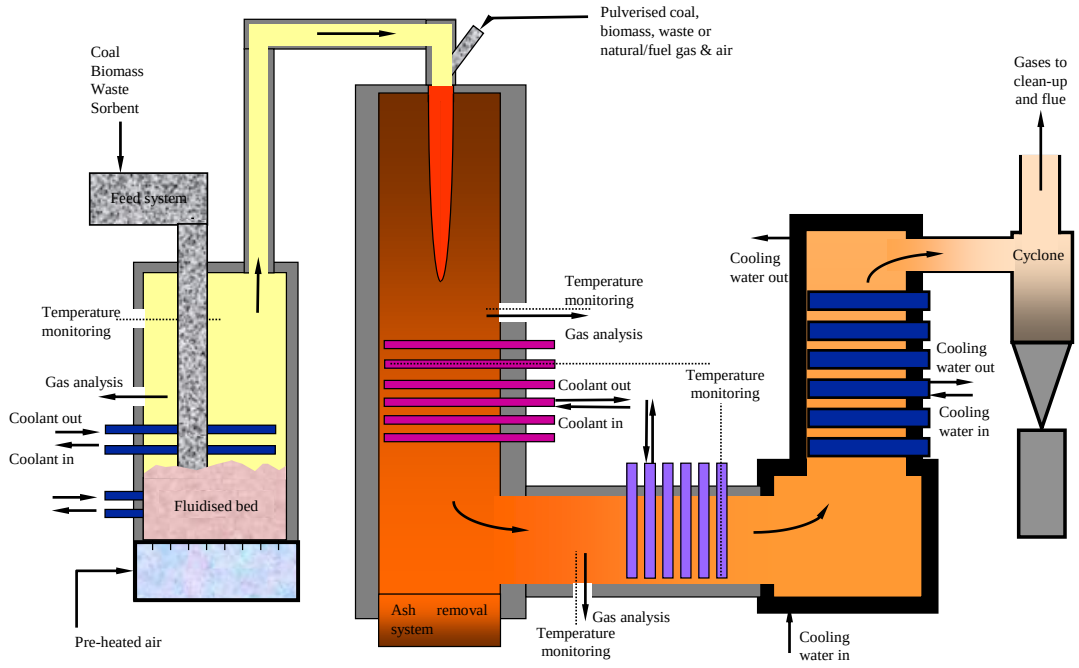


**Figure 46 Schematic diagram of FB (left) and PF (right) combustors prior to the retrofitting process**

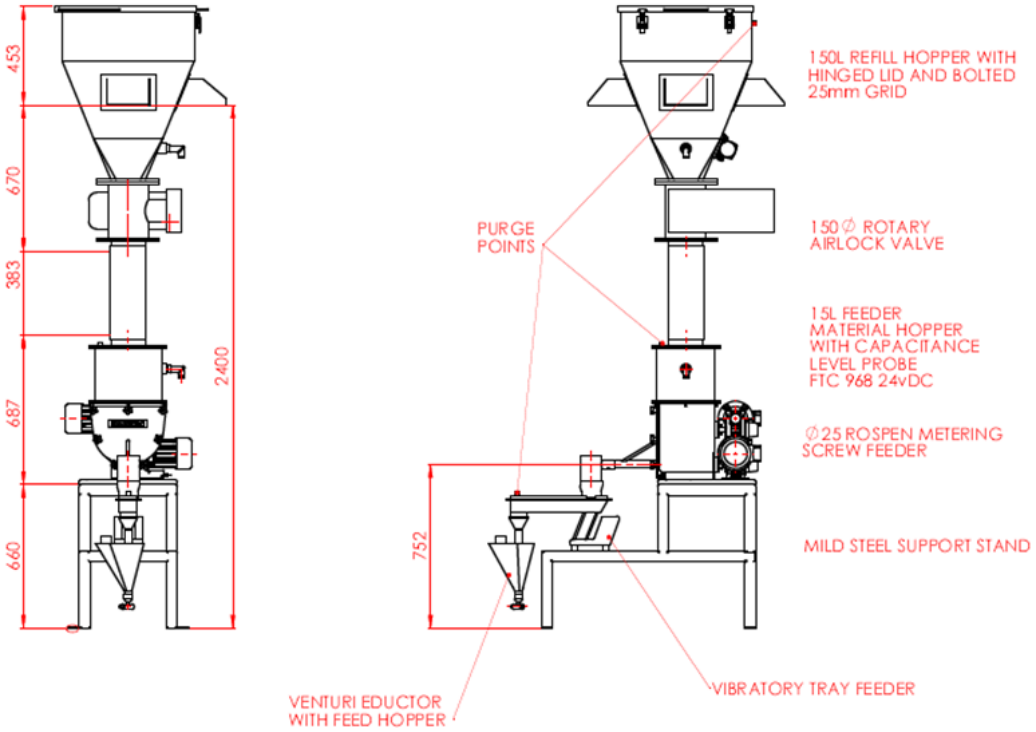


**Figure 47 Schematic of the air-tight PF feeder**

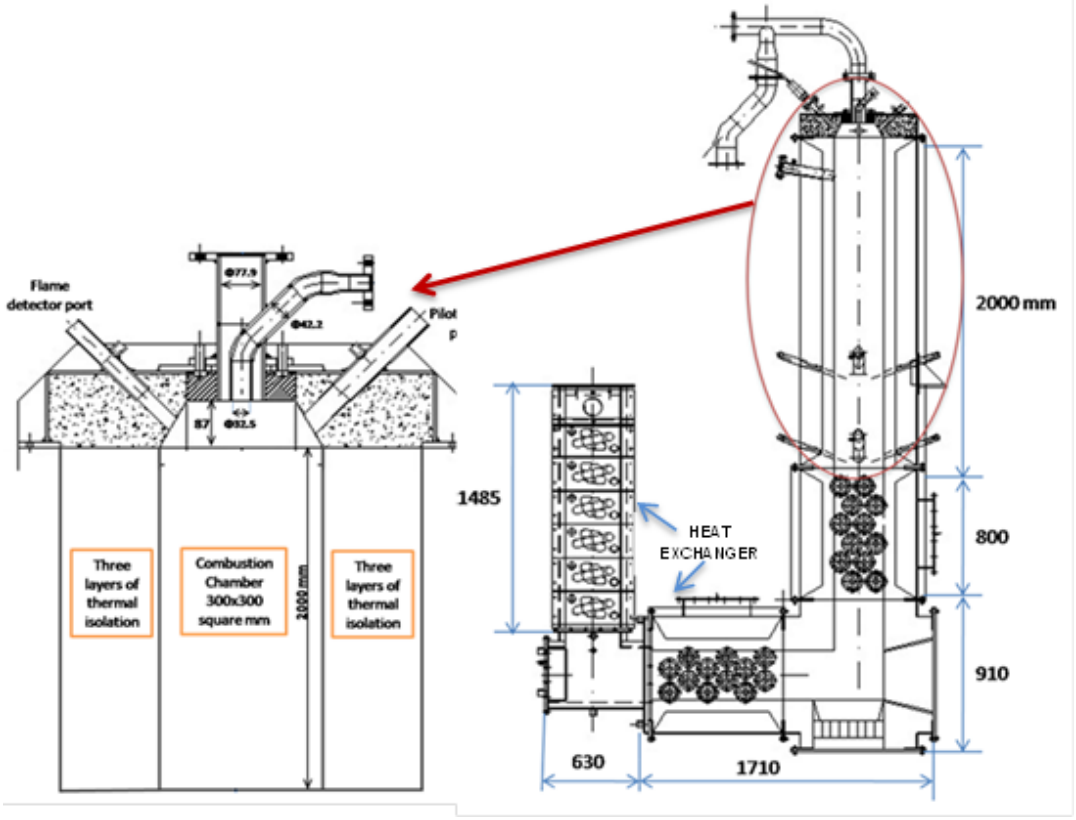


**Figure 48 Overall dimensions of the PF combustor**

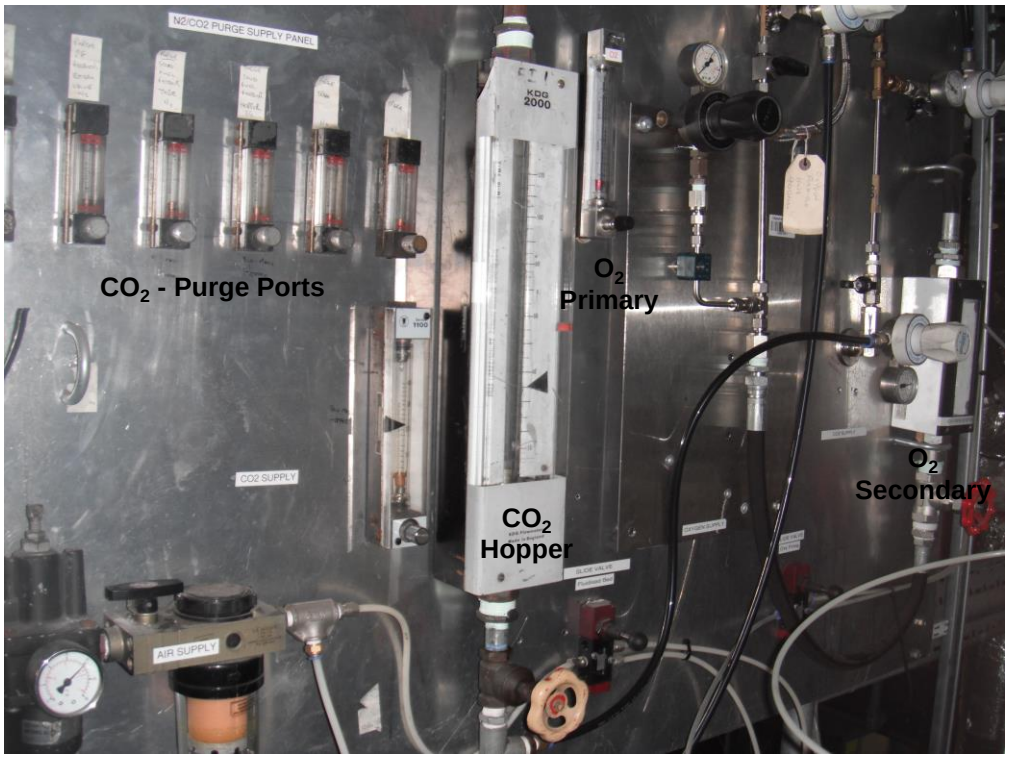


**Figure 49 Gas panel - $CO_2$ and $O_2$ into the process**

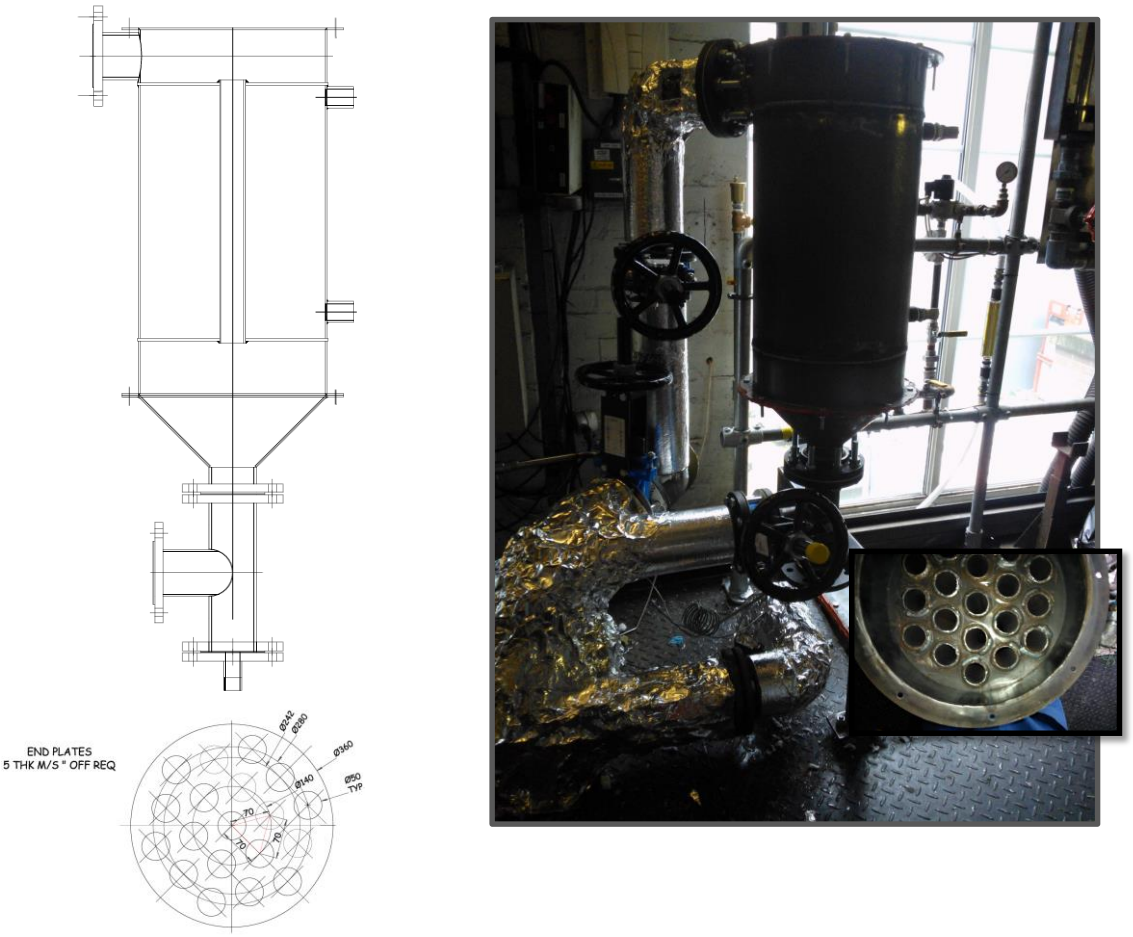


**Figure 50 Image of condenser installed and detail of technical schematic**

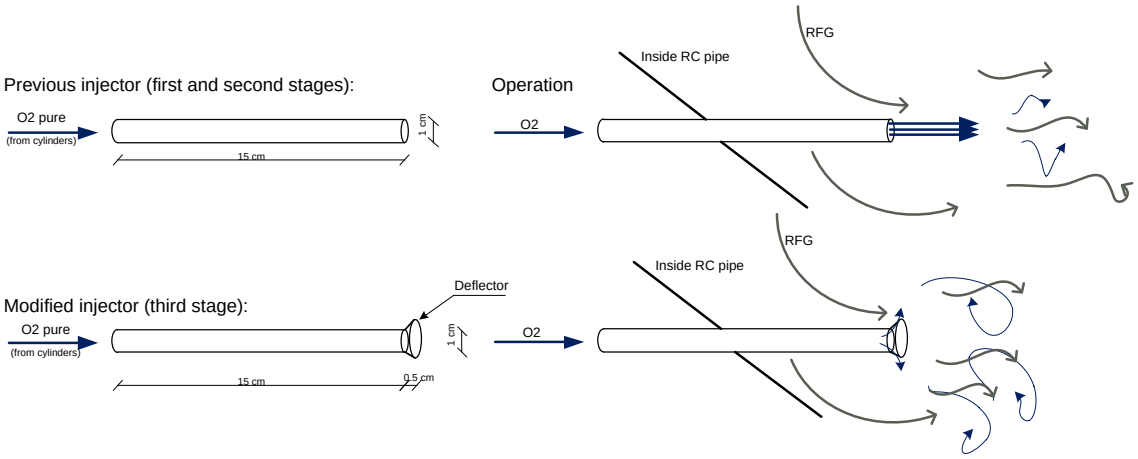


**Figure 51 Technical schematic of $O_2$ injector and its modification**

Standard

| Component | Standard Range / mg/m³ |
|---|---|
| CO | 0 – 75 mCerts |
| NO | 0 – 200 mCerts |
| $NO_2$ | 0 – 200 |
| $N_2O$ | 0 – 100 |
| $SO_2$ | 0 - 75 mCerts |
| $NH_3$ | 0 - 15 mCerts |
| HCl | 0 - 15 mCerts |
| HF | 0 – 15 |
| HBr | 0 - 200 |
| $CH_4$ (Methane) | 0 – 70 |
| $C_2H_6$ (Ethane) | 0 – 50 |
| $C_3H_8$ (Propane) | 0 – 50 |
| $C_4H_{10}$ (n-Butane) | 0 – 50 |
| $C_6H_{14}$ (n-Hexane) | 0 - 50 |
| $C_2H_4$ (Ethene) | 0 - 25 |
| $CH_3OH$ (Methanol) | 0 – 70 |
| HCHO (Formaldehyde) | 0 – 20 |
| $C_6H_6$ (Benzene) | 0 – 250 |
| $C_6H_6O$ (Phenol) | 0 – 100 |
| HCN | 0 – 15 |
| $CCl_4$ | 0 - 200 |
| $CS_2$ | 0 - 100 |
| COS | 0 – 50 |
| $CF_4$ | 0 - 40 |
| $SF_6$ | 0 – 65 |
| TOC (Indication only) | 0 – 50 |
| $H_2O$ | 0 – 40 % mCerts |
| $CO_2$ | 0 – 20 % |
| $O_2$ (via zirconia sensor) | 0 – 20.9% mCerts |

Upgraded

| Component | Standard Range / mg/m³ |
|---|---|
| CO | 0 – 75 mCerts |
| NO | 0 – 200 mCerts |
| $NO_2$ | 0 – 200 |
| $N_2O$ | 0 – 100 |
| $SO_2$ | 0 - 75 mCerts |
| $NH_3$ | 0 - 15 mCerts |
| HCl | 0 - 15 mCerts |
| HF | 0 – 15 |
| HBr | 0 - 200 |
| $CH_4$ (Methane) | 0 – 70 |
| $C_2H_6$ (Ethane) | 0 – 50 |
| $C_3H_8$ (Propane) | 0 – 50 |
| $C_4H_{10}$ (n-Butane) | 0 – 50 |
| $C_6H_{14}$ (n-Hexane) | 0 - 50 |
| $C_2H_4$ (Ethene) | 0 - 25 |
| $CH_3OH$ (Methanol) | 0 – 70 |
| HCHO (Formaldehyde) | 0 – 20 |
| $C_6H_6$ (Benzene) | 0 – 250 |
| $C_6H_6O$ (Phenol) | 0 – 100 |
| HCN | 0 – 15 |
| $CCl_4$ | 0 - 200 |
| $CS_2$ | 0 - 100 |
| COS | 0 – 50 |
| $CF_4$ | 0 - 40 |
| $SF_6$ | 0 – 65 |
| TOC (Indication only) | 0 – 50 |
| $H_2O$ | 0 – 40 % mCerts |
| $CO_2$ | 0 – 80 % |
| $O_2$ (via zirconia sensor) | 0 – 20.9% mCerts |

**Figure 52 Calibration ranges for the FTIR analyser**

**Table 28 Calibration ranges for the ADC MGA 3000 Multi Gas Analyser**

| | Standard | Upgraded |
|---|---|---|
| $CO_2$ | 0-15 % (v/v) | 0-100 % (v/v) |
| $O_2$ | 0-30% (v/v) | 0-40% (v/v) |
| CO | 0-4% (v/v) | 0-4% (v/v) |
| $SO_2$ | 0-1000 ppm | 0-1000 ppm |

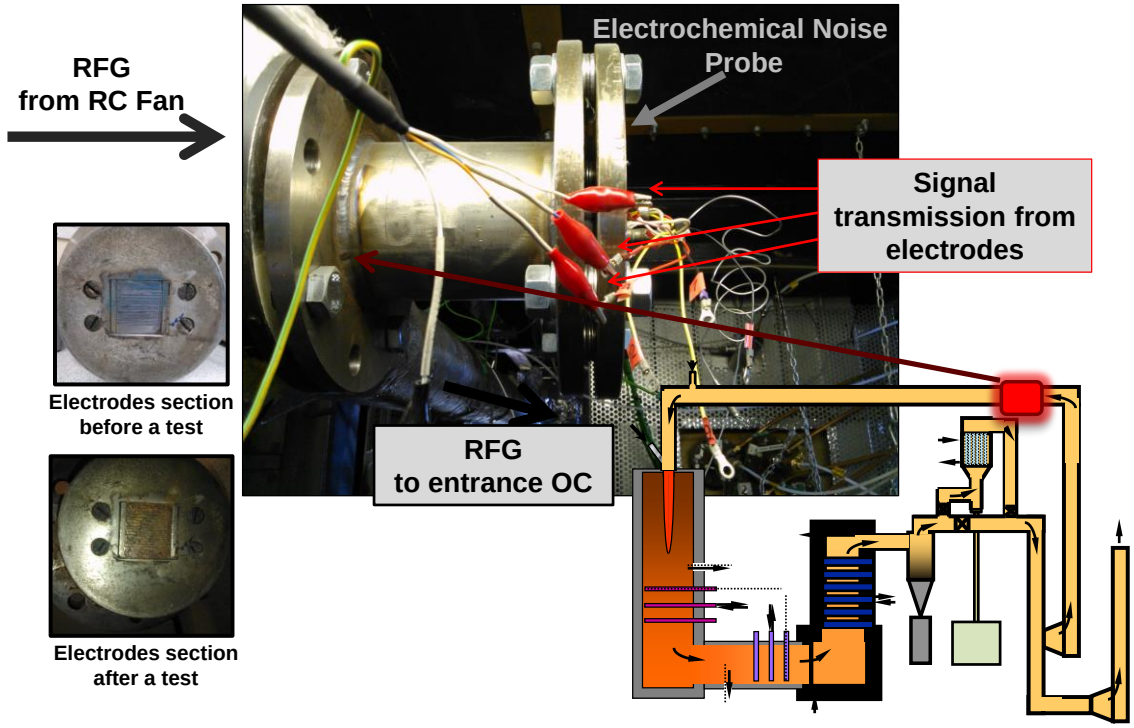


**Figure 53 Electrochemical noise probe location. Detail of electrodes before and after a test**

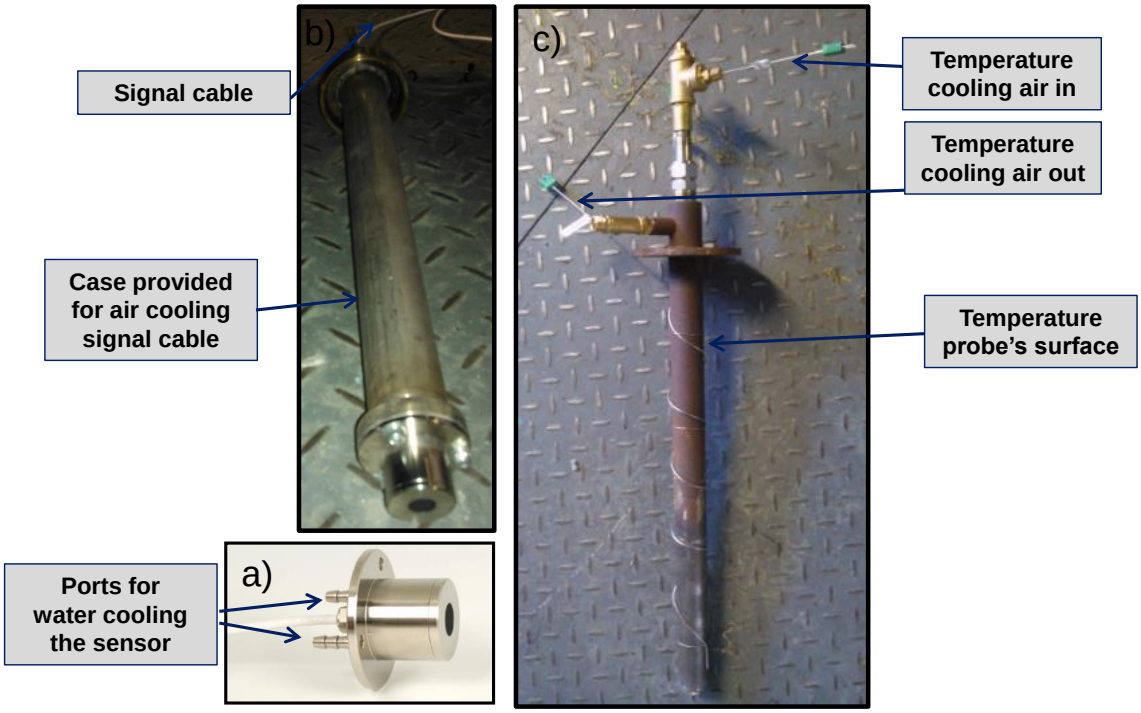


**Figure 54 Heat flux sensors: Global [a), b)] and convective [c)]**

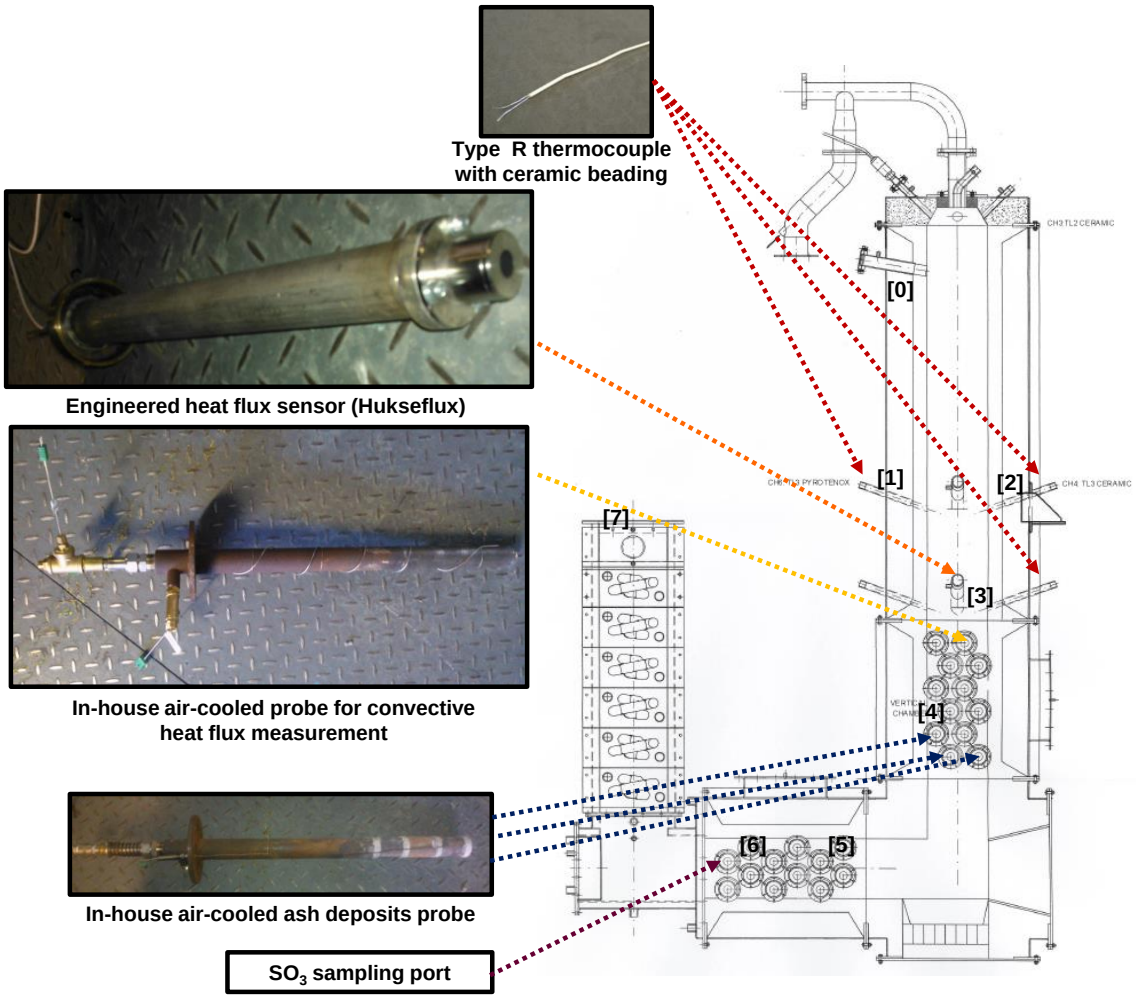


**Figure 55 Location for several measurement systems: R type thermocouples [1-3], K type thermocouples [0-4-5-6-7], heat flux sensors, ash deposits probes and $SO_3$ sampling port**

# B.1 Operational aspects

TEST: DATE:

| CONDITIONS | | TIME | CH1 | CH2 | CH3 | CH4 | FANS | | | TEMPERATURE | | | | | | | | | H FLUX | CAPCIS PROBE | | | INLET GAS | | | | | FTIR (EXHAUST GAS) | | | | RFG | |
|---|---|---|---|---|---|---|---|---|---|---|---|---|---|---|---|---|---|---|---|---|---|---|---|---|---|---|---|---|---|---|---|---|---|
| NG:Natural gas C:Coal/CCP | AF: Air -Firing OF:Oxy - Firing 1:Main FTIR Sampling Point 2: FTIR Sampling Point after condenser | | (FLOWMETER [orifice-plate] ID FAN) (Pa) | (FLOWMETER [orifice-plate] RECIRC FAN) (Pa) | (RIG DRAUGHT) (Pa) | (FLUE DRAUGHT) (Pa) | ID ( Hz) | RC (Hz) | RFG (%) | Ch 3 TL2 ceramic Top vert Cham (°C) | Flame 1 (°C) | Flame 2 (°C) | Flame 3 (°C) | Vert ChambBottm (°C) | Hor Cham 1 (°C) | Hor Chamb 2 (°C) | Before Cyclone (°C) | After Cond (°C) | Hukseflux (kW/m2) | T (°C) | Cooling air? | Noise? | PRIMARY $O_2$ (l/min) | PRIMARY $O_2$ P M1 (bar-man) | SECONDARY $O_2$ (l/min) | $CO_2$ (l/min) | $CO_2$ P M2 (bar-man) | $O_2$ (%) | $CO_2$ (%) | $H_2O$ (%) | CO (ppm) | $O_2$ (%) | $CO_2$ (%) |
| | | | | | | | | | | | | | | | | | | | | | | | | | | | | | | | | | |

**DOUBLE CHECK:**

Temperatures of Deposit Probes are 500, 600 and 700°C
Cooling water and air are fed to Hukseflux sensor
Cooling water of heat exchanger
There is liquid seal at the exit (bottom) of condenser
The glass has grease on the joints

CAPCIS: Working 1-------1
Reference------4
White----------5

SO3 SAMPLING TRAIN

| TIME | SAMPLING TIME | TEMP INSIDE | TEMP FILTER AND TUBE | TEMP CONDENSER | FLOW (l/min) |
|---|---|---|---|---|---|
| | | | | | |
| | | | | | |
| | | | | | |
| | | | | | |

Initial Dry Gas meter reading

Final Gas meter reading

Volume sampled

FUEL IN FEEDER:

HOPPER SPEED:
Vib tray:
Massflow(kg/h)

REMAINING FUEL IN FEEDER(kg):

INCIDENTS:

CONDENSATES:

TEST DURATION:

COAL CONSUMPTION:

**Figure 56 Datasheet for data acquisition during operation**

### B.1.1 Limitations during operation

During the experimental tests, a number of limitations for the operation of the rig were identified and are explained below. Some of them were specific for one of the campaigns, and others have been common during the course of the PhD.

- Limitations during first campaign:
  - The rudimentary design of the fuel feeder used during this campaign caused several deviations from the optimal operation:
    - ✓ Due to its low storage capacity, it had to be refilled every 30 minutes, causing a massive air ingress into the process
    - ✓ The vibratory tray associated to the feeder did not provide with a constant flowrate of fuel, causing noticeable fluctuations in the characteristics of the flame and the flue gas.
- Limitations during second campaign:
  - The main difficulty found in this campaign was in relation to controlling the recycle flue gas, as it is the consequence of the interaction of fans considering also the specification of keeping negative pressure inside the combustor
  - This campaign was the first one in which biomass was used, and its high water content effect on the flue gas was pointed out as a possible source of operational problems: possible condensation in the recycle line, in the fans or in the exhaust duct. This led to increased attention to the trace heating system's maintenance and its re-design to be effective with the new operating conditions
  - Another issue associated with the use of the biomass, was related to its fibrous form. Some straw would pass the sieve with mesh size of 1.7 mm (if they achieved an orientation to the sieve longitudinally, during the preparation of the fuel) but during the operation, they could obstruct the posterior part of the Venturi eductor, blocking the fuel ability to reach the burner

- Some problems were associated with the controllability of the gas-tight fuel feeder, as sometimes there was not good communication between the level controllers associated with it. This on some occasions stopped the test as no fuel was fed into the burner even though the hopper was not empty.

– Limitations during third campaign:
  - Some difficulty was found in controlling the percentage of recycle flue gas and the pressure inside the combustor, when the condenser was used. This is thought to be consequence of the pressure drop created by the column of water that appeared inside the condenser after some time of operation. The solution found after the initial tests of this campaign, was to partially bypass the condenser, intermittently, to allow for the draining of the condensates
  - The efficiency of the condenser was found to drop sharply after two hours of operation. Additionally, for those tests using 100% biomass, the condenser had to be used from the beginning, as otherwise it would achieve minimal efficacy
  - The improved performance of the oxy-combustor allowed one to reach high temperatures in the area close to the bottom of the vertical section, which in turn made it necessary to change the location of the deposit probes (towards inferior sampling ports)
  - Some air ingress into the process was found to occur through the deposit probes, as consequence of the cooling air used in them
  - Moving the FTIR sampling point from the vertical section of the oxy-combustor to the exit of the condenser took ten minutes, and during this time no flue gas analysis could be done. This change in location was made after having after having reached almost completely steady state inside the combustor, so not to lose crucial data

- Despite calibrating the fuel feeder several times for a specific flowrate (coal, biomass or blends), the flowrate during the experiment would always differ from the calibration settings
- The heat flux sensor (manufactured by Hukseflux) had only one possible location, so if the flame was much higher or lower in the vertical section of the oxy-combustor, this affected the measurements
- The wet gas meter used for the $SO_3$ sampling train based its measurements on having a certain quantity of water. Sometimes, during a sampling period, this meter had to be refilled as it was noticed it was not measuring properly (after some time, part of the water had evaporated)
- Although the controlled condensation method used for this PhD work recommends the use of a dry gas meter to sample $SO_3$, this was not available. The alternative of using a wet gas meter is thought to produce measurements sufficiently accurate, with the error for $SO_3$ and $SO_2$ levels calculated to be around 0.5%.

– Limitations common to all the campaigns:
  - Time limitations: due to the time necessary for the combustor to heat up, also given the maximum capacity of the hopper, the tests could not last more than 3-4 hours. However, it is believed that after this time the steady state had been reached or at least conditions were very close to stead state conditions.
  - During the preparation of the fuels, previously to each test, the blend of coal and biomass was done manually, so there is always a risk of non-homogeneity in the blend or possible stratification inside the feeder hopper.
  - The gases into the process, $O_2$ and $CO_2$, were manually controlled
  - For the first a second campaigns, gas cylinders were used to supply $O_2$ and $CO_2$. Due the high flowrate necessary, special attention had to be paid during the test to check that the supply pressure was high enough; otherwise, the cylinder had to be

changed. In the last campaign this supply system was changed to high capacity vessels of compressed gases.

### B.1.2 Preparation tasks

- Start logging data from:
  - ✓ FTIR
  - ✓ Data logger (downstairs and upstairs)
  - ✓ Electrochemical noise probe
- Open valves for $O_2$ cylinders
- Open valves for $CO_2$ from the BOC tank
  - ✓ Set up rotameters for viewports
  - ✓ Set up rotameters for hopper
- Set up $O_2$ analyser:
  - ✓ Make sure that the rock wool is clean, if not replace it
  - ✓ Flasks in containers with water and ice blocks
- Open valves for compressed air and set up air-cooling rotameters
- Open valves for cooling water to Hukseflux sensor
- Set up the cooling water of the combustor heat exchanger at a enough flowrate to be around 100-150°C before the cyclone
- Turn on trace heating for recirculation line
- Set up $SO_3$ sampling train:
  - ✓ Set up glassware
  - ✓ Attach heating tapes
  - ✓ Insulation
  - ✓ Impingers filled with $H_2O_2$, $H_2O$ and silica
- Prepare fuel for 3,5 hours of operation for oxy-firing and 2.5 hours for air-firing (minimum)
  - ✓ 100% Coal: 13.5kg/h (Total O-F:47.3kg; Total A-F:33.75kg)
  - ✓ 100% Biomass:22kg/h (Total O-F:77kg; Total A-F:55kg)
  - ✓ 50% Coal-50% Biomass: 16.7kg/h (Total O-F: 58.5 kg [Coal: 29.25kg/ Biomass: 29.25kg]; Total A-F: 42kg [Coal: 21/ Biomass: 21kg])

- ✓ 75% Coal-25% Biomass: 15kg/h (Total O-F:52.5 kg [Coal: 39.4/ Biomass: 13.1kg]; Total A-F:37.5kg [Coal:28.1/ Biomass: 9.4kg]).

### B.1.3 Maintenance tasks

- Disassemble electrochemical noise probe, polish it and re-install it
- Clean ceramic filter of FTIR
  - ✓ Ultrasonic bath during 30 minutes for two consecutive times (changing water of the glass where the filter is placed)
  - ✓ Dry it for 12-24 hours on a radiator
  - ✓ Apply compressed air (from the inside)
- Empty container below cyclone (take sample for burnout test)
- Hoover horizontal section of combustor (through bottom hexagonal plates)
- Empty the fuel feeder and weight the remaining fuel
- Take ash samples
- Take burnout samples (inside the furnace and cyclone)
- Measure volume of condensates
- Clean $SO_3$ sampling train, take samples and analyse them.

# Appendix C Simulation model description

**Table 29 Reactors definition for the equilibrium model**

| Phenomena | Reactor Type | Input Parameters |
|---|---|---|
| Drying | RSTOIC | Pressure, heat duty, reactions, reaction's selectivity, final moisture |
| | FLASH2 | Pressure, heat duty |
| Oxy-combustion | | |
| - DEVOLATILIZATION | RYIELD | Pressure, temperature, yield of each component |
| - COMBUSTION | RGIBBS | Pressure, existing phases |
| Heat transfer | Heater | Pressure, exit temperature |
| Solid removal | SSPLIT | Split fraction for each stream |
| Heat loss | Heater | Pressure, exit temperature |

**Table 30 Reactors description for equilibrium and rate-based model**

| Reactor Type | Description |
|---|---|
| RSTOIC | Stoichiometric reactor based on known fractional conversions or extents of reaction |
| RYIELD | Nonstoichiometric reactor based on known yield distribution |
| RGIBBS | Rigorous reaction and/or multiphase equilibrium based on Gibbs free energy minimization |
| RPLUG | Rigorous plug reactor with rate-controlled reactions based on known kinetics |
| REQUIL | Rigorous equilibrium reactor based on stoichiometric approach |
| FLASH2 | Two-outlet flash. Models flash drums, evaporators…,using rigorous V-L or V-L-L equilibrium |
| SSPLIT | Sub-stream splitter. Divides feed based on splits specified for each sub-stream |
| Heater | Thermal and phase changer |

**Table 31 Reactors definition for kinetic model with partial condensation in the RFG**

| Phenomena | Reactor Type | Input Parameters | Kinetics | | | | Specification Type |
|---|---|---|---|---|---|---|---|
| | | | Reactions | A | $A_{HR}$ | E | |
| Drying | RSTOIC | P, heat duty, reactions, reaction's selectivity, final moisture | | | | | |
| | FLASH2 | P, heat duty | | | | | |
| Oxy-combustion | | | | | | | |
| -DEVOLATILIZATION | RYIELD | P, T, yield of each component | | | | | |
| -VOLATILE COMBUSTION | RSTOICH | P, fractional conversion | $CO + 0.5O_2 \rightarrow CO_2$<br>$S + O_2 \rightarrow SO_2$<br>$H_2 + 0.5O_2 \rightarrow H_2O$ | | | | Fractional conversion<br>Xc =VM-H-S<br>$Xc_{(DM)}$=0.2564<br>$Xc_{(CCP)}$=0.6484<br>$X_S$=1; $X_{H2}$=1 |
| -CHAR COMBUSTION | RPLUG | P, heat duty, reactor dimensions, kinetic parameters | $C(s) + 0.5O_2 \rightarrow CO$<br>$C(s) + CO_2 \rightarrow 2CO$<br>$C(s) + H_2O \rightarrow CO + H_2$<br>$CO + 0.5O_2 \rightarrow CO_2$<br>$H_2 + 0.5O_2 \rightarrow H_2O$ | $5 \cdot 10^{-3}$<br>$6.35 \cdot 10^{-3}$<br>$1.92 \cdot 10^{-3}$ | <br><br><br>$2.5 \cdot 10^{8}$<br>$7.9 \cdot 10^{10}$ | $7.4 \cdot 10^{4}$<br>$1.62 \cdot 10^{5}$<br>$1.47 \cdot 10^{5}$<br>8.052<br>17.614 | |
| -THERMAL $NO_x$ GENERATION | REQUIL | P, heat duty | $0.5N_2(air) + 0.5O_2 \rightarrow NO$<br>$0.5N_2(air) + 0.5O_2 \rightarrow NO_2$<br>$N_2 + 0.5O_2 \rightarrow N_2O$ | | | | Temperature approach<br>$\Delta T$=0 |
| -FUEL $NO_x$ GENERATION | RSTOICH | P, heat duty | $0.5N_2(Fuel) + O_2 \rightarrow NO_2$ | | | | Partial conversion<br>$X_{N(Fuel)}$=1 |
| Heat transfer | Heater | P, $T_{exit}$ | | | | | |
| Solid removal | SSPLIT | Split fraction for each stream | | | | | |
| Heat loss | Heater | P, $T_{exit}$ | | | | | |
| Partial condenser | Component separator | P, T, split fraction for each stream, valid phases | | | | | Max $P_{H2O)RFG}]_{EXIT}$ = $P^{o}_{H2O,Sat}(T_{min\ reached})$ |
| Heat conditioning | Heater | P, $T_{exit}$ | | | | | |

**Table 32 Value of the fixed parameters used in the kinetic model-Different stages**

| Parameter | Value in stage K3 (Wet recycle with partial condensation) | Value in stage K6 (Dry recycle) |
|---|---|---|
| $r_{fuel\ part}$ (μm) | 250 | 250 |
| $MW_C$ (g/mol) | 12 | 12 |
| Flowrate $_{coal}$(kg/h) | 14.93 | 13.5 |
| $\rho_{coal}$ (kg/m$^3$) | 1836 | 1836 |
| $\rho_{B,\ coal}$ (kg/m$^3$) | 431 | 431 |
| Flowrate $_{CCP}$(kg/h) | 22.03 | 22.03 |
| $\rho_{CCP}$ (kg/m$^3$) | 503 | 503 |
| $\rho_{B\ CCP}$ (kg/m$^3$) | 96 | 96 |
| *Combustor geometry (flame section)* | | |
| - Cross section( m$^2$) | 0.09 | 0.09 |
| -Length (m) | 2 | 2 |
| Cyclone efficiency (%) | 90 | 100 |
| $T_{exit\ H\ –EXCH}$ (K) | 640 | 640 |
| $T_{exit\ H\ –LOSS}$ (K) | 360 | 360 |
| $T_{exit\ TRACE\ HEATING\ SYSTEM}$ (K) | 400 | 400 |
| Convergence Method | Broyden | Broyden |
| Tolerance $_{PRODUCTS}$ | 0.001 | 0.001 |
| Tolerance $_{CHARPRODUCTS}$ | 0.0001 | 0.0001 |
| Tolerance $_{VOLPRODUCTS}$ | 0.0001 | 0.0001 |

**Table 33 Reactors definition for kinetic model with dry recycle-Stages K4 and K6**

| Phenomena | Reactor Type | Input Parameters | Kinetics | | | | Specification Type |
|---|---|---|---|---|---|---|---|
| | | | Reactions | A | $A_{HR}$ | E | |
| Oxy-combustor | | | | | | | |
| VOLATILE COMBUSTION | RSTOICH | P, fractional conversion | $CO + 0.5O_2 \rightarrow CO_2$<br>$S + O_2 \rightarrow SO_2$<br>$H_2 + 0.5O_2 \rightarrow H_2O$<br>$H_2O + Cl_2 \rightarrow 2HCl + 0.5O_2$ | | | | Fractional conversion<br>Xc =VM-H-S<br>$Xc_{(El\ Cerrejon)}$=0.2942<br>$Xc_{(CCP)}$=0.6484<br>$X_S$=1; $X_{H2}$=1; $X_{Cl2}$=1 |
| CHAR COMBUSTION | RPLUG | P, heat duty, reactor dimensions, kinetic parameters | $C(s) + 0.5O_2 \rightarrow CO$<br>$C(s) + CO_2 \rightarrow 2CO$<br>$C(s) + H_2O \rightarrow CO + H_2$<br>$CO + 0.5O_2 \rightarrow CO_2$<br>$H_2 + 0.5O_2 \rightarrow H_2O$ | $5 \cdot 10^{-3}$<br>$6.35 \cdot 10^{-3}$<br>$1.92 \cdot 10^{-3}$ | <br><br><br>$2.5 \cdot 10^{8}$<br>$7.9 \cdot 10^{10}$ | $7.4 \cdot 10^{4}$<br>$1.62 \cdot 10^{5}$<br>$1.47 \cdot 10^{5}$<br>8.052<br>17.614 | |
| THERMAL NOx GENERATION | REQUIL | P, heat duty | $0.5N_2(air) + 0.5O_2 \rightarrow NO$<br>$0.5N_2(air) + 0.5O_2 \rightarrow NO_2$<br>$N_2 + 0.5O_2 \rightarrow N_2O$ | | | | Temperature approach<br>ΔT=0 |
| FUEL NOx GEN | RSTOICH | P, heat duty | $0.5N_2(Fuel) + O_2 \rightarrow NO_2$ | | | | $NO_2$ molar extent<br>$2.4 \cdot 10^{-8}$ kmol/s |
| Condenser | | | | | | | |
| CONDENSER | REQUIL | P, T | $NO + 0.5\ O_2 \leftrightarrow NO_2$<br>$2\ NO_2 + H_2O + 0.5\ O_2 \leftrightarrow 2\ HNO_3$<br>$SO_2 + 0.5\ O_2 \leftrightarrow SO_3$<br>$SO_3 + H_2O \leftrightarrow H_2SO_4$ | | | | Temperature approach<br>ΔT=0 |
| ACID SEP | SEP | Split fraction | | | | | $SF_{H2O}$=0.95; $SF_{HCl}$=0.98; $SF_{H2SO4}$= $SF_{HNO3}$=1 |

**Table 34 Variable split fractions (SF) applied in kinetic model with dry recycle (K7) depending of fuel**

| | $SF_{H2O}$ | $SF_{HCl}$ | $SF_{H2SO4}$ | $SF_{HNO3}$ |
|---|---|---|---|---|
| 100% El Cerrejon coal | 0.33 | 1 | 1 | 1 |
| 75%El Cerrejon-25% CCP (wt.) | 0.535 | 1 | 1 | 1 |
| 50%El Cerrejon-50% CCP (wt.) | 0.57 | 1 | 1 | 1 |
| 100% Cereal co- product | 0.86 | 1 | 1 | 1 |

# Appendix D Experimental data

**Table 35 Fuel flowrates used for each experiment and power associated**

| | $\dot{m}_{\text{Daw Mill}}$ (kg/h) | $\dot{m}_{\text{El Cerrejon}}$ (kg/h) | $\dot{m}_{\text{Cereal co-product}}$ (kg/h) | Potential power generated (kW) |
|---|---|---|---|---|
| FC.DM.A | 8.4 | - | - | 56 |
| FC.DM.O(a) | 8.4 | - | - | 56 |
| FC.DM.O(b) | 8.4 | - | - | 56 |
| FC.DM.O(c) | 8.4 | - | - | 56 |
| FC.DM.O(d) | 13.1 | - | - | 88 |
| SC.DM.O | 18.0 | - | - | 120 |
| SC.CC.O | - | - | 17.6 | 80 |
| SC.B1.O | 8.8 | | 8.8 | 99 |
| TC.EC.A | - | 14.4 | - | 108 |
| TC.B1.A | - | 9 | 9 | 108 |
| TC.CC.A | - | - | 22.3 | 101 |
| TC.EC.O.(a) | - | 15.8 | - | 119 |
| TC.EC.O.(b) | - | 13.5 | - | 101 |
| TC.EC.O.(c) | - | 16.7 | - | 125 |
| TC.B2.O | | 11.6 | 3.9 | 105 |
| TC.B1.O.(a) | - | 9.5 | 9.5 | 114 |
| TC.B1.O.(b) | - | 8.7 | 8.7 | 105 |
| TC.CC.O | - | - | 26 | 118 |

## D.1 Gas composition and temperature

### D.1.1 First campaign

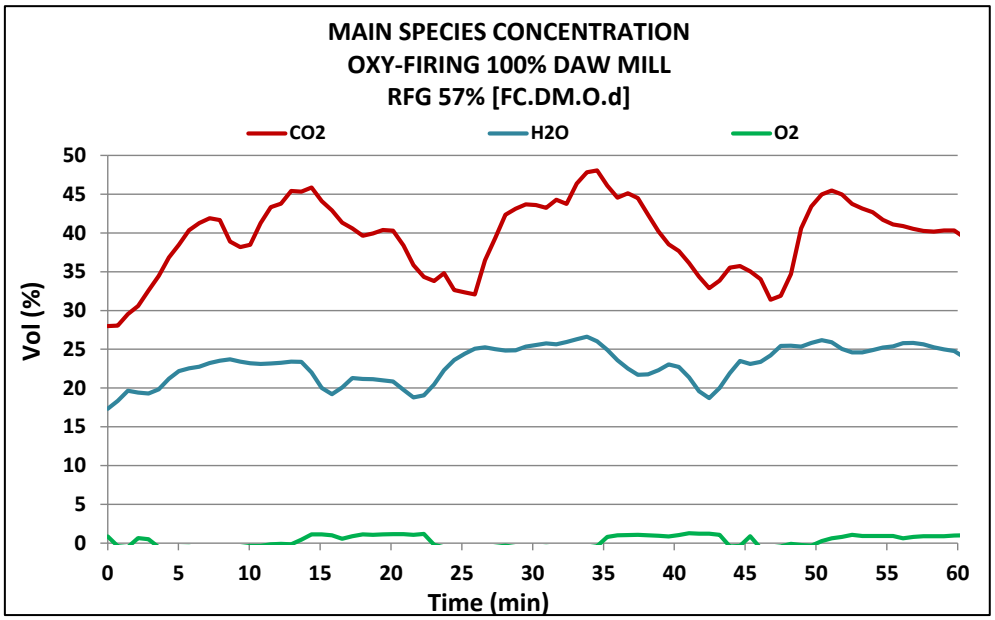


**Figure 57 Gas composition_ Main species evolution for oxy-firing test FC.DM.O.d**

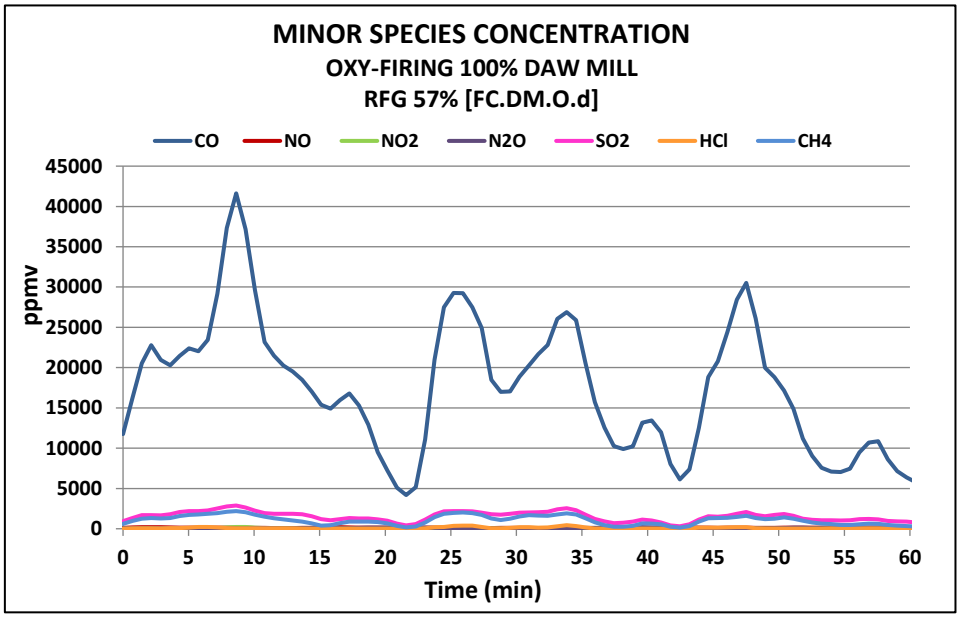


**Figure 58 Gas composition_ Minor species evolution for oxy-firing test FC.DM.O.d**

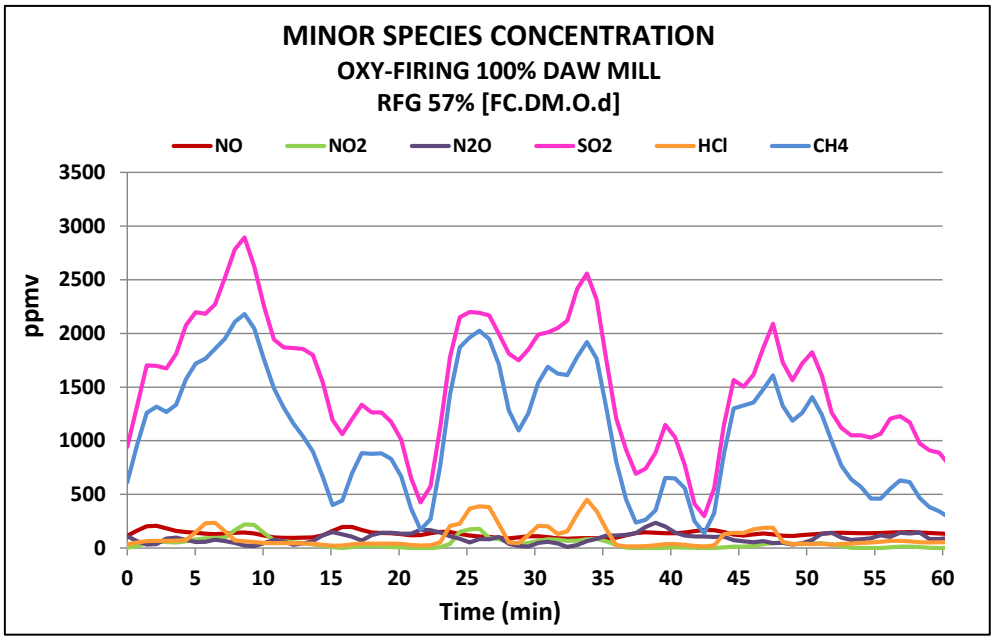


**Figure 59 Gas composition_ Minor species evolution (without CO) for oxy-firing test FC.DM.O.d**

## D.1.2 Second campaign

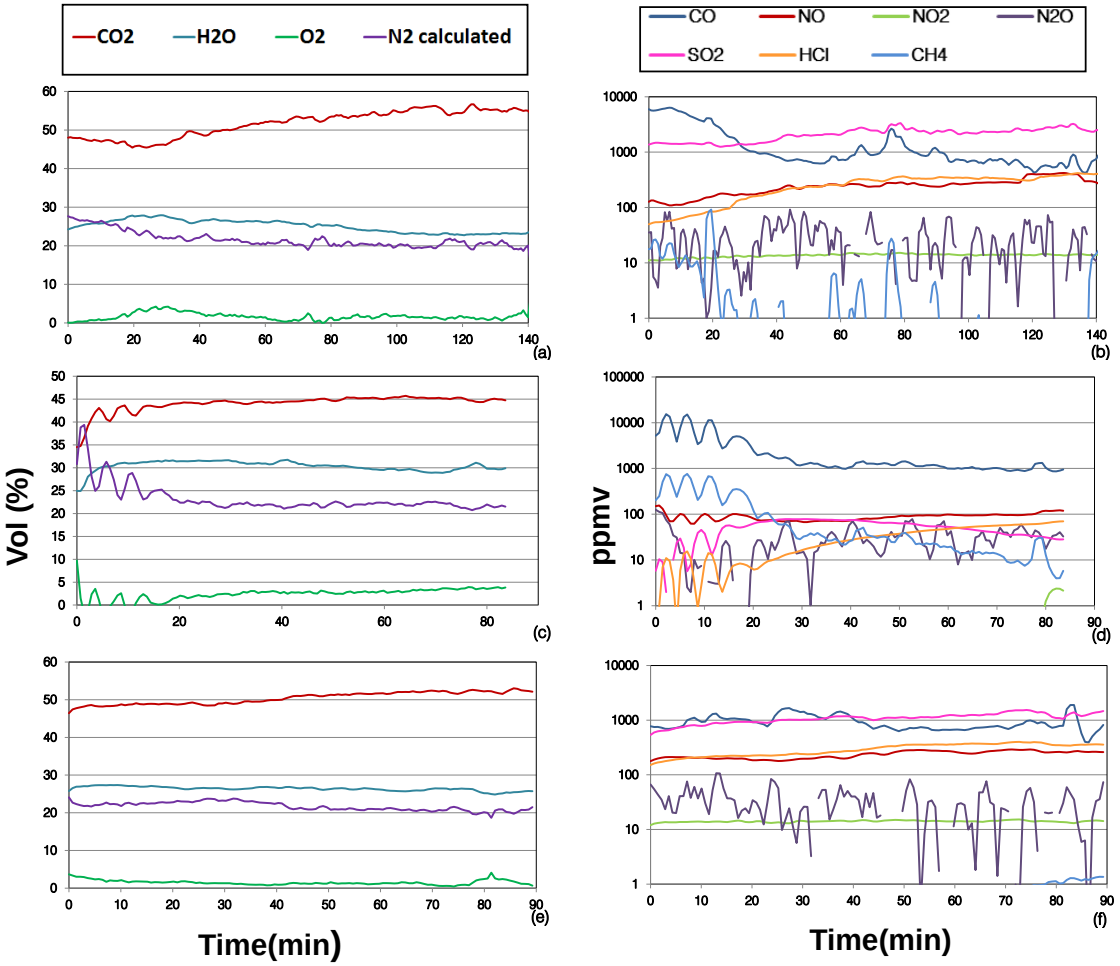


**Figure 60 Gas composition of the flue gas in second campaign. (a) Main species 100% Daw Mill [SC.DM.O] (b) Minor species 100% Daw Mill [SC.DM.O] (c) Main species 100% CCP [SC.CC.O] (d) Minor species 100% CCP[SC.CC.O] (e) Main species 50% Daw Mill-50% CCP [SC.B1.O] (f) Minor species 50% Daw Mill-50% CCP [SC.B1.O]**

## D.1.3 Third campaign

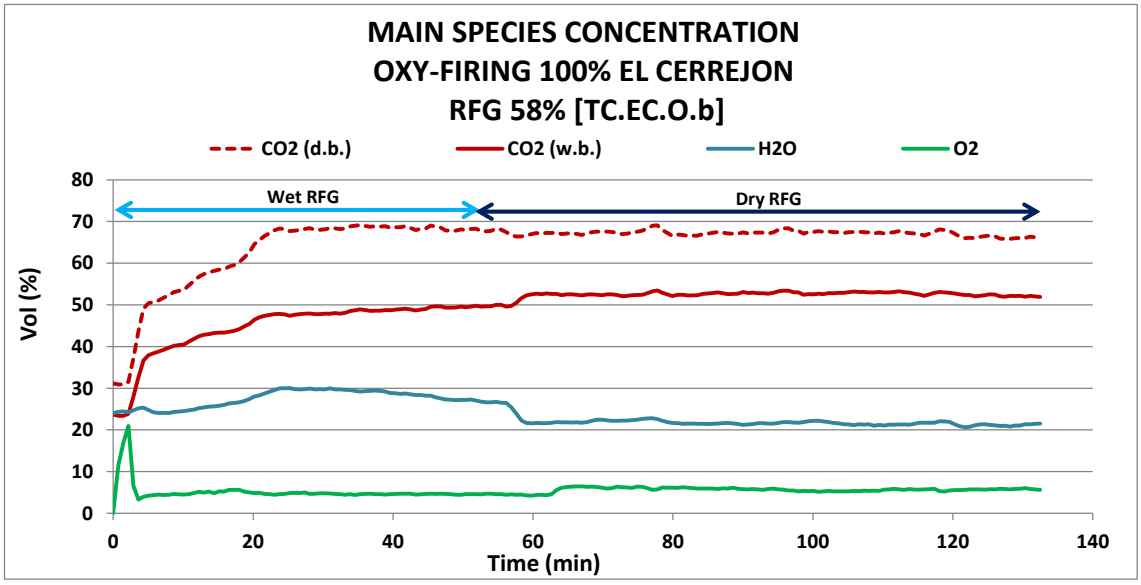


**Figure 61 Gas composition_ Main species for oxy-firing test TC.EC.O.b. Transition from wet to dry RFG**

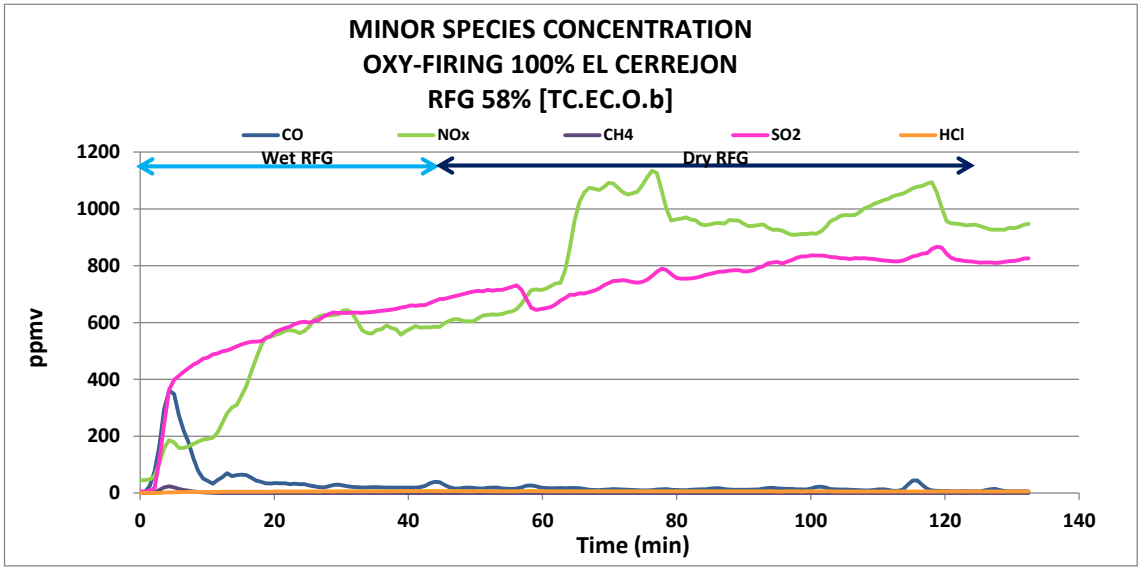


**Figure 62 Gas composition_ Minor species evolution for oxy-firing test TC.EC.O.b. Transition from wet to dry RFG**

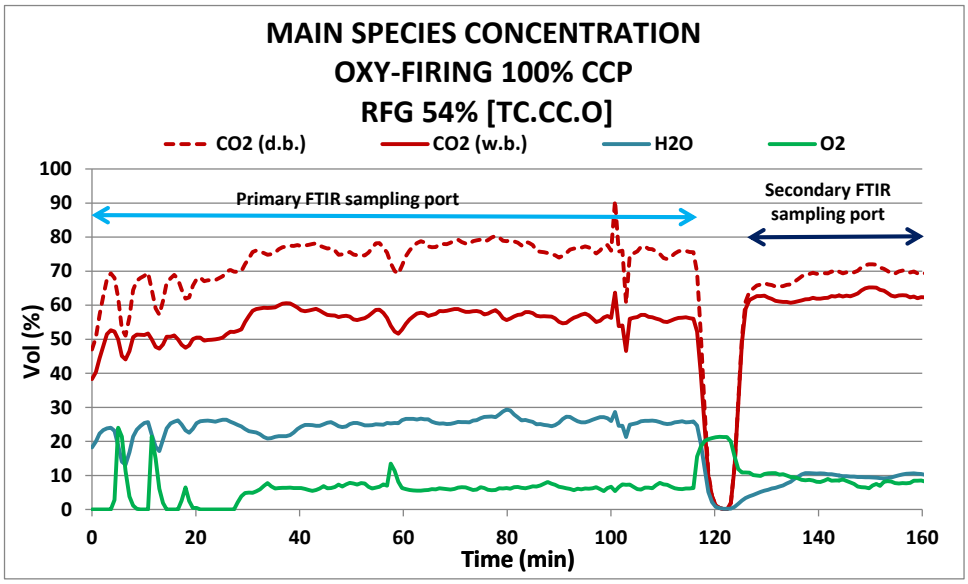


**Figure 63 Gas composition_ Main species for oxy-firing test TC.CC.O. Samples using primary and secondary FTIR ports**

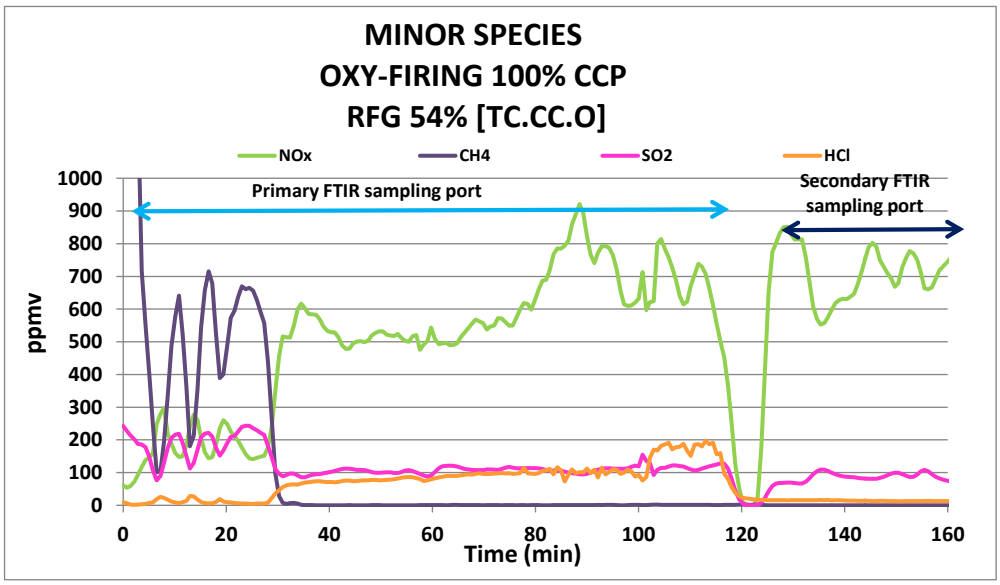


**Figure 64 Gas composition_ Minor species (without CO) for oxy-firing test TC.CC.O. Samples using primary and secondary FTIR ports**

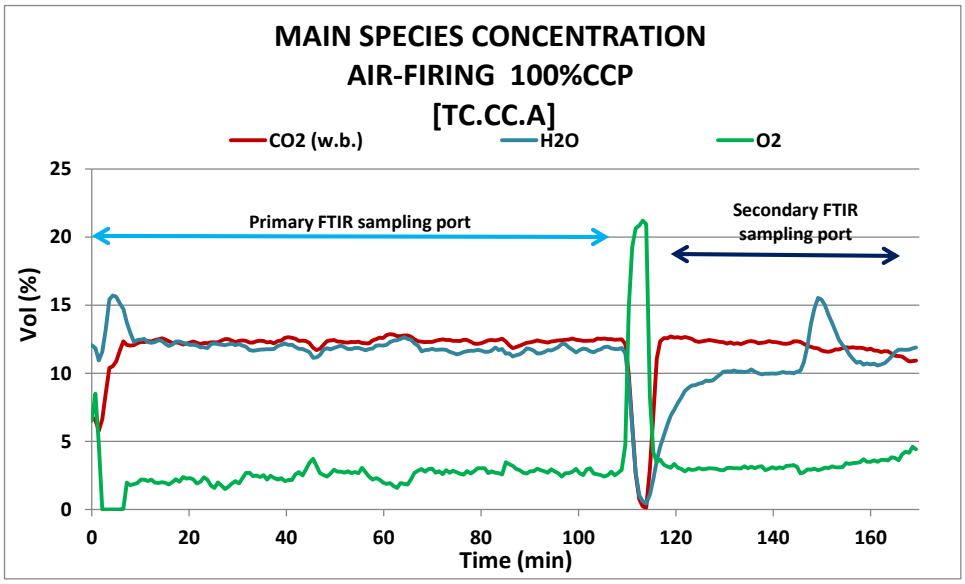


**Figure 65 Gas composition_ Main species for oxy-firing test TC.CC.A. Samples using primary and secondary FTIR ports**

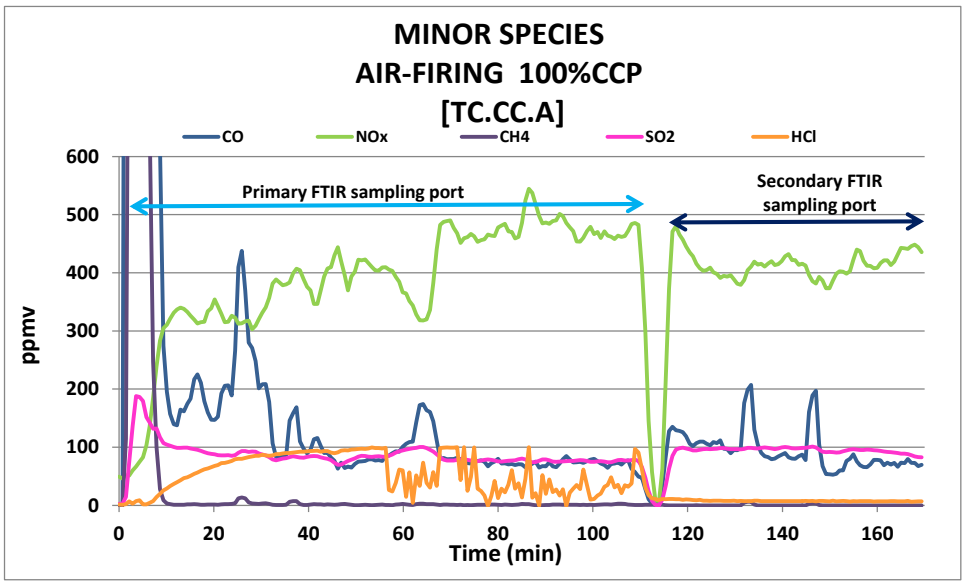


**Figure 66 Gas composition_ Minor species for oxy-firing test TC.CC.A. Samples using primary and secondary FTIR ports**

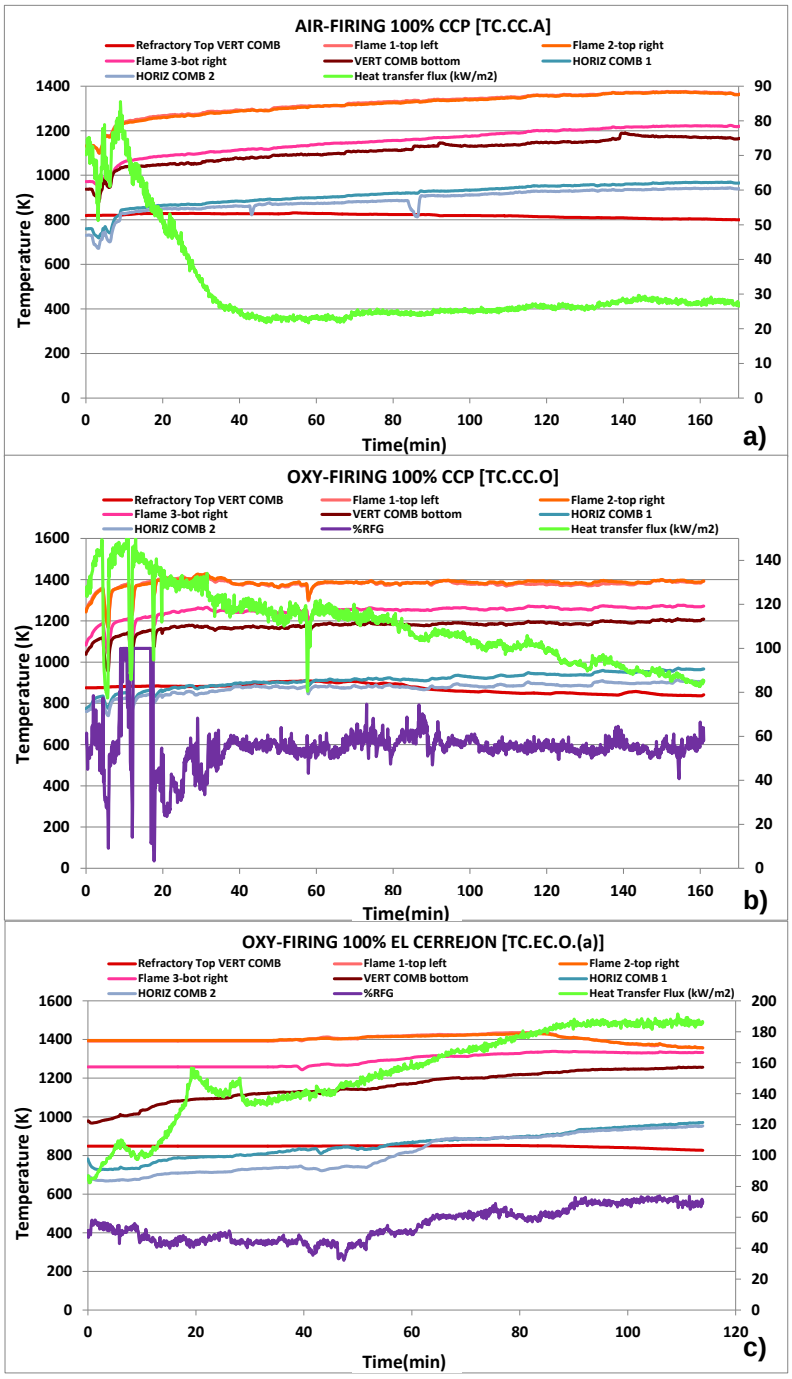


**Figure 67 Temperatures and heat fluxes during tests: a) [TC.CC.A] b) [TC.CC.O] c) [TC.EC.O.(a)]**

## D.2 ESEM/EDX Analysis

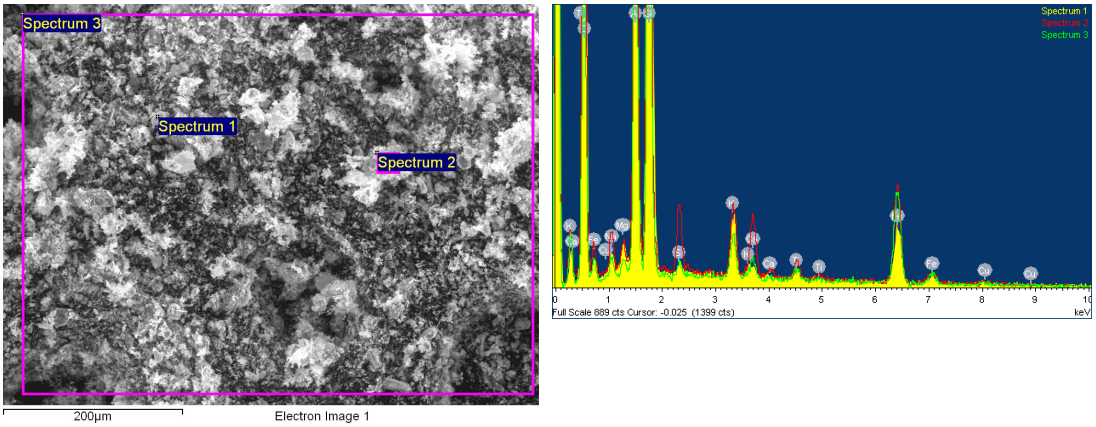


**Figure 68 ESEM/EDX Results from ash sampled after test FC.DM.O(d)**

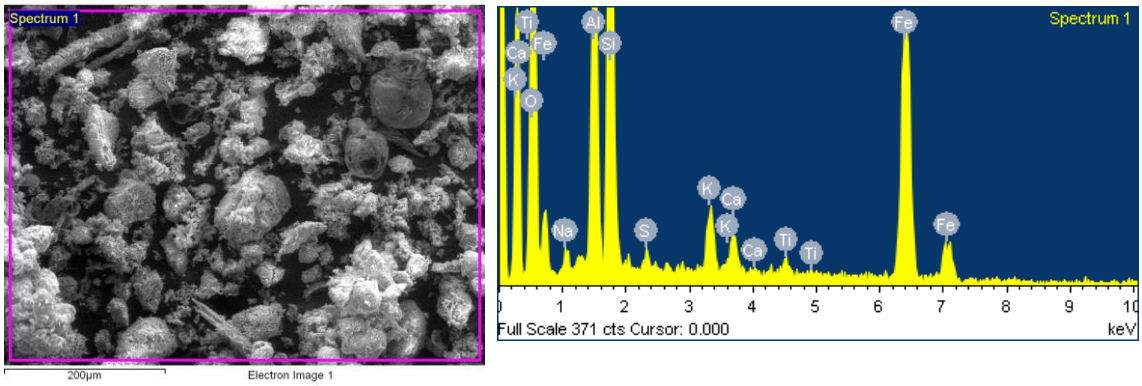


**Figure 69 ESEM/EDX Results from ash sampled after test SC.DM.O**

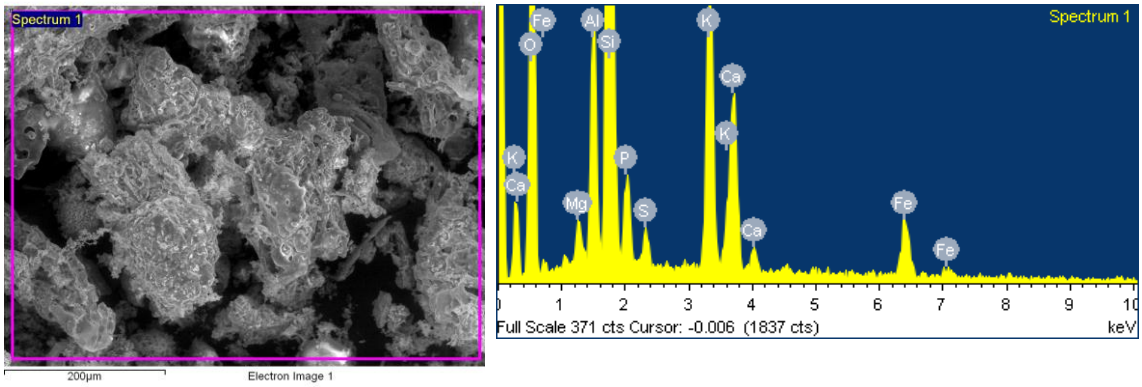


**Figure 70 ESEM/EDX Results from ash sampled after test SC.B1.O**

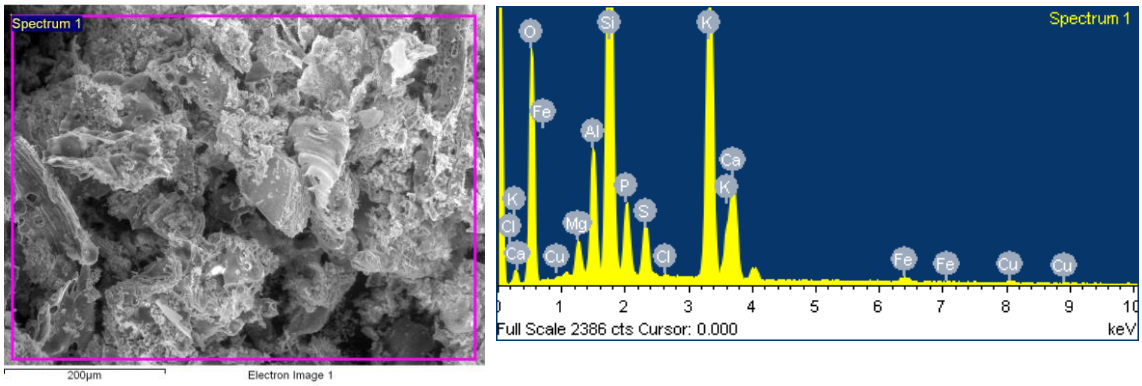


**Figure 71 ESEM/EDX Results from ash sampled after test SC.CC.O**

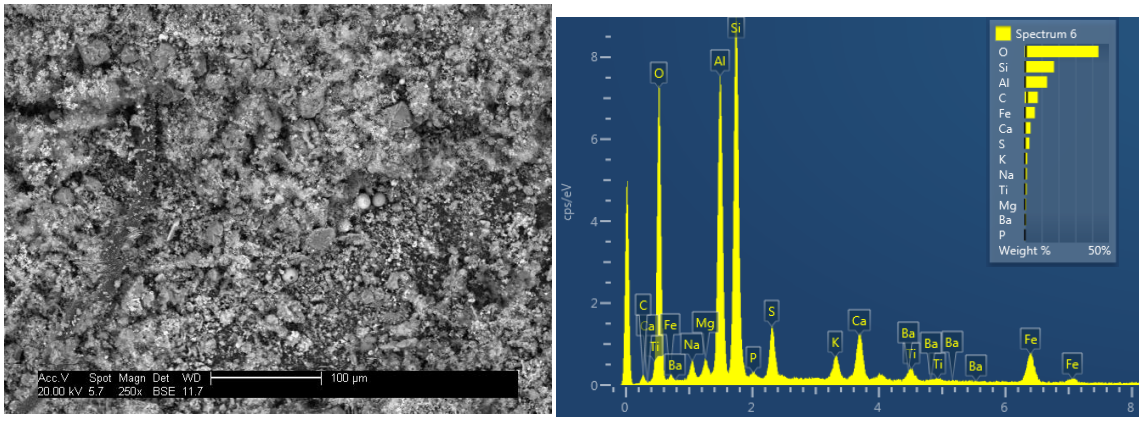


**Figure 72 ESEM/EDX Results from ash sampled after test TC.EC.A**

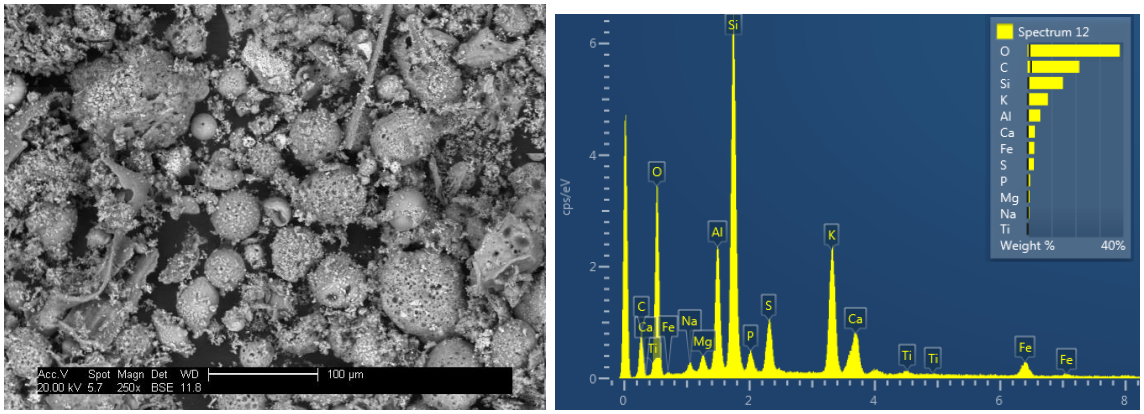


**Figure 73 ESEM/EDX Results from ash sampled after test TC.B1.A**

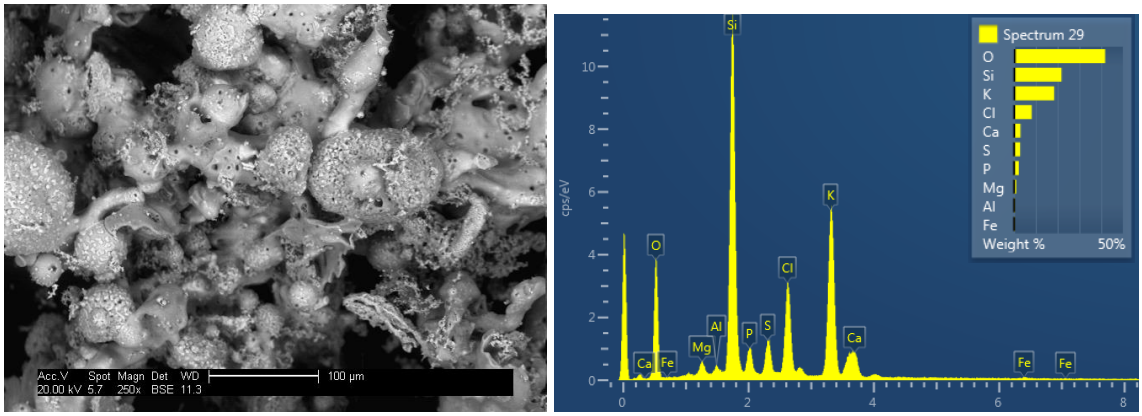


**Figure 74 ESEM/EDX Results from ash sampled after test TC.CC.A**

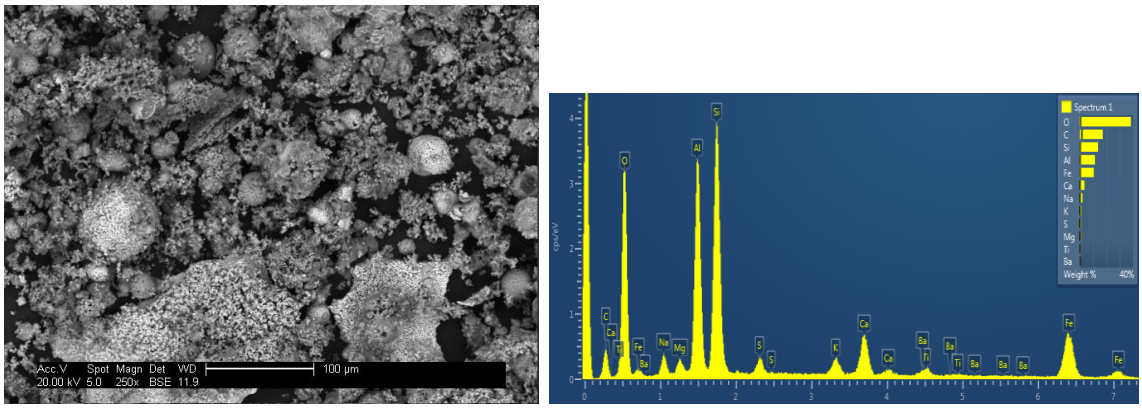


**Figure 75 ESEM/EDX Results from ash sampled after test TC.EC.O.(c)**

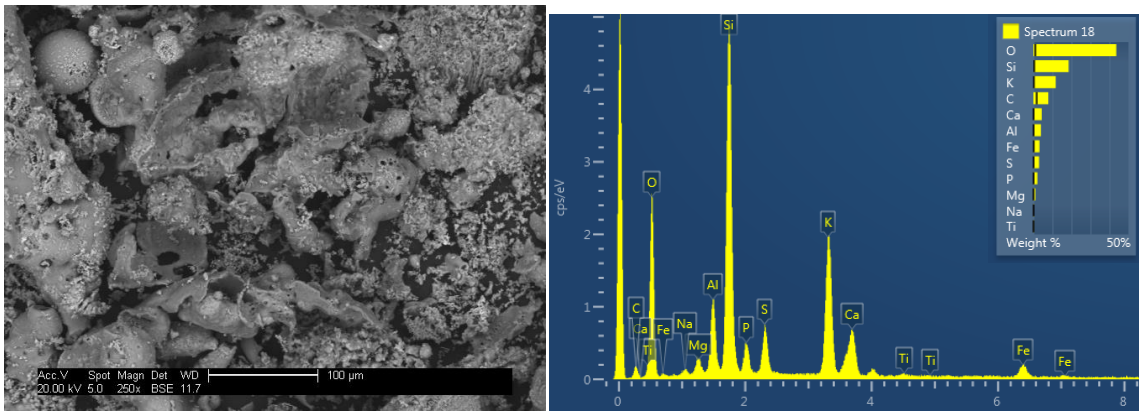


**Figure 76 ESEM/EDX Results from ash sampled after test TC.B1.O.(a)**

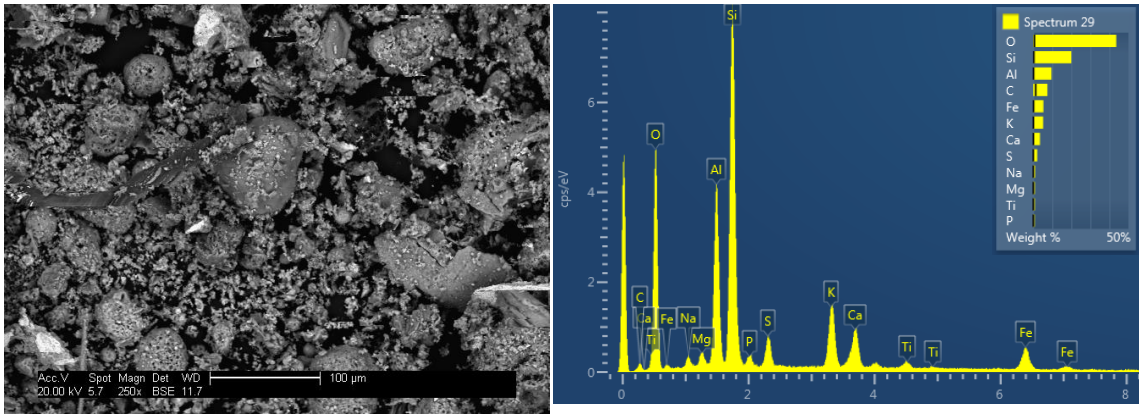


**Figure 77 ESEM/EDX Results from ash sampled after test TC.B2.O**

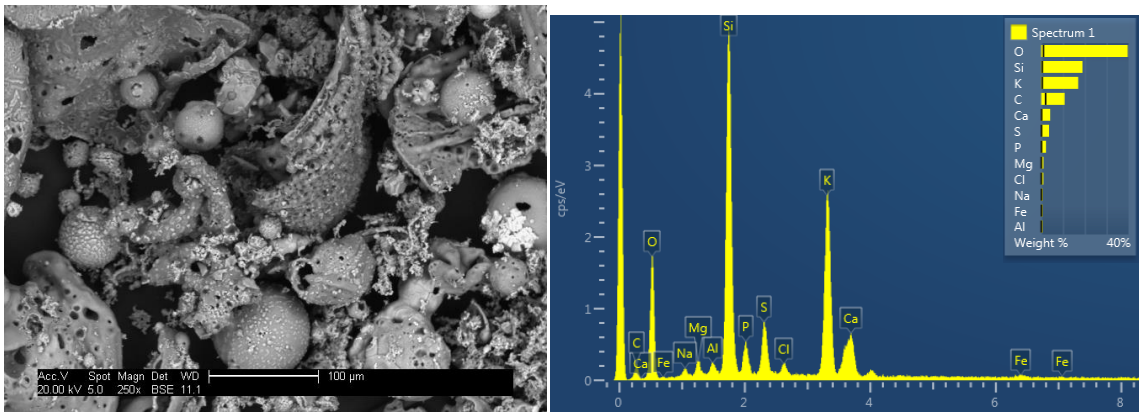


**Figure 78 ESEM/EDX Results from ash sampled after test TC.CC.O**

## D.3 XRD Analysis

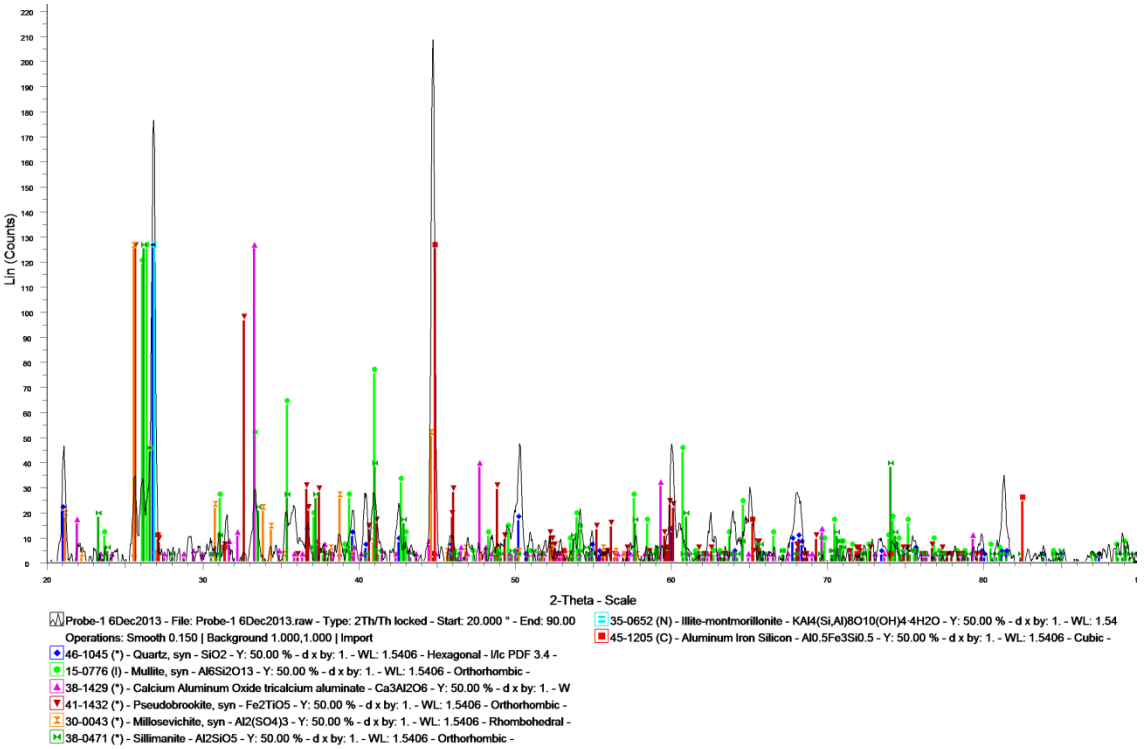


**Figure 79 XRD chart for ashes from air-firing El Cerrejon coal [TC.EC.A]**

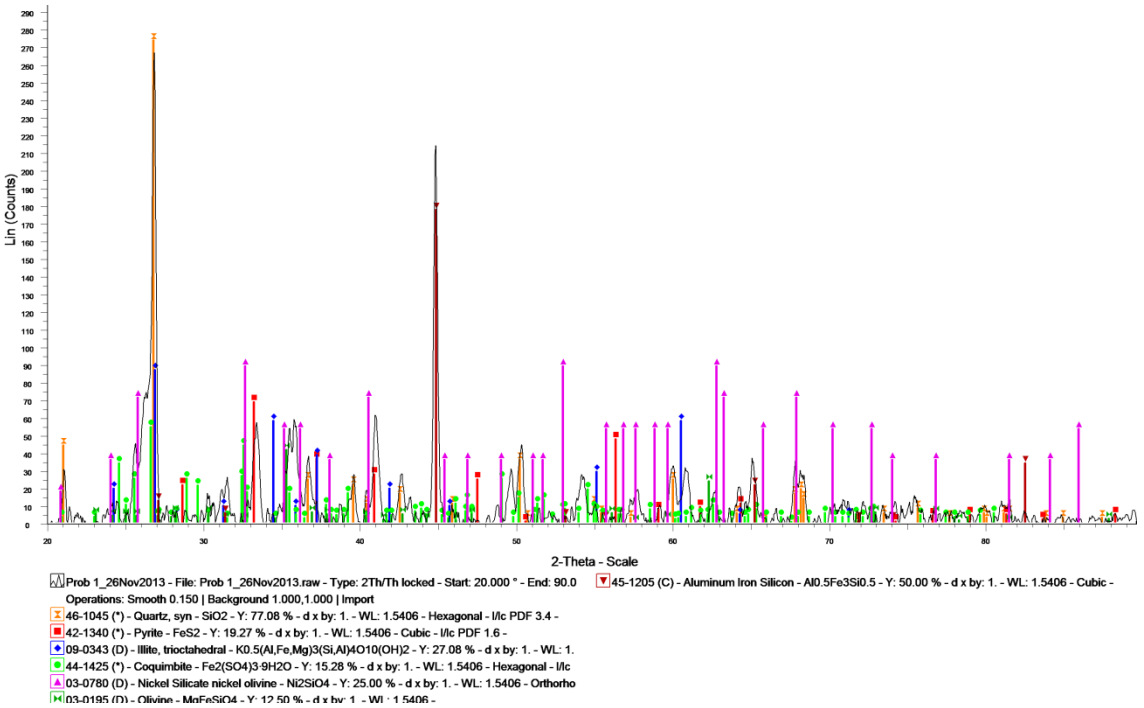


**Figure 80 XRD chart for ashes from oxy-firing El Cerrejon coal [TC.EC.O (c)] at 973K**

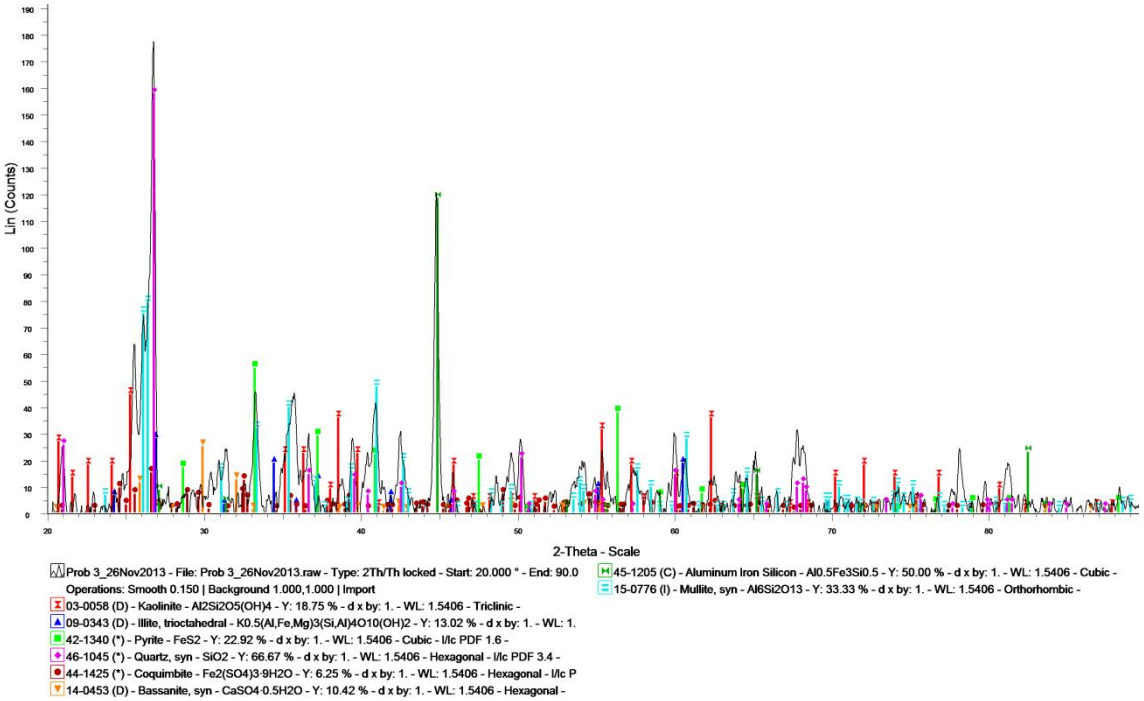


**Figure 81 XRD chart for ashes from oxy-firing El Cerrejon coal [TC.EC.O (c)] at 1130K**

## D.4 Ash deposits: size distribution and shape

These analyses were performed on an area with dimensions 600µm x 600µm.

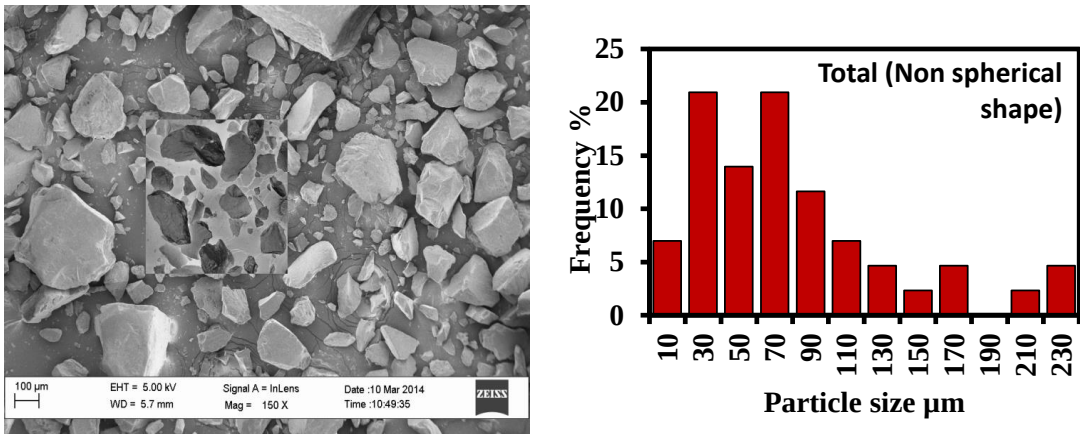


**Figure 82 Size distribution and shape for El Cerrejon coal, as received**

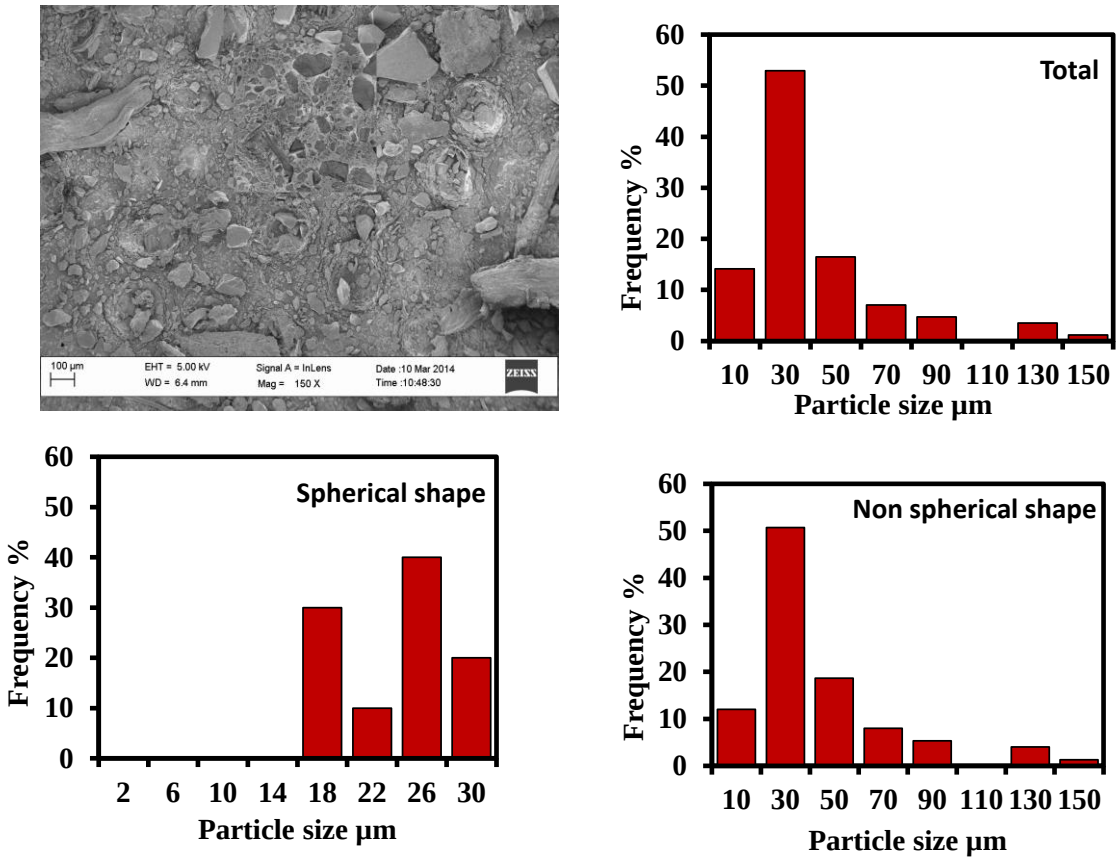


**Figure 83 Size distribution and shape for CCP, after sieving**

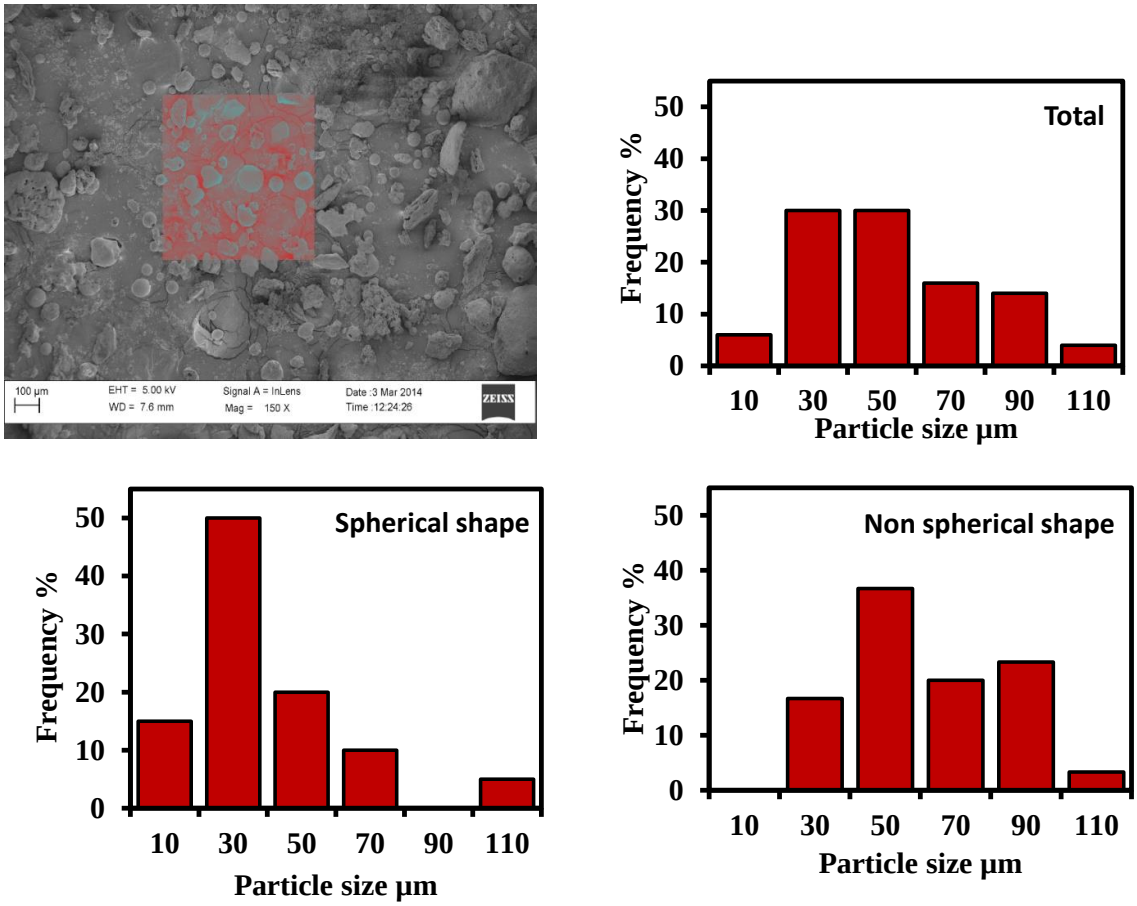


**Figure 84 Size distribution and shape for ash deposits generated oxy-firing 100% El Cerrejon coal [TC.EC.O.(c)]**

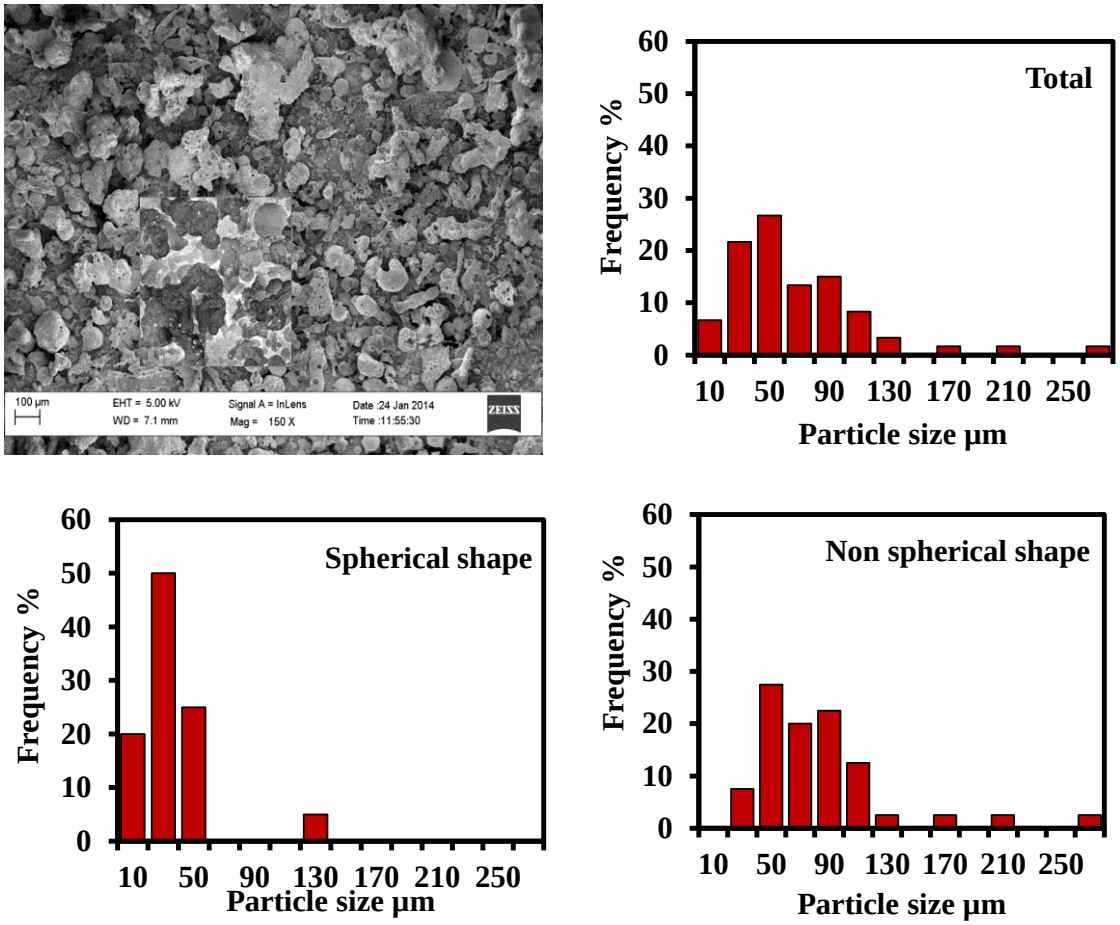


**Figure 85 Size distribution and shape for ash deposits generated oxy-firing 100% CCP [TC.CC.O]**

## D.5 Carbon in ash

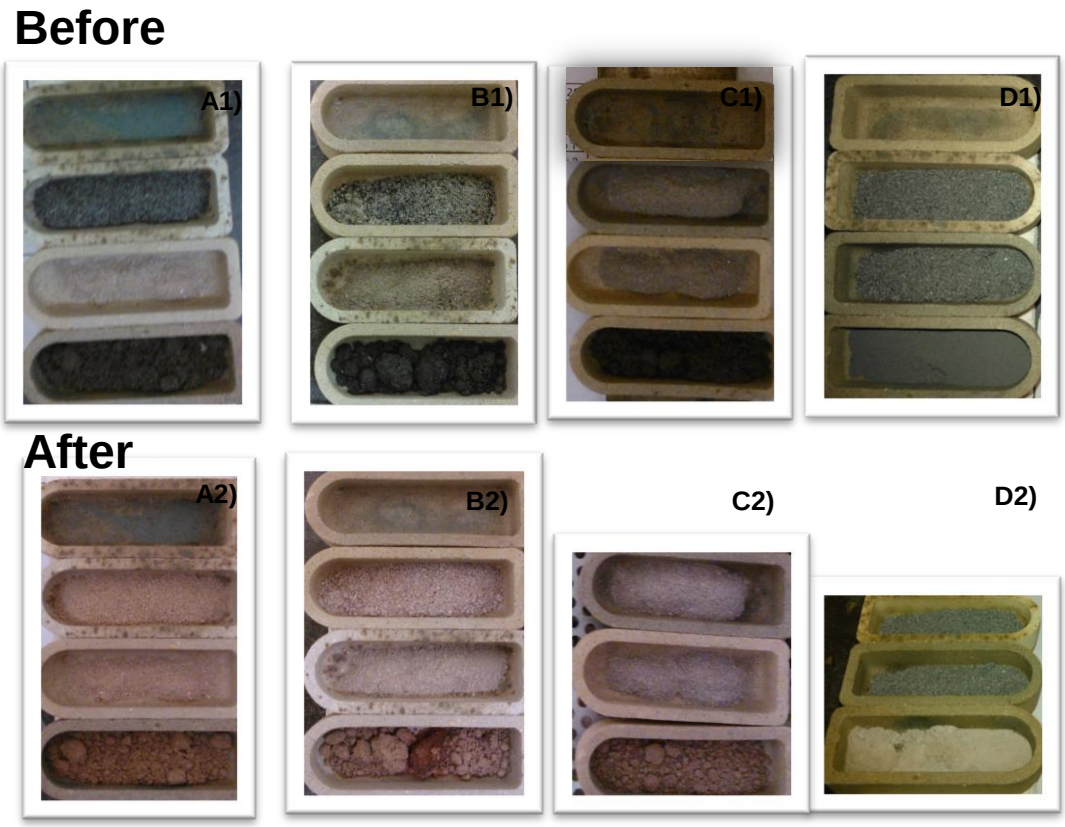


**Figure 86 Samples for carbon in ash tests A)[TC.EC.O(c]); B)[TC.B2.O]; C)[TC.B1.O(b)]; D)[TC.CC.O]**

# Appendix E Modelling data

**Table 36 Simulation results_ Gas composition and temperatures using 5%$O_{2,excess}$ and several percentages of RFG-Stage K2**

| RFG (%) | Fuel | Air Ingress (%) | $O_{2,IN}$ %(v/v) | $O_{2,OUT}$ %(v/v) | $H_2O$ %(v/v) | $CO_2$ %(v/v) | CO (ppmv) | $SO_2$ (ppmv) | T (K) | Heat Transfer (kW) |
|---|---|---|---|---|---|---|---|---|---|---|
| | DM | 2 | 40.21 | 4.23 | 22.77 | 64.29 | 0 | 4030 | 2412 | 81.9 |
| 55 | B1 | 2 | 34.98 | 3.32 | 30.93 | 57.32 | 5 | 2526 | 2278 | 78.63 |
| | CCP | 2 | 31.32 | 0.98 | 42.7 | 48.27 | 0 | 650 | 2105 | 74.99 |
| | DM | 2 | 35.87 | 4.46 | 22.59 | 63.81 | 0 | 4000 | 2205 | 80.77 |
| 60 | B1 | 2 | 32.85 | 3.64 | 30.57 | 56.95 | 0 | 2510 | 2083 | 77.17 |
| | CCP | 2 | 25.73 | 0 | 46.46 | 43.99 | 4427 | 606 | 1927 | 76.69 |
| | DM | 2 | 31.64 | 4.64 | 22.61 | 63.32 | 0.00 | 3970 | 1997 | 79.34 |
| 65 | B1 | 2 | 28.21 | 3.15 | 31.5 | 56.3 | 0.00 | 2480 | 1902 | 76.94 |
| | CCP | 2 | 24.23 | 2.15 | 41.22 | 48 | 1.00 | 647 | 1748 | 70.27 |
| | DM | 2 | 27.1 | 4.68 | 22.28 | 63.02 | 0.00 | 3936 | 1801 | 79.19 |
| 70 | B1 | 2 | 24.85 | 3.99 | 30.27 | 56.09 | 0.00 | 2471 | 1697 | 73.86 |
| | CCP | 2 | 23.01 | 4.92 | 39.68 | 46.38 | 0.00 | 624 | 1553 | 68.38 |

**Table 37 Simulation results_ Gas composition in volume, temperatures and net power generated using 10% air ingress-Stage K6**

| Fuel | RFG (%) | $O_{2,Exc}$ (%) | $O_2$ (%) | $H_2O$ (%) | $CO_2$ (%) | CO (ppm) | $SO_2$ (ppm) | HCl (ppm) | NO (ppm) | $NO_2$ (ppm) | T (K) | Net power ($kW_e$) |
|---|---|---|---|---|---|---|---|---|---|---|---|---|
| EC | 55 | 0 | 3.97 | 12.38 | 63.71 | 0 | 890 | 27 | 914 | 69 | 2822 | 17.8 |
| EC | 60 | 0 | 4.03 | 11.00 | 63.75 | 0 | 788 | 25 | 810 | 62 | 2587 | 17.6 |
| EC | 65 | 0 | 4.84 | 9.42 | 62.05 | 0 | 672 | 20 | 691 | 54 | 2314 | 17.1 |

| Fuel | RFG (%) | $O_{2,Exc}$ (%) | $O_2$ (%) | $H_2O$ (%) | $CO_2$ (%) | CO (ppm) | $SO_2$ (ppm) | HCl (ppm) | NO (ppm) | $NO_2$ (ppm) | T (K) | Net power ($kW_e$) |
|---|---|---|---|---|---|---|---|---|---|---|---|---|
| EC | 55 | 5 | 7.29 | 11.95 | 61.36 | 0 | 857 | 25 | 880 | 66 | 2765 | 17.4 |
| EC | 60 | 5 | 7.65 | 10.59 | 61.14 | 1 | 759 | 23 | 779 | 59 | 2529 | 17.0 |
| EC | 65 | 5 | 8.19 | 9.07 | 59.59 | 0 | 647 | 20 | 665 | 51 | 2265 | 16.5 |
| B1 | 55 | 0 | 3.52 | 17.57 | 60.45 | 0 | 658 | 154 | 566 | 63 | 2637 | 16.7 |
| B1 | 60 | 0 | 3.03 | 16.38 | 60.61 | 15 | 586 | 137 | 504 | 57 | 2453 | 16.9 |
| B1 | 65 | 0 | 2.44 | 13.85 | 60.58 | 5490 | 503 | 118 | 435 | 50 | 2185 | 15.8 |
| B1 | 55 | 5 | 7.26 | 17.21 | 56.79 | 1363 | 624 | 147 | 539 | 58 | 2574 | 16.1 |
| B1 | 60 | 5 | 7.38 | 14.75 | 56.73 | 1 | 560 | 128 | 467 | 52 | 2344 | 15.8 |
| B1 | 65 | 5 | 7.81 | 12.95 | 56.94 | 0 | 482 | 113 | 415 | 47 | 2137 | 15.4 |
| CCP | 55 | 0 | 1.80 | 24.09 | 56.61 | 0 | 343 | 148 | 132 | 56 | 2444 | 15.9 |
| CCP | 60 | 0 | 0.58 | 23.03 | 57.18 | 0 | 310 | 133 | 124 | 50 | 2236 | 16.7 |
| CCP | 65 | 0 | 1.33 | 19.75 | 53.49 | 15200 | 509 | 109 | 73 | 23 | 2057 | 16.3 |
| CCP | 55 | 5 | 5.62 | 22.45 | 54.59 | 0 | 331 | 142 | 128 | 54 | 2366 | 15.0 |
| CCP | 60 | 5 | 2.73 | 23.17 | 56.45 | 0 | 304 | 131 | 117 | 50 | 2318 | 16.7 |
| CCP | 65 | 5 | 2.12 | 20.45 | 50.47 | 4870 | 255 | 107 | 96 | 40 | 2106 | 15.2 |